THE DESIGN AND OPTIMIZATION OF A SYSTEM USING AN INDUCTION MOTOR DRIVEN PUMP, POWERED BY SOLAR PANELS

J.L.Davies, BSc(Elec Eng),UCT

Department of Electrical and Electronic Engineering, University of Cape Town

30 April 1992

Thesis prepared in partial fulfillment of the requirements for the Degree of MSc in Electrical and Electronic Engineering

ACKNOWLEDGEMENTS

The Author wishes to thank the following people for assistance received during the course of the project.

Mr Michel Malengret for his supervision, technical contribution and many positive suggestions towards the project.

Jochen Roeber for his help with the field tests and array tracker.

Professor Gieraz for his constructive criticism concerning the chapter on the motor analysis.

Glynn Morris from the Energy Research Institute for assessing the solar literature review.

Dave Kenyon for his help in mounting the system components for experimentation in the laboratory.

The Kirsten family for the hospitality I received during the field tests, which were carried out on their farm near Prince Albert.

TERMS OF REFERENCE

This project was proposed by Mr M. Malengret at the University of Cape Town. The project involves the development and evaluation of an induction motor driven solar water pumping system. Mr Malengret's specific instructions were:

1) To develop the system for application to borehole pumping with a positive displacement pump.

2) To optimize the performance of the system in order to maximize the water delivery. This involves:

   - Developing an efficient and robust variable speed drive for the induction motor.

   - Optimizing the performance of the induction motor at all speeds of operation.

   - Controlling the system in such a way that the solar panels are utilized to their full potential despite variations in the irradiance level.

SYNOPSIS

This thesis describes the design and evaluation of an induction motor driven water pumping system which is powered by solar panels. The system consists of a positive displacement pump, solar panels and an induction motor with a microprocessor controlled inverter. The reason that an induction motor has been chosen for the project is that these motors are cheaper and more robust than the more conventional DC motors. It is expected that by using an induction motor, the system performance will improve significantly for the same investment.

The motor has a power rating of 0.75kW and it has been specially designed for a solar application. The system has been designed to operate from between five and seven solar panels, which yields a system capacity of 350W. The capacity could be extended to operate up to the full rating of the motor.

A variable frequency drive has been designed to control the motor speed. The drive consists of a power MOSFET inverter bridge which is controlled by an 8031 microcontroller. Software has been written for the controller to generate the required pulse-width modulated signals to the inverter. Also included in the system design is an array tracker which optimizes the power output of the solar panels.

The efficiency of the motor has been optimized for the torque requirements of the pump. This has been achieved by implementing an optimized voltage frequency curve and by providing for operation above the rated frequency of the motor. The motor has been operated in the frequency range of 5 - 80Hz.

The inverter efficiency was high at 87% and this is expected to increase at higher power ratings. The combined motor and inverter efficiency was found to be 67% over a frequency range of 45 - 80Hz. This is only marginally less than the efficiency found in DC systems where a DC-DC converter is required to drive the motor.

The control method for the system incorporated a method of maximizing the water delivery. This was achieved by optimizing the motor speed while monitoring the panel voltage. The voltage was monitored because of the high inertia of the pump, which made pure speed control difficult to implement.

A field test was conducted to compare the developed AC system with a Mono DC system. The gearing of the DC system was not optimal and hence a higher flow rate was achieved with the AC system. However, the efficiency of the DC motor and converter combination proved to be slightly higher than that of the AC system. This comparison neglected the effect of poor maximum power point tracking of the DC system.

In conclusion, the implementation of an AC induction motor system offers significant advantages over a DC system in terms of cost and reliability, while similar efficiencies are expected from the two systems. The cost reduction with a seven panel system will more than cover the cost of another panel, which represents a 15% increase in the system input power. The speed control of the system ensures that the water delivery is maximized at all operating irradiance levels and hence the panel output is fully utilized. The system performance is further enhanced with the use of an array tracker, which will improve the panel output by approximately 20%.

CONTENTS

Chapter	Page
Acknowledgements	i
Terms of Reference	ii
Synopsis	iii
List of Illustrations	viii
Glossary	xi
1. INTRODUCTION	1
2. SOLAR LITERATURE REVIEW	3
2.1 Photovoltaic Panels	3
2.1.1 History of Converting Light to Electricity	
2.1.2 Future Developments in Photovoltaic Technology	
2.1.3 Economics of Photovoltaic Power	
2.1.4 Operation and Characteristics of Solar Panels	
2.2 Application of Photovoltaic Power to Water Pumping	11
2.2.1 The Mono System	
2.2.2 The solar Jack System	
2.2.3 Other Systems in Southern Africa	
2.3 Most Effective Motor and Pump Combination	14
2.3.1 Most Suitable Pumps for Solar Application	
2.3.2 Most Suitable Motor for Solar Application	
3. SYSTEM DESCRIPTION	18
3.1 Solar Panels Used for Project	19
3.2 Pump Operation and Characteristics	19
3.3 Induction Motor Description	21
3.4 Inverter and Controller Description	21
4. DESIGN OF SYSTEM COMPONENTS	22
4.1 Inverter Design	22
4.1.1 Base Drive Circuit	
4.1.2 Switching Aid Network	
4.2 Microcontroller Design	23
4.2.1 Allocation of Memory Space	
4.2.2 Interfacing with ROM	
4.2.3 Interfacing with RAM	
4.2.4 Interfacing with the ADC	
4.2.5 Watchdog Circuit	
4.3 Speed Monitoring Circuit	28
4.4 DC-DC Converter Design	28
4.5 Array Tracking Design	29

5 SOFTWARE STRUCTURE AND GENERATION OF PWM 31
5.1 Choice of PWM Strategy 31
5.1.1 Carrier Modulated Sine PWM
5.1.2 Programmed PWM Techniques
5.2 Microcontroller Software Structure 34
5.3 Generation of PWM 36
5.3.1 Operation of Timer 1 Service Routine
5.3.2 Creating a Three-Phase Sequence in RAM
5.3.3 Operation of Timer 0 Service Routine
5.3.4 Software Optimization of Starting Torque

6. MOTOR EFFICIENCY ANALYSIS 45
6.1 Derivation of Maximum Efficiency Curve 45
6.2 Derivation of Equivalent Circuit Parameters 48
6.2.1 Calculation of Fundamental Circuit Parameters
6.2.2 Harmonic Frequency Equivalent Circuit
6.3 Evaluation of Motor Performance 55
6.3.1 Evaluation of Optimum voltage Frequency Curve
6.3.2 Experimental Evaluation of Motor Performance
6.3.3 Effects of Oversizing the Induction Motor

7. INVERTER PERFORMANCE ANALYSIS 63
7.1 Assessment of PWM Harmonic Losses 63
7.2 Assessment of Switching Losses 66
7.3 Assessment of Conduction Losses 69
7.4 Assessment of Control circuit Losses 71
7.5 Inverter Efficiency and Total Losses 71

8. CONTROLLER FOR MAXIMIZATION OF DELIVERY 75
8.1 Constant voltage Tracking 75
8.2 Maximum Power Point Tracking 76
8.3 Speed Maximization Controller 76
8.4 Controller Requirements 77
8.5 Designing a Suitable Controller 78
8.5.1 Hill-Climbing Algorithm Approach
8.5.2 Constant Slip Controller
8.5.3 Slip Controller with Offset
8.5.4 Combination of Voltage and Speed Control

9. FIELD TEST EVALUATION 90
9.1 System Optimization for Field Test Conditions 91
9.2 Factors Affecting System Performance During Test 92
9.3 Measurements taken During Field Tests 92
9.4 Assessment of Pump Characteristics 93
9.5 Comparative Tests Between DC and AC Systems 95
9.5.1 Panel Optimization Assessment
9.5.2 Performance Comparison Between Two Systems
9.6 Improvements with Array Tracker 100

10. CONCLUSIONS 101

11. RECOMMENDATIONS 103

REFERENCES 104

APPENDICES

LIST OF ILLUSTRATIONS

Figures	Page
1. PV Module Cost Versus Time	6
2. Unit Costs of Pumped Water in South Africa	7
3. Schematic of a Photo-Voltaic Cell	8
4. Characteristic Curves for Panels at Different Temperature and Insolation Levels	10
5. Performance Curves for Mono Water Pumping System	12
6. Efficiencies of Solar Jack System	13
7. Comparison Between a Mono and a Centrifugal Pump at 20m Head	15
8. Induction Motor Driven Solar Pumping System	18
9. Panel Characteristics Supplied by Siemens	19
10. Mono Positive Displacement Rotor and Stator	20
11. Allocation of Memory Space	24
12. Interfacing with ROM	25
13. Interfacing with RAM	25
14. Interfacing with the ADC	26
15. Implementation of Natural Sampled PWM	32
16. Implementation of Regular Sampled PWM	32
17. Software Structure for Microcontroller	35
18. Timer 1 Service Routine	36
19. Phase Shift due to Changing Modes	38
20. Reading in Voltage Table from ROM	40
21. Generating Single-Phase Sequence in RAM	41
22. Generating Three-Phase Sequence in RAM	42
23. Operation of Timer 0 Service Routine	43
24. Routine to Overcome Starting Torque	44
25. Approximate Equivalent Circuit for Best Efficiency Derivation	46
26. Equivalent Circuit to Predict Motor Performance	49
27. Secondary Resistance and Secondary Leakage Inductance for Operating Frequency Range	50
28. Harmonic Frequency Equivalent Circuit	54
29. Derived Optimum Voltage Frequency Curve for Different Torques	56

30. Voltage and Efficiency as a Function of Frequency for Derived and Exact Circuit Optimum Performance 57
31. Efficiency Sensitivity for Changing Torque 58
32. Efficiency Sensitivity for Changing Voltage 59
33. Experimental and Theoretical Motor Efficiency (T = 1 Nm) 60
34. Motor Characteristics at Rated Frequency and Voltage ($V=63.5v_{ln}$) 61
35. Motor Characteristics at Rated Frequency and Below Rated Voltage 61
36. Harmonic Losses at 20 Hz 64
37. Harmonic Losses at 35 Hz 64
38. Harmonic Losses at 50 Hz 65
39. Table of Harmonic Losses for Sine and Harmonic Elimination PWM 65
40. Inverter Turn-on Switching Waveforms 67
41. Linearized Current Switching Waveform 68
42. Table of Switching losses for Sine and Harmonic Elimination PWM 69
43. Motor and Combined Inverter and Motor Efficiency 71
44. Inverter Efficiency versus Frequency 72
45. Bar Chart of Different Inverter Losses 73
46. Correlation of Two Methods of Harmonic Loss Prediction 73
47. Control Method Whereby Small Changes in Frequency are Used to Obtain Maximum Speed 78
48. Operation of Constant Slip Controller 80
49. Linearity of F_n With Respect to the Actual Frequency 81
50. Phase Delay of Motor Speed with Collapsing Supply Voltage 82
51. Operation of Controller with Crossover Point 83
52. Controller Performance Following a Step Change in Irradiance 84
53. Flow Diagram of Controller with Offset 85
54. Controller Performance Once Oscillations have Settled 86

55. Evaluation of Speed Controller Performance 87
56. Laboratory Simulation of Pumping System 88
57. Flow Diagram of Voltage and Speed Controller 89
58. The Borehole Pump Used for the Field Tests 90
59. Torque Speed Curve for Field Test Pump 94
60. Experimental Curve of Flow Rate Versus Speed 95
61. Panel Voltage for AC and DC Systems 96
62. Irradiance versus Time for a Clear Day 97
63. Flow Rate of AC and DC Systems 98
64. Comparative Efficiency of AC and DC Systems 99
65. Irradiance with Directional and Fixed Array 100

GLOSSARY

ADC - Analogue to digital converter

DPTR - Pointer of 8031 microcontroller for addressing external data

IC - Integrated circuit

I_D - Current through drain of MOSFET

Monocrystalline - Single crystal structure of silicon

MOSFET - Metal oxide silicon field effect transistor

Oversizing - Operation of motor below its rated power

PDP - Positive displacement pump

Photovoltaic - Operation by means of photo-electric effect

PWM - Pulse-width modulation

pyranometer - Device used to measure light irradiance levels

RAM - Random access memory

ROM - Read only memory

Snubber - Switching aid circuit to protect the MOSFET from current or voltage transients

V_{DS} - Voltage across the drain and source of a MOSFET

w - Angular velocity measured in rad/s

W_p - Peak power output of solar panels

CHAPTER 1: INTRODUCTION

The aim of this thesis was the design and evaluation of a solar powered, water pumping system driven by an induction motor. Solar powered water pumping is fast becoming an accepted means of obtaining water in remote areas where national grid connection is not viable. The low maintenance requirements and the cost reduction of solar panels over the past few years have made such systems highly competitive against diesel and windmill energy generation.

Many commercial systems are being made available and these comprise various types of pumps and motors. The most popular system is the positive displacement pump by Mono Pumps, which uses a DC motor. The disadvantage of using a DC motor is the high cost and periodic maintenance requirement of replacing brushes. AC systems offer the advantage of being both inexpensive and more robust than their DC counterparts, but the drawback of these systems has been their low efficiency.

Following a BSc thesis by the author, it was established that an induction motor could provide a viable means of obtaining an inexpensive and efficient pumping system. The reason for this is that the low efficiency of small induction motors is not caused by physical constraints on the motor, but rather by manufacturers believing their is only a limited market for highly efficient small motors.

The Energy Research Institute at UCT have also been investigating the viability of using an induction motor for a solar pumping application. A motor manufacturing firm was requested to design and produce an efficient small induction motor and such a motor has been produced. The motor has an efficiency similar to a DC

motor and it is this motor which has been used for the project.

The objectives of this thesis are to develop a three-phase system which maximizes the water delivery of the pump. Particular attention has been given to the control and performance optimization of the motor and inverter. The system is controlled by a microcontroller which both adjusts the speed of the pump to optimize the water delivery. Since the main aim is to maximize the water delivery, an array tracker has been included in the system design to improve the panel delivery.

This report starts off by presenting the research progress that has been made in the field of solar water pumping which is relevant to the project. This is followed by the design of the controller, inverter and array tracker. Following this the microcontroller software structure and method of generating the PWM is described. Optimization of the motor and inverter are then discussed and the method of controlling the speed of the pump is presented. To give an indication of the system performance, a field test was conducted and these results are presented. Finally, conclusions are drawn and recommendations are made concerning the further development and commercialization of such a system.

CHAPTER 2: SOLAR LITERATURE REVIEW

This review discusses recent literature relevant to solar water pumping. Efficiencies and future trends of solar panels are discussed and the characteristics of the panels are analyzed. Various types of available pumping systems are discussed and compared to the potential of developing an induction motor driven positive displacement system.

2.1. PHOTOVOLTAIC PANELS

Photovoltaic power is the quintessential energy source, creating electricity with no pollution, no noise and often no moving parts. Photovoltaic systems are well suited to remote or arid regions and they can also operate on any scale[1]. This section looks at the development and expected trends of solar panels.

2.1.1. History of Converting Light to Electricity

The phenomenon of converting light to electricity was first observed in 1839 by Edmund Becquerel. He noticed that a voltage appeared when one of two electrodes in a conducting solution was illuminated. In the 1920s quantum mechanics laid the theoretical foundation for our understanding of the physics of PV phenomena. This was followed in the 1950s with the development of the Czochralski method of producing high quality crystalline silicon. In 1954 Bell Telephone laboratories developed a silicon cell with an efficiency of 4%. This was soon bettered to 6% and then 11% efficiency.

The development of the solar cell was greatly encouraged by the realization that PV could be an effective source for powering space missions. Another factor that contributed greatly to solar-cell technology was the

transistor industry. Transistors and PV cells are made from similar materials and their workings are determined by many of the same mechanisms. Today, photovoltaic systems are capable of transforming one kilowatt of solar energy falling on one square meter into about one hundred watts of electricity[2].

2.1.2. Future Developments in Photovoltaic Technology

Research and development is an ongoing process in the PV panel industry and the main areas of technological development are briefly listed below:

- Polycrystalline silicon cells have a lower efficiency, but the cost saving in manufacture could make these a viable alternative.

- Amorphous silicon appears to have an efficiency limitation of 12-14%, but it shows promise because of its ability to absorb light well.

- Thin film multi-junction cells, whereby a thin film is deposited on a substrate, could also provide a means of lowering the cost of solar cells[3]

The disadvantage of monocrystalline silicon is its high manufacturing costs compared to the polycrystalline and amorphous silicon cell. Kamper[4] suggests that the amorphous cell will be used more in the future, while Sinclair[5] argues that thin film multi-junction cells are more hopeful.

The improvement of efficiency and reduction in cost of solar panels is a much sought after goal and many developments are taking place to achieve this. An example of such a development is the unveiling of the first solar photovoltaic technology using silicon ribbon by Ferrofluidics and the Blue Ridge group in March 1992. This technology uses crystal growing in a process that enables growth of solar cells from a continuous

ribbon of silicon. Such ribbons have proven to be more efficient , lighter in weight, more flexible and less costly than traditional energy conversion technologies such as silicon wafers[6].

Another new development in the photovoltaic industry comes from the Southern California Edison Company. This company has developed a solar cell that uses inexpensive, low-impurity silicon - considered unusable until now - to convert sunlight into electricity. This method is expected to surpass contemporary photovoltaic processes by combining common, abundant materials with low-cost manufacturing equipment. Edison quotes commercially available solar cells at $5/watt, while it predicts that this cost can be reduced to under $1/watt[7]. More information on this technology has been included in Appendix 2.

Although it is not yet clear which type will offer the best combination of efficiency and cost, the trend of photovoltaic technology clearly indicates a reduction in the overall cost of solar systems.

2.1.3. Economics of Photovoltaic Power

For most commercial solar applications, the monocrystalline silicon PV cell is used. This type of cell has an efficiency of around 15%. The PV modules mostly in demand in terms of peak power are between 45 and 55 Wp and these cost about R22/Wp (July 1990)[8].

The fact that solar energy is free does not mean that it will have a low utilization cost. The capital costs of solar systems are still too high to compete with electrical grid connections. Regions of developing countries where rural electrification is embryonic are important early markets for PV systems. Extending power lines from centralized sources to rural areas is often not yet economical, and so decentralized power sources such as PV are a promising alternative. On a lifetime

cost basis, PV is now cost effective compared with diesel generators at capacities below 20 KW[9].

Ultimately the potential of photovoltaics is determined by the cost of electricity production compared to competing electricity generating technologies. As the cost of photovoltaics falls, solar applications closer to the national grid will become competitive. The graph below shows clearly how the cost of PV power has fallen over the last decade and this trend is expected to continue in the foreseeable future[10].

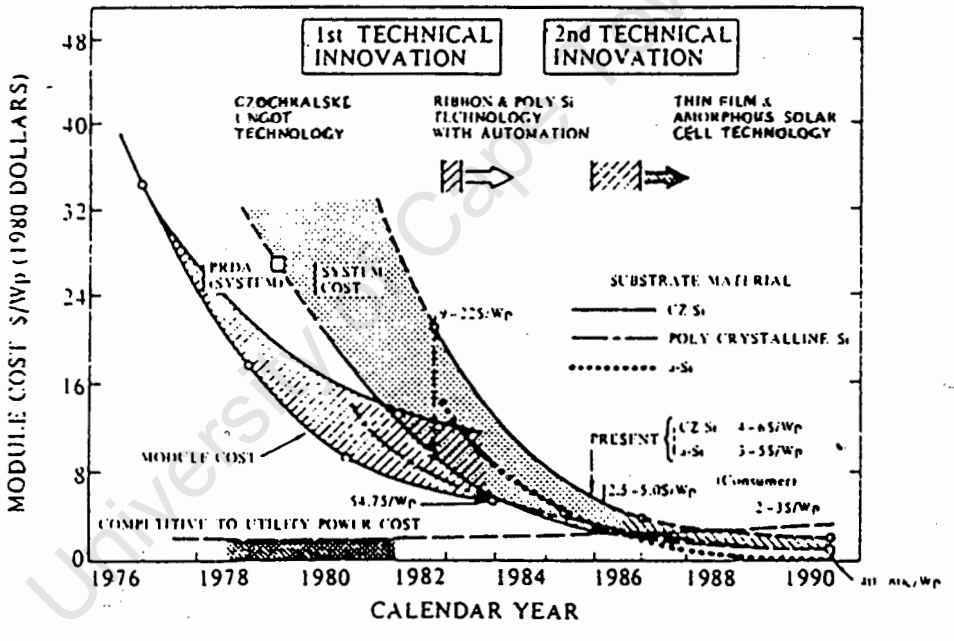

Figure 1: PV Module Cost Versus Time [Hamakawa cited by Sinclair]

Two studies have been made by Wiseman and Halcroft to compare the cost between PV and diesel water pumping. Gosnell[11] has combined these two studies and adapted them for application in South Africa. The bar chart

below shows that in most cases, PV power offers a cheaper alternative to diesel power.

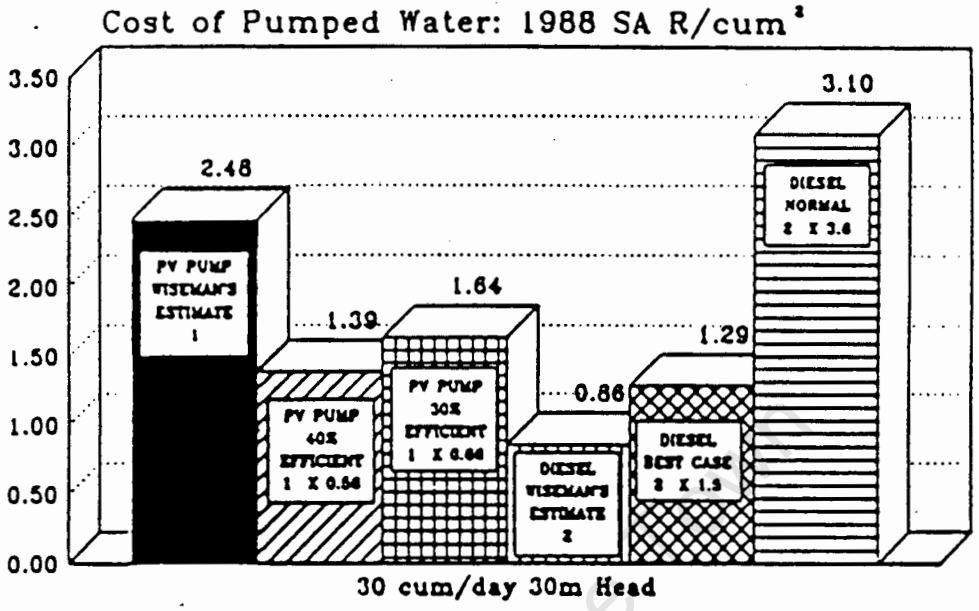

Figure 2: Unit Costs of Pumped Water in South Africa

2.1.4. Operation and Characteristics of Solar Panels

In order to optimize the system efficiency of any solar application it is necessary to have some knowledge of the operating characteristics of solar panels.

2.1.4.1. Operation of Solar Panels

The single crystal photovoltaic cell is made of two layers of silicon each doped with an impurity. The layer on which the sun shines is doped with phosphorus, which creates an n-type semi-conductor. The other layer is doped with boron and is a p-type semi-conductor. Together the two layers form a p-n junction similar to those used in transistors.

Because the phosphorus atom has five valence electrons as opposed to the four of silicon, the n-layer has free electrons which are not bonded. Similarly, in the p-

layer there are spaces for extra electrons which the boron atoms have created as they have only three valence electrons.

When the two layers are bonded a depletion region forms at the interface and a potential difference is built up across the junction. This is caused by the free electrons from the n-layer flowing into the p-layer and filling the electron holes. At any time some valence electrons may have enough energy to overcome their bonds to the nuclei and are thus mobile. The electric field sweeps these mobile electrons across the junction and an equilibrium is established. In sunlight the photons of light liberate a large number of electrons from their bonds. Most of these are swept out of the depletion zone before they recombine with the nuclei and they form the current of the PV cell. The following figure shows a schematic of the operation of a PV cell.

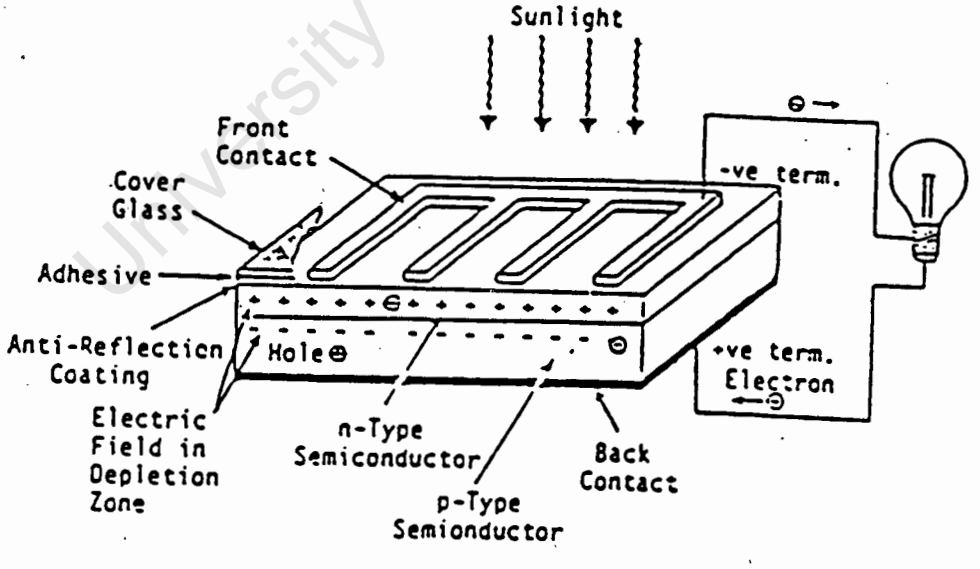

Figure 3: Schematic of a Photo-Voltaic Cell[12]

2.1.4.2. Characteristics of Solar Panels

A photovoltaic cell behaves similarly to a diode with a photo-voltage. The photo-voltage arises from the dissociation of electron-hole pairs which are created by incident photons within the built-in field of the diode junction.

According to Lasnier, the operating equation of I = f(V) characteristics of a solar cell can be derived as:

$$I = I_l - I_o\left[e^{\frac{q(V+R_sI)}{nKT}} - 1\right] - \frac{V+R_sI}{R_{sh}}$$

where I_l = Photocurrent (A/m^2)
I_o = Saturation current (A/m^2)
n = Ideality factor
q = Electronic charge (C)
K = Boltzman's constant (J/K)
T = Junction temperature (K)
R_s = Series resistance
R_{sc} = Shunt resistance[13]

As can be seen from the figure below, the characteristic curve varies substantially with different temperature and insolation levels.

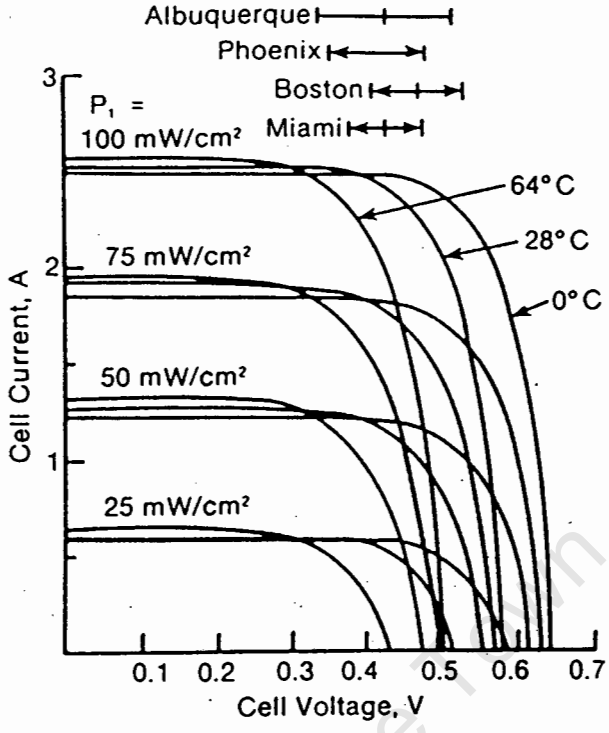

Figure 4: Characteristic Curves for Panels at Different Temperature and Insolation Levels[14]

In order for any solar system to operate efficiently, it is necessary for the panels to operate at the maximum power point. This can be achieved either by keeping the voltage constant or by tracking the maximum power point directly. Voltage tracking offers the advantage of simplicity, but it is not as efficient as maximum power point tracking.

As far as the author knows, all the available commercial water pumping systems either use voltage tracking or direct coupling (in the case of some centrifugal pumps). However, maximum power point tracking is widely documented in the application of battery chargers. Both Enslin and Van den Heever[15] and Lasnier[16] estimate that a 25% improvement to the panel efficiency can be achieved by maximum power point tracking in the use of battery chargers. These estimates take into account the variation in the battery voltage due to ageing,

temperature and charge level of the battery. These are factors which are not present in a water pumping application.

According to Lasnier, variations of the panel voltage are due to solar radiation (10%), temperature (10%) and ageing. Another factor which affects the panels is the scattering effect of the electrical characteristics of solar cells. This is due to the imperfect repeatability of the technical processes of solar cell fabrication[17].

It is therefore evident that for solar water pumping systems, as for battery charging applications, significant improvements to the panel efficiency can be achieved by implementing maximum power point tracking as opposed to constant voltage control.

2.2. APPLICATION OF PHOTOVOLTAIC POWER TO WATER PUMPING

Water pumping is a relatively new application of photo-voltaic power in South Africa. In July 1991 a thesis was submitted by R.J.Gosnell to the Energy Research Institute (UCT) which could be considered to be the first thorough evaluation of a photovoltaic water pumping system in South Africa. Gosnell's study evaluated the technical, social and economic aspects of a solar water pumping system. The system that was evaluated consisted of a positive displacement pump driven by a permanent magnet DC motor.

A feasibility study for a PV pumping system has been submitted to the National Energy Council by M.J.Kamper from the University of Stellenbosch. This study examines the available photovoltaic water pumping systems in South Africa and discusses the feasibility of developing a submersible system using either a brushless DC motor or a reluctance motor. From Kamper's report, the market share of PV powered deep well pumps is held

predominantly by two types of pumps in South Africa. These are the Mono PV pump and the Solar Jack pump.

2.2.1. The Mono System

The Mono system consists of a positive displacement pump with a permanent magnet DC motor driven via a DC-DC converter. The motor tested by Gosnell showed a constant efficiency of 76%, which is in agreement with Halcrow's estimated efficiencies for DC permanent magnet motors of between 76% and 82%. The pump used by Gosnell yielded an efficiency of around 40%, which is a typical value to be expected from the characteristic curves supplied by Mono Pumps (Appendix 1.2). The graphs in figure 5 show the performance curves for Gosnell's system.

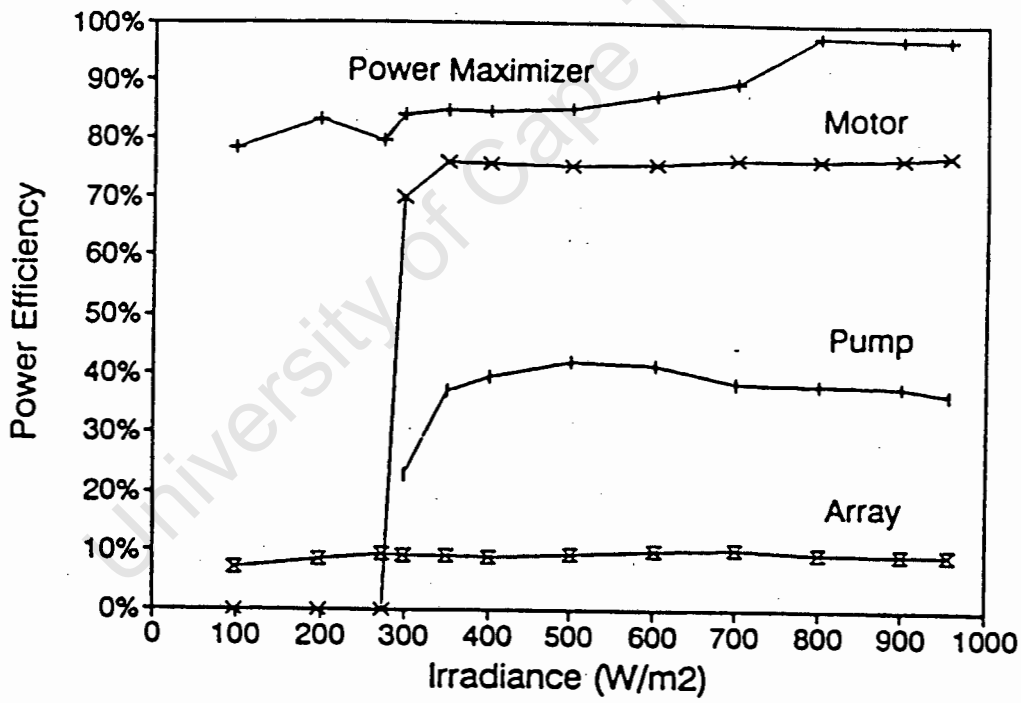

Figure 5: Performance Curves for Mono Water Pumping System[18]

2.2.2. The Solar Jack System

The Solar Jack system comprises a submersible pump with a DC-DC converter situated above ground. A

diaphragm pump is used which is driven by a permanent magnet brushed DC motor.

This pump is the smallest commercial PV pumping system available and it has been designed to operate efficiently at low flow rates and low heads. Only two PV modules (47 - 60 Wp) are required. Such a system has been tested by the ERI at UCT and the efficiency of the system is shown in the following figure.

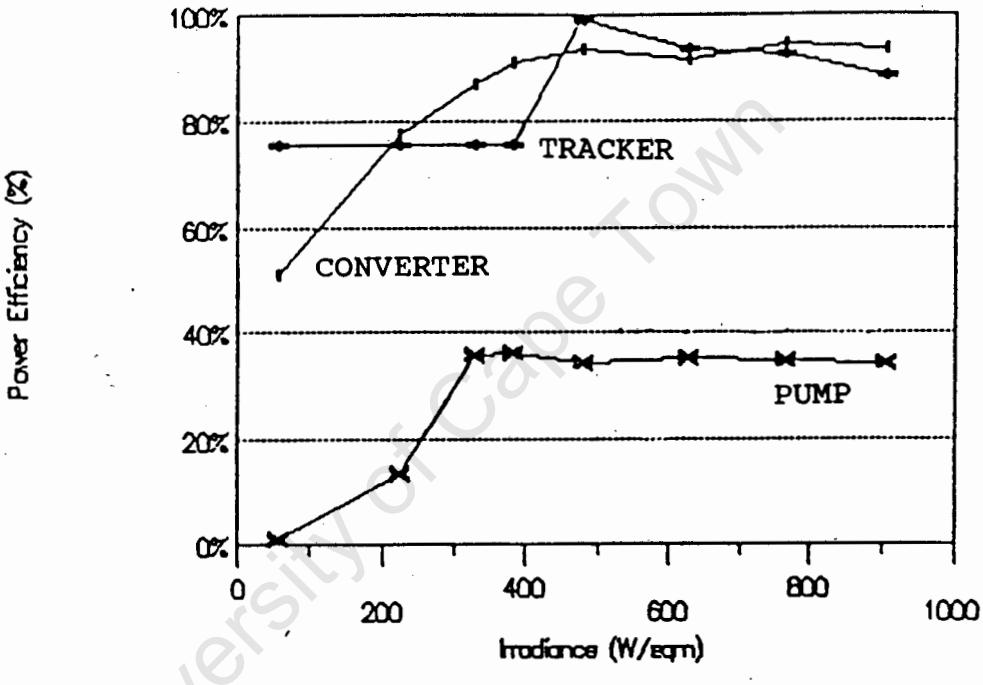

Figure 6: Efficiencies of Solar Jack System[19]

2.2.3. Other Systems in Southern Africa

Siemens and AEG provide submersible systems which are driven by an induction motor with constant voltage control. The motor is manufactured by Franklin and has been specially designed for a submersible pumping application. The efficiency of this motor is between 68% and 72%. The Siemens systems have a capacity greater than 1 kWp, but it would appear that none of these systems have yet been installed in South Africa[20].

The system of AEG operates in the power range of 1 to 3.8 kW at a head of between 10 and 80m. This system has an inverter efficiency of 95% at rated output[21]. The pump is a centrifugal pump manufactured by Grundfos and the characteristic curves are shown in Appendix 1.2.

Because solar water pumping is a developing field, new systems are fast appearing on the market. Some of these systems use a submersible pump driven by an AC motor. The Tescon system of National Lunar consists of a motor with a battery to provide sufficient starting torque. The motor runs until the battery dischages to a certain level and then the inverter is switched off and the battery is recharged. The continual cycling of the battery is not an optimal solution and these systems are not considered to be highly reliable.

2.3. MOST EFFECTIVE MOTOR AND PUMP COMBINATION

The main requirements of a solar pumping system are reliability, efficiency and cost. Reliability is an important factor because the system must be designed for rural areas which have little technical support and may not be easily accessible. Cost and efficiency are closely linked and because of the high cost of the solar panels, the motor/pump combination should be as efficient as possible to minimize the overall system cost.

2.3.1. Most Suitable Pumps for Solar Application

Pumps can be broadly classified into centrifugal and positive displacement types and these are described in detail by Fraenkel[22]. The centrifugal pumps are used by the larger systems of AEG and Siemens, while Mono Pumps and Solar Jack use positive displacement pumps.Centrifugal pumps have the disadvantage that they need to be run at constant speed in order to operate efficiently. Since solar powered systems have a variable input power, this type of pump is not optimal. As can be

seen from the Grundfos characteristic curves, no data is supplied for insolation levels below 4 kWh/day and this suggests that the performance of the pump is low in this region. Gosnell did comparative tests on centrifugal pumps and the graph below shows the efficiencies of the positive displacement and centrifugal pumps.

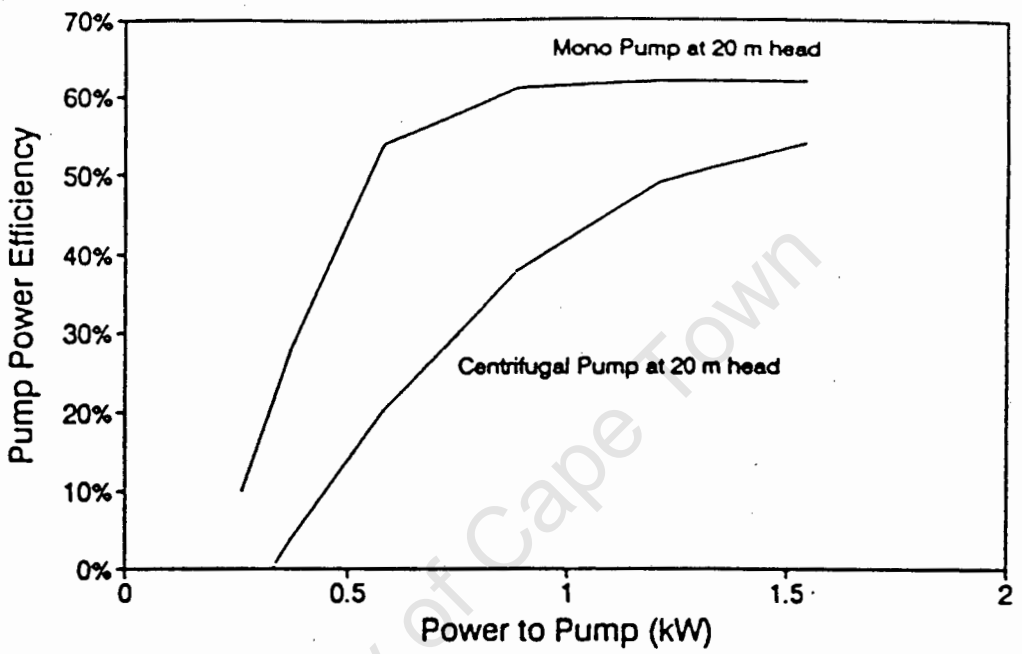

Figure 7: Comparison Between a Mono and a Centrifugal Pump at 20m Head[23]

Positive displacement pumps have the advantage that they are capable of operating efficiently over a wide speed range and this makes them highly suited to a solar application. This type of pump can be divided into the Helical screw type of Mono Pumps and the diaphragm type of the Solar Jack pump.

Because of the wear and tear on the diaphragm of the Solar Jack pump, this pump is not considered to be as reliable as the Helical screw pump. The disadvantages of the Mono pump is that it operates with a drive shaft and it requires a high starting torque. The problem of high

starting torque can be overcome by storing energy in a capacitor[24].

The efficiency of the Mono pump is between 45% to 55% for heads of 25 and 35m, and 26% to 53% for a 55m head[Pulfrey cited by Gosnell]. From Appendix 1.2, the efficiency of the Solar Jack varies from 27% at a head of 30m to 30% at a head of 60m (this is the efficiency of the motor/pump combination). The efficiency of the Mono motor and controller is around 66% [Mono Pumps, SA] and if this value is used, the Mono system efficiency is between 18% and 37%. It is therefore difficult to draw conclusions as to the most efficient system, but from a reliability point of view, the Mono positive displacement pump has significant advantages over the diaphragm pump.

2.3.2. Most Suitable Motor for Solar Application

Apart from the large systems of Siemens and AEG, the permanent magnet DC motor is the predominant motor used for solar water pumping. This type of motor has the advantage of being both efficient (76% - 82%) and simple to control.

The disadvantage of using a DC motor is that it has a high cost and it is not maintenance-free, as the brushes need periodic replacing. It is these factors that has led Kamper to investigate the feasibility of developing a permanent magnet brushless machine or, alternatively, a reluctance machine.

The reason that induction motors have not been considered for small and medium systems is that manufacturers have not optimized the efficiency of these motors. It is these motors that form the workhorse of industry and they are usually connected to the ESCOM grid where power is cheap and the capital cost of the machine rather than its efficiency has been optimized. Small induction motors are being produced with efficiencies of between 60% and 72% for sizes ranging from 0.25 to 1 kW.

Apart from the low efficiency of the induction motor, because of its reliability and low cost, this would be an ideal motor to use for solar water pumping. It was with this in mind that GEC has developed an induction motor designed specifically for a solar water application. The motor is rated at 0.75 kW and has an efficiency of 80%. This compares very favorably with the DC motor. In addition, DC motors cost around R2400, while the GEC motor costs only R675 (this price is likely to be reduced if more motors are required). This represents a significant cost saving with the system having the potential of obtaining a similar efficiency to that of a DC system.

It would appear that the diameter constraint of submersible induction motors does not have a significant adverse effect on the motor efficiency, as the Franklin induction motors have a similar efficiency to normal application motors. The Franklin motor is around 72% efficient.

The induction motor system requires an inverter to run off the solar panels, and the cost of this should be similar to that of a DC-DC converter as required by a DC system. The high efficiency of inverters, as reported by AEG indicates that an inverter has comparable performance capabilites to that of a DC - DC converter. It would therefore appear that despite the increased losses due to the power factor of the AC drive, the induction motor offers significant advantages over the DC motor in terms of cost and reliability, while similar efficiencies are expected.

The main components of the pumping system as used by this project are the solar panels, positive displacement pump, induction motor, three-phase inverter and microcontroller. The system is illustrated below and each of the components is discussed further.

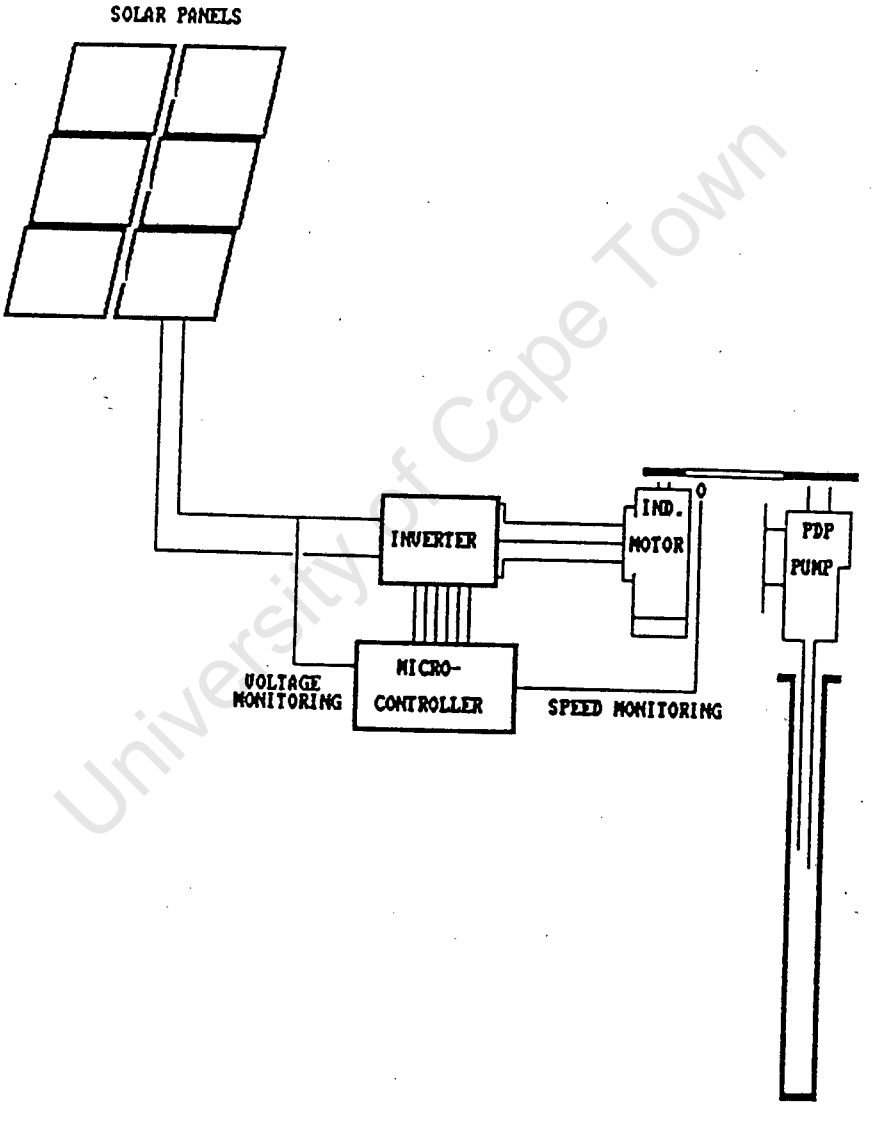

Figure 8: Induction Motor Driven Solar Pumping System

3.1. SOLAR PANELS USED FOR PROJECT

For experimental purposes, seven 53 W_p panels were obtained. The manufacturer characteristic curves of these panels are shown in the figure below and information on these panels is included in Appendix 1.3.

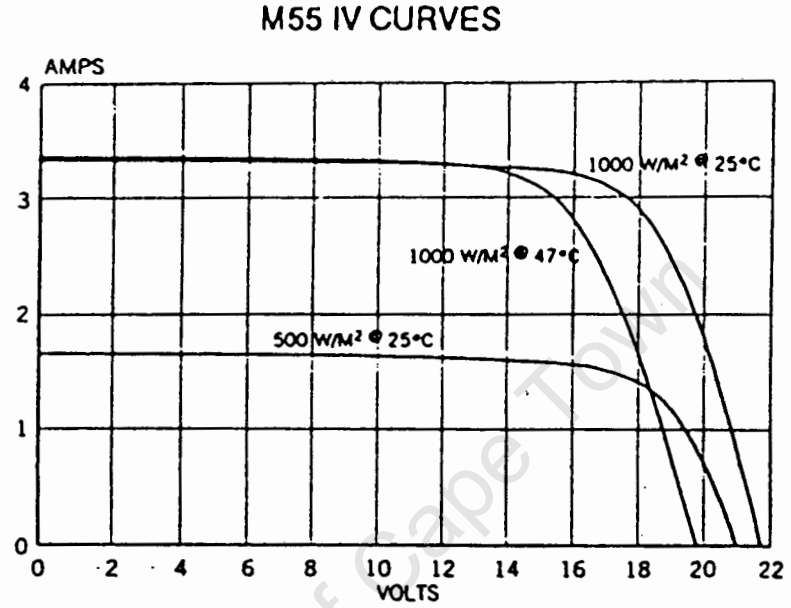

Figure 9: Panel Characteristics Supplied by Siemens

In order to maximize the power delivery, the panels were mounted on a single axis array tracker. This is a stand alone unit and has not been incorporated in the rest of the system electronics.

3.2. PUMP OPERATION AND CHARACTERISTICS

The positive displacement pump used for this project can be used with a wide range of heads and power requirements. The pumps have been designed especially for solar application, where the power rating is lower than that for normal windmill pumps. In order to achieve a lower operating and starting torque, the seal on the

solar pumps is less tight and this causes a reduction in the efficiency of the pump. The pump characteristic curves in Appendix 1.2 also include curves for a windmill pump, and it can be seen that because of the very high starting torque and operating power requirements these pumps are not suitable for a solar application.

The pumps operate with the use of a helical screw in a rubber seal and is shown below.

Figure 10: Mono Positive Displacement Rotor and Stator

For the purposes of this project a pump model SW4L was obtained and mounted in a closed circuit configuration so that the water was continually recycled. The head was simulated with a valve and measured with a pressure gauge. This does not exactly simulate a pumping system as the head is dependant on the pressure which in turn varies with the pump speed. Therefore, in order to simulate a particular head at different speeds, the valve needed continual adjustment.

3.3. INDUCTION MOTOR DESCRIPTION

The motor is a 4-pole machine rated at 0.75 kW and has been designed to operate at 110v at a frequency of 50Hz. The efficiency of the motor is 80% at full load. In order to predict the performance of the motor, it was mounted on bearings so that the torque could be measured. The motor was characterized at different voltages and supply frequencies and these curves are shown in Appendix 4.1.

From the characterization curves, it can be seen that at lower supply voltages the peak of the efficiency curve drops slightly. This is predominantly due to the increase in the proportion of power that is lost due to windage losses. For this reason a system which uses this motor would not be suitable for very low power applications.

3.4. INVERTER AND CONTROLLER DESCRIPTION

The inverter is a fully controlled bridge which converts the panel DC voltage to three-phase AC by means of pulse width modulation. Low impedance MOSFETs were used to minimize the inverter losses.

The microcontroller both monitors the speed of the pump to operate the panels close to the peak power point and supplies the PWM signals to switch the inverter MOSFETs. The microcontroller that was chosen for the project is the 8031 from Intel. The device has sufficient speed to generate high resolution PWM signals and it can easily interface with other devices. A brief description of the 8031 is included in Appendix 6.

CHAPTER 4: DESIGN OF SYSTEM COMPONENTS

4.1. INVERTER DESIGN

Low impedance power MOSFETs were used in the inverter design. MOSFETs can offer significant advantages over bipolar transistor designs because of their reduced drive power requirements and improved safe operating area[25]. Another advantage of using MOSFETs is their ease of paralleling for a higher output power. Thus the system can be easily modified to operate on a larger system.

4.1.1. Base Drive Circuit

The main requirements of the base drive circuit are to provide an isolated signal to the gate and to switch the capacitive load of the gate at an acceptable speed. A circuit diagram of the base drive is shown in Appendix 5.1.

4.1.1.1. Switching of the Gate

The rate of change of V_{DS} and I_D depend on the gate current, which determines how fast the device capacitances are charged and discharged. The MOSFET switching times can therefore be controlled by controlling the gate current supplied by the drive circuit. It is therefore advantageous for the base drive to have a high current pulse capability.

A totem pole configuration provides a faster turn-off time than an open collector and can be realized either by using discrete transistors or an IC. Use of an IC offers the advantage that the device is modular and the components can therefore be arranged closer to minimize stray inductance. Switching of the gate was achieved with the use of the DS0026 IC which is a high speed

totem-pole driver capable of supplying high current pulses.

4.1.1.2 Floating Power Supply

The load of the upper MOSFETs in the bridge configuration is connected to the source of these devices. For these MOSFETs to be driven into saturation it is necessary for the gate drive circuit to be referenced to the source and not the ground. This can be achieved by means of optically coupled isolators, pulse transformers or a DC to DC chopper with transformer isolation.

Pulse transformers can only transfer to the secondary the AC component of the input signal. Consequently, their output swings from negative to positive by an amount that changes with the duty cycle. Chopper circuits are expensive, complex and have a limited bandwidth. These two methods are therefore not suitable for a variable frequency drive system.

Since only a small amount of power is required for the base drive, it is possible to develop a supply to the gate from the drain voltage[26].

When the lower MOSFET is switched on, the source voltage of the upper MOSFET is close to zero and C_s charges and is used to supply the upper base drive. This circuit will only operate effectively at low frequencies or high duty cycles and this makes it ideal for application in PWM systems.

The PWM signal from the microcontroller is referenced to the source via an optocoupler. This also serves to protect the microcontroller from possible voltage surges caused by the power switching. It is for this reason that optocouplers were used on all six PWM signals.

4.1.2. Switching Aid Network

Switching aid circuits are used to protect the Mosfets by improving their switching trajectory. Three types of circuits exist, namely turn-off, turn-on and overvoltage snubbers.

Turn-on snubbers are used only to reduce the power dissipated by the switching device during turn-on. These snubbers have been designed for use in transistor circuits and they operate by reducing the voltage across the switch as the voltage builds up. Generally Mosfets do not require turn-on snubbers because of their large peak current handling capability[27].

Turn-off snubbers provide a means for reducing the losses during turn-off and an RCD snubber was used. Calculations for determining the component values of the snubber have been included in Appendix 5.1.

The main objective of the turn-off snubber is to reduce the rate of rise of the applied voltage. Its effect as a surge voltage limiter is small[28]. The presence of wiring inductance results in the generation of surge voltages which can be reduced by a protection network which behaves similarly to a zener diode. It was not necessary to implement such a snubber as the IRFP250 MOSFET has a built in zener diode to clamp such overvoltages. In order to limit voltage surges, the component layout was arranged in such a way as to provide for the shortest routes possible to minimize stray inductance.

4.2. MICROCONTROLLER DESIGN

The 8031 microcontroller from Intel proved to be well suited for the application of both generating the PWM signals and controlling the speed of the motor. The hardware structure of the device provides for easy external interfacing and it has sufficient speed to

provide both an acceptable PWM resolution and a fast response for the control function.

The dual functions of controlling the motor and generating the PWM were simplified because the device has two on-board timers and no external timing interrupts were required. One timer was used to output the PWM at the required frequency, while the other determined the sampling period for the controller.

A circuit using the 8031 with ROM, RAM and an ADC was designed and implemented. The complete circuit diagram and the PC board layout is shown in Appendix 5.2.

4.2.1. Allocation of Memory Space

The 8031 interfaces with program memory (ROM) and data memory (RAM) differently. To access Program Memory the PSEN line is used, while to access Data Memory the RD and WR lines are used. Program Memory consists of both program instructions and tables of constants. Data Memory comprises RAM and the multiplexed ADC. The allocation of memory space is shown below.

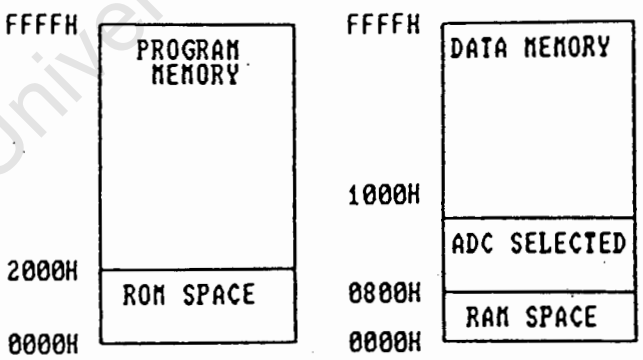

Figure 11: Allocation of Memory Space

4.2.2. Interfacing with ROM

The circuit was designed to interface with 8 kilobytes of ROM and is shown below.

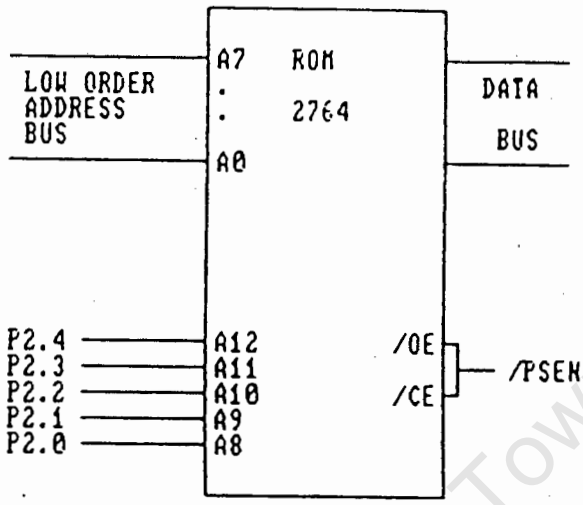

Figure 12: Interfacing with ROM

4.2.3. Interfacing with RAM

Although the 8031 has 128 bytes of RAM as part of its architecture, this was not sufficient and 2 kilobytes of external RAM were added to this.

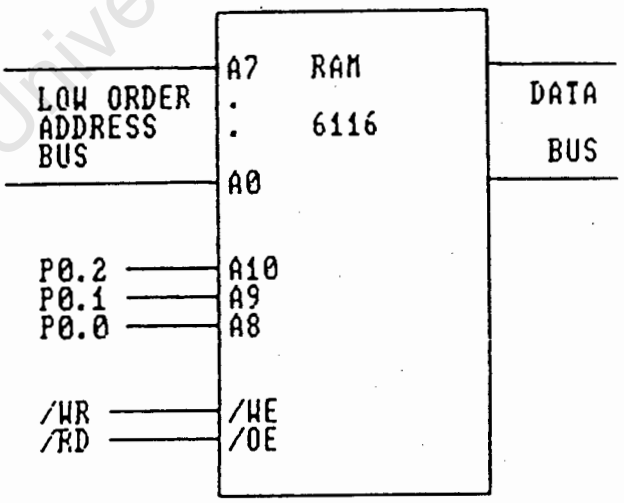

Figure 13: Interfacing with RAM

4.2.4. Interfacing With the ADC

The ADC is used to monitor any external variables that are required for the control process. For this purpose, the ADC0809 converter made by National Semiconductors was ideal as it is an 8-bit converter which multiplexes 8 channels. The maximum clock frequency of the ADC is 1280 kHz and this is obtained from the output clock of the 8031. The ADC was clocked at 625 kHz by dividing the output clock frequency of the 8031 with the use of D-type flip-flops.

The device receives the address of the signal to be multiplexed on the system data bus and interfacing with the device is shown below.

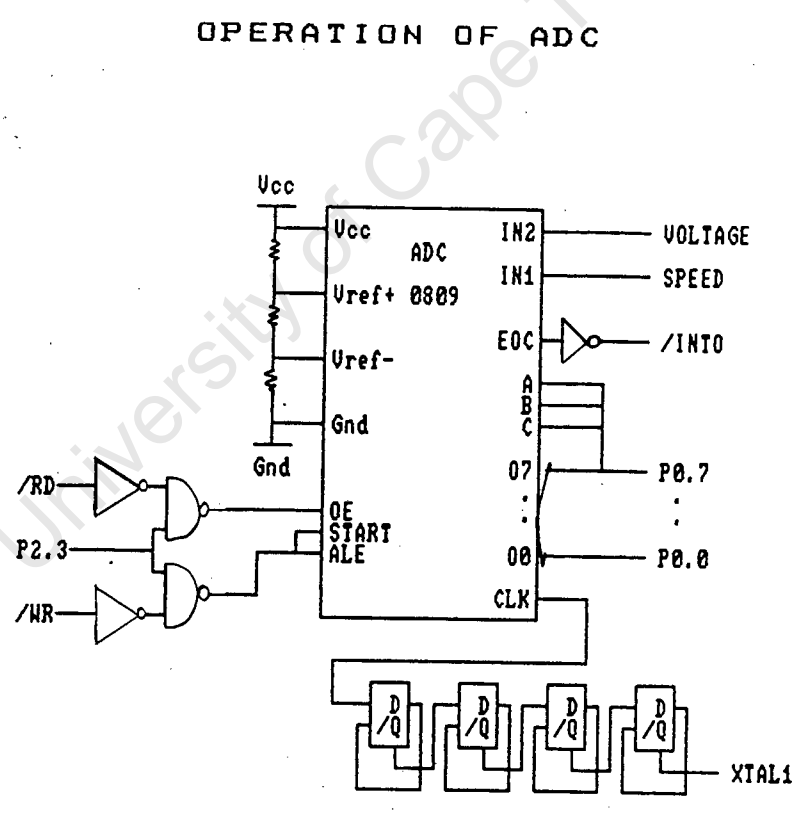

Figure 14: Interfacing with the ADC

The 8031 reads data from and writes data to the ADC as if it were accessing RAM. To read in a value from a particular channel, the following procedure is followed:

- The 8031 places the address of the required channel on the data bus and writes it to the ADC.

- Combinational logic is provided such that when bit 3 of Port 2 goes high (ie the ADC is addressed) and the /WR line of the 8031 goes low, the address to the ADC is latched and the conversion is started.

- Once the conversion has been started, the 8031 waits until the EOC line of the ADC goes high.

- After the EOC line has gone high, data can be read in from the ADC. To achieve this, the ADC is addressed (bit 3 of Port 2 goes high) in a read instruction. Combinational logic is provided such that when the /RD line goes low and bit 3 of Port 2 goes high, the output of the ADC is enabled. The converted signal is then read in via the data bus to the 8031.

4.2.5. Watchdog Circuit

In order to ensure that the microcontroller resets properly, a watchdog circuit was designed which resets the 8031 when a pulse at its input is discontinued. Such a pulse could be received either from the output of one of the PWM signals from the 8031 or from a pulse in the speed measuring circuit. Receiving the pulse from the speed measuring circuit is a more robust form of control and works on the principle that if the motor stalls the controller is reset.

The watchdog was implemented using a 555 timer IC and the circuit diagram is shown with the controller circuit in Appendix 5.2.

4.3. SPEED MONITORING CIRCUIT

The speed was monitored by an optical sensor mounted on the motor and the circuit diagram is shown in Appendix 5.2. The pulses received from the sensor were converted to an analogue signal by means of an LM331 configured as a frequency to voltage converter. The signal was then filtered and used as an input to the ADC. The circuit has been designed to monitor the speed in the range from 150 to 2500 Rpm.

The op-amp used to filter the signal from the LM331 is the CA7140, which is capable of delivering an output signal very close to ground and this eliminates the need for a negative rail.

4.4. DC-DC CONVERTER DESIGN

The combined current requirement of the microcontroller and inverter amounts to 200mA. This supply can be obtained either by tapping off from two panels or by using the full panel voltage. Tapping off from two panels is not a desirable solution as this has a similar effect as selective shading of the array. This method will adversely affect the performance of all the panels as they are connected in series. Another disadvantage of tapping off two panels is that the voltage of these two will collapse before the others in the event of a disturbance to the panels and this could cause problems with the controller power supply.

It is therefore necessary to use the full array voltage in providing the power supply for the control circuitry. A current of 200mA from an 85v supply represents a loss of 17W where only 3W are being used effectively. Clearly therefore, it would be advantageous if a DC-DC converter were to be used in supplying this power.

Low power DC-DC converters are commercially available and have an efficiency of around 50%. The specifications

for converters available from a local supplier are included in Appendix 1.1. After some investigation it was found that commercially available converters do not have an input voltage rating capable of running off a multi-panel solar array. For this reason it was necessary to design a DC-DC converter capable of running off a 150v supply to cater for worst case open-circuit conditions.

The TL494 switchmode PWM control circuit by Motorola was used in implementing a DC-DC converter. The TL494 is a fixed frequency control circuit which has been designed for switchmode power supply control. The device operates at a maximum supply voltage of 40v and therefore a separate supply was necessary for the IC. A supply current of 10mA was required and this was obtained via a Darlington and zener diode configuration. The circuit diagram for the converter is shown in Appendix 5.3.

The efficiency of the converter was found to be 55% and this compares favourably with commercially available converters. The efficiency is low because the power to the TL494 is obtained from the high array voltage. By using the DC-DC converter, a power reduction of 11.5W was achieved and hence only 5.45W were lost to the control circuitry.

4.5. ARRAY TRACKING DESIGN

A single axis array tracker was designed to maximize the panel delivery. It is estimated that the tracker will cost around R400 and an estimated 20% to the panel output could be achieved[29]. Since panels cost around R1000 each, the use of an array tracker would improve the panel delivery without increasing the cost of the system proportional to the saving.

With the help of J.Roeber, University of Cape Town, a tracking system was realized by using two photocells on

either side of a pointer which was mounted perpendicularly to the panels. The system works on the principle that when either of the photocells is obstructed from the sun, a high torque DC motor is used to turn the array until the intensity level of the two cells is the same. Logic is provided to reset the panels at the end of each day and to charge the battery from which the motor obtains its power. The circuit diagram of the array tracker is shown in Appendix 5.4.

CHAPTER 5: SOFTWARE STRUCTURE AND GENERATION OF PWM

It is widely recognized that PWM inverters offer a number of advantages over other converter techniques. These advantages are usually gained at the expense of more complex control configurations, but with the use of a microprocessor the task is made simpler.

This chapter discusses the different types of PWM strategies employed and the software implementation of the PWM is then described.

5.1. CHOICE OF PWM STRATEGY

Present-day available schemes can be broadly classified as carrier-modulated sine PWM and pre-calculated programmed PWM schemes. These two methods are briefly discussed and the most suitable method is then chosen to be implemented by the software.

5.1.1. Carrier Modulated Sine PWM

Carrier modulated sine PWM can be divided into natural and regular sampling. Natural sampling has been most widely used because of its ease of implementation using analogue techniques. This mode of sampling is obtained by comparing a triangular carrier wave signal directly with a sinusoidal modulating wave to determine the switching instants, and therefore the resulting pulse widths. This method is illustrated in figure 15.

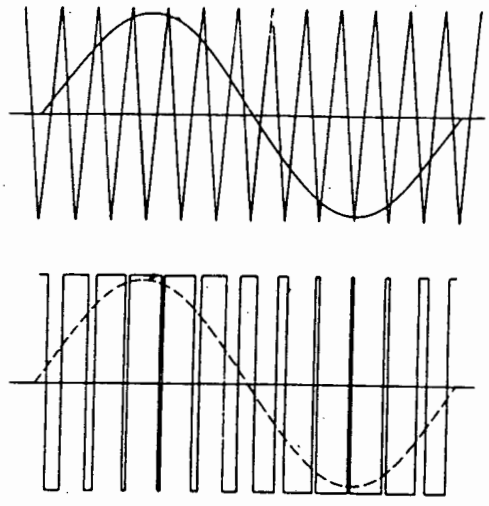

Figure 15: Implementation of Natural Sampled PWM

Regular sampled PWM has been designed for implementation for digital or microprocessor techniques. In this mode of control, the amplitude of the modulating signal is stored by a sample-and-hold circuit and is maintained at a constant level during the intersample period until the next sample is taken. This method is illustrated in figure 16.

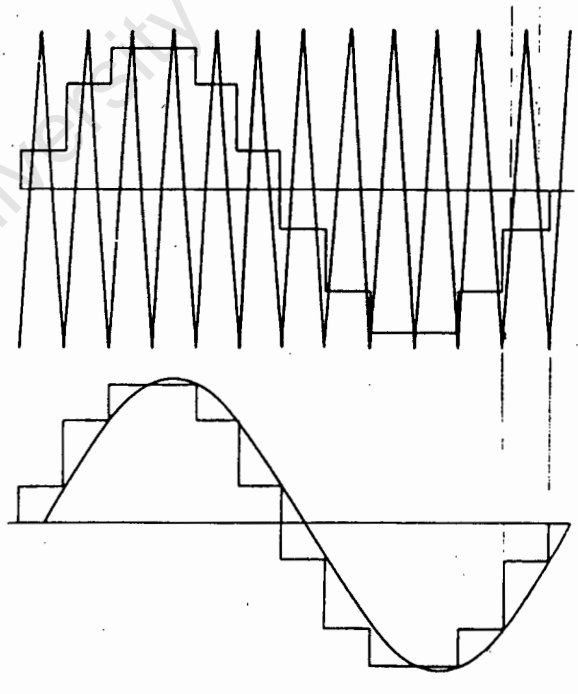

Figure 16: Implementation of Regular Sampled PWM[31]

5.1.2. Programmed PWM Techniques

Programmed PWM techniques optimize a particular objective function such as to obtain minimum losses and reduced torque pulsations by selective minimization of harmonics. These methods are considered to be the most effective means of obtaining high performance results. Programmed PWM's exhibit several distinct advantages in comparison to the conventional carrier-modulated sine PWM schemes and these are listed below:

1) With programmed techniques, a reduction of about 50% in switching frequency is achieved and this represents a reduction in the switching losses of the inverter.
2) Higher voltage gain due to overmodulation is possible with programmed techniques.
3) Because of the low current ripple obtained with programmed techniques, a smaller DC link filter can be used.
4) Programmed elimination of low-order harmonics causes no harmonic interference with line filtering networks typically employed in inverter power supplies

The disadvantage of using programmed techniques is that each technique is associated the difficult task of computing specific PWM switching instants to optimize a particular objective function. This difficulty is especially encountered at a lower output frequency range due to the necessity of a large number of switching instants[32]. Zuckerberger[33] describes an 8085 micro-computer controlled three-phase inverter which operates in the 1-45 Hz interval with the 5th, 7th and 11th harmonics eliminated. Tables have been provided which include elimination up to and including the 13th harmonic.

Since the inverter is required to operate efficiently even at low frequencies, it was decided to use tables for the generation of the PWM signals. This ensures flexibility in implementing either sinusoidal or

harmonic elimination PWM. At higher frequencies, the harmonic elimination PWM would enable the inverter to operate efficiently because the switching frequency could be minimized. At lower frequencies, sinusoidal modulation could yield a better performance because a reduction in the higher order harmonics could be achieved.

By using the programmed tables in Appendix 7.3, elimination of the 5th, 7th, 11th and 13th harmonics was obtained. Tables for sinusoidal modulation were generated by a True Basic program which is also included in Appendix 7.3.

5.2. MICROCONTROLLER SOFTWARE STRUCTURE

The software structure of the controller operates with the use of the two on-board 8031 timers. A brief description of the operation of the 8031 has been included in Appendix 6. Timer 1 is used to determine at which voltage and frequency to operate (controller function) and to provide a sequence of bytes in RAM for timer 0 to access. The sequence in RAM comprises the six signals to control the six MOSFETs. For frequencies ranging from 0-40Hz a full cycle consists of 256 bytes, while for the frequency range of 40 - 80Hz, 256 bytes represents two full cycles. High frequency is obtained at the expense of resolution, but this only occurs at a high modulation index where good resolution is not required.

Timer 0 is responsible for accessing the table that has been set up in RAM and sequentially writing these values to the output port at the required speed. The basic structure of the software is illustrated below.

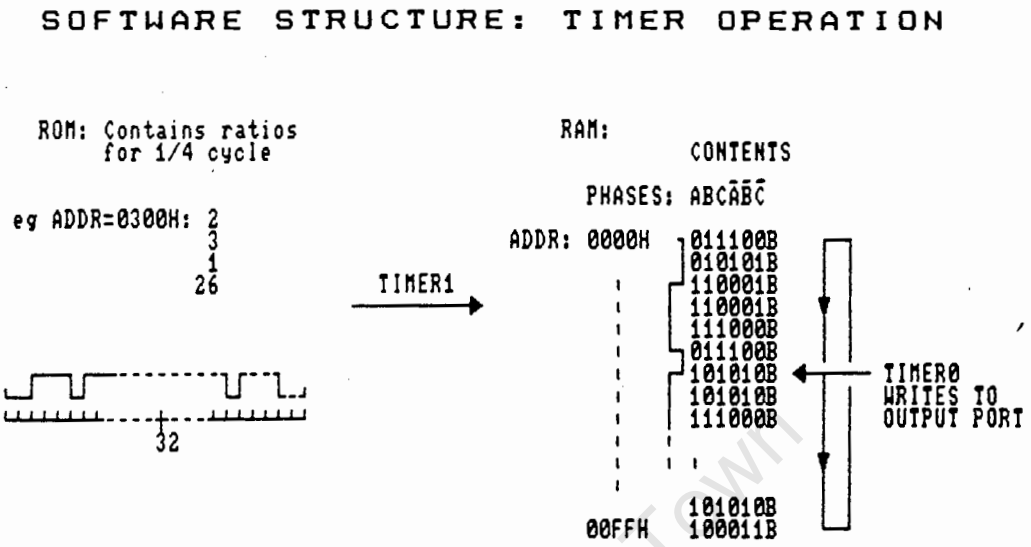

Figure 17: Software Structure for Microcontroller

It is necessary that timer 0 has the highest priority as its speed must be fixed in order to obtain a uniform output. The 8031 architecture provides for two priority levels, but a third level can be simulated with software . The controller function is responsible for reading in any external variables and this occurs while timer 1 is being serviced. Since reading an external variable involves receiving an external interrupt, it is necessary to create a third priority level. The external interrupt therefore has the second priority and timer 1 has the third priority. The third priority level is established in the service routine INTRPT which is shown in Appendix 7.1.

5.3. GENERATION OF PWM

Software operation to generate the required PWM has been described by means of flow diagrams and the program software is included in Appendix 7.1.

5.3.1. Operation of Timer 1 Service Routine

The operation of timer 1, which is responsible for generating the PWM is illustrated below.

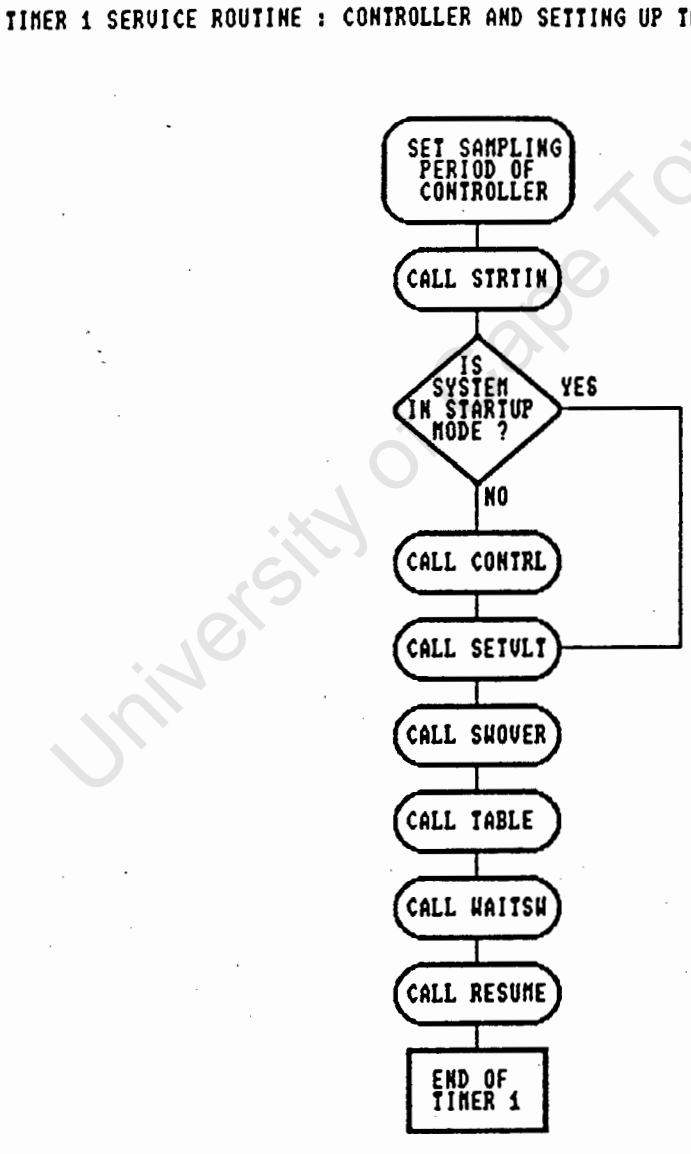

Figure 18: Timer 1 Service Routine

The routine operates by determining the new output frequency from the either the control or startup subroutines. These routines load register R7 with a number which provides the address of the new frequency and corresponding voltage. The frequency constitutes two bytes which are loaded into the 16-bit timer speed setting of timer 0, while the voltage setting contains the start address of the voltage table to be accessed. The subroutine SETVLT loads DPTR with the start address of the voltage table and the subroutine RESUME switches timer 0 to the new speed of operation. TABLE is used to convert the voltage table into the three-phase sequence in RAM.

Because timer 1 has two modes of operation for high and low frequencies (above and below 40 Hz), it is necessary to ensure a smooth transition from one mode to another. Such a transition is detected by the subroutine SWOVER and when it occurs the flag SWITCH is set. When a new voltage table is being implemented, a sequence is written to RAM over the existing sequence. This occurs while timer 0 is continually accessing the sequence. When the new frequency is in the same mode as the old frequency this is acceptable as the voltage simply changes slightly. However, when the frequency changes modes a phase shift could occur that could damage the inverter. This phase shift arises due to the fact that a different number of bytes is required to represent a full cycle for the two modes and such an occurrence is illustrated in the following figure.

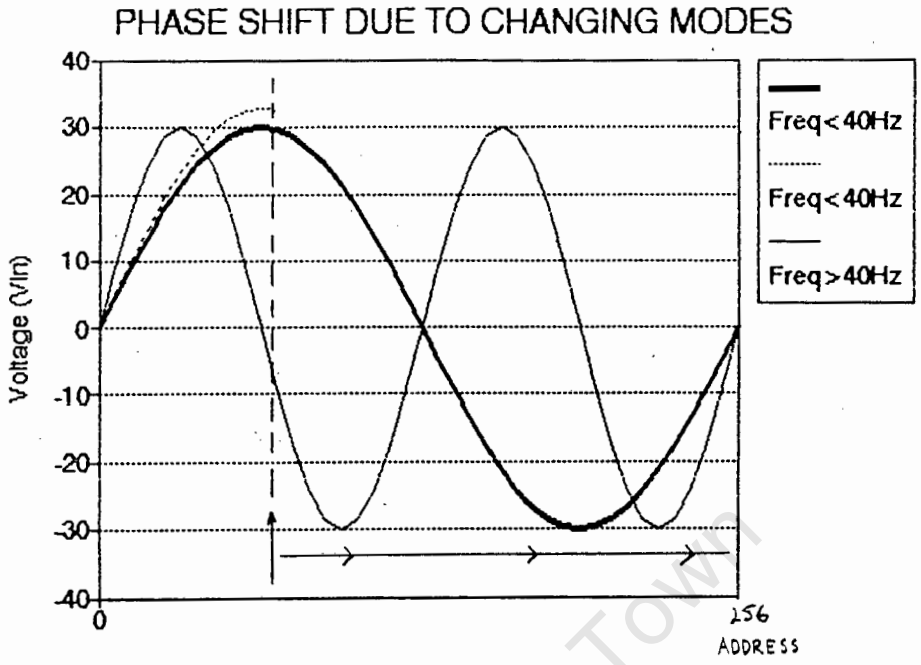

Figure 19: Phase Shift due to Changing Modes

In order to prevent such a phase shift occurring, it is necessary when changing modes to create a new table instead of overwriting the existing table. When the two tables are in phase, synchronous switching can occur and a smooth transition is ensured. The subroutine WAITSW sets the bit READY when timer 0 passes through the start of the table. This indicates to timer 0 that it must now access the second table in RAM. Immediately after READY is set, the speed of timer 0 is adjusted in the subroutine RESUME.

5.3.2. Creating a Three-Phase Table in RAM

The subroutine TABLE converts the PWM ratios stored in ROM into the three-phase sequence in RAM. This is done in three stages and are as follows:

1) The PWM ratios of the relevant voltage table are transferred to internal RAM (subroutine READBL). There can be between 1 and 32 ratios to represent a quarter cycle and the end of the table is indicated by the

number FFH. The sum of these ratios must equal 64 or 32, depending on the mode of operation.

2) A single-phase sequence is generated in external RAM (subroutine SNGSEQ). The start address of this table is 0200H and it requires 256 bytes. If operation is in the high frequency mode, these 256 bytes represent two cycles.

3) By providing the single-phase table with the necessary offset, a three-phase table is generated (subroutine THRSEQ). The start address of this table is 0000H at frequencies below 40Hz and 0100H for frequencies above 40Hz. In each case this table also requires 256 bytes.

The above subroutines have been illustrated with the use of the following flow diagrams:

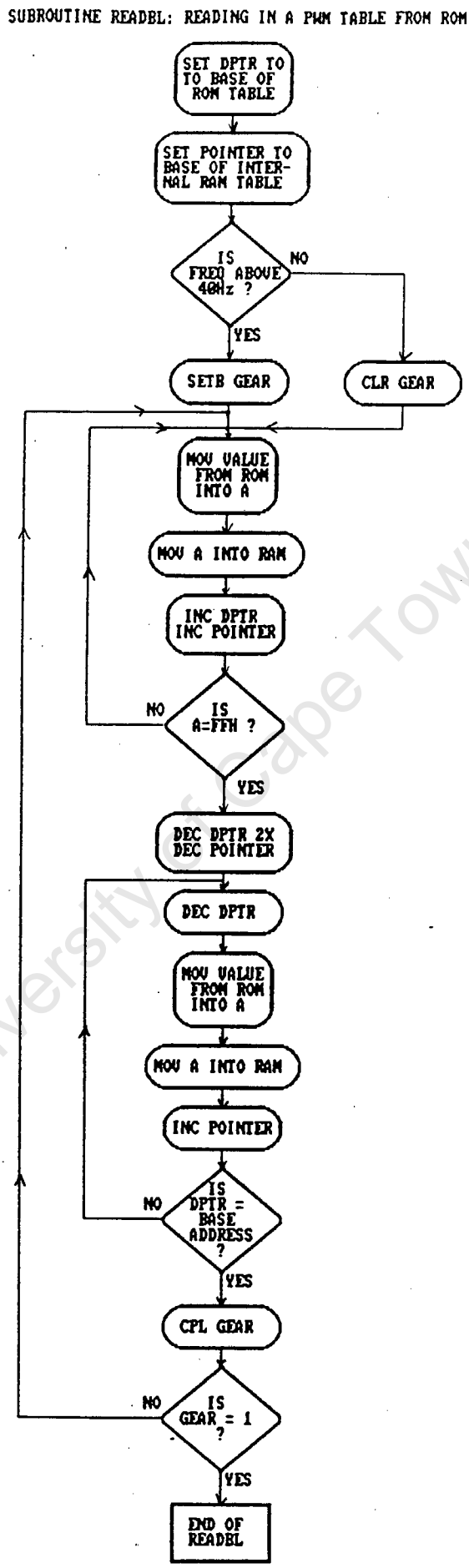

Figure 20: Reading in Voltage Table from ROM

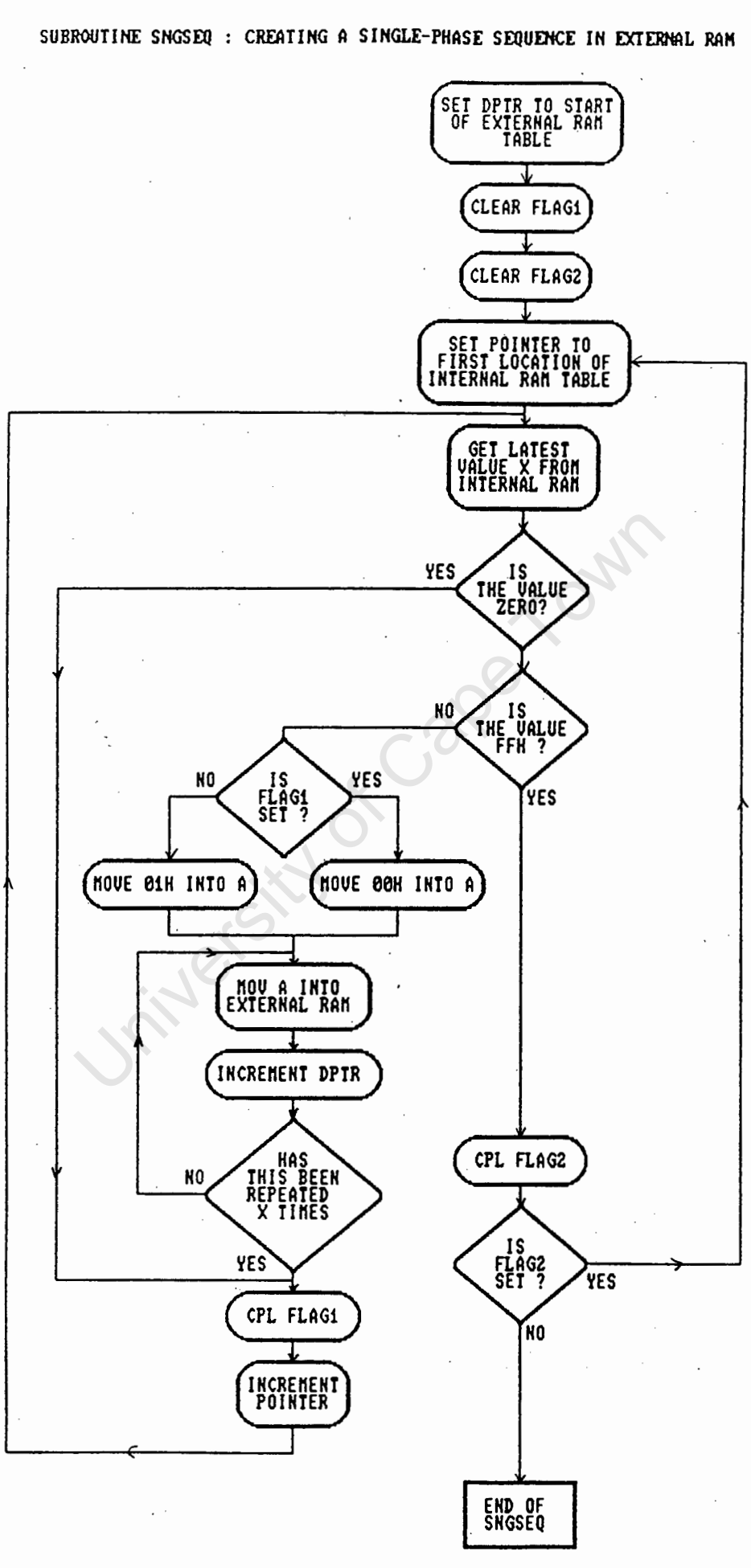

Figure 21: Generating Single-Phase Sequence in RAM

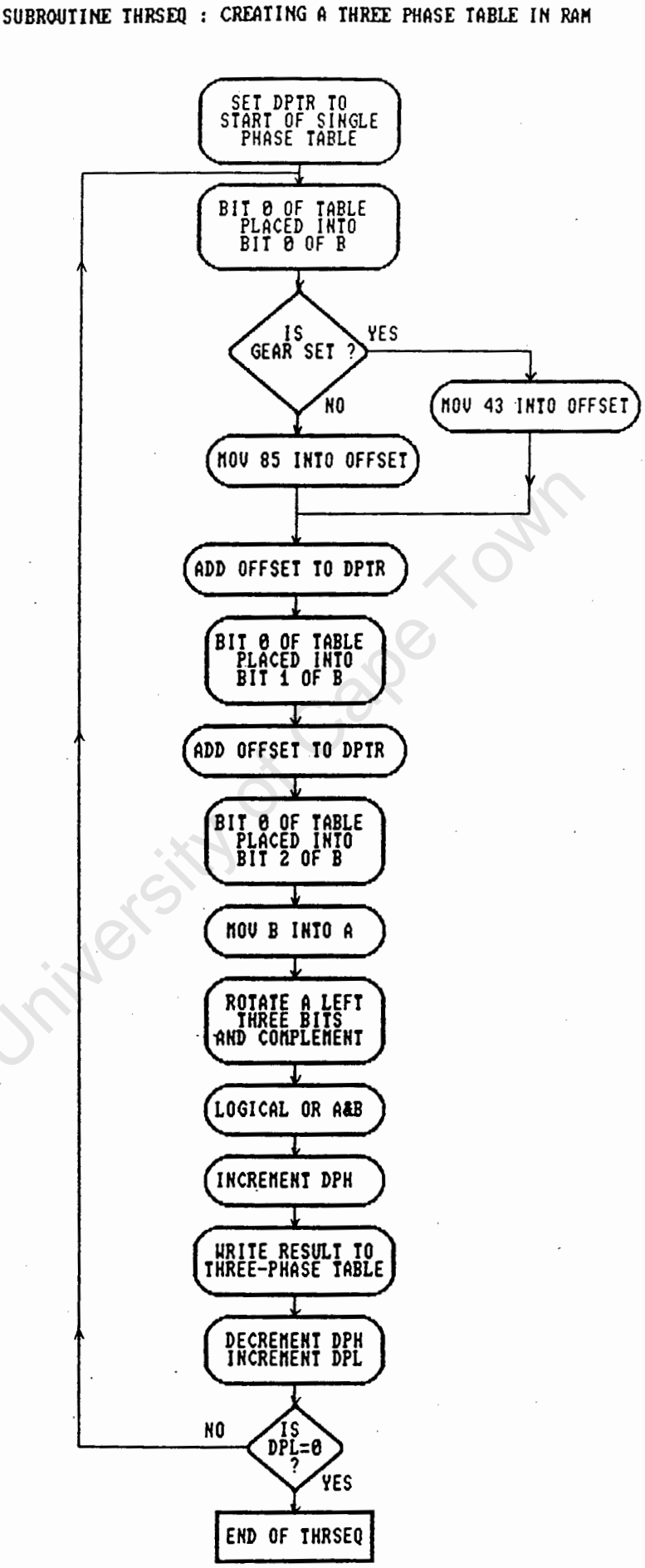

Figure 22: Generating Three-Phase Sequence in RAM

5.3.3. Operation of Timer 0 Service Routine

Timer 0 accesses the required three-phase sequence in RAM and writes it to the output port. If the bit SWITCH is set and the pointer is at the start of the sequence, the address of the sequence to be accessed is alternated. Another function of this service routine is to provide an overlap for the MOSFETs if a transition in one of the phases occurs. The operation of timer 0 is illustrated in the flow diagram below.

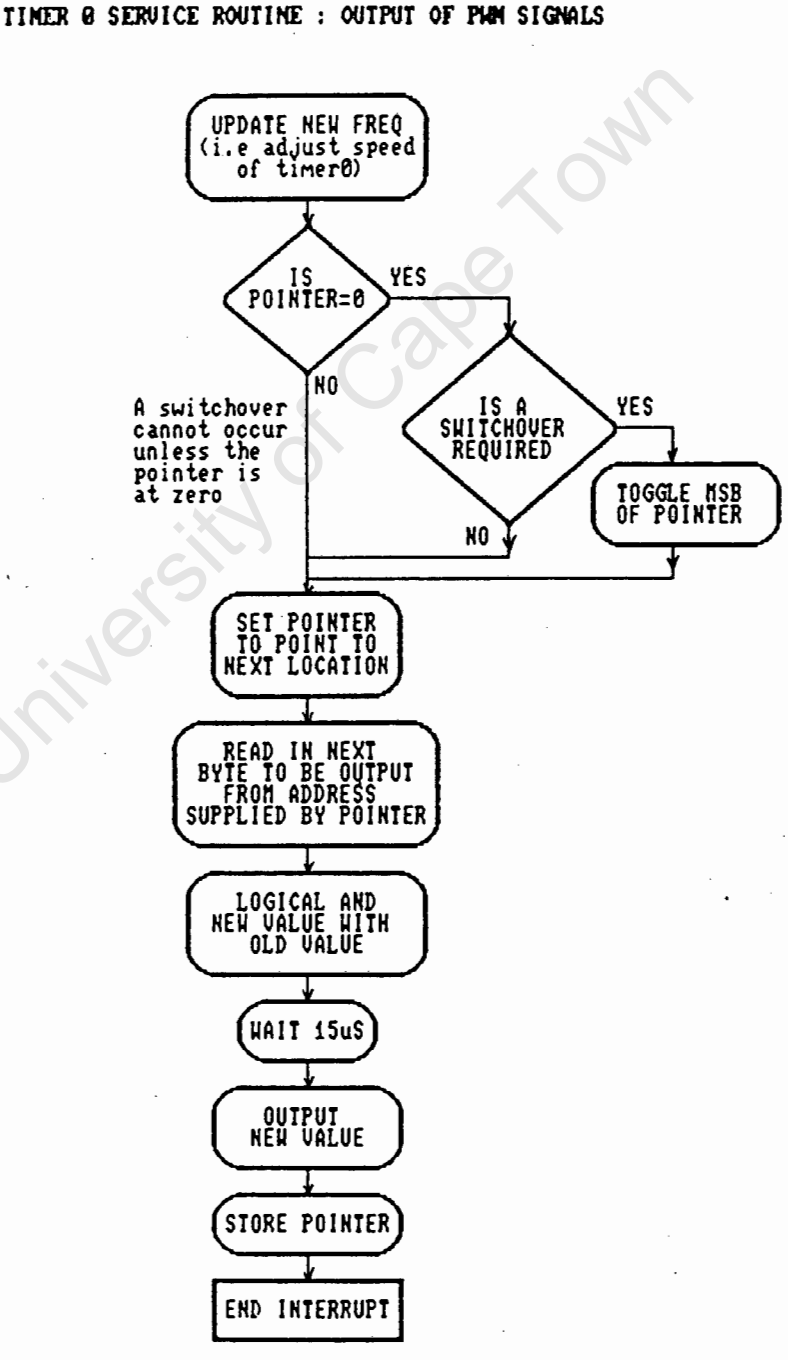

Figure 23: Operation of Timer 0 Service Routine

5.3.4. Software Optimization of Starting Torque

The high starting torque of the pump was overcome by using the energy from the DC-link capacitors. The software routine to do this is illustrated below.

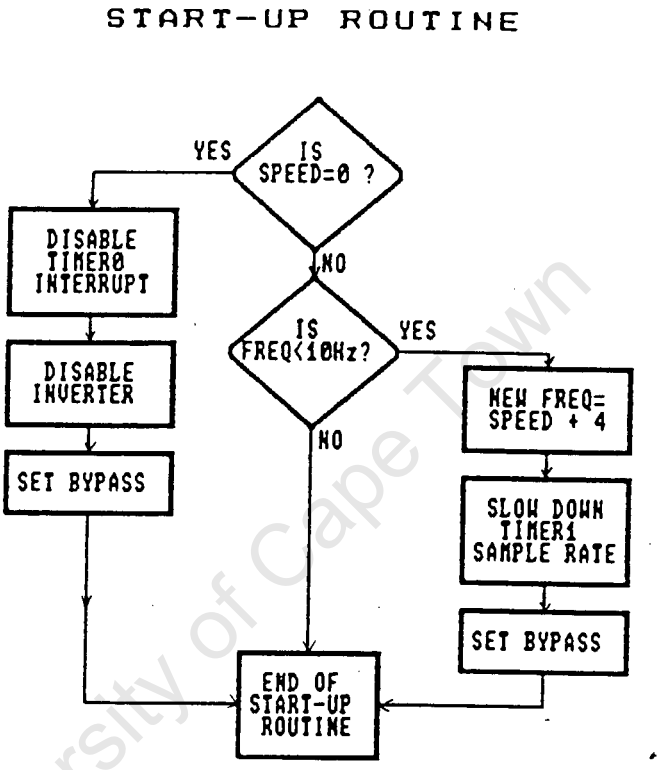

Figure 24: Routine to Overcome Starting Torque

When the controller senses that the motor is not turning, the inverter is switched off to allow the capacitors to charge up. After a set time, the watchdog circuit reboots the controller and a large current pulse is obtained to start the motor. By experimentation at different frequencies, a pump torque of 1 Nm could be sustained with a DC current of 0.74A. Hence, from the panel characteristic curves, the pump will be able to start at an irrandiance level of around 175 W/m².

CHAPTER 6: MOTOR EFFICIENCY ANALYSIS

In order to optimize the performance of the motor, it is necessary to operate at maximum efficiency over the full frequency range. The machine must be run efficiently even at low frequencies so that the motor speed and hence water delivery can be maximized at all irradiance levels.

In most applications of variable speed drives, a linear voltage versus frequency curve is followed. This ensures a constant airgap flux which prevents saturation and avoids damage to the motor. The motor is usually used at its full capacity and hence the voltage frequency curve passes through the point at rated voltage and frequency.

The limitation of implementing such a curve is that below rated frequency the efficiency is not maximized. This is mainly due to the fact that the motor is being run close to saturation and if the supply voltage were to be increased above the constant flux line, any theoretical improvements to the efficiency would be offset by losses due to saturation. However, if the motor is oversized, considerable flexibility can be achieved by implementing a voltage frequency curve that ensures maximal efficiency over a wide frequency range. This is due to the fact that at rated frequency the supply voltage is less than rated voltage and hence the motor does not operate close to saturation.

6.1. DERIVATION OF MAXIMUM EFFICIENCY CURVE

In deriving the maximum efficiency curve, it is assumed that the slip is small and hence approximations have been made to the equivalent circuit. The circuit used in the derivation is shown in figure 1. Although this circuit would be unacceptable in predicting the

motor performance accurately, it is only being used to predict the voltage at which maximum efficiency occurs.

APPROXIMATE EQUIVALENT CIRCUIT

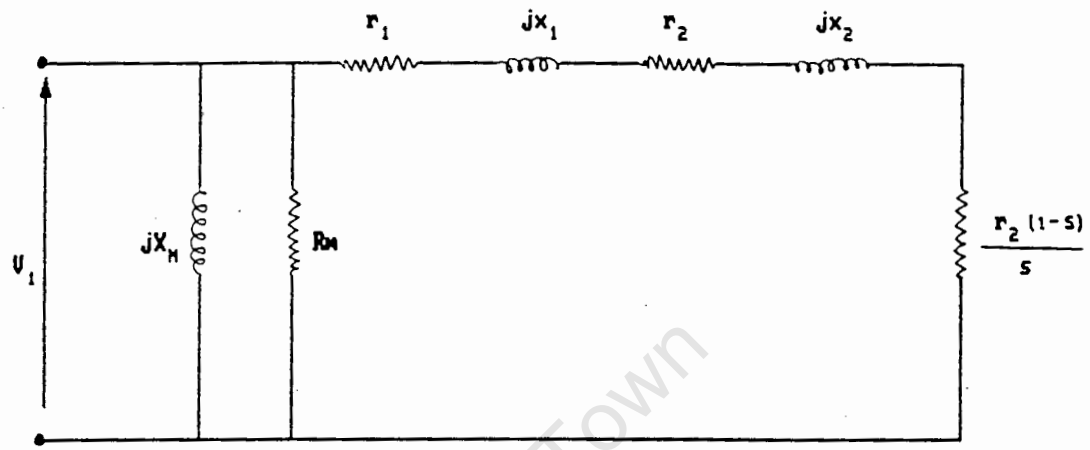

Figure 25: Approximate Equivalent Circuit for Best Efficiency Derivation

From the above circuit, the following equations are given[34]:

$$I2_{mod} = \frac{sV}{[r_2^2 + s^2(x_1+x_2)^2]^{1/2}} \quad \text{----- [1]}$$

$$T = \frac{3V^2 r2}{1/2.sw_s \times [x_1+x_2)^2 + (r_1+r_2/s)^2]} \quad \text{----- [2]}$$

Since the slip is assumed to be small, the secondary current can be simplified to:

$$I2_{mod} = \frac{sV}{r_2} \quad \text{----- [3]}$$

and hence

$$T = \frac{6V^2 s}{w_s r_2} \qquad \text{----- [4]}$$

Before Eqn's 3 and 4 can be implemented, it is necessary to verify the above assumption for a small motor. Parameters obtained from a test motor[35] rated at 200v and 0.75 kW were used to compare current values according to Eqn's 1 and 3.

At rated frequency(50Hz), the parameters were given as $r_1 = 2.89$; $x_1 = 1.91$; $r_2 = 2.14$; $x_2 = 2.325$; $r_m = 135.5$; $x_m = 48.147$. At rated voltage and for a slip of 0.05, Eqn 1 gives the current as $I2_{mod} = 2.685A$, while Eqn 3 gives the current as $I2_{mod} = 2.698A$.

The parameters were also given at half rated frequency and these were: $r_1 = 2.89$; $x_1 = 0.955$; $r_2 = 2.14$; $x_2 = 1.1625$; $r_m = 106.957$; $x_m = 22.305$. In this case, at half rated voltage, Eqn 1 gives $I2_{mod} = 1.347A$, while Eqn 3 gives $I2_{mod} = 1.349A$. Clearly, therefore, the above approximation for the secondary current is valid for small values of slip over a wide frequency range. Eqn's 3 and 4 can now be used to determine the efficiency of the motor.

Efficiency is given by:

$$E = \frac{P_{out}}{P_{out} + P_{lost}}$$

$$= \frac{R_m r_2 s - R_m r_2 s^2}{R_m r_1 s^2 + R_m r_2 s + r_2^2} \qquad \text{----- [5]}$$

By differentiating the efficiency with respect to slip, a local maximum is obtained:

$$\frac{dE}{ds} = \frac{r_2 R_m[(1-2s)(R_m r_1 s^2 + R_m r_2 s + r_2^2) - s(1-s)(2R_m r_1 s + R_m r_2)]}{(R_m s^2 r_1 + R_m r_2 s + r_2^2)^2}$$

$$= 0$$

Hence $$R_m(r_1 + r_2)s^2 + 2r_2^2 s - r_2^2 = 0$$

and $$s = \frac{-r_2^2 + r_2[r_2^2 + R_m(r_1 + r_2)]^{\frac{1}{2}}}{R_m(r_1 + r_2)} \quad \text{----- [6]}$$

Substitution of eqn. 6 into eqn. 4 gives the optimum efficiency curve for voltage as a function of frequency:

$$V = \sqrt{w_s} \left[\frac{T/6}{\frac{-r_2 + [r_2^2 + R_m(r_1 + r_2)]^{\frac{1}{2}}}{R_m(r_1 + r_2)}} \right]^{\frac{1}{2}}$$

As can be seen from the above equation, the supply voltage is proportional to the square root of the operating frequency. It should be noted, however, that the circuit parameters are frequency dependent and hence it is necessary to estimate the effect of frequency on the equivalent circuit before the above relationship can be evaluated.

6.2. DERIVATION OF EQUIVALENT CIRCUIT PARAMETERS

In order to predict the performance of the motor, the equivalent circuit was found for both fundamental and harmonic frequencies.

6.2.1. Calculation of Fundamental Circuit Parameters

The motor performance was evaluated with the use of the equivalent circuit shown below. A method which uses the blocked rotor and no-load tests at rated and half-

rated frequency has been used to evaluate the variation in parameters with the fundamental frequency[36].

The no-load tests were conducted at both rated voltage and at a voltage which was close to the expected operating voltage for the system. Because of magnetic saturation, the two tests yielded slightly different results and it was therefore decided to use the lower voltage. Similarly the blocked rotor tests were done at a current similar to that expected during normal operation and not at the rated current of the motor. The blocked rotor and no-load tests have been included in Appendix 4.3.

FUNDAMENTAL FREQUENCY EQUIVALENT CIRCUIT

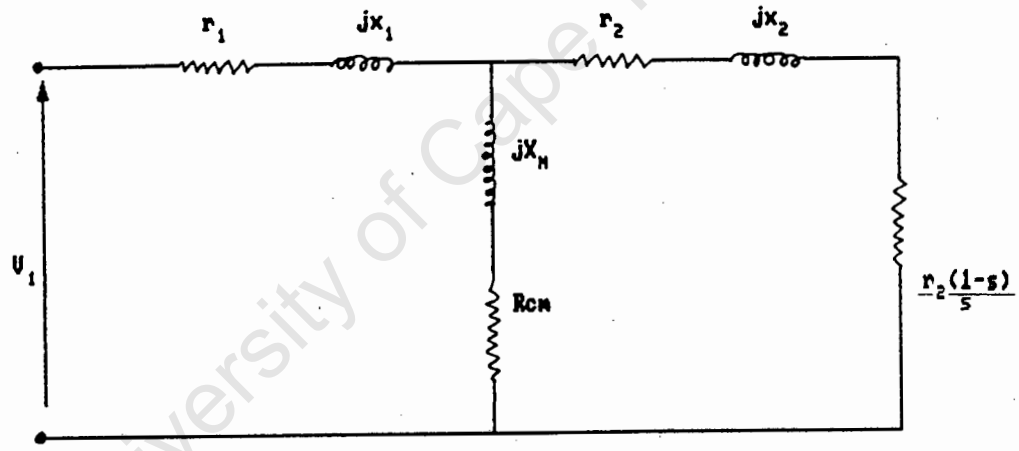

Figure 26: Equivalent Circuit to Predict Motor Performance

6.2.1.1. Calculation of r_1, r_2, l_1 and l_2

For a conductor of circular cross section with its diameter d < 2mm, the skin effect is negligible and r_1 is constant[37]. The values of the secondary circuit parameters change considerably due to skin effect[38] and l_2 and r_2 are obtained by extrapolation as shown in

Figure 27. These values were found by using the blocked rotor tests and are shown below. Since the tests have not been done for double-cage or deep-bar rotors, it was not necessary to conduct the tests at slip frequency.

r_1 = 0.737; --- Temperature corrected DC resistance

l_1 = 3.251 mH; --- Found by assuming that at rated frequency $l_1 = l_2$

r_{2n} = 0.500; l_{2n} = 3.521 mH; -- rated frequency

r_{2n}'= 0.363; l_{2n}'= 3.925 mH; -- 1/2 rated frequency

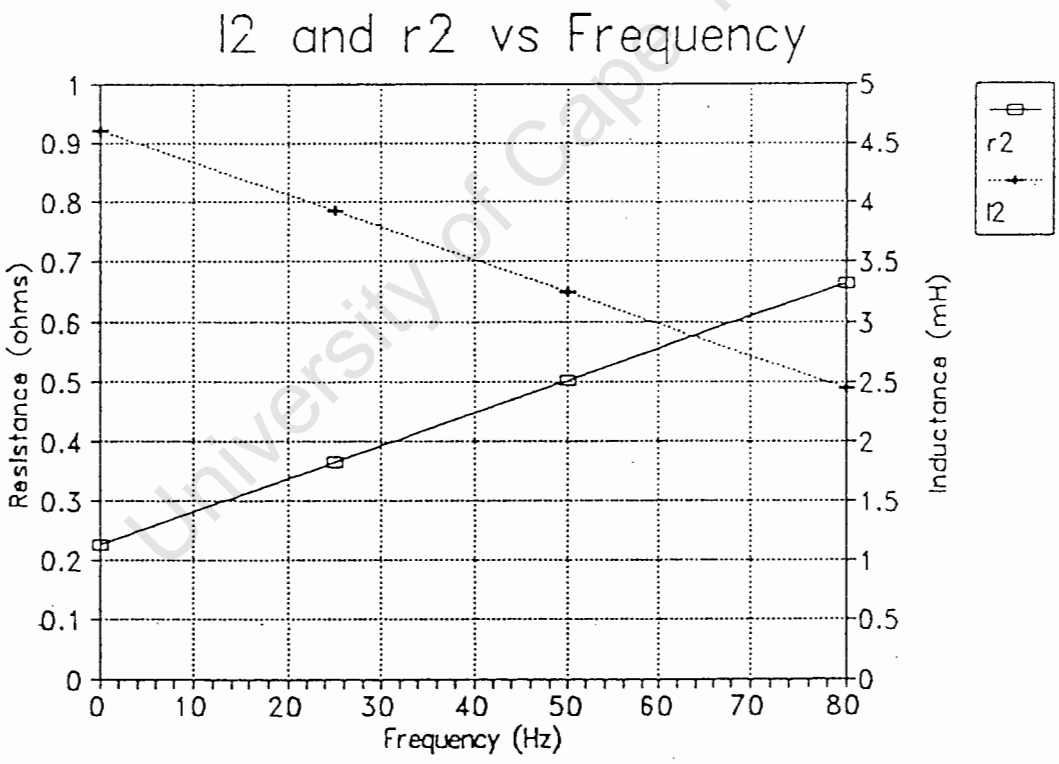

Figure 27: Secondary Resistance and Secondary Leakage Inductance for Operating Frequency Range

From the values obtained above, the secondary resistance and leakage inductance are given by:

$l_2 = 4.599 - 0.02696f$ mH;

$r_2 = 0.226 + 0.00548f$ ohms.

6.2.1.2. Calculation of Magnetizing Reactance

Since the supply voltage is below rated voltage, the effect of magnetic saturation in the exciting inductance has been neglected and hence this value is constant[39]. The magnetizing inductance was found from the no-load tests and results were obtained at 25 and 50 Hz to give $L_{m25} = 0.0537$H and $L_{m50} = 0.054$H. Clearly the assumption that the magnetizing inductance is constant is valid and the average value was taken to give $L_m = 0.0539$H.

6.2.1.3. Calculation of Mechanical Losses

Friction and windage losses can be predicted by

$$Wm = K_m(1-s)^z f^z \quad \text{-------} \quad [8]$$

where K_m and z are constants. The mechanical losses at rated and half-rated frequency were obtained from the no-load curves and substituted into the above equation to give

$$z = 1.24 \text{ and } K_m = 0.1094.$$

For the purposes of determining the mechanical losses the dependance of the circuit parameters on frequency have been neglected in determining the slip. The slip was determined according to eqn. 6 at rated frequency and expected load. This yielded s = 0.022 and hence

$$Wm = 0.106f^{1.24}$$

6.2.1.4. Calculation of Iron Losses

The iron losses can be divided into hysteresis and eddy current losses, where

$$Wc = Wh + We$$

$$= k_h f\Phi^2 + k_e f^2\Phi^2 \quad \text{------ [9]}$$

The dependance of mutual flux on the induced emf is given by

$$E1 = 4.44k_{m1}fn\Phi$$

and the assumption that $V1 = 4.44k_{m1}fn\Phi$ is valid except for very low frequencies[40]. For a constant voltage versus frequency relationship, this would mean that constant flux would be maintained. However, the maximum efficiency curve best approximates a square root curve of voltage versus frequency and hence

$$V = k\sqrt{f} \; ; \qquad \Phi = k'/\sqrt{f}$$

where k,k′ are constants

Using the above relationship of flux to frequency and eqn. 9, the iron losses can be calculated as follows:

$$Wc = k_h' + k_e'f, \quad \text{------- [10]}$$

where $k_h' = k_h k'$ and $k_e' = k_e k'$.

From the no-load test, $Pin = 3Io^2r_1 + Wc + Wm$.

Wc can thus be calculated from the results at rated and half-rated frequency to give:

$$Wc = 5.585 + 0.131f$$

6.2.1.5. Calculation of Iron and Mechanical Loss Resistance

Since the voltage frequency curve has been calculated in terms of the circuit parameters and the dependance of r_2 on frequency is known, the mechanical and iron losses can be taken into account by R_{cm}.

By combining eqn's 8 and 10, the power dissipated by Rcm is given by:

$$W_{Rcm} = Wc + Wm$$

$$= k_h' + k_e'f + K_m(1-s)^z f^z \quad \text{-------} \quad [11]$$

The iron and mechanical loss resistance is given by:

$$R_{cm} = \frac{W_{Rcm}}{3I_o^2} \quad \text{-----} \quad [12]$$

In order to calculate the iron and magnetic loss resistance, it is necessary to determine the no-load current as a function of frequency. In determining the no-load current, it was necessary to assume that this current is primarily determined by the magnetizing impedance and that the supply voltage follows a square root curve with respect to frequency.

Using the above assumptions the no-load current is given by:

$$I_o = k_o/\sqrt{f} \quad \text{-------} \quad [13]$$

Since the no-load tests were conducted with the supply voltage following a square root curve, the accuracy of the above equation can be assessed:

At a frequency of 50 Hz the no-load current was measured to be 1.9A and this yielded $k_o = 13.44$. At 25 Hz the no-load current was 2.75A and this yielded $k_o = 13.75$. Clearly the equation 13 is a good approximation in determining I_o.

By combining equations 11,12 and 13, the iron and mechanical loss resistance is given by:

$$R_{cm} = (k_h' + k_e'f + K_m(1-s)^z f^z)f/(3k_o^2)$$

It should be noted that because a fixed voltage frequency relationship has been assumed, this value of R_{cm} has been estimated only in terms of the frequency.

For changes in the supply voltage, as would occur for different load torques, this value will not predict constant losses accurately. Hence for lower torques, the equivalent circuit will predict a slightly higher efficiency than that found experimentally. However, within the operating range of torques, a fairly accurate prediction of the motor performance is obtained.

6.2.2 Harmonic Frequency Equivalent Circuit

The harmonic equivalent circuit of an induction motor under normal operating conditions can be represented by an equivalent circuit similar to that of the locked-rotor equivalent circuit[41].

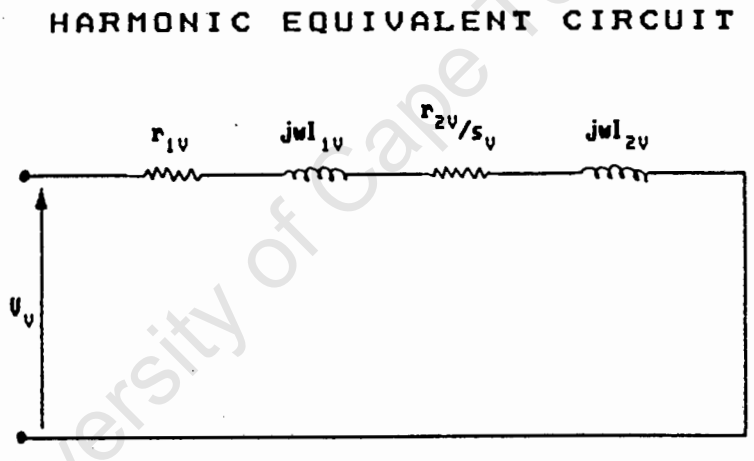

Figure 28: Harmonic Frequency Equivalent Circuit

The primary resistance and leakage reactance is assumed to be constant and therefore $r_{1v} = r_1$ and $l_{1v} = l_1$. The secondary resistance can be expressed approximately as a linear function of the frequency and is given by $r_{2v} = af_v + b$, where a and b have already been determined from the fundamental equivalent circuit.

The secondary leakage inductance has a linear function of frequency in the logarithmic domain and therefore l_{2v} can be expressed by the power function of the harmonic

frequency[42]. l_{2v} is determined from the blocked rotor tests at 25 and 50Hz a follows:

$$l_{2v} = Kf_v^c$$

$$\text{where} \quad c = \log_2 \frac{l_{2(50Hz)}}{l_{2(25Hz)}}$$

$$K = \frac{l_{2(50Hz)}}{f_n^c}$$

From the blocked rotor test results and solving the above equations, l_{2v} is given by:

$$l_{2v} = 6.507f_v^{-0.157}$$

6.3. EVALUATION OF MOTOR PERFORMANCE

Before the motor performance can be evaluated, it is necessary to determine the accuracy of the derived optimum voltage frequency curve. The experimental efficiency of the motor is compared with the theoretically predicted efficiency and the effects of oversizing the motor are also discussed.

6.3.1. Evaluation of Optimum Voltage Frequency Curve

In this section the optimum voltage frequency curve is evaluated against the equivalent circuit and the effectiveness of implementing such a curve in a production environment is discussed.

6.3.1.1. Evaluation of Approximated Equivalent Circuit Derivation

Since $r_2(f)$ and Rcm(f) are known, the curve for optimum efficiency can be obtained by substituting these values

into eqn 7. The following graph shows the derived optimum voltage frequency curve for different torques.

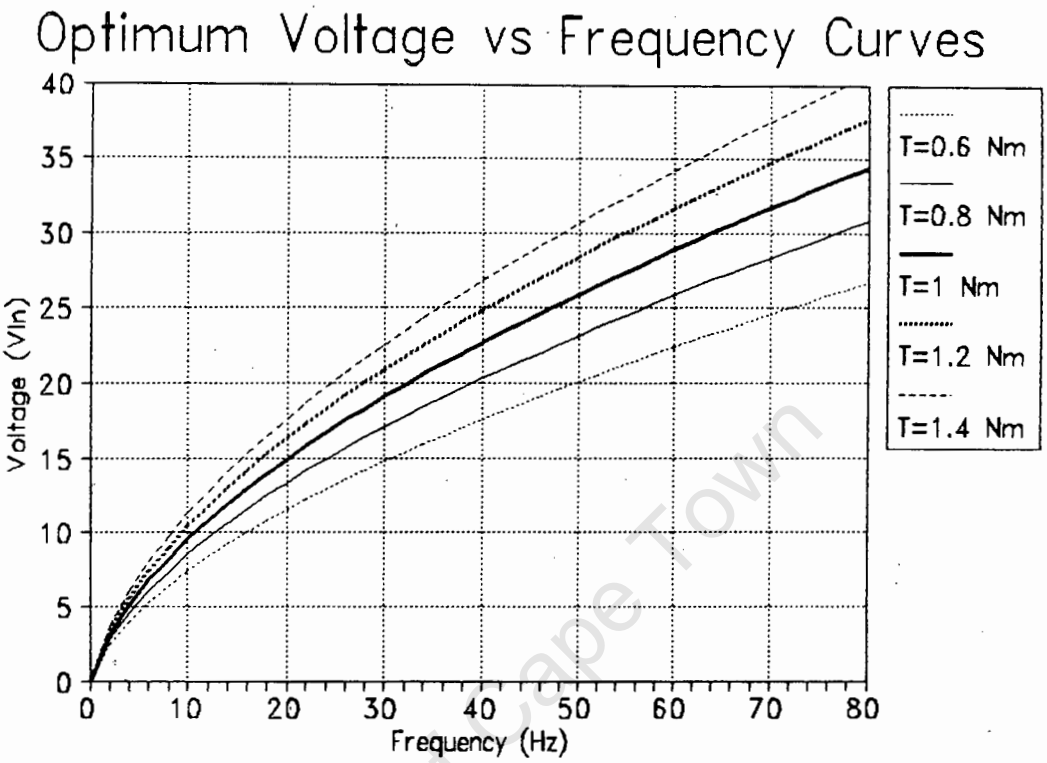

Figure 29: Derived Optimum Voltage Frequency Curve for Different Torques

Since only an approximate circuit was used to obtain the above curves, it is necessary to verify these relationships against the unsimplified equivalent circuit. This circuit was simulated with the use of a MATHSCAD program included in Appendix 4.2. The motor efficiency was predicted for different values of voltage and frequency in order to find the optimum voltage for a torque of 1Nm. The efficiency at different frequencies of the derived curve was also obtained with the unsimplified equivalent circuit. The graph below shows the derived and unsimplified circuit best voltage frequency curves with the corresponding calculated efficiencies.

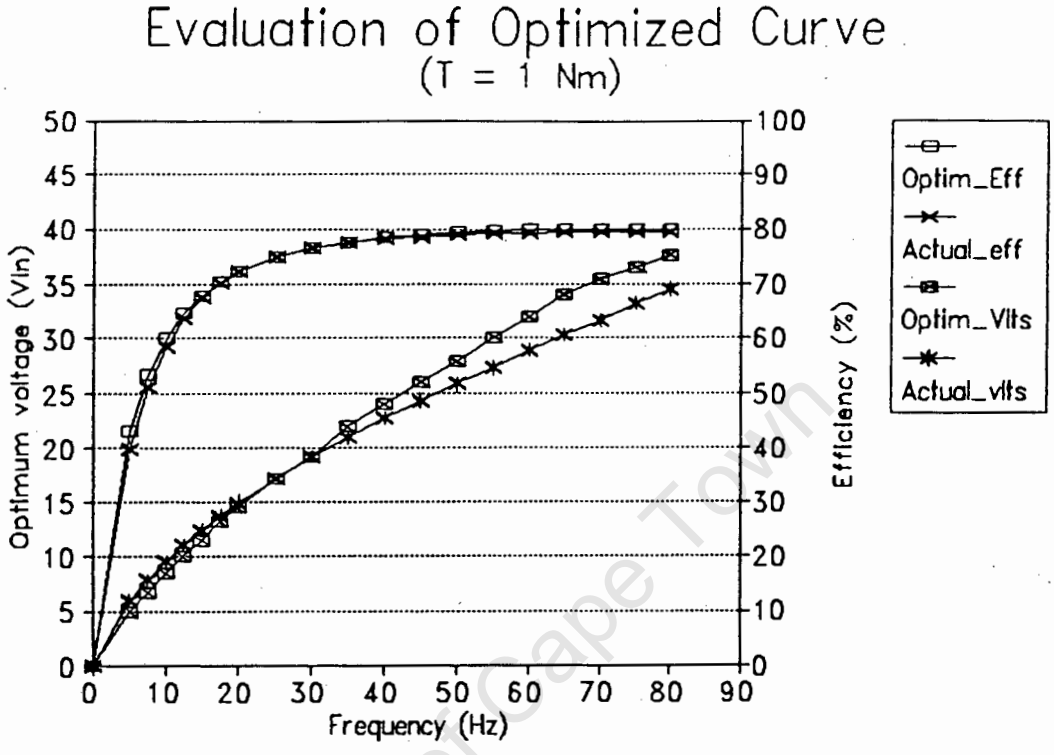

Figure 30: Voltage and Efficiency as a Function of Frequency for Derived and Exact Circuit Optimum Performance

As can be seen from the above graph, there is a good correlation between the two voltage frequency curves. Deviations between the two curves are due to the effects of the circuit inductances. At higher frequencies the series winding leakage inductance has a higher impedance, while at low frequencies the parallel magnetizing impedance begins to have an influence on the efficiency. These deviations at high and low frequencies do not have a significant effect on the motor efficiency and therefore the derived best efficiency curve can implemented in the microcontroller software for the required torque.

6.3.1.2. Effect of Mismatching on Motor Performance

The voltage frequency curve has been derived to optimize the motor performance at a particular torque and supply voltage. In a production environment these variables are likely to vary and hence the performance of the motor will be affected.

The torque of a pumping system varies directly with the head and this will fluctuate seasonally. The graph below shows the effect of changing torque around the designed value (0.85 Nm) on the motor efficiency. Clearly the efficiency of the motor has an inelastic relationship to the torque and the system will still operate efficiently despite fairly large changes in torque.

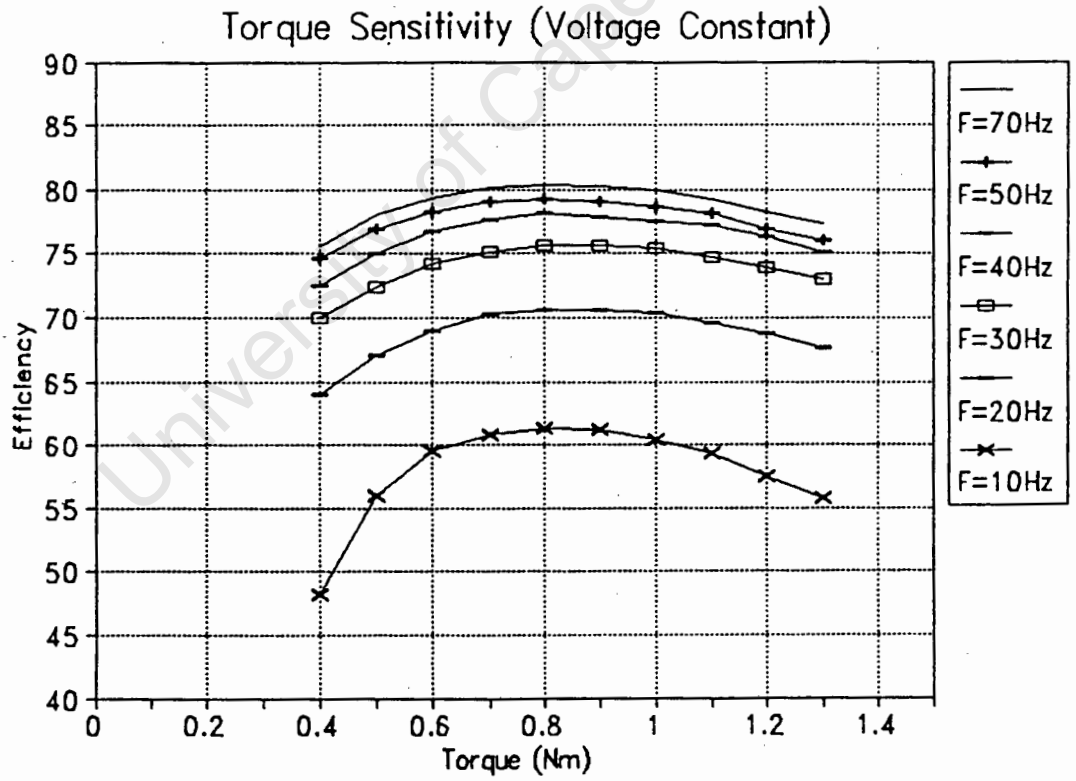

Figure 31: Efficiency Sensitivity for Changing Torque

The panel voltage changes due to temperature and irradiance level and these changes also affect the motor performance. The sensitivity of the motor due to changes in voltage is shown below, with markers showing the efficiency at 20% from the optimum voltage. Even with such a large voltage deviation the efficiency of the motor is maintained to within 3% from its maximum.

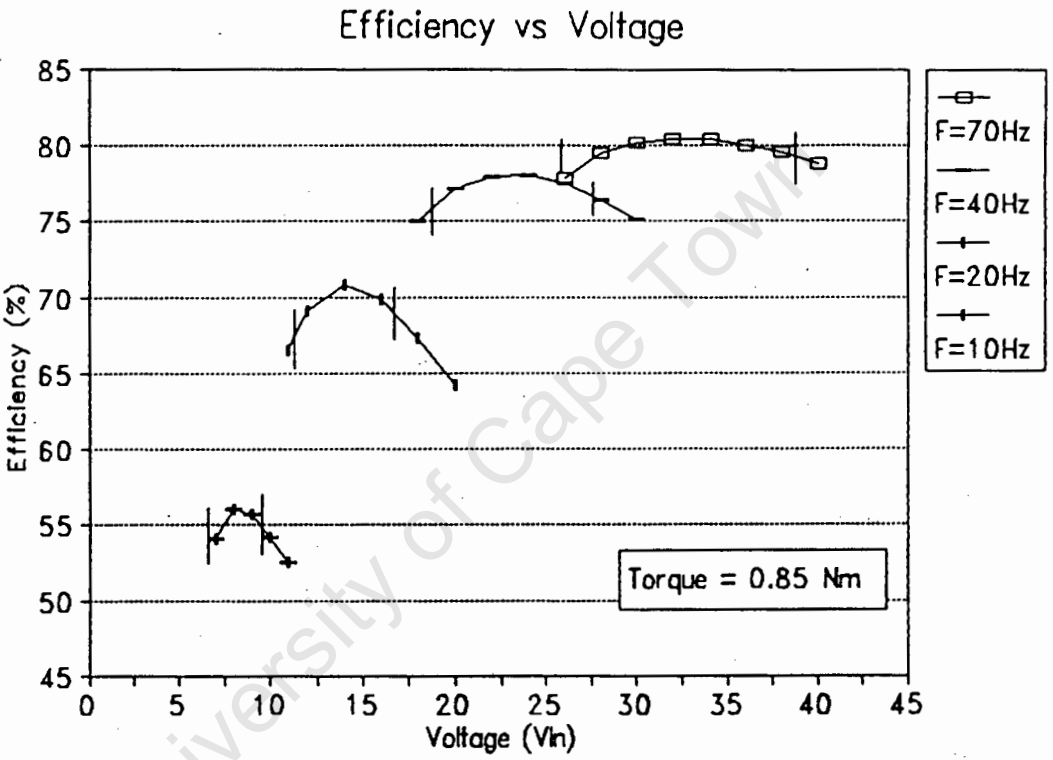

Figure 32: Efficiency Sensitivity for Changing Voltage

6.3.2. Experimental Evaluation of Motor Performance

The efficiency of the motor was measured experimentally at a fixed torque and these results were compared with the predicted efficiency from the equivalent circuit.

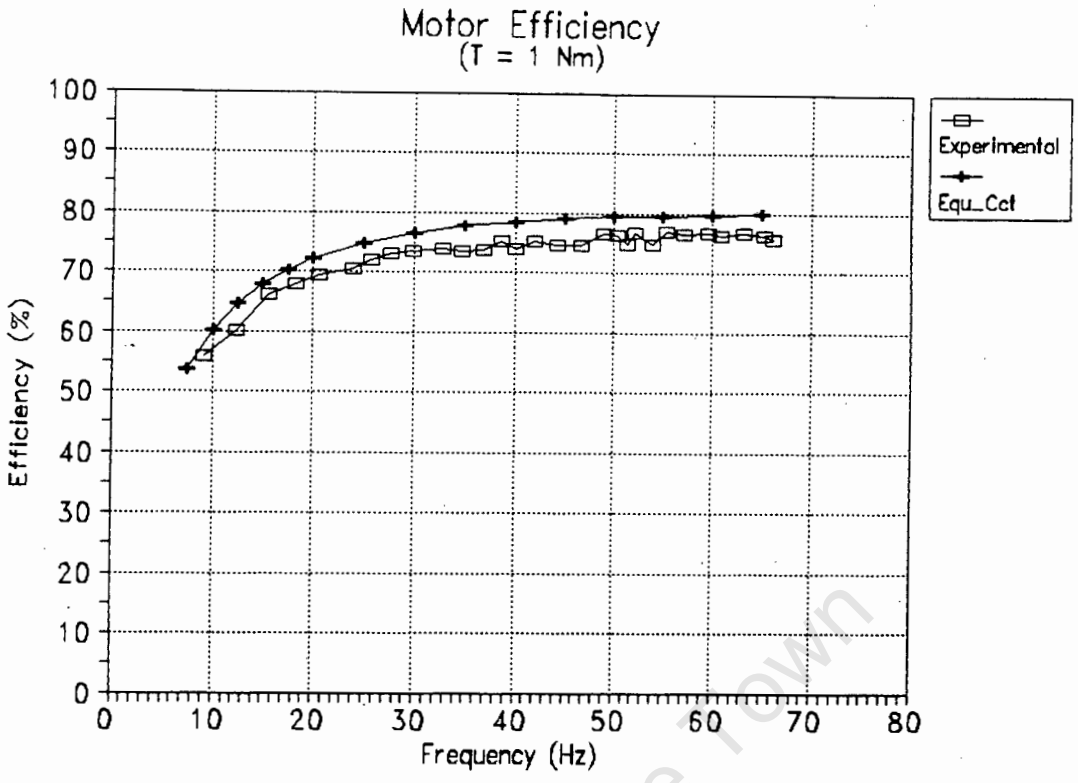

Figure 33: Experimental and Theoretical Motor Efficiency (T = 1 Nm)

From the above graph it can be seen that the experimental efficiency is slightly lower than the calculated efficiency. This is due to the fact that the motor has been lightly loaded and because of the low supply voltage, the losses of R_{cm} have not been adequately estimated. Despite this, the two graphs are very similar in shape and this indicates that the frequency dependance of the circuit parameters has been correctly estimated.

6.3.3. Effects of Oversizing the Induction Motor

The graphs below show plots of the motor characteristics at rated voltage and at a lower voltage at which the efficiency is maximized for a particular torque. The curves were obtained from the equivalent circuit for which the parameters were determined

separately at rated voltage and current and lower voltage and current. The motor curves are therefore shown at rated output and at a typical power output.

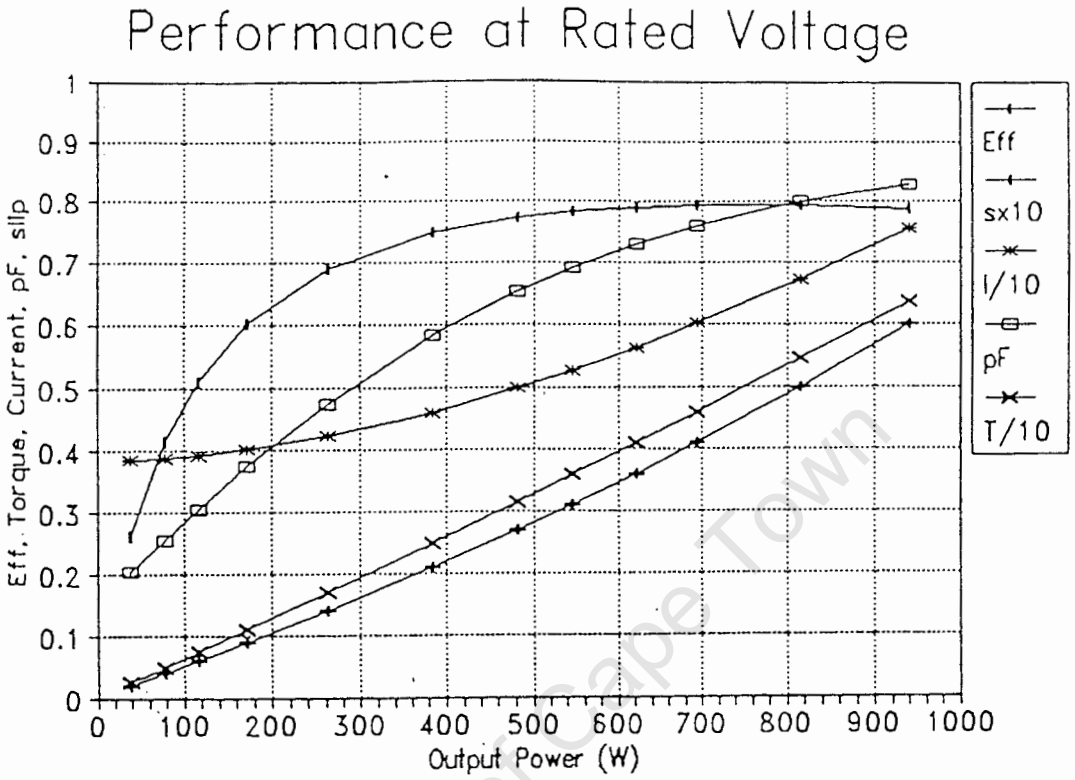

Figure 34: Motor Characteristics at Rated Frequency and Voltage ($V=63.5v_{ln}$)

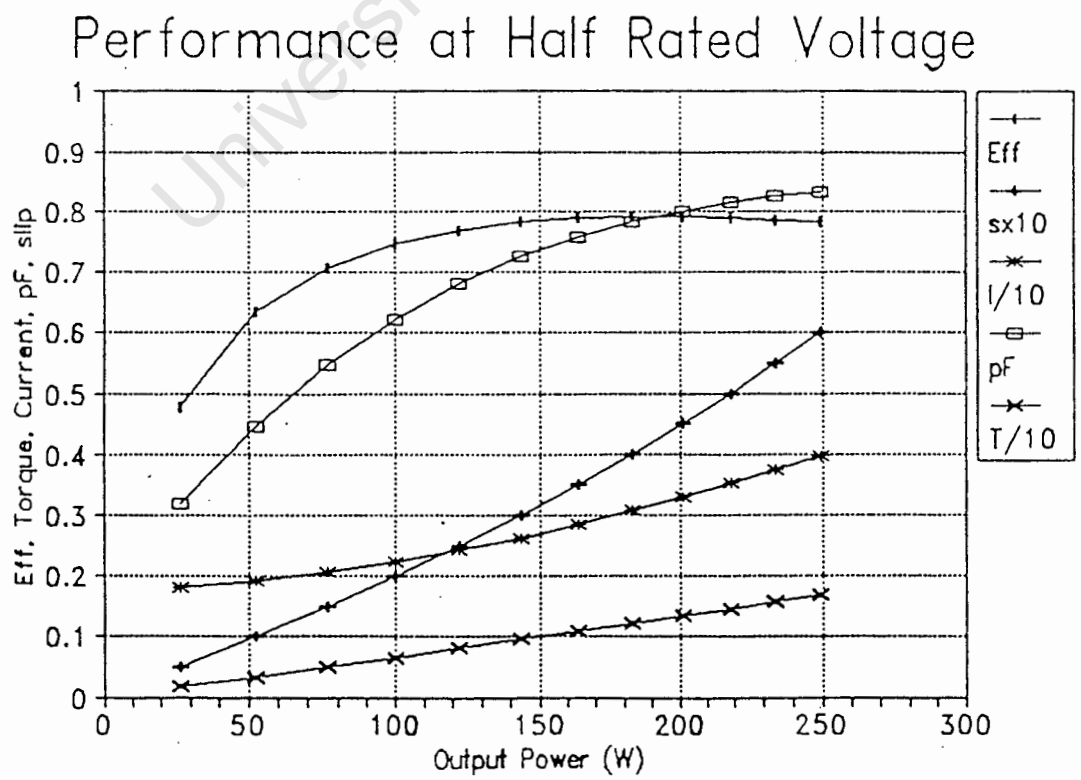

Figure 35: Motor Characteristics at Rated Frequency and Below Rated Voltage ($V=32v_{ln}$)

From the graphs, the efficiency of the motor is virtually the same in both cases. The power factors at the operating points of the two curves are similar and this means that the inverter losses will not increase due to oversizing.

From the motor curves in Appendix 4.1, the motor efficiency at very light loads tends to decrease. This is to be expected due to the increased effect of constant losses on the motor performance. A limit therefore exists to the extent the motor can be oversized while maintaining an acceptable efficiency level. For ratings down to around 150W, the motor efficiency is still acceptable and hence the motor is suitable for a large power range.

CHAPTER 7: INVERTER PERFORMANCE ANALYSIS

For the system to operate efficiently the inverter performance must be optimized over a wide frequency range. The inverter losses are classified as the losses which have been introduced by the inverter and these have been divided into harmonic, switching, conduction, and control circuit losses. In this chapter the different losses are estimated and combined to form the total inverter losses.

7.1. ASSESSMENT OF PWM HARMONIC LOSSES

Both sinusoidal and harmonic elimination PWM techniques were implemented and the two methods were compared to determine which would yield the highest efficiency. For the harmonic elimination method, the effectiveness of the microcontroller in eliminating the required harmonics was evaluated by obtaining harmonic traces of the output voltage at 20, 35 and 50Hz. These traces have been included in Appendix 8. From the graphs in the appendix, it can be seen that the 5th, 7th, 11th and 13th harmonics have been successfully eliminated subject to small rounding errors.

In order to assess the harmonic losses caused by the inverter, the current waveform was decomposed into its fourier elements. These elements were used as inputs to the harmonic equivalent circuit and the losses were predicted. The losses for both sinusoidal PWM and programmed harmonic elimination PWM were examined and comparisons were drawn between the two methods. In the figures below, the losses at different frequencies for harmonic and sinusoidal PWM are shown. The current harmonic spectrum has been included in Appendix 8.

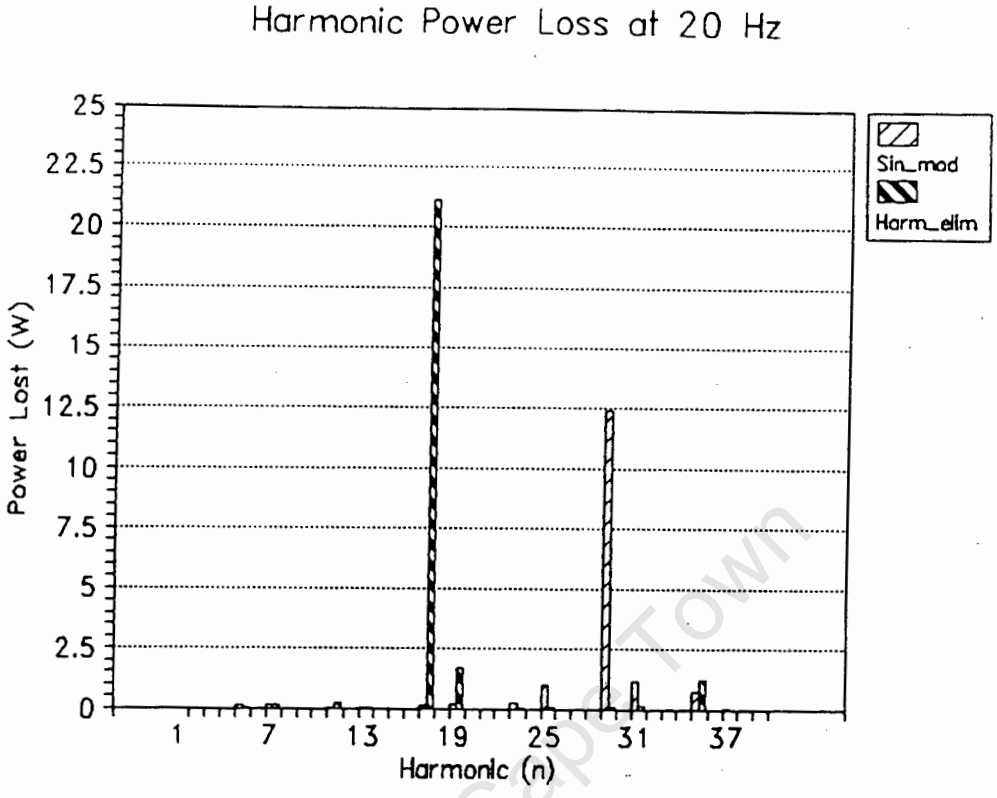

Figure 36: Harmonic Losses at 20 Hz

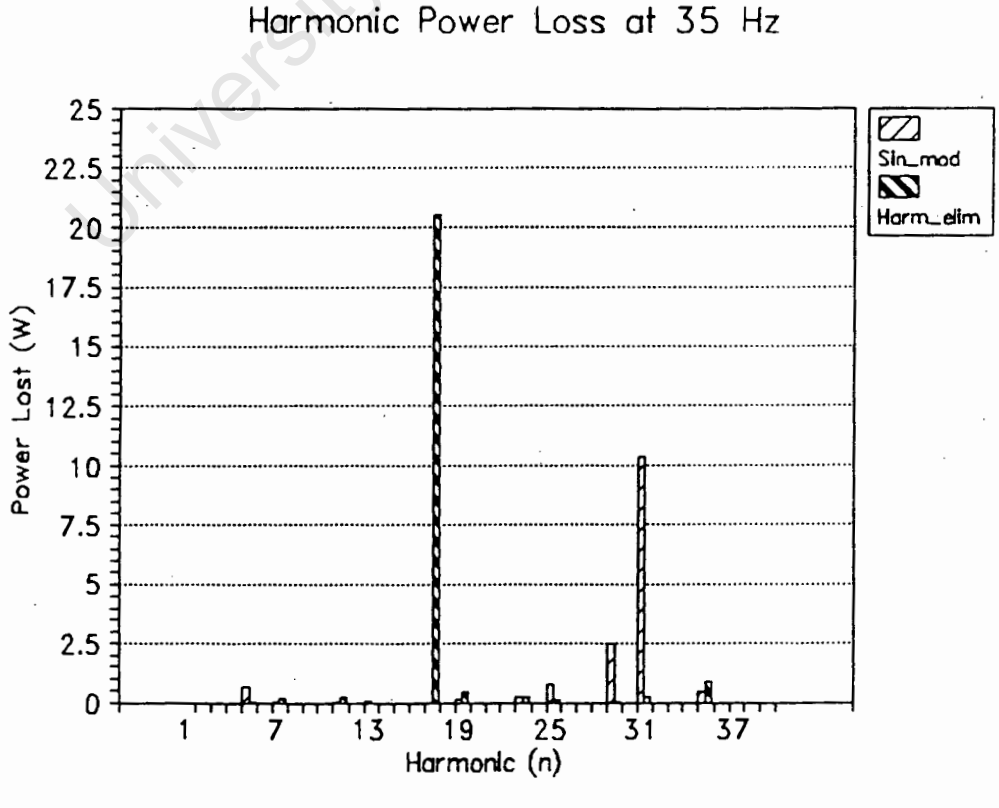

Figure 37: Harmonic Losses at 35 Hz

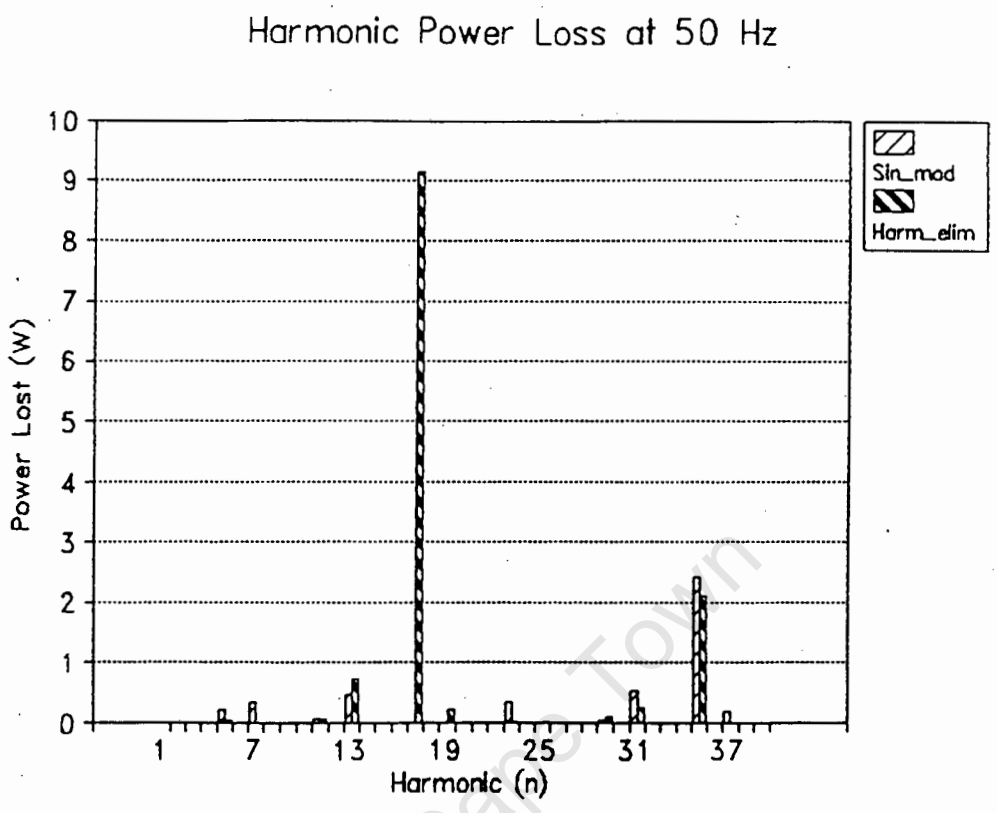

Figure 38: Harmonic Losses at 50 Hz

The total harmonic losses of each method were obtained and are shown below:

HARMONIC LOSSES	Harm_Elim	Sine_Mod
Frequency = 20 Hz:	24.9 W	16.3 W
Frequency = 35 Hz:	23.1 W	15.2 W
Frequency = 50 Hz:	12.7 W	4.6 W

Figure 39: Table of Harmonic Losses for Sine and Harmonic Elimination PWM

As can be seen from the above table, sinusoidal modulation has an advantage over the harmonic elimination method in reducing the total harmonic losses. This is due to the fact that harmonics above the 13th have a significant influence on the total losses. In order to fully assess the optimum method for the

generation of the PWM signals, it is necessary to take into account the switching losses caused by the two methods.

7.2. ASSESSMENT OF SWITCHING LOSSES

The switching losses have been estimated by the method set out in the Hexfet Designers Manual which has been included in Appendix 1.4. Only turn-on losses have been considered as turn-off losses are small compared to the conduction and diode recovery losses found during turn-on[43]. The turn-on waveforms of the MOSFETs are shown below and it these waveforms that have been used to predict the switching losses. A description of these waveforms is given in Appendix 1.4.

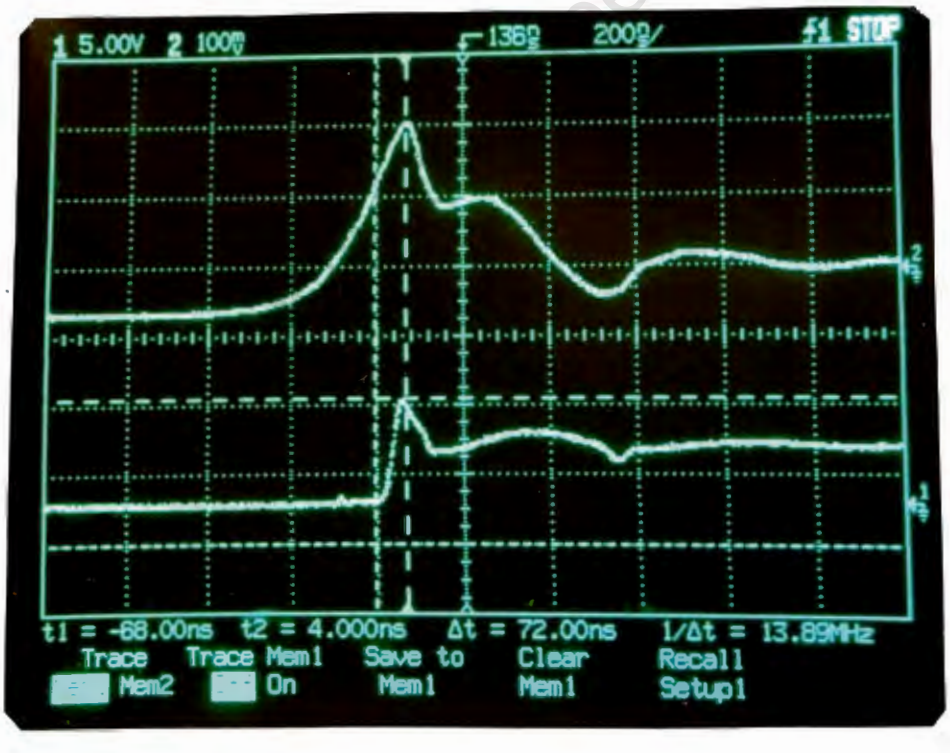

40a) Voltage and Current Trace of Upper MOSFET

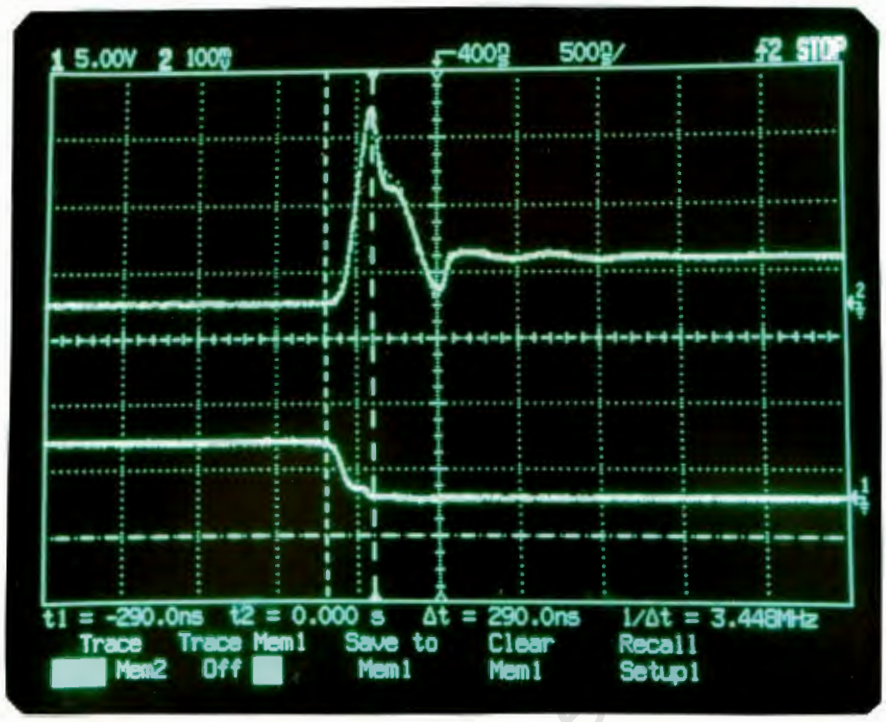

40b) Voltage and Current Trace of Lower MOSFET

Figure 40: Inverter Turn-on Switching Waveforms.

For the switching losses to be calculated at different supply frequencies, the panel voltage and AC line current must be known. The panel voltage is constant due to the array characteristics and it was also found that for a torque of 1 Nm the line current remained within the limits of 2.7 to 3 A_{rms} over a wide range of frequencies. Hence both voltage and line current could be assumed constant when determining the switching losses. From the switching waveform, the peak current was found to be 7.4A. This is larger than the RMS current because of distortion caused because the inverter current is not purely sinusoidal. In order to determine the switching losses, the current switching waveform has been approximated by the diagram shown below.

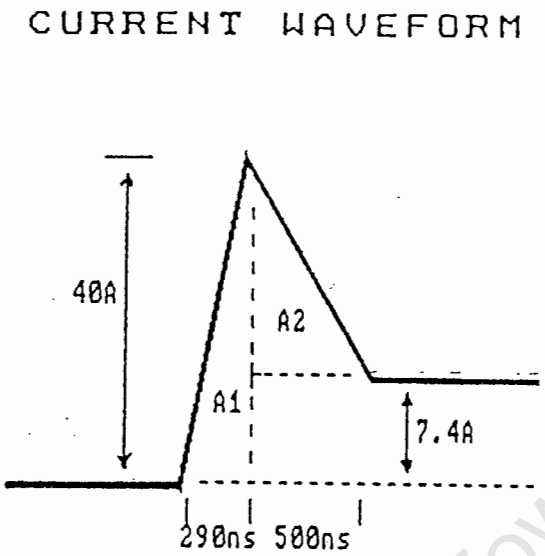

Figure 41: Linearized Current Switching Waveform

From Appendix 1.4, the total commutation energy loss may be expressed as

$$E = V_{dc}(\text{Area1} + \text{Area2})$$
$$= V_{dc}(\tfrac{1}{2}b_1h_1 + \tfrac{1}{2}b_2h_2)$$
$$= 1.19 \cdot 10^{-3} \text{ J}$$

The switching losses are therefore given by $P_{sw} = 3 \cdot f_s \cdot 1.19 \cdot 10^{-3}$ W, where f_s is the switching frequency. Power dissipated by the snubber circuit has been neglected in determining the switching losses because the tests were conducted only with small snubber capacitors and these had a negligible effect on the system losses. The switching losses were obtained at frequencies of 20, 35 and 50 Hz in order to compare the two methods of generating PWM.

SWITCHING LOSSES	Harm_Elim	Sine_Mod
Frequency = 20 Hz:	1.4 W	6.5 W
Frequency = 35 Hz:	2.5 W	7.5 W
Frequency = 50 Hz:	3.6 W	5 W

Figure 42: Switching losses for Sine and Harmonic Elimination PWM

When combining the harmonic and switching losses of the two methods of PWM, it can be seen that the sine modulated method is more efficient than the harmonic elimination method. This is especially true at lower frequencies. Therefore, for frequencies below 50 Hz sine modulation was used, while for frequencies above 50 Hz the harmonic elimination method was used.

7.3. ASSESSMENT OF CONDUCTION LOSSES

In order to minimize the conduction losses, MOSFETs with the lowest on-resistance in the required voltage range were chosen. The IRFP250 MOSFETs are rated at 200v with an on-resistance of only 0.085 ohms. The normalized on-resistance versus temperature graph for this device is shown in Appendix 1.4. During normal operation, it was found that the Mosfets did not heat up considerably and only small heatsinks were used. From the voltage versus temperature graph, the on-resistance at 60 C is 0.106 ohms.

The load current is carried either by the channel of one MOSFET or by the body-drain diode of the other. When the channel is conducting, the power dissipated by that MOSFET is given by

$$P_d = i_d^2 R_{DSon}.$$

During the period when the body-drain diode of a MOSFET conducts, the power dissipated by that MOSFET is given by

$$P_d = i_d V_{sd},$$

where V_{sd} is the forward drop of the diode and is a function of the load current. Since the load current for the motor has been assumed constant for all frequencies, V_{sd} can be obtained from current compensation graph Appendix 1.4. For a peak current of 7.4A, V_{ds} was found to be approximately 0.75v.

According to the calculations supplied by the Hexfet Designers Manual and included in Appendix 1.4, the average power in one leg of the inverter due to channel conduction is given by

$$P_{chan} = 0.462 I_1^2 R_{DSon}, \quad \text{------ [1]}$$

where I_1 is the peak AC current. The average power loss due to diode conduction is given by

$$P_{diode} = 0.068 I_1 V_{SD}. \quad \text{------ [2]}$$

The motor operates at a power factor of around 0.8 and this must be taken into account according to the loss factor graph in Appendix 1.4. For a loss factor of 1.7, the total conduction losses are given by:

Channel Conduction Losses:	8.045W
Diode Conduction Losses:	1.925W
Total Conduction Losses:	9.97W

This power is easily dissipated by the six MOSFETs and there is therefore no need for large heatsinks.

7.4. ASSESSMENT OF CONTROL CIRCUIT LOSSES

The control circuit losses are constant and these are determined by the microcontroller and base drive current requirements.

The combined microcontroller and base drive circuit requires a current of approximately 200mA. For a supply voltage of 15v, this represents a power loss of 3W. It should be noted, however, that this supply voltage must be obtained from the full dc supply rail by means of a dc-dc converter The dc-dc converter as described in the hardware design chapter yielded an efficiency of 55% and the power lost was therefore 5.45W.

7.5. INVERTER EFFICIENCY AND TOTAL LOSSES

The inverter efficiency was found experimentally by measuring the efficiency of the motor with pure sinusoidal excitation and comparing it to the efficiency obtained when the motor was supplied by the inverter. This method incorporates the harmonic losses with the inverter losses. The graph below shows the motor and combined motor/inverter efficiency.

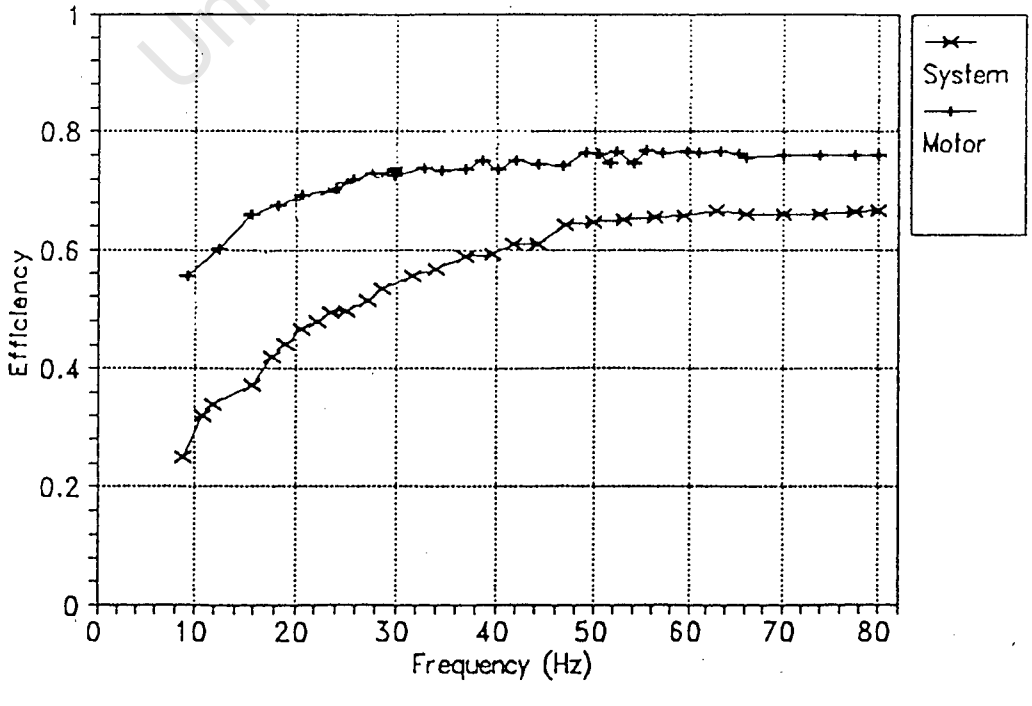

Figure 43: Motor and Combined Inverter and Motor Efficiency

Figure 44 shows the inverter efficiency as a function of frequency for a torque of 1 Nm. At frequencies above 50Hz, the inverter efficiency is close to 87%, which compares favourably with a typical inverter efficiency of 85% as quoted by Lasnier[44]. It is expected that at higher power ratings the efficiency of the bridge should increase as the constant control circuit and modulation frequency harmonic losses will become less significant. The slight bumps in the inverter efficiency curve are caused by the microcontroller changing from one voltage table to the next.

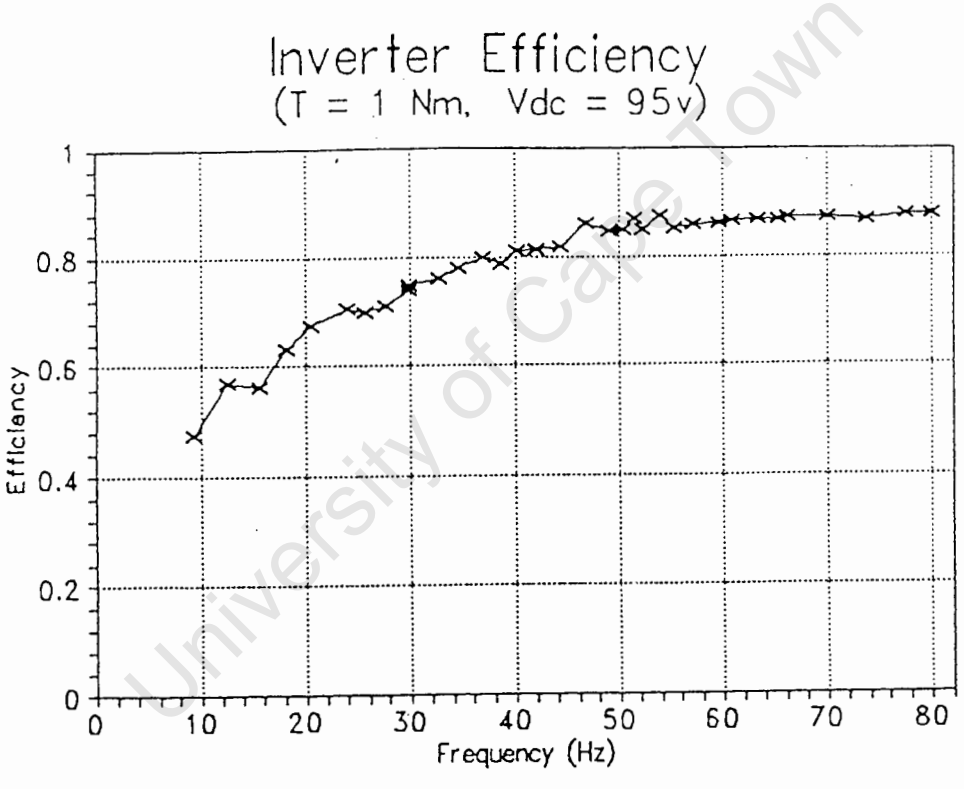

Figure 44: Inverter Efficiency versus Frequency

The harmonic losses have been obtained by deducting the switching, conduction and control circuit losses from the total inverter losses. The bar chart shown below provides an estimated breakdown of the different losses and these are discussed further.

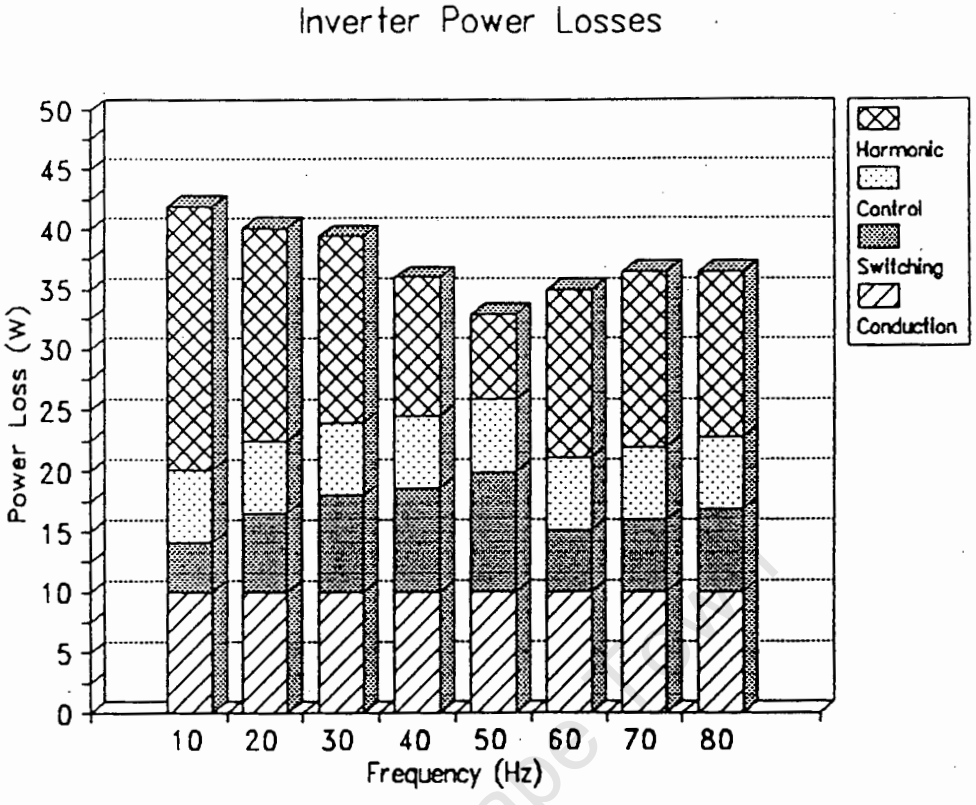

Figure 45: Bar Chart of Different Inverter Losses

The accuracy of determining the harmonic losses by the above method can be verified against the harmonic equivalent circuit results obtained previously:

HARMONIC LOSS PREDICTION		
	Harm_Equ Cct	Eff Method
Frequency = 20 Hz:	16.3 W	17.7 W
Frequency = 35 Hz:	15.2 W	13.5 W
Frequency = 50 Hz:	4.6 W	7.1 W

Figure 46: Correlation of Two Methods of Harmonic Loss Prediction

Clearly the two methods are in good agreement at these frequencies.

The switching losses increase steadily with frequency up to 50Hz, while the harmonic losses decrease accordingly. Although there is a decrease in the number of switches per cycle with frequency, the frequency increases at a higher rate and hence the switching losses increase. For frequencies above 40 Hz, the generation of PWM takes place in the second mode of operation. Although the resolution is not as fine here, this has no ill effects on the harmonic losses as the trend of decreasing harmonics continues to 50 Hz.

Above 50 Hz, the harmonic elimination method has been used and here the harmonic losses increase substantially. This is probably due to the introduction of additional harmonics due to overmodulation at these high frequencies.

CHAPTER 8: CONTROLLER FOR MAXIMIZATION OF DELIVERY

The main function of the controller for any solar water pumping system is to ensure that the water delivery of the pump is maximized. In conventional solar pumping applications, two methods of control can be implemented and these are constant voltage control and maximum power point tracking. For this project, a third method of control is presented, namely speed control.

8.1. CONSTANT VOLTAGE TRACKING

This is the simplest and most commonly used method of ensuring that the system is run close to the maximum power point of the solar panels. The method is based on the assumption that the maximum power point of the panels is found at constant voltage for all levels of irradiance. A control system that uses such a method would simply adjust the load (i.e. vary the pump speed) in such a way that the voltage remains fixed at a predetermined level. This method is used widely in many solar applications which include battery charging and water pumping. The DC positive displacement systems of Mono Pumps uses this method of control.

The main disadvantage of this method is that the voltage at which the peak power point occurs can vary substantially due to factors such as temperature, insolation and production spread. Another disadvantage of this method is that the system must be set to operate at the correct voltage and this could be difficult if different types of panels are being used in a production environment.

Voltage tracking can be used successfully if the operating voltage is determined as a fixed percentage of the open circuit voltage. This implies that the load

must be briefly disconnected in order to determine the open circuit voltage. Such a method has been developed that enables the panels to operate close to the peak power point[45].

8.2. MAXIMUM POWER POINT TRACKING

This method of control can be used to ensure that the panels deliver their maximum power over a wide rage of solar insolation. In order to realize such a controller, it is necessary to multiply the instantaneous current and voltage and to implement some form of hill-climbing algorithm to operate on the peak power point. Usually such systems are implemented with the use of a microcontroller.

8.3. SPEED MAXIMIZATION CONTROLLER

In feedback control systems, it is advisable wherever possible to use the final output variable in the feedback path. This ensures that if there are any parameter variations to the transfer function, these do not significantly affect the output. It is obvious that the primary task of the controller is to maximize the water delivery, and although this is usually coincidental with operating on the peak power point, it is not always the case. This is especially true for a three-phase motor drive, where a change in the harmonic content of the motor current could cause more power to be used at a lower operating speed than a higher speed. This would only be noticeable for small changes in supply frequency and hence there would be 'glitches' where the motor would operate below maximum speed. This is also only likely to occur at low speeds where the harmonic losses have more influence on the system motor performance.

Using conventional feedback theory, the optimum approach would be to maximize the water flow rate. However, this would not give a very constant reading because of oscillations and phase shifts in the pump itself. These fluctuations could be filtered out, but this is not necessary if the speed of the pump is used as the control variable. This is because the pump has a large flywheel on it and this acts as a low-pass filter. Another reason to use a speed transducer is that it is both cheap and robust. Since the motor speed is higher than the pump speed, it is advantageous to place the speed transducer on the motor to enable faster sampling times at low speeds.

It is for the above reasons that a controller was designed which used the motor speed as the input variable in order to maximize the water delivery.

8.4. CONTROLLER REQUIREMENTS

The controller must ensure that the motor is run as fast as possible over a wide range of insolation levels. This is a dynamic process in which the controller is continually varying the supply frequency in order to obtain maximum speed. The controller must therefore minimize its hunting operation around the maximum speed point as this will lead to a reduced flow rate.

Another requirement of the controller is to have an adequate dynamic response to ensure that the system remains stable. Although the time constant of insolation for a clear day is very slow, the controller must provide a fast dynamic response in the event of changes in insolation due to clouds or other disturbances. In lightly overcast conditions the irradiance level fluctuates often and it is not acceptable to have the motor stalling and restarting during such conditions.

8.5. DESIGNING A SUITABLE CONTROLLER

Initially the pump characteristics were simulated by coupling the induction motor to a DC generator loaded to a torque of 1 Nm, which is a typical value to be expected for a PDP pumping system. The solar panels were simulated by a 110v DC bus with a variable internal resistor. Such a configuration yields a parabolic power curve with a peak power point at half the open circuit voltage.

8.5.1. Hill-Climbing Algorithm Approach

Since the panel characteristics are not known and are variable, a formula cannot be applied in determining the maximum power point. A conventional control system would use a hill-climbing algorithm to operate at the peak power point. This approach was implemented and is illustrated in the following figure.

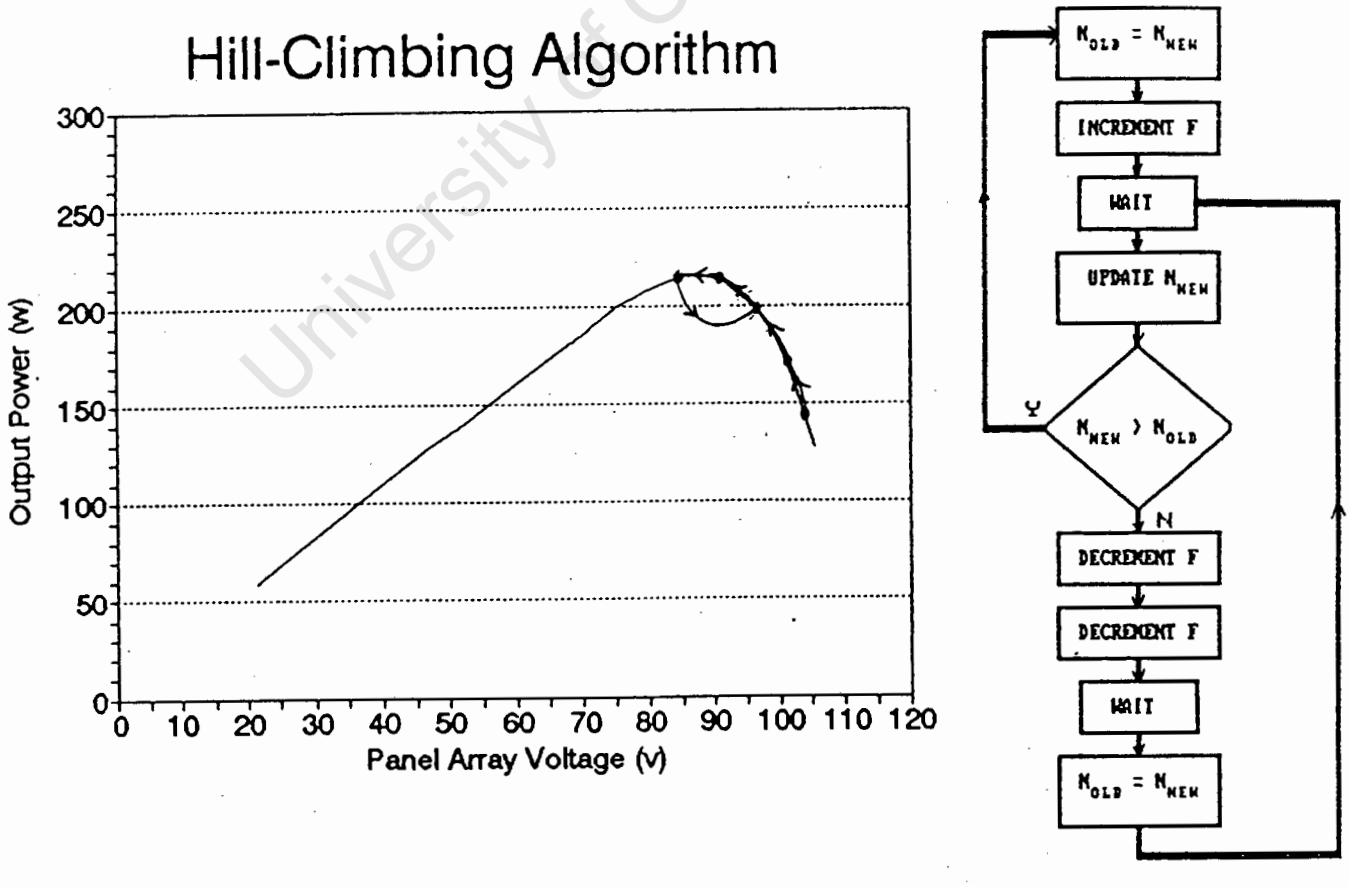

Figure 47: Control Method Whereby Small Changes in Frequency are Used to Obtain Maximum Speed

Although the above method was capable of tracking the peak power point, it was only stable for slow changes of the internal resistor.

A controller was needed that could find the peak operating point despite large steps in irradiance levels. Such a controller was obtained by following a constant slip curve.

8.5.2. Constant Slip Controller

A controller was implemented which ensured that the motor operated at a constant slip. This gave the advantage that if there were large changes in irradiance, a frequency could be selected that would enable the motor to accelerate to its maximum speed. This method worked on the principle that

$$F_n = kN_{n-1},$$

where F_n = New frequency

N_{n-1} = Previous speed

k = Scaling constant

The speed was scaled in such a way that kN_{n-1} was always slightly greater than F_{n-1} when the motor was undergoing normal operation. When the peak point was exceeded, the slip would start to increase and kN_{n-1} would decrease. Hence F_n would be lower than F_{n-1} and the motor would oscillate slowly between two frequencies at the peak point. This method is illustrated in the graph below.

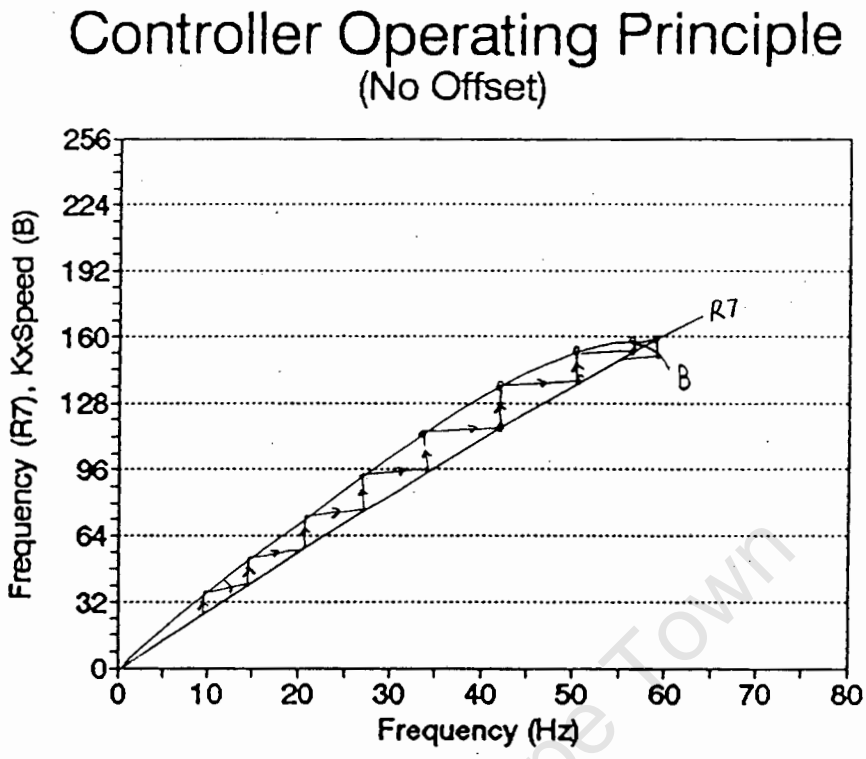

Figure 48: Operation of Constant Slip Controller

In order for the above system to operate effectively, it was necessary for the two bytes containing the frequency Fn and speed Nn to have a linear relationship with respect to the actual speed and frequency. The accuracy of the speed tracking was determined by the linearity of these two variables. Any deviations from a linear relationship would lead to glitches in the controller which could only be overcome by increasing k and hence increasing the oscillations at the peak power point. The hardware for reading in the speed used an LM331 which provides a very linear response (0.01%). The output frequency, however, was determined by the timer speed values and these followed a hyperbolic curve with respect to frequency. A look-up table was implemented to provide a linear relationship with frequency and this is shown in the graph below.

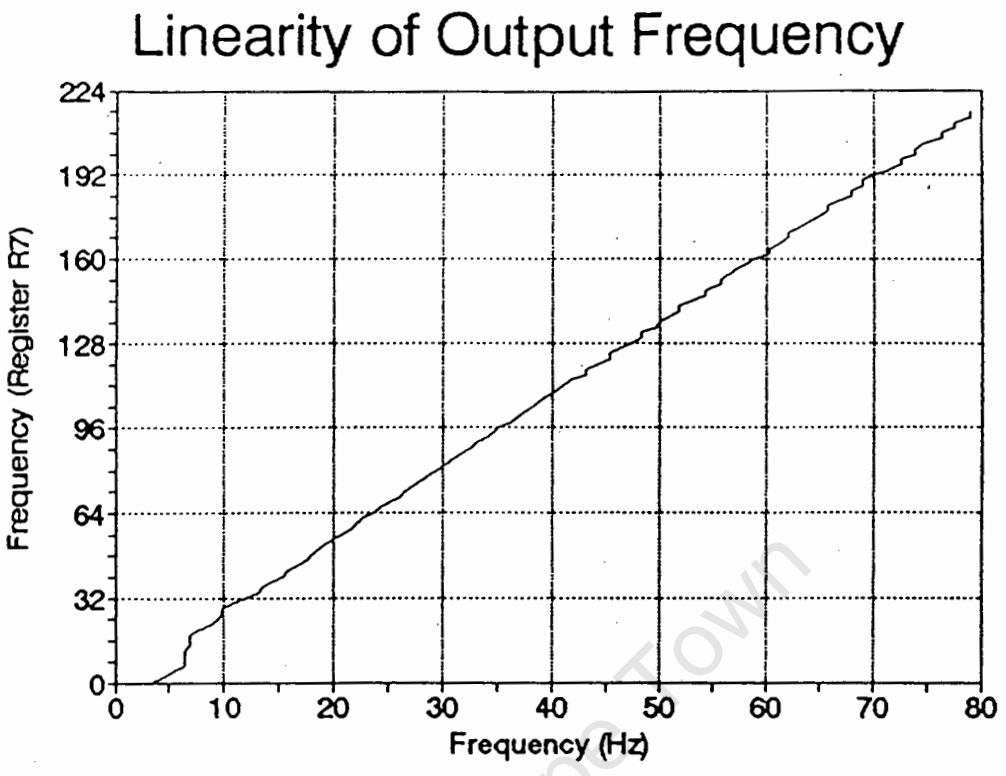

Figure 49: Linearity of F_n With Respect to the Actual Frequency

Although this method provided both stable operation at the peak point and a fast dynamic response, it was still not acceptable because k had to be carefully adjusted to prevent the controller from becoming unstable. If kN_{n-1} was slightly too large then the system would start oscillating and if it was too small the motor would remain at constant speed or even converge to the lowest frequency. This placed a fine tolerance on k which was unacceptable for the robust requirements of a solar water pump.

In addition to this, when the system was run from the solar panels, it became more difficult to control. This was due to the fact that the short circuit current of the panels is close to the operating current and if the slip increased, the motor would require more current and the voltage would quickly collapse.

With the use of a data acquisition system, it was possible to obtain plots of the voltage and speed against time. The collapsing voltage of figure 50 was caused by the controller trying to operate at a frequency slightly above that for optimum speed. From the graph it is clear that the dips in the speed are inevitable because of the phase delay of the load caused by the high inertia of the pump.

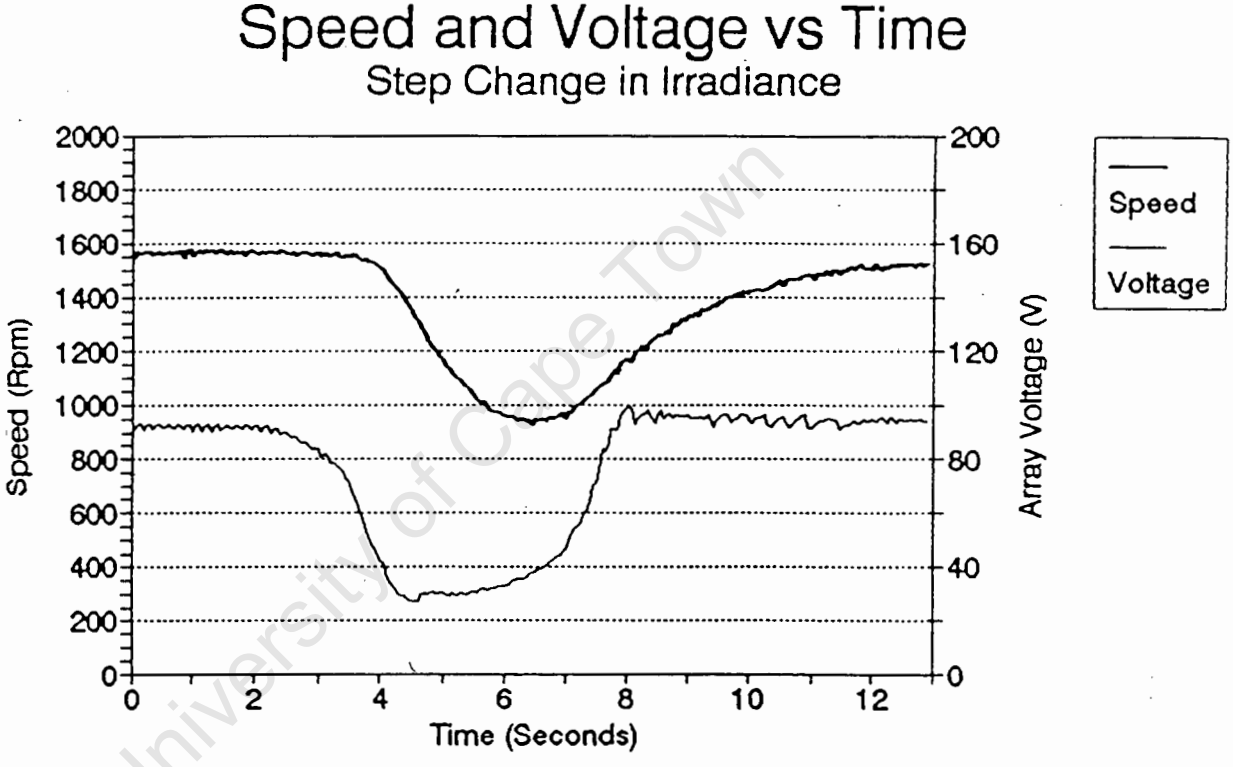

Figure 50: Phase Delay of Motor Speed with Collapsing Supply Voltage

8.5.3. Slip Controller with Offset

In an attempt to avoid the problem of the load phase delay, an offset was provided to kN_{n-1} so that the two lines of figure 48 would have a definite crossover point. By introducing such a crossover point, the controller would operate at a fixed frequency. After a predetermined time, k was increased to cause a higher operating frequency. If the peak point was exceeded, k

was decreased until the speed oscillations had fallen below a certain level.

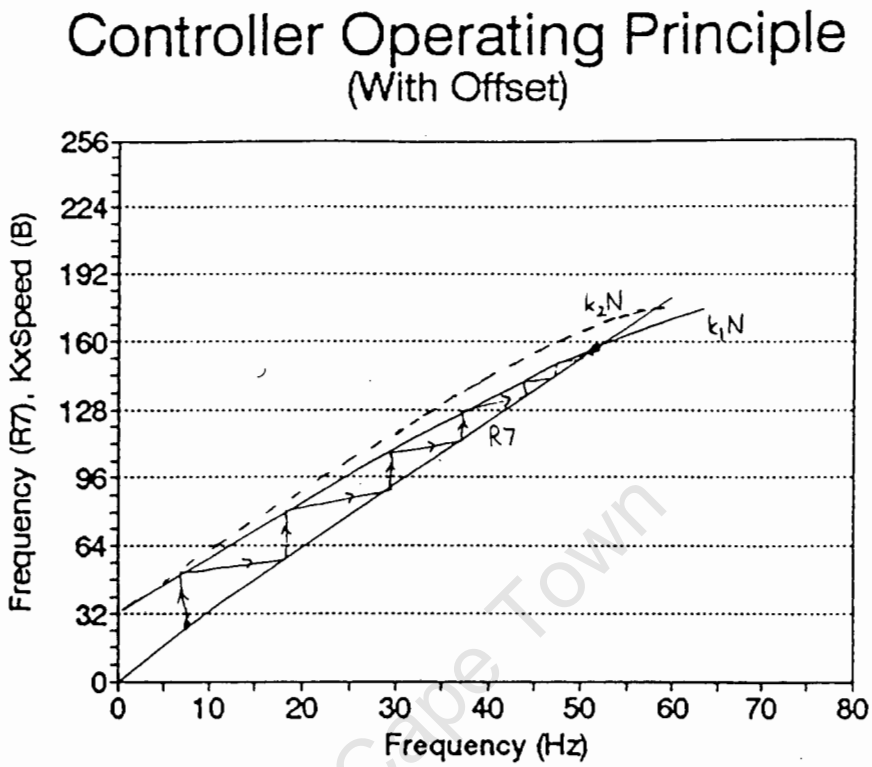

Figure 51: Operation of Controller with Crossover Point

The advantage of this method was that the voltage did not collapse unnecessarily and the controller was still capable of a fast dynamic response. In figure 52 the controller response is shown after a step disturbance to the panel irradiance level. The disturbance was achieved by tilting the panels away from the sun and returning them back to their original position.

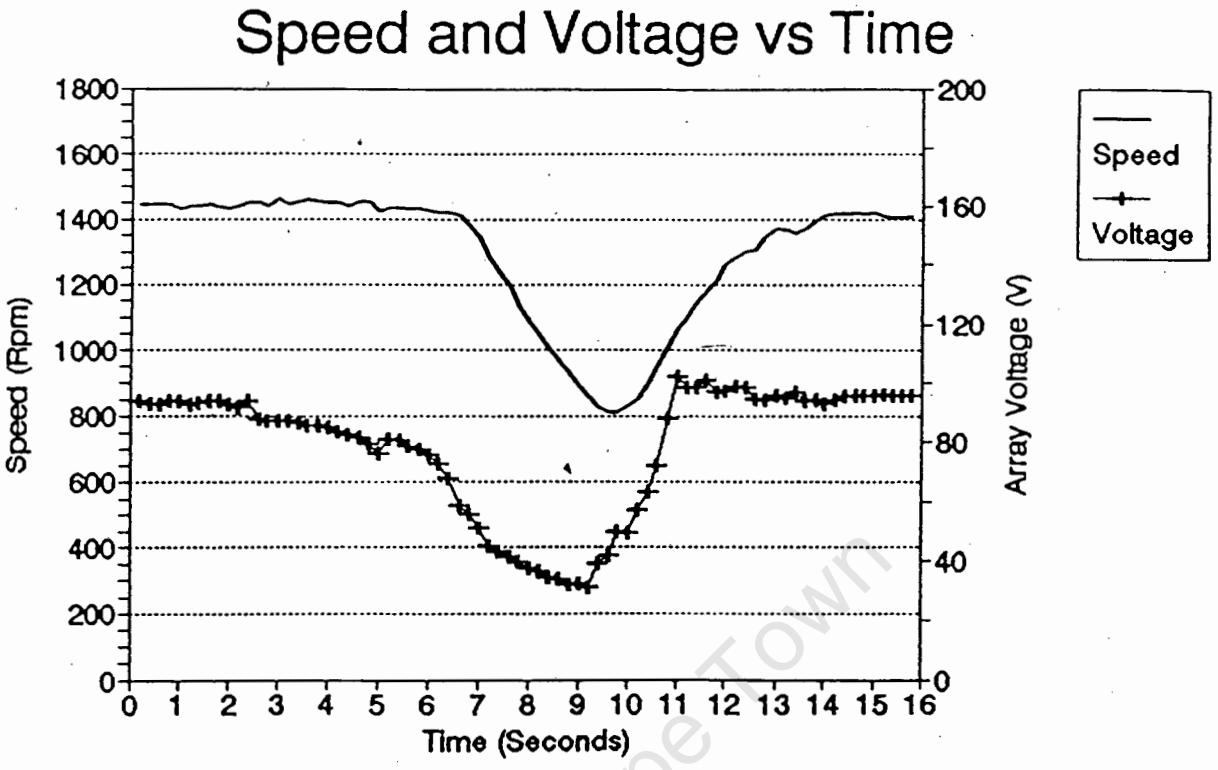

Figure 52: Controller Performance Following a Step Change in Irradiance.

The software implementation of this control method is illustrated in the following flow diagram.

SPEED CONTROLLER WITH OFFSET

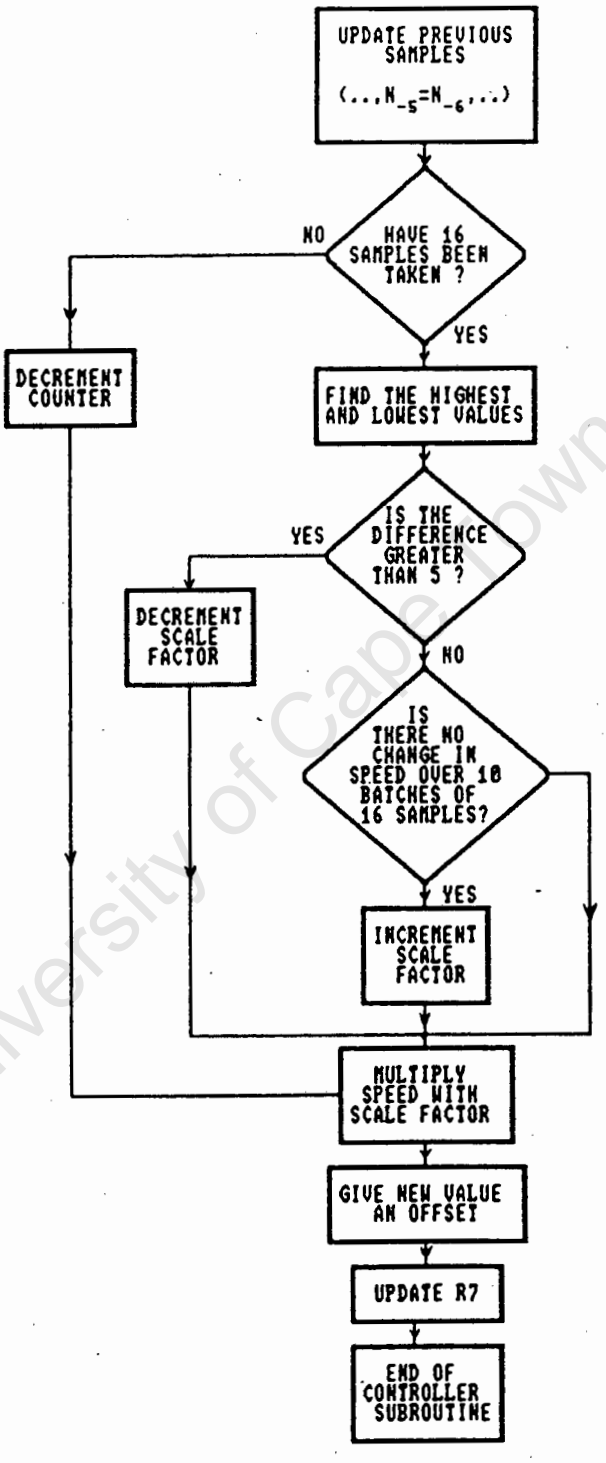

Figure 53: Flow Diagram of Controller with Offset

The microcontroller software thus ensured that if the speed remained constant too long, k was increased and if the speed oscillated too much then k was decreased. If oscillations were present then k would be decreased immediately, but the time constant to increase k was much slower. The graphs in figure 54 show the controller performance once the oscillations have settled to an acceptable level.

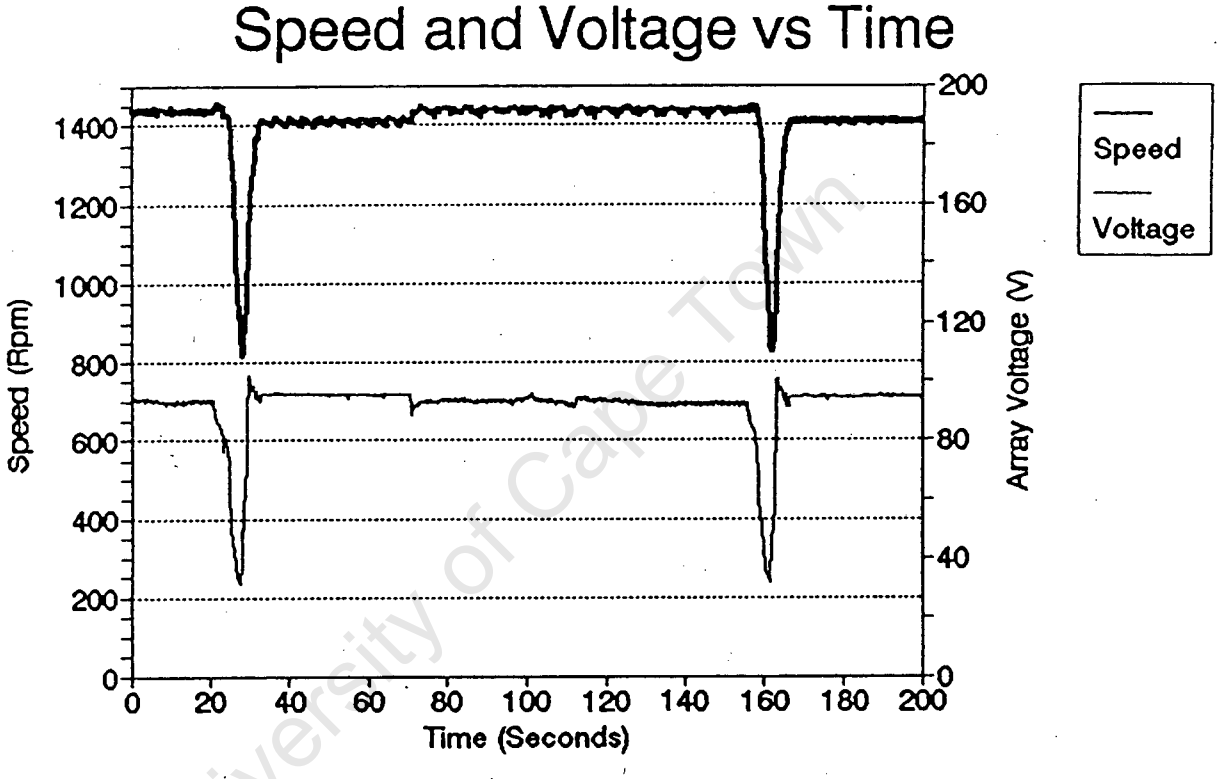

Figure 54: Controller Performance Once Oscillations have Settled

In order to evaluate the effectiveness of the controller, the position at which the motor operated on the power curve was monitored. The power curve of the panels was logged by connecting a variable resistor across the array output and measuring the voltage and current from the panels. Immediately thereafter the motor was run from the panels and once the motor had settled, the voltage and current were measured. In figure 55 the results of this test have been plotted at

different levels of insolation. As can be seen from the graph, the controller adequately tracks the peak power point.

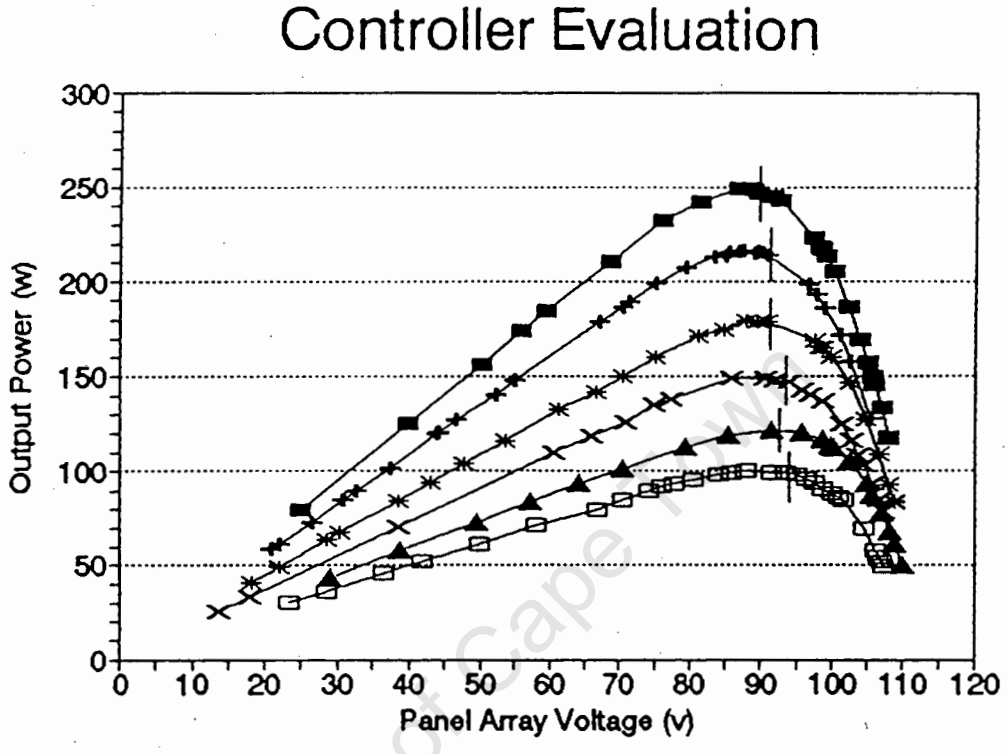

Figure 55: Evaluation of Speed Controller Performance

In order to simulate the pumping system as closely as possible, the motor was mounted to a closed circuit Mono positive displacement pump. The required head was simulated by means of a pressure gauge and a photograph of the experimental set-up is shown below.

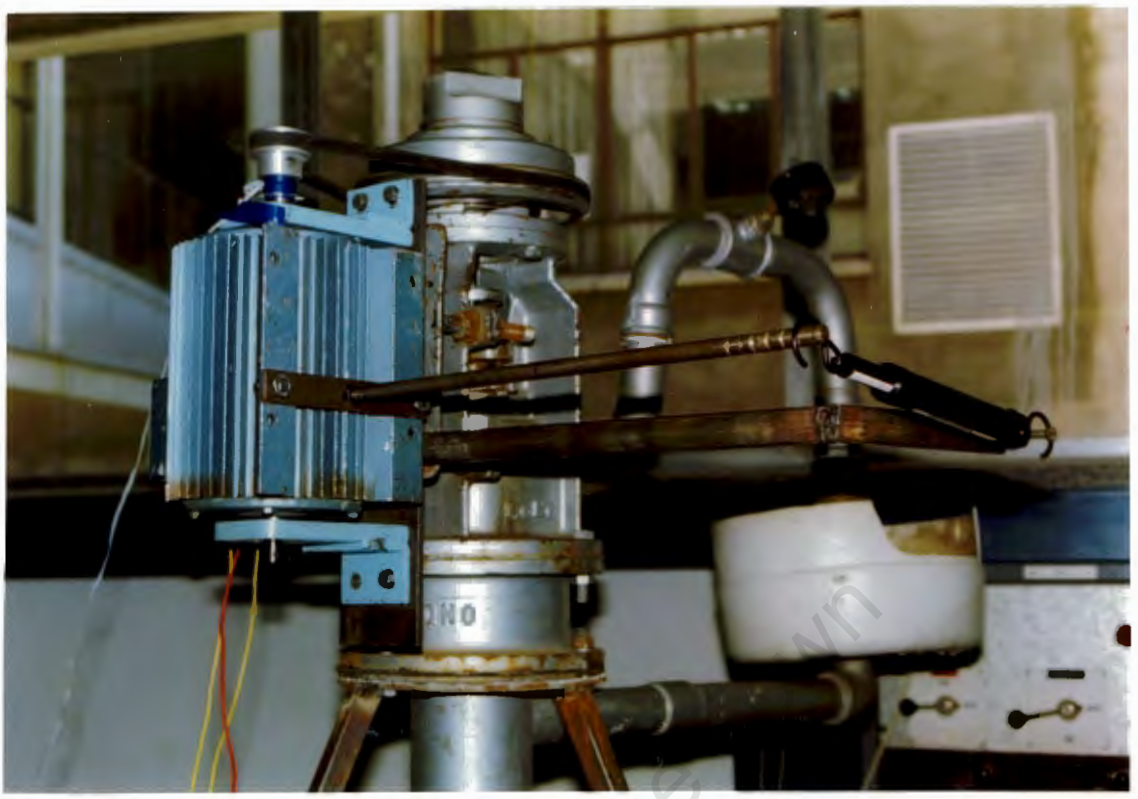

Figure 56: Laboratory Simulation of Pumping System

Although the periodic dips in the speed did not seriously affect the water delivery at most levels of irradiance, at lower levels the pump would stall after each oscillation. This was undesirable and a controller was designed which incorporated a combination of both speed and voltage control.

8.5.4. Combination of Voltage and Speed Control

By introducing the voltage as a control variable, the problem of pump inertia was eliminated. Operation of this controller combines constant voltage control with speed monitoring. The controller maintains the panel voltage at a reference value and this value is slowly adjusted until maximum speed is obtained. Although there is interaction between the two control loops, this can be neglected due to the large difference between the speed and voltage sampling times. The flow diagram on the following page illustrates the software

implementation of this controller. This controller proved to be the most effective as it ensured operation to within 1v of the voltage corresponding to the peak power point. This controller also provided a fast dynamic response which was able to maintain correct operation during shading of the array.

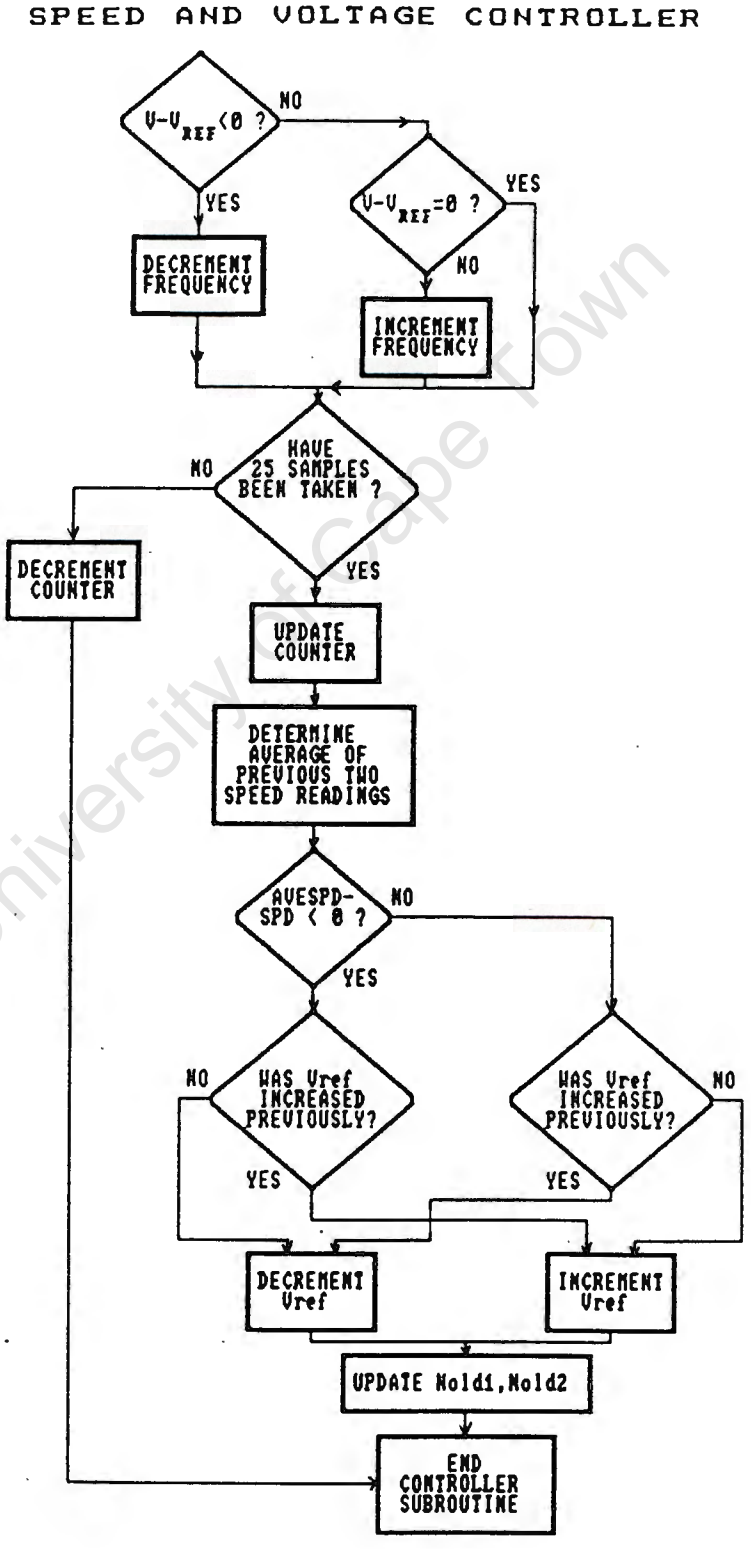

Figure 57: Flow Diagram of Voltage and Speed Controller

CHAPTER 9: FIELD TEST EVALUATION

A field test was conducted to compare the AC system with a Mono DC system. The pump that was chosen for the experiment was on a farm in the Middle Karoo, approximately 50 km from Oudshoorn. The farm requirements were ideal for the installation of a solar system. The farm does not have access to the ESCOM grid and the borehole is situated far from the homestead where access with normal vehicles has been denied. According to the farmer, significant savings have been made due to the minimal maintenance requirement of the solar pump as opposed to the previously used windmill.

A Mono solar pump had been installed on the farm and this made it possible to conduct comparative tests between the two systems. The size of the Mono system and the depth of the borehole were suitable for easy adaptation to the AC induction motor system.

Figure 58: The Borehole Pump Used for the Field Tests

9.1. SYSTEM OPTIMIZATION FOR FIELD TEST CONDITIONS

In order for the AC system to operate efficiently, it was necessary to determine the most suitable pulley ratio and to implement the optimum voltage frequency curve for the required torque.

The DC system installed by Mono Pumps comprised a positive displacement pump (Model S2M) powered by seven 49Wp panels. This delivers a peak input power of 343W, although this is unlikely to be realized due to the decreased performance of the panels at higher temperatures. According to Mono Pumps, the panels are derated by as much as 60% when determining the required system components. From the Siemens characteristic curves in Appendix 1.3, the panels can be derated by approximately 10% due to the effect of temperature.

At maximum input power it is desirable to run the motor at full speed in order to operate the motor efficiently over a wide speed range. At 80Hz the efficiency of the motor/inverter combination was assumed to be 70% and hence the input power to the pump was 216W. Since $T=P_o/w$, the desired torque of the motor is 0.89Nm.

The torque of the pump is not given directly from the manufacturer curves, but it can be calculated because the efficiency and input power as a function of speed are given. According to Mr M. van der Westhuizen, who installed the system, the head of the pump is 40m. From the characteristic curves of the pump at higher speeds, the torque of the pump at this head is 2.6 Nm. This is only a rough estimate as the characteristic curves do not appear to be accurate. From the characteristic curves, at lower speeds the torque increases, which is unlikely because of the constant torque speed characteristic of the pump.

9.2. FACTORS AFFECTING SYSTEM PERFORMANCE DURING TEST

The induction motor was mounted on the pump and supported on bearings so that the torque of the pump could be measured. The torque was found to be fairly constant and less than the expected value. The DC system had a pulley ratio of 3.6:1, which inhibited its performance because the gear ratio was too high. The DC-DC converter went into straight-through mode at fairly low irradiances and this imposed a limitation on the maximum speed of the DC motor.

For the AC system, a pulley ratio of 2.2:1 was chosen and this provided a maximum motor speed of 1725 Rpm, which was significantly less than the designed maximum speed of 2300 Rpm. The reason for this low speed was that the panels were only capable of delivering 255Wp, as opposed to an expected 308Wp. The poor performance of the panels was due to the fairly low irradiance levels which occurred during testing.

A further limitation on the AC system was that the controller did not yet operate effectively, as the controller was not yet fully refined. For the purposes of the field test, the output frequency of the controller was adjusted manually in order to operate at the peak power point of the panels. This did not prove to be an effective means of controlling the system because of the sensitivity of the panels when the peak power point was exceeded. In order to take measurements, the panels were operated slightly to the right of the maximum power point.

9.3. MEASUREMENTS TAKEN DURING FIELD TESTS

The field tests took place over two clear days, one day was used for the DC system, while the other was used for the AC system. The performance of each system was measured at different irradiance levels and the

irradiance was plotted as a function of time. The results of the two systems could then be plotted on the same time axes for comparative purposes.

In order to ensure that the two days had similar insolence levels, a pyranometer calibrated by the UCT Energy Research Institute was used. Although the meter has no guaranteed accuracy, it was judged to be accurate to within 2%. Since estimates of the irradiance were only required for comparative tests, this meter proved to be adequate for the purposes intended.

No temperature measurements were taken of the panels as the primary aim of the experiment was to assess the drive and pump performances. The pyranometer used was of a similar technology to the panels, so any deviations due to temperature change were automatically compensated for by this device, as it was also temperature sensitive.

For each system the operating characteristics were obtained at different irradiance levels. The variables which were measured were flow rate, pump speed, current, voltage, torque and irradiance level. Torque could only be measured on the AC system as the motor had to be mounted on bearings.

9.4. ASSESSMENT OF PUMP CHARACTERISTICS

The torque of the pump was measured over the required speed range and this is shown in the following graph.

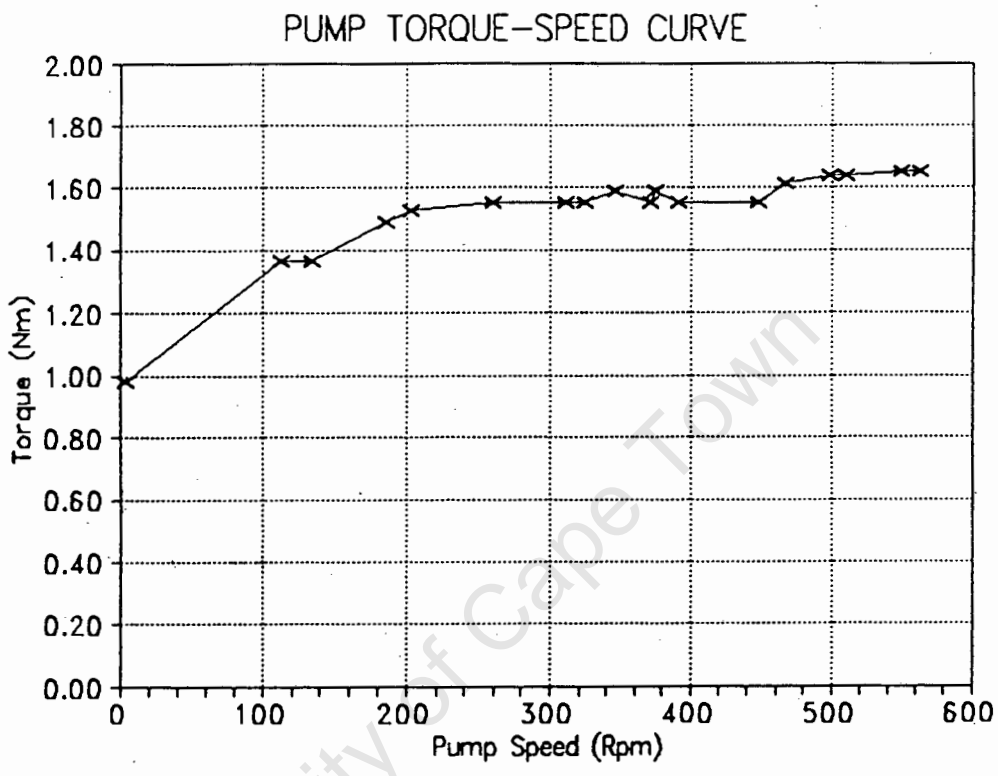

Figure 59: Torque Speed Curve for Field Test Pump

The pump torque levels off at 1.62 Nm, which is less than the expected torque of 2.6 Nm. Unfortunately the head could not be measured as it would have been necessary to remove the pump from the borehole with heavy lift equipment.

The flow rate was also measured as a function of speed and this was plotted in the graph below. Here there was good correlation between the experimental graph and the graph obtained from the Mono curves.

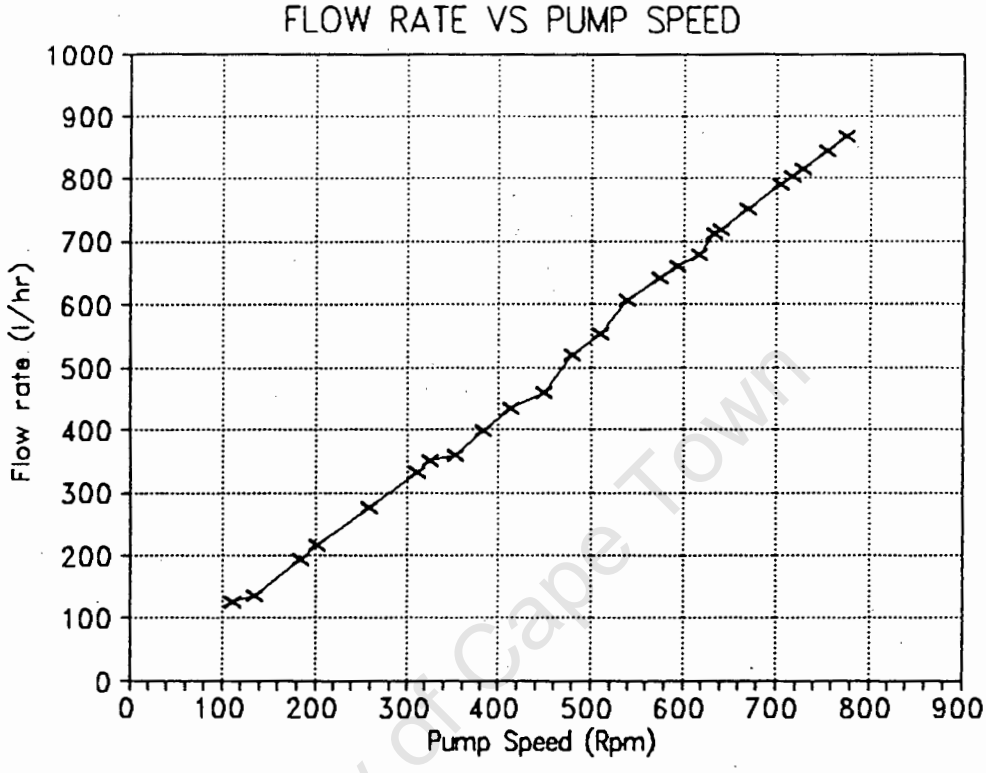

Figure 60: Experimental Curve of Flow Rate Versus Speed

9.5. COMPARATIVE TESTS BETWEEN DC AND AC SYSTEMS

The performance of the two systems was measured and compared. Particular attention has been given to the flow rate and efficiency of the two systems.

9.5.1. Panel Optimization Assessment

The graph in figure 61 shows the voltage of the two systems at different levels of irradiance. The DC system is not being used optimally, as at high levels of irradiance, when the converter goes into straight-

through mode, the voltage of the panels increases and the panels do not operate at their peak power point. It would appear that even at low levels of irradiance, the system operates sub-optimally, as the voltage is below that for maximum power point operation. The voltage of the AC system operates much closer to the peak power point, which is close to 90v.

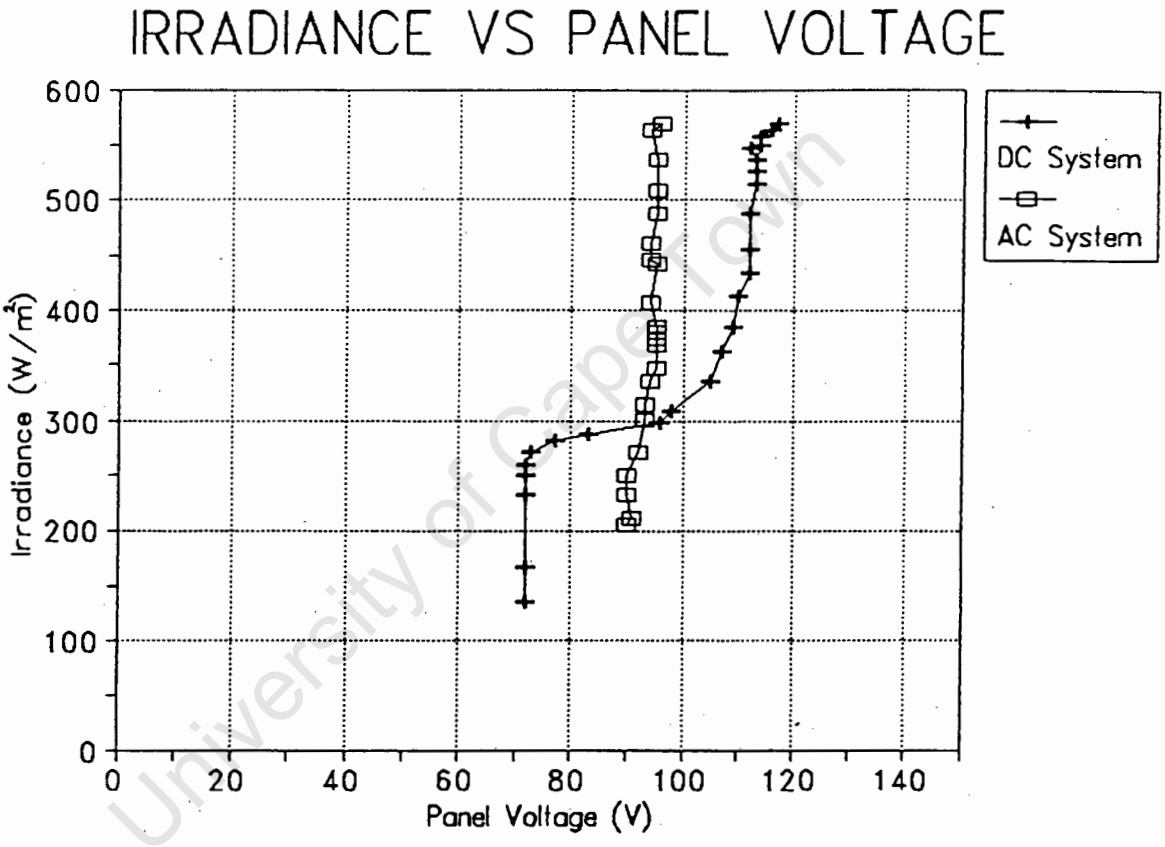

Figure 61: Panel Voltage for AC and DC Systems

9.5.2. Performance Comparison Between Two Systems

In order to compare the water delivery of the two systems, it was necessary to determine the irradiance level as a function of time for a typical clear day. Since the performance of the two systems was measured as

a function of irradiance, the graphs for both systems could be plotted as a function of time. The graph below shows the irradiance plotted over a half day.

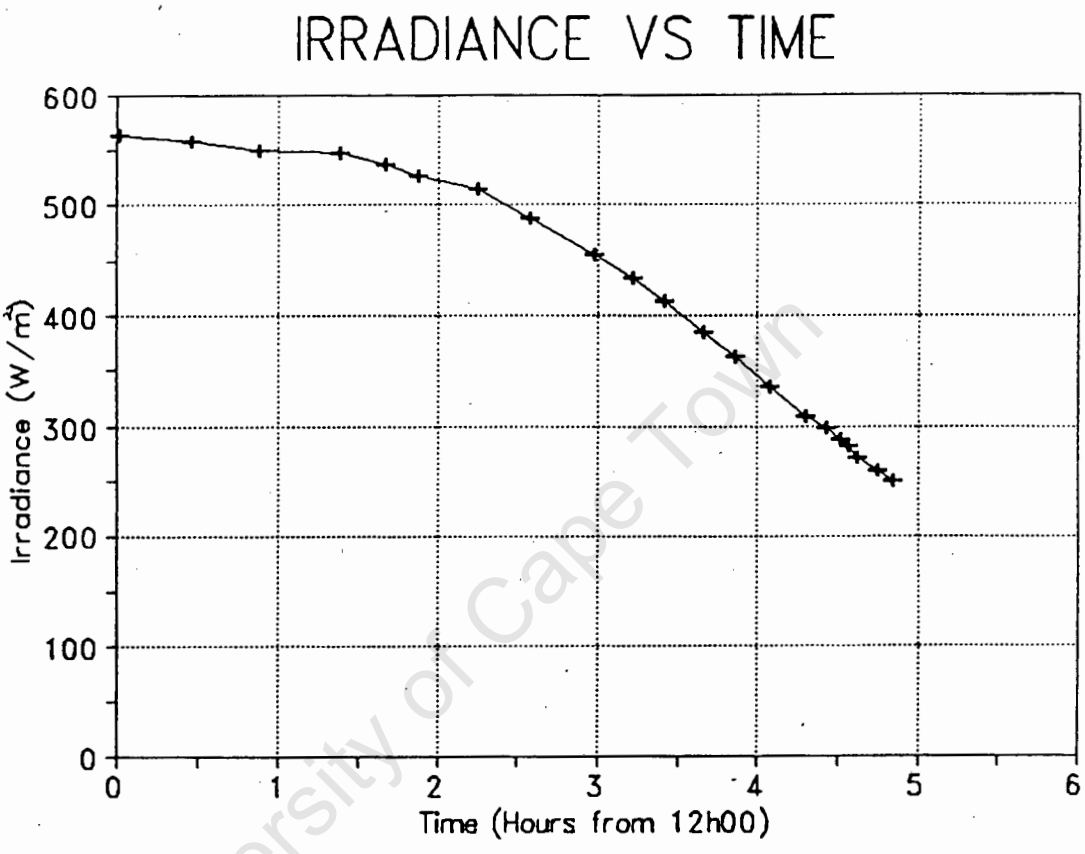

Figure 62: Irradiance versus Time for a Clear Day

Because of the lower pulley ratio of the AC system, it was capable of attaining a higher speed at high levels of irradiance than the DC system. As can be seen from the graph below, the efficiency of the AC system decreased relative to the DC system at lower levels of irradiance. This is to be expected as at low frequencies both the efficiency of the inverter and motor of the AC system decreases. The efficiency of the DC motor, on the other hand, remains constant over a wide speed range and

only the efficiency of the converter decreases at lower speeds.

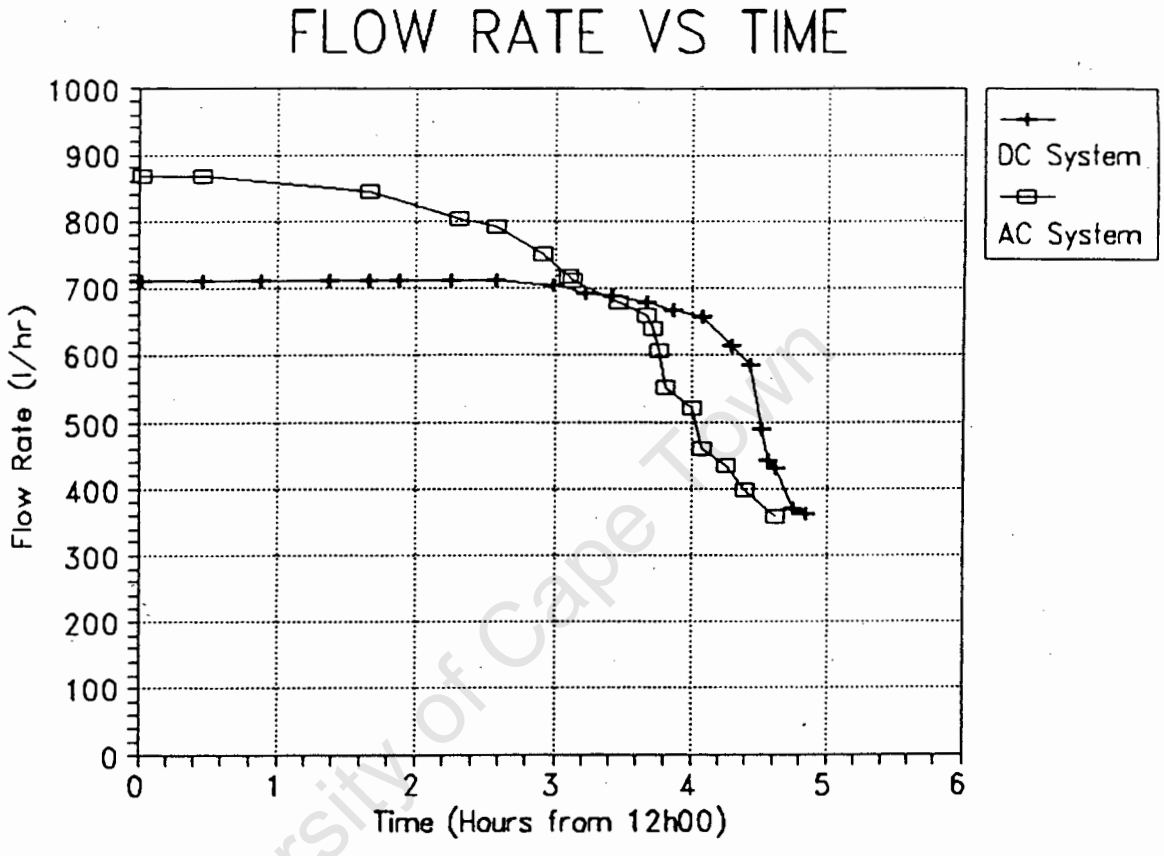

Figure 63: Flow Rate of AC and DC Systems

The efficiency of the two systems was also compared. In these tests the sub-optimal utilization of the panels in the DC system was not taken into account. The efficiency was determined from

$$E = \frac{P_{out}}{V_{dc} \cdot I_{dc}}$$

where P_{out} is determined from the flow rate and head of the system. Although the head has not been accurately determined, this is not necessary as the test is only being used for comparative purposes.

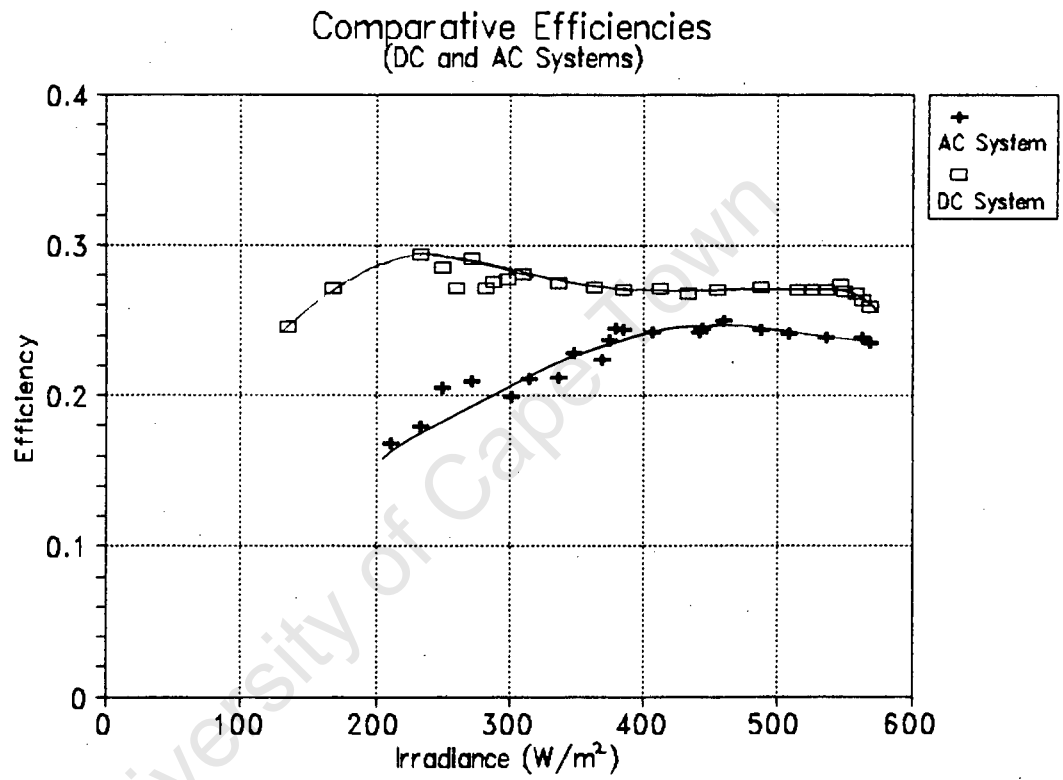

Figure 64: Comparative Efficiency of AC and DC Systems

The efficiency of the DC system increases with irradiance and peaks when the DC-DC converter goes into straight-through mode. Thereafter the efficiency decreases slightly because the panel voltage increases as operation moves away from the peak power point.

The efficiency of the AC system increases steadily and levels off at around 380 W/M^2. A larger portion of the

level efficiency would have been observed for either higher irradiance levels or a higher gear ratio. This is because operation in the 50 - 80 Hz range, at which the AC system is most efficient, was not obtained.

9.6. IMPROVEMENTS WITH ARRAY TRACKER

A graph was obtained of irradiance with the array in a fixed position and with the array facing the sun directly.

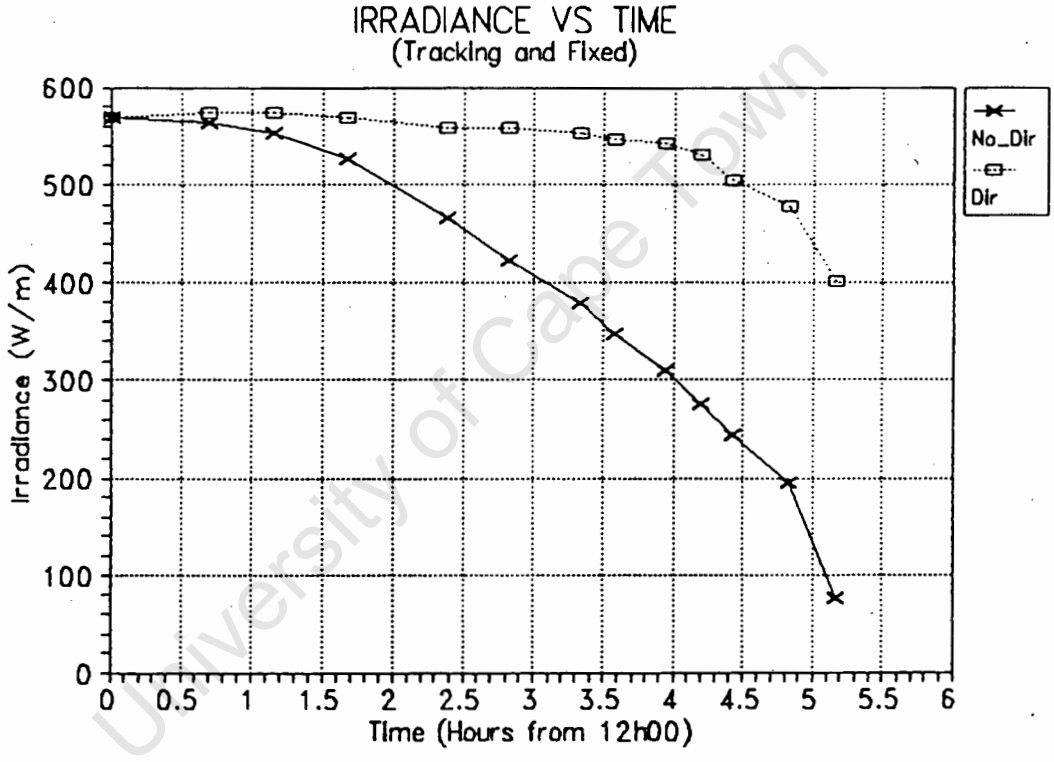

Figure 65: Irradiance with Directional and Fixed Array

Clearly a tracking device contributes significantly towards improving the system efficiency and particularly the motor and inverter efficiencies. With correct matching the motor would virtually always operate in the 40-80Hz region, where the efficiency of the motor and inverter is high.

CHAPTER 10: CONCLUSIONS

By using an induction motor system as opposed to a DC system, significant benefits can be obtained in terms of cost and reliability. The efficiency of the AC drive for a 300 Wp system was found to be 67%, which is only marginally less than that found in DC systems. For the seven panel system that was developed, the cost saving of the AC system more than covers the cost of an extra solar panel. This represents a 15% increase in the system input power and hence for the same investment the AC system provides a far better performance.

Based on the performance of the developed system the following conclusions can be drawn regarding the induction motor, inverter, microcontroller and array tracker:

1) The **induction motor** is a highly suited machine for a solar water pumping application for the following reasons:

   - The efficiency of the machine is 80% at its rated output and for a 300Wp system it is slightly less at 77%. This compares favourably with the DC motors which are being used commercially.

   - The cost of the induction motor is significantly less than that of a DC motor and it is a more reliable motor. If the trend of lower panel costs continues, the argument for using a cheaper motor will become stronger.

   - The efficiency of the induction motor decreases at lower supply frequencies, but this effect can be reduced by operating the motor above its rated frequency. This creates a wider frequency range (45 - 80Hz) over which the motor runs at maximum efficiency.

- The efficiency of the motor is optimized by implementing the derived optimum voltage frequency curve for the required load torque.

2) For a 300Wp system, the **inverter** efficiency proved to be high at 87%, which is adequate for this application. The motor and inverter combination therefore yielded an efficiency of 67%, which was maintained over a frequency range of 45 -80 Hz.

3) The flexibility in using a **microcontroller** has proved to be advantageous in the following areas:

   - Sufficient starting torque was obtained by pulsing the motor in such a way as to utilize the energy stored in the DC link capacitors.

   - Implementing a variable voltage frequency curve for different torques has been simple to achieve with pre-programmed tables.

   - A robust control method of optimizing the water delivery has been obtained by monitoring the pump speed and panel voltage. The peak power point of the panels has been very accurately tracked using this method.

4) With the incorporation of an array tracker into the system, the panel output will improve by approximately 20%. The use of a tracker for medium and large systems is justified because of the high cost of the panels.

CHAPTER 11: RECOMMENDATIONS

Based on the findings and conclusions of this thesis, the following recommendations are made:

1) All indications from the test results show that the system has been adequately developed and that it is ready for the industrialization phase to make it into a marketable product.

2) The system could be expanded to cover the following applications range:

   - A solar power range from 200 to 1000 Wp. To cover this range, the inverter capacity would have to be increased, but this is simple to achieve by paralleling the MOSFETs. For larger systems a larger motor would be required as the rating of the 0.75kW motor would be exceeded.

   - The Mono pump range allows for flexibility in applying the system to various heads. For the required power range the system can be applied to heads ranging from 15 - 140m. The pumps are not designed to operate efficiently for heads below 15m.

3) The motor should be matched to the pump so that the maximum frequency of operation continues up to 80Hz. This will provide a greater range of operation at a higher efficiency.

4) The microprocessor allows for the development of self-diagnosis software. With the addition of an inexpensive LCD display, it will be possible for untrained personnel to easily maintain the system.

5) Because the array tracker is a stand alone unit, it can be marketed separately for use in solar applications such as water pumping and battery charging.

REFERENCES

1: C.J.Weinberg, R.H.Williams: Energy from the Sun, Scientific American, Volume 263, Number 3, September 1990, p101.

2: K.Zweibel, P.Hersch: Basic Photovoltaic Principles and Methods, Van Nostrand Reinhold, New York, 1984, pp 6-9.

3: D.J.Sinclair: A Review of International and Local Developments in Photovoltaic Technology and Economics for Developing Areas, 1989, p 39.

4: M.J.Kamper: Photovoltaic Powered Water Pumps: A Feasibility Study, 1990, p5.

5: D.J.Sinclair: A Review of International and Local Developments in Photovoltaic Technology and Economics for Developing Areas, 1989, p 54.

6: R.Falzone: CSIRIS World Weekly, New Solar Device Using Silicon Technology Unveiled, March 19, 1992, p1.

7: N.W.Patapoff: Advanced Solar Energy Research May Yield Breakthrough, Research Newsletter, Southern California Edison, Vol. 20, No. 2, pp 1-4.

8: M.J.Kamper: Photovoltaic Powered Water Pumps: A Feasibility Study, 1990, pp 5-7.

9: C.J.Weinberg, R.H.Williams: Energy from the Sun, Scientific American, Volume 263, Number 3, September 1990, p102

10: D.J.Sinclair: A Review of International and Local Developments in Photovoltaic Technology and Economics for Developing Areas, 1989, pp 74-77.

11: R.G.Gosnell: Photovoltaic Water Pumping: A Case Study in Kwazulu, ERI, University of Cape Town, 1991, pp 51-52.

12: R.G.Gosnell: Photovoltaic Water Pumping: A Case Study in Kwazulu, ERI, University of Cape Town, 1991, p9.

13: F.Lasnier, T.G.Ang, K.S.Lwin: Solar Photovoltaic Handbook, 1st Edition, Thailand, 1988, pp 53-69.

14: K.Zweibel, P.Hersch: Basic Photovoltaic Principles and Methods, Van Nostrand Reinhold, New York, 1984, p 196.

15: P.D. van den Heever, J.H.R.Enslin: Preliminary Results of Comparative Tests Between a High-Efficiency Solar Panel/Wind Turbine Converter with Maximal Power Control and a Normal Regulator, p7.

16: F.Lasnier, T.G.Ang, K.S.Lwin: Solar Photovoltaic Handbook, 1st Edition, Thailand, 1988, p151.

17: F.Lasnier, T.G.Ang, K.S.Lwin: Solar Photovoltaic Handbook, 1st Edition, Thailand, 1988, p71.

18: R.G.Gosnell: Photovoltaic Water Pumping: A Case Study in Kwazulu, ERI, University of Cape Town, 1991, p88.

19: R.G.Gosnell: The Efficiency and Cost Effectiveness of the BP Submersible (Solar Jack) Photovoltaic Pump, Energy for Development Research Center, UCT, August 1991, p15.

20: M.J.Kamper: Photovoltaic Powered Water Pumps: A Feasibility Study, 1990, pp 7-8.

21: Space and New Technologies, AEG

22: P.Fraenkel: Water Pumping devices, Intermediate Technology Publications, London 1986, pp 40,53.

23: R.G.Gosnell: Photovoltaic Water Pumping: A Case Study in Kwazulu, ERI, University of Cape Town, 1991, p139.

24: R.G.Gosnell: Photovoltaic Water Pumping: A Case Study in Kwazulu, ERI, University of Cape Town, 1991, p

25: International Rectifier: HEXFET Designer's Manual, 4th Ed., California 1987, p I-29.

26: International Rectifier: HEXFET Designer's Manual, 4th Ed., California 1987, p I-74.

27: Mohan, Undeland, Robbins: Power Electronics: Converters, Applications and Design, Singapore 1989, p566.

28: Thomson Semiconductor Division: The Power Transistor in Its Environment, 1978, p192.

29: P.D.van den Heever, J.H.R.Enslin: Preliminary Results of Comparative Tests Between a High Efficiency Solar Panel/Wind Turbine Converter with Maximal Power Control and a Normal Regulator, University of Pretoria, p6.

30: Bosterling W, Keuter W, Tscharn M: To Control IGBT Modules: Characteristics-Electronics-Drives; AEG Technical Information, 1990, p13.

31: S.R.Bowes, R.R.Clements: Computer-Aided Design of PWM Inverter Systems; IEEE PROC, Vol 129, January 1982, p1.

32: P.N.Enjeti, P.D.Ziogas, J.F.Lindsay: Programmed PWM Techniques to Eliminate Harmonics: A Critical Evaluation; IEEE trans on Industry, Vol 26, No 2, March 1990, p302.

33: A.Zuckerberger, A.Alexandrovitz: Determination of Commutation Sequence with a View to Eliminating Harmonics in Microprocessor-Controlled PWM Voltage Inverter; IEEE Transactions on Industrial Electronics, Vol IE-33, No 3, August 1986, pp 262-270.

34: F.S.van der Merwe, N.C.Enslin: Extract from Electrical Machines and Their Applications, University of Stellenbosch, p145.

35: I.Miki, K.Matsuse, S.Nishiyama, A.Nassirharand: A Method of Determining Equivalent Circuit Parameters of an Induction Motor Fed from Various Inverters; Electric Energy Conference, Adelaide 1987, p416.

36: I.Miki, K.Matsuse, S.Nishiyama, A.Nassirharand: A Method of Determining Equivalent Circuit Parameters of an Induction Motor Fed from Various Inverters; Electric Energy Conference, Adelaide 1987, p413.

37: J.F.Gieras: Computation of Power losses of an Inverter-Fed Double Cage Induction Motor; 6th Mediteranean Electrotechnical Conference, 1991; IEEE Proceedings, Vol II, p1298.

38: P.L.Alger: Induction Machines, Their Behaviour and Uses; New York,1970; p417.

39: I.Miki, K.Matsuse, S.Nishiyama, A.Nassirharand: A Method of Determining Equivalent Circuit Parameters of an Induction Motor Fed from Various Inverters; Electric Energy Conference, Adelaide 1987, p413.

40: T.Kataoka, Y.Kandatsu, T.Akasaka: Measurement of Equivalent Circuit Parameters of Inverter Fed Induction Motors; IEEE transactions, 1987, p3015.

41: I.Miki, K.Matsuse, S.Nishiyama, A.Nassirharand: A Method of Determining Equivalent Circuit Parameters of an Induction Motor Fed from Various Inverters; Electric Energy Conference, Adelaide 1987, p414.

42: I.Miki, K.Matsuse, S.Nishiyama, A.Nassirharand: A Method of Determining Equivalent Circuit Parameters of an Induction Motor Fed from Various Inverters; Electric Energy Conference, Adelaide 1987, p41.

43: Hexfet Power Mosfet Designers Manual, International Rectifier; 1987; pI-144.

44: F.Lasnier, T.G.Ang, K.S.Lwin, T.Hemasuk: Photovoltaic Tests and Instrumentation: Pumping System, 1st Edition, Asian Institute of Technology, Thailand, 1988, p23.

45: J.J.Schoeman, J.D.van Wyk; A Simplified Maximal Power Controller for Terrestrial Photovoltaic Panel Arrays; IEEE Power Electronics Specialists Conference, June 1982; PESC '82 Record, pp 361-367.

APPENDICES

CONTENTS

1 COMPONENT CHARACTERISTICS
- 1.1 Electronic Components
- 1.2 Pump Characteristics
- 1.3 Solar Characteristics
- 1.4 Inverter Loss Calculation

2 PHOTOVOLTAIC TECHNOLOGY WITH IMPURE SILICON

3 FEASIBILITY OF USING INDUCTION MOTOR FOR SOLAR APPLICATION

4 MOTOR PERFORMANCE
- 4.1 Experimental Motor Characterization Curves
- 4.2 Predicted Motor Performance
- 4.3 Calculation of Motor Parameters

5 DESIGN OF SYSTEM COMPONENTS
- 5.1 Inverter Circuit
- 5.2 Microcontroller Circuit
- 5.3 DC-DC Converter Circuit
- 5.4 Array Tracking Circuit

6 OPERATION OF 8031 MICROCONTROLLER

7 PROGRAM LISTING
- 7.1 Microcontroller Program Listing
- 7.2 PWM ratios

8 HARMONIC CONTENT OF PWM WAVEFORMS

APPENDIX 1: COMPONENT CHARACTERISTICS

INTERNATIONAL RECTIFIER IOR

REPETITIVE AVALANCHE AND dv/dt RATED*

HEXFET® TRANSISTORS

N-CHANNEL

IRFP250
IRFP251
IRFP252
IRFP253

200 Volt, 0.085 Ohm HEXFET
TO-247AC (TO-3P) Plastic Package

The HEXFET® technology is the key to International Rectifier's advanced line of power MOSFET transistors. The efficient geometry and unique processing of this latest "State of the Art" design achieves: very low on-state resistance combined with high transconductance; superior reverse energy and diode recovery dv/dt capability.

The HEXFET transistors also feature all of the well established advantages of MOSFETs such as voltage control, very fast switching, ease of paralleling and temperature stability of the electrical parameters.

They are well suited for applications such as switching power supplies, motor controls, inverters, choppers, audio amplifiers and high energy pulse circuits.

Product Summary

Part Number	BV_{DSS}	$R_{DS(on)}$	I_D
IRFP250	200V	0.085Ω	33A
IRFP251	150V	0.085Ω	33A
IRFP252	200V	0.120Ω	27A
IRFP253	150V	0.120Ω	27A

Features:

- Isolated Central Mounting Hole
- Repetitive Avalanche Ratings
- Dynamic dv/dt Rating
- Simple Drive Requirements
- Ease of Paralleling

CASE STYLE AND DIMENSIONS

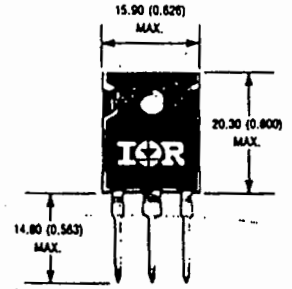

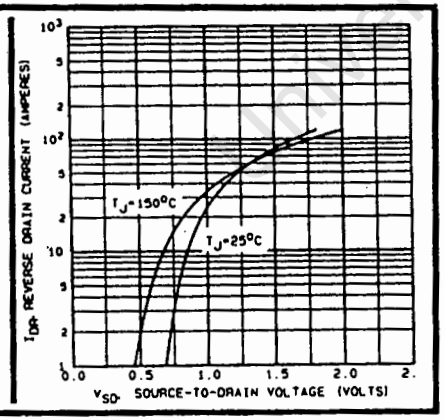

National Semiconductor

DS0026/DS0056 5 MHz Two Phase MOS Clock Drivers

General Description

DS0026/DS0056 are low cost monolithic high speed two phase MOS clock drivers and interface circuits. Unique circuit design provides both very high speed operation and the ability to drive large capacitive loads. The device accepts standard TTL outputs and converts them to MOS logic levels. They may be driven from standard 54/74 series and 54S/74S series gates and flip-flops or from drivers such as the DS8830 or DM7440. The DS0026 and DS0056 are intended for applications in which the output pulse width is logically controlled; i.e., the output pulse width is equal to the input pulse width.

The DS0026/DS0056 are designed to fulfill a wide variety of MOS interface requirements. As a MOS clock driver for long silicon-gate shift registers, a single device can drive over 10k bits at 5 MHz. Six devices provide input address and precharge drive for a 8k by 16-bit 1103 RAM memory system. Information on the correct usage of the DS0026 in these as well as other systems is included in the application note AN-76.

The DS0026 and DS0056 are identical except each driver in the DS0056 is provided with a V_{BB} connection to supply a higher voltage to the output stage. This aids in pulling up the output when it is in the high state. An external resistor tied between these extra pins and a supply higher than V^+ will cause the output to pull up to ($V^+ - 0.1V$) in the off state

For DS0056 applications, it is required that an external resistor be used to prevent damage to the device when the driver switches low. A typical V_{BB} connection is shown on the next page.

These devices are available in 8-lead TO-5, one watt copper lead frame 8-pin mini-DIP, and one and a half watt ceramic DIP, and TO-8 packages.

Features

- Fast rise and fall times—20 ns 1000 pF load
- High output swing—20V
- High output current drive—± 1.5 amps
- TTL compatible inputs
- High rep rate—5 to 10 MHz depending on power dissipation
- Low power consumption in MOS "0" state—2 mW
- Drives to 0.4V of GND for RAM address drive

PHOTODARLINGTON OPTOCOUPLERS

4N32
4N33

DESCRIPTION

The 4N32 and 4N33 have a gallium arsenide infrared emitter optically coupled to a silicon planar photo-darlington.

FEATURES & APPLICATIONS

- High isolation resistance – $10^{11}\Omega$
- High dielectric strength, input to output 2500 V RMS – 1 minute
- Low coupling capacitance – 1.0 pF
- Convenient package – plastic dual-in-line
- Long lifetime, solid state reliability
- Low weight – 0.4 grams
- UL recognized – File E50151

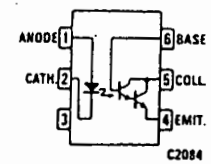

Equivalent Circuit

DC/DC Converters

800 Series 10 & 12 Watt

MODEL NUMBERS		INPUT VOLTAGE	OUTPUT VOLTAGE	OUTPUT CURRENT	INPUT CURRENT	
					NO LOAD	FULL LOAD
801	UM501	5 VDC	5 VDC	2000 mA	60 mA	3340 mA
803	UM502	5 VDC	12 VDC	940 mA	80 mA	3500mA
804	UM503	5 VDC	15 VDC	800 mA	100 mA	3670 mA
851	UM504	5 VDC	±12 VDC	±525 mA	130 mA	3840 mA
852	UM505	5 VDC	±15 VDC	±412 mA	180 mA	3780 mA
811	UM506	12 VDC	5 VDC	2000 mA	30 mA	1400 mA
813	UM507	12 VDC	12 VDC	940 mA	40 mA	1450 mA
814	UM508	12 VDC	15 VDC	800 mA	50 mA	1540 mA
861	UM509	12 VDC	±12 VDC	±525 mA	80 mA	1600 mA
862	UM510	12 VDC	±15 VDC	±412 mA	90 mA	1570 mA
821	UM511	24 VDC	5 VDC	2000 mA	20 mA	700 mA
823	UM512	24 VDC	12 VDC	940 mA	25 mA	700 mA
824	UM513	24 VDC	15 VDC	800 mA	25 mA	730 mA
871	UM514	24 VDC	±12 VDC	±525 mA	50 mA	780 mA
872	UM515	24 VDC	±15 VDC	±412 mA	50 mA	760 mA
831	UM516	28 VDC	5 VDC	2000 mA	20 mA	600 mA
833	UM517	28 VDC	12 VDC	940 mA	25 mA	590 mA
834	UM518	28 VDC	15 VDC	800 mA	30 mA	620 mA
881	UM519	28 VDC	±12 VDC	±525 mA	50 mA	650 mA
882	UM520	28 VDC	±15 VDC	±412 mA	50 mA	650 mA
841	UM521	48 VDC	5 VDC	2000 mA	20 mA	350 mA
843	UM522	48 VDC	12 VDC	940 mA	25 mA	350 mA
844	UM523	48 VDC	15 VDC	800 mA	25 mA	360 mA
891	UM524	48 VDC	±12 VDC	±525 mA	30 mA	390 mA
892	UM525	48 VDC	±15 VDC	±412 mA	40 mA	380 mA

MOTOROLA

TL494

SWITCHMODE PULSE WIDTH MODULATION CONTROL CIRCUITS

The TL494 is a fixed frequency, pulse width modulation control circuit designed primarily for Switchmode power supply control. This device features:

- Complete Pulse Width Modulation Control Circuitry
- On-Chip Oscillator With Master Or Slave Operation
- On-Chip Error Amplifiers
- On-Chip 5 Volt Reference
- Adjustable Dead-Time Control
- Uncommitted Output Transistors Rated to 500 mA Source Or Sink
- Output Control For Push-Pull Or Single-Ended Operation
- Undervoltage Lockout

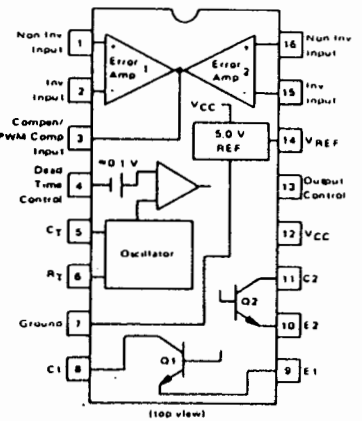

The TL494C is specified over the commercial operating range of 0°C to 70°C. The TL494I is specified over the industrial range of – 25°C to 85°C. The TL494M is specified over the full military range of – 55°C to 125°C.

SWITCHMODE PULSE WIDTH MODULATION CONTROL CIRCUITS

SILICON MONOLITHIC INTEGRATED CIRCUITS

J SUFFIX
CERAMIC PACKAGE
CASE 620-10

N SUFFIX
PLASTIC PACKAGE
CASE 648-06

ORDERING INFORMATION

Device	Temperature Range	Package
TL494CN	0° to + 70°C	Plastic DIP
TL494CJ	0° to + 70°C	Ceramic DIP
TL494IN	– 25° to + 85°C	Plastic DIP
TL494IJ	– 25° to + 85°C	Ceramic DIP
TL494MJ	– 55° to + 125°C	Ceramic DIP

SOLAR / SONKRAG | TYPICAL AVERAGE PERFORMANCE / TIPIESE GEMIDDELDE POMPPRESTASIE | PUMP SIZE / POMP GROOTTE S2M

MAX HEAD 150m / MAKS HOOGTE
MAX SPEED 1200 r/min / MAKS SPOED
40 mm COLUMN 13mm SHAFT UP TO 150 m — 40 mm PYPE 13mm STANGE TOT OP 150 m
mm COLUMN mm SHAFT UP TO m — mm PYPE mm STANGE TOT OP m
MONOSTROOM DISCHARGE HEAD UP TO 150 m — MONOSTROOM ONTSLAGKOP TOT OP 150 m
DISCHARGE HEAD UP TO m — ONTSLAGKOP TOT OP m
MINIMUM STARTING TORQUE 3 N.m — MINIMUM DRAAIMOMENT

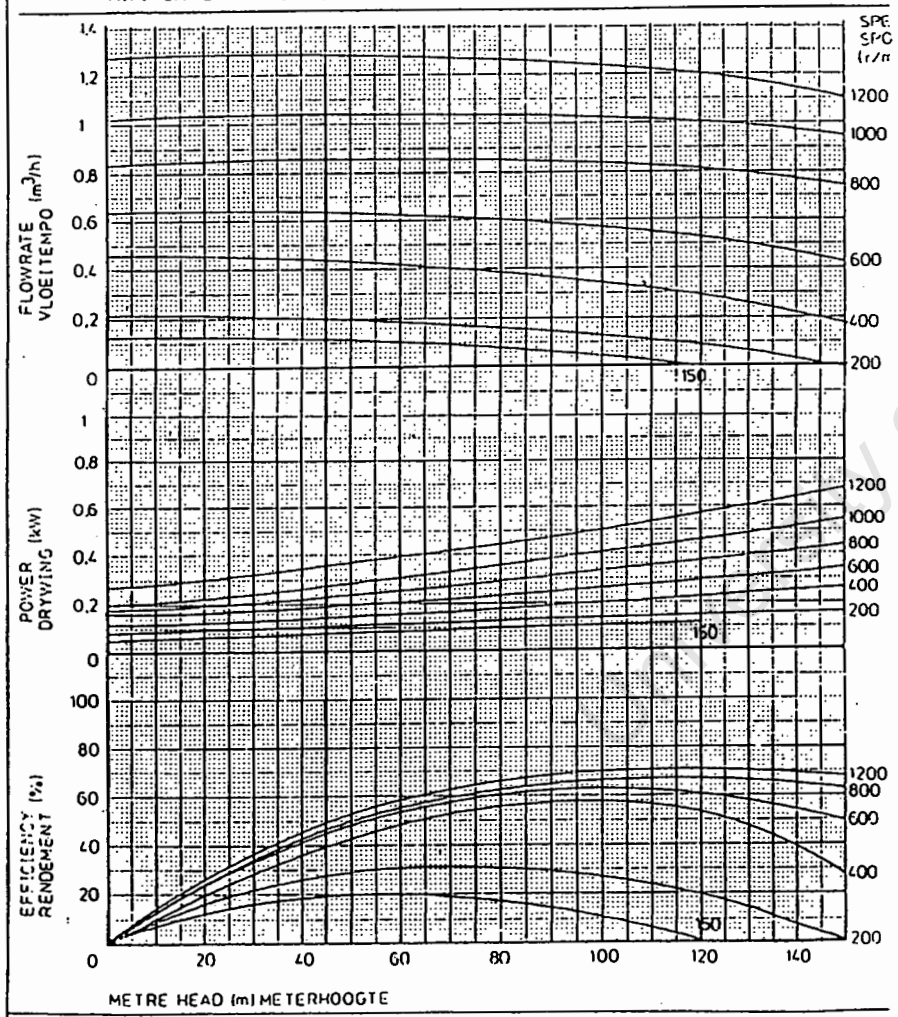

ISSUE 09/89 — MONO PUMPS — PAGE NO: TA4.8-1

SOLAR / SONKRAG | TYPICAL AVERAGE PERFORMANCE / TIPIESE GEMIDDELDE POMPPRESTASIE | PUMP SIZE / POMP GROOTTE S9M

MAX HEAD 150m / MAKS HOOGTE
MAX SPEED 1000 r/min / MAKS SPOED
40 mm COLUMN 13mm SHAFT UP TO 150m — 40 mm PYPE 13mm STANGE TOT OP 150m
50 mm COLUMN 16mm SHAFT UP TO 150m — 50mm PYPE 16mm STANGE TOT OP 150m
MONOSTROOM DISCHARGE HEAD UP TO 150m — MONOSTROOM ONTSLAGKOP TOT OP 150m
DISCHARGE HEAD UP TO m — ONTSLAGKOP TOT OP m
MINIMUM STARTING TORQUE 6 N.m — MINIMUM DRAAIMOMENT

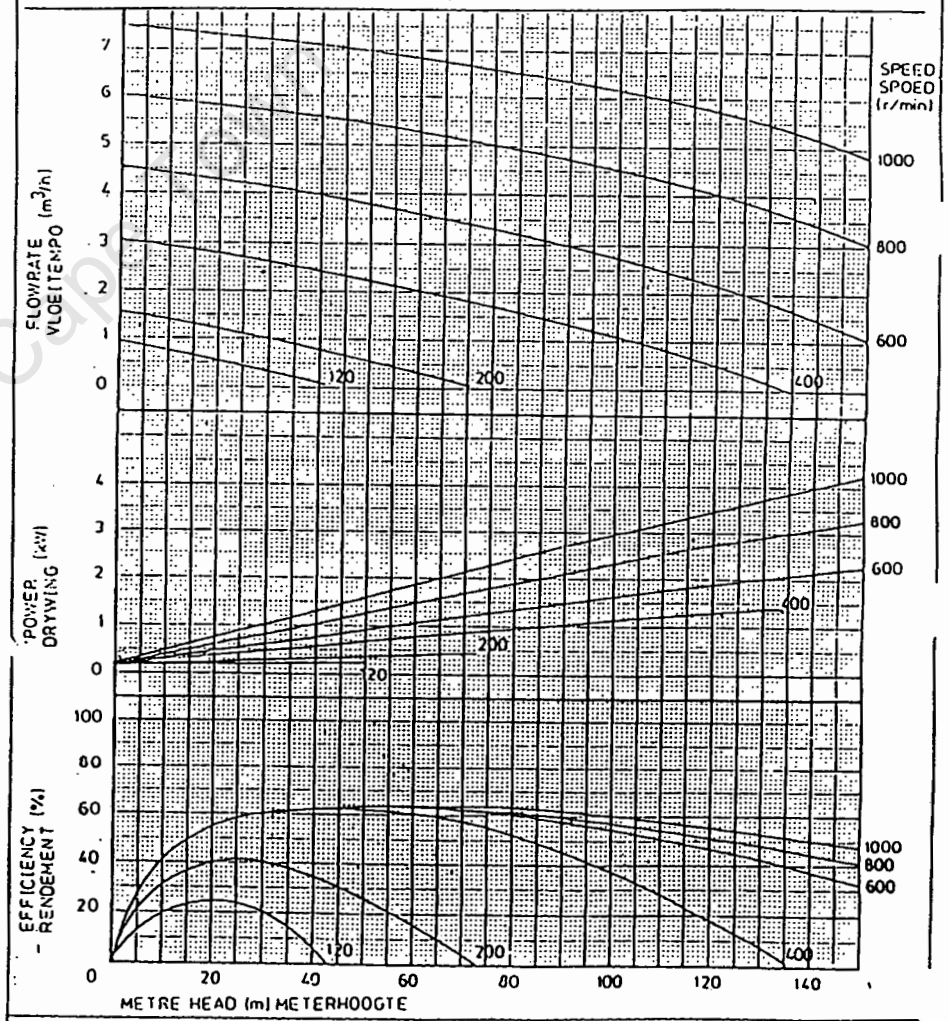

ISSUE 09/89 — MONO PUMPS — PAGE NO: TA4.8-4

SOLAR SONKRAG	TYPICAL AVERAGE PERFORMANCE TIPIESE GEMIDDELDE POMPPRESTASIE	PUMP SIZE POMP GROOTTE S6L

MAX HEAD		75m	MAKS HOOGTE		
MAX SPEED		1500 r/min	MAKS SPOED		
40mm COLUMN	13mm SHAFT UP TO	75m	40mm PYPE	13mm STANGE TOT OP	75m
mm COLUMN	mm SHAFT UP TO	m	mm PYPE	mm STANGE TOT OP	m
MONOSTROOM DISCHARGE HEAD UP TO		75m	MONOSTROOM ONTSLAGKOP TOT OP		75m
DISCHARGE HEAD UP TO		m	ONTSLAGKOP TOT OP		m
MINIMUM STARTING TORQUE		5.5 N.m.	MINIMUM DRAAIMOMENT		

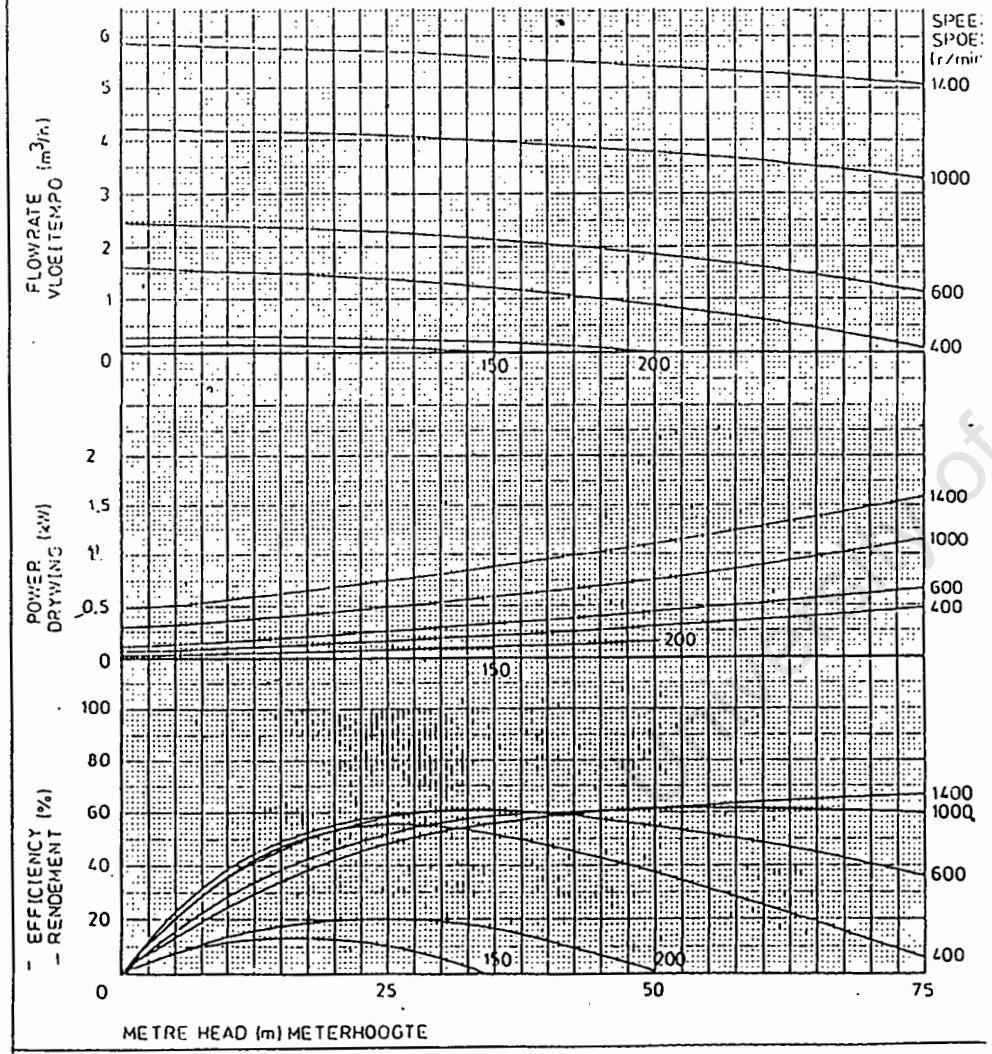

SOLAR SONKRAG	TYPICAL AVERAGE PERFORMANCE TIPIESE GEMIDDELDE POMPPRESTASIE	PUMP SIZE POMP GROOTTE S4L

MAX HEAD		75m	MAKS HOOGTE		
MAX SPEED		1500 r/min	MAKS SPOED		
40mm COLUMN	13mm SHAFT UP TO	75m	40mm PYPE	13mm STANGE TOT OP	75m
mm COLUMN	mm SHAFT UP TO	m	mm PYPE	mm STANGE TOT OP	m
MONOSTROOM DISCHARGE HEAD UP TO		75m	MONOSTROOM ONTSLAGKOP TOT OP		75m
DISCHARGE HEAD UP TO		m	ONTSLAGKOP TOT OP		m
MINIMUM STARTING TORQUE		4.5 N.m.	MINIMUM DRAAIMOMENT		

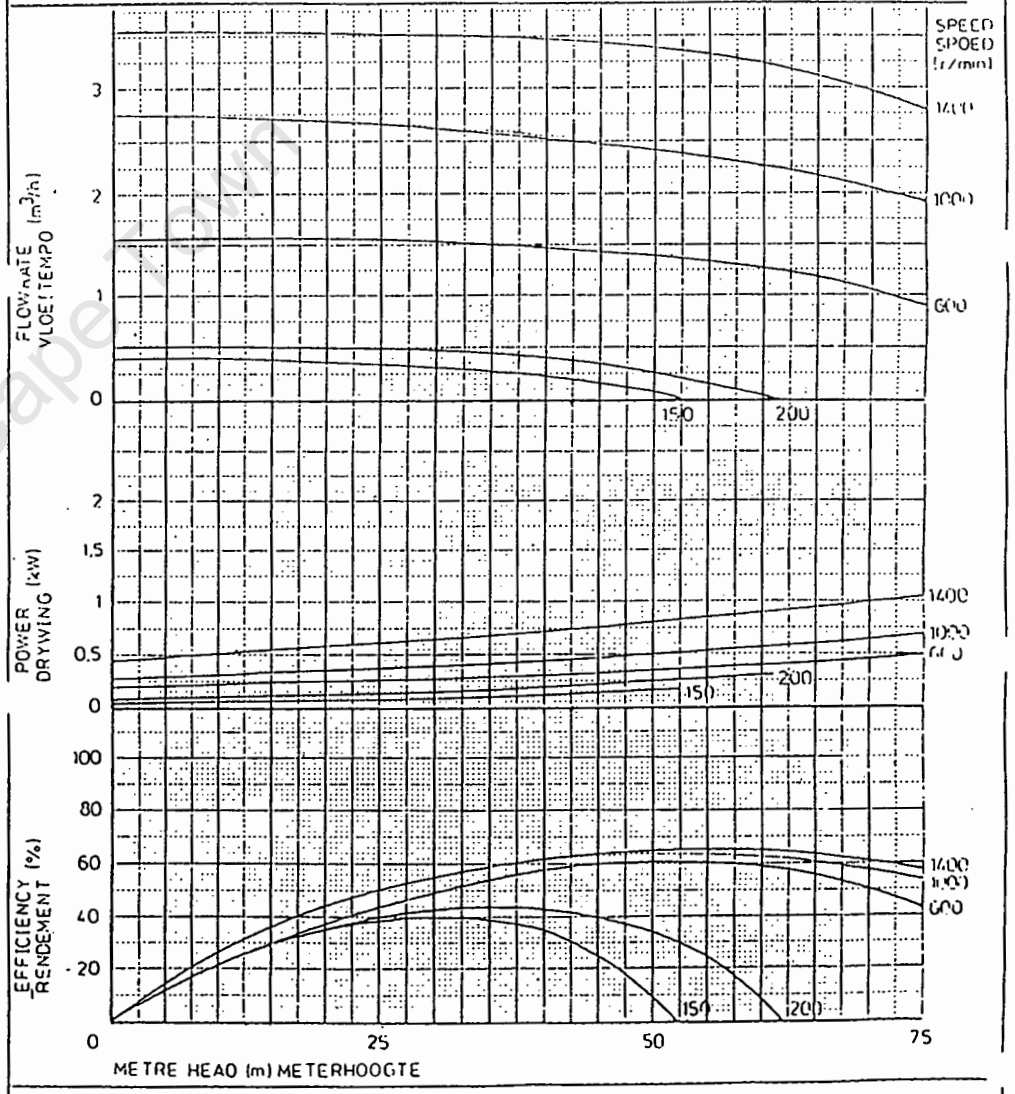

SOLAR / SONKRAG	TYPICAL AVERAGE PERFORMANCE / TIPIESE GEMIDDELDE POMPPRESTASIE	PUMP SIZE / POMP GROOTTE	S 12 L

MAX HEAD	75m	MAKS HOOGTE	
MAX SPEED	1100 r/m	MAKS SPOED	
50 mm COLUMN 16 mm SHAFT UP TO	75m	50 mm PYPE 16 mm STANGE TOT OP	75m
mm COLUMN mm SHAFT UP TO	m	mm PYPE mm STANGE TOT OP	m
MONOSTROOM DISCHARGE HEAD UP TO	75m	MONOSTROOM ONTSLAGKOP TOT OP	75m
DISCHARGE HEAD UP TO	m	ONTSLAGKOP TOT OP	m
MINIMUM STARTING TORQUE	5.8 N.m.	MINIMUM DRAAIMOMENT	

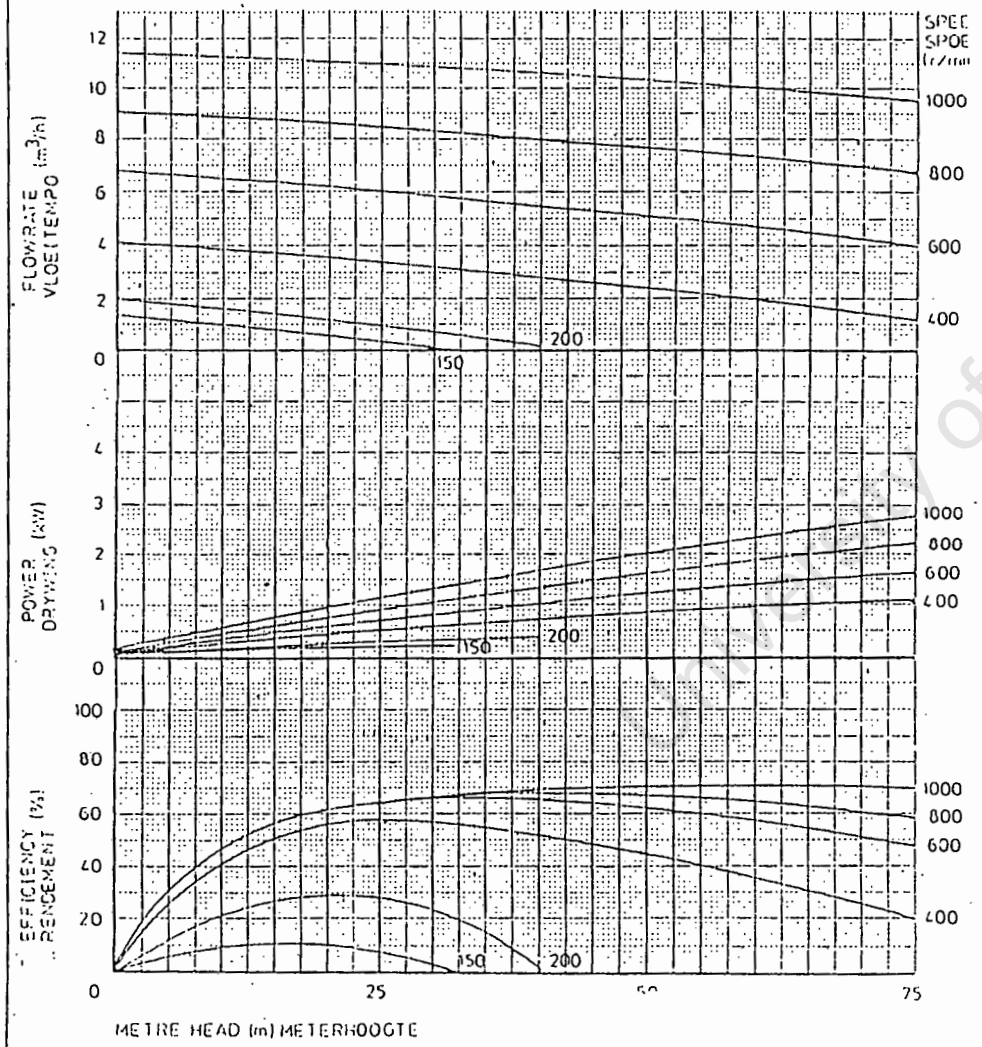

WINDMILL / WINDMEUL	TYPICAL AVERAGE PERFORMANCE / TIPIESE GEMIDDELDE POMPPRESTASIE	PUMP SIZE / POMP GROOTTE	W30L

MAX HEAD	75 m	MAKS HOOGTE	
MAX SPEED	1500 r/min	MAKS SPOED	
80 mm COLUMN 22 mm SHAFT UP TO	75 m	80 mm PYPE 22 mm STANGE TOT OP	75 m
mm COLUMN mm SHAFT UP TO	m	mm PYPE mm STANGE TOT OP	m
MONOMEESTER DISCHARGE HEAD UP TO	75 m	MONOMEESTER ONTSLAGKOP TOT OP	75 m
DISCHARGE HEAD UP TO	m	ONTSLAGKOP TOT OP	m
MINIMUM STARTING TORQUE	25 N.m	MINIMUM DRAAIMOMENT	

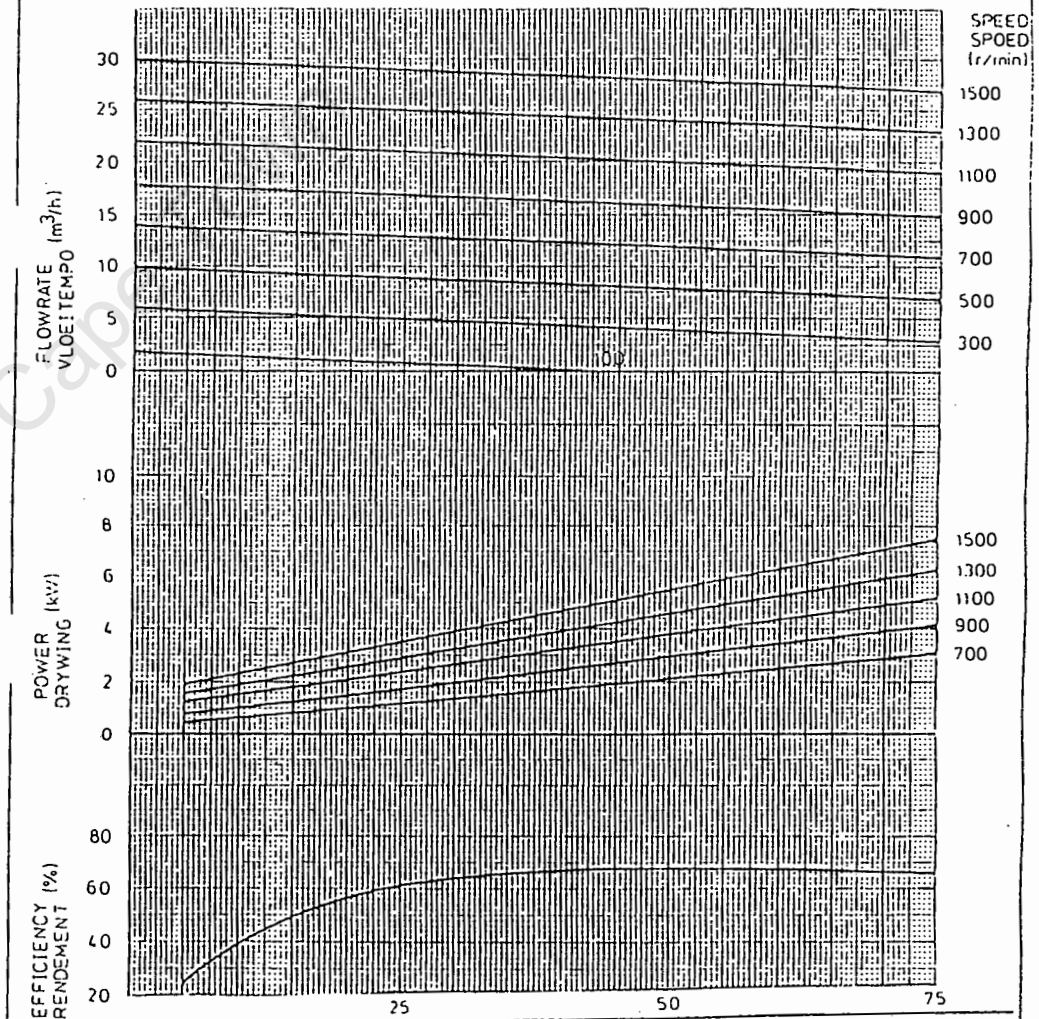

ISSUE Nº 1
DATE 25/10/85

CURVE Nº C 259

1 PANEL (47Wp) TESTED @ 900 W/M²					2 PANEL (94Wp) TESTED @ 900 W/M²				
TOTAL HEAD		FLOW RATE		MOTOR CURRENT	TOTAL HEAD		FLOW RATE		MOTOR CURRENT
FEET	METERS	GPH*	LPH Δ	AMPS	FEET	METERS	GPH	LPH	AMPS
5	1.5	60	227	1	5	1.5	120	454	1.65
25	7.6	54	204	1.2	25	7.6	108	409	2.0
50	15.2	45	182	1.3	50	15.2	99	375	2.2
75	22.8	39	147	1.95	75	22.8	90	341	2.5
100	30.4	33	125	2.1	100	30.4	81	307	2.9
125	38.1	30	114	2.5	125	38.1	75	284	3.0
150	45.7	27	102	2.75	150	45.7	66	250	3.1
175	53.3	24	91	2.92	175	53.3	57	216	3.15
200	60.9	21	79	3.05	200	60.9	45	170	3.2
225	68.6	19	72	3.2	225	68.5	33	125	3.25

BATTERY (12V)					BATTERY (24V)				
TOTAL HEAD		FLOW RATE		MOTOR CURRENT	TOTAL HEAD		FLOW RATE		MOTOR CURRENT
FEET	METERS	GPH	LPH	AMPS	FEET	METERS	GPH	LPH	AMPS
5	1.5	48	182	1	5	1.5	102	386	1.2
25	7.6	45	170	1.3	25	7.6	96	363	1.7
50	15.2	39	148	1.5	50	15.2	90	341	2.0
75	22.8	36	136	1.7	75	22.8	85	322	2.3
100	30.4	35	132	2.1	100	30.4	81	307	2.6
125	38.1	30	114	2.5	125	38.1	75	284	3.0
150	45.7	27	102	2.75	150	45.7	71	269	3.1
175	53.3	24	91	3.0	175	53.3	66	250	3.2
200	60.9	18	68	3.1	200	60.9	60	227	3.25
225	68.6	13	50	3.2	225	68.6	55	208	3.3

* GPH - U.S. GALLONS PER HOUR Δ LPH - LITERS PER HOUR

PLEASE NOTE: 1) PUMP OUTPUTS AND MOTOR CURRENTS MAY VARY
2) PUMPS RUN ON SOLAR PANELS SHOULD USE A CURRENT BOOSTER TYPE CONTROLLER

FOR MORE INFORMATION AND TO ORDER, CONTACT:

OTTO SOLAR

R. W. Otto

P.O. BOX 276
UPINGTON
8800
TEL/054 2 3878
STEENKAMPSPAN

PHOTOVOLTAIC SOLAR PANELS
WINDCHARGERS
BATTERIES & LIGHTS
INVERTERS
PUMPS & FILTERS
DC MOTORS & SOLAR HEATING
AND INTERRELATED PRODUCTS

ALL POWER
E.P.c.c. Q.P. b.k.

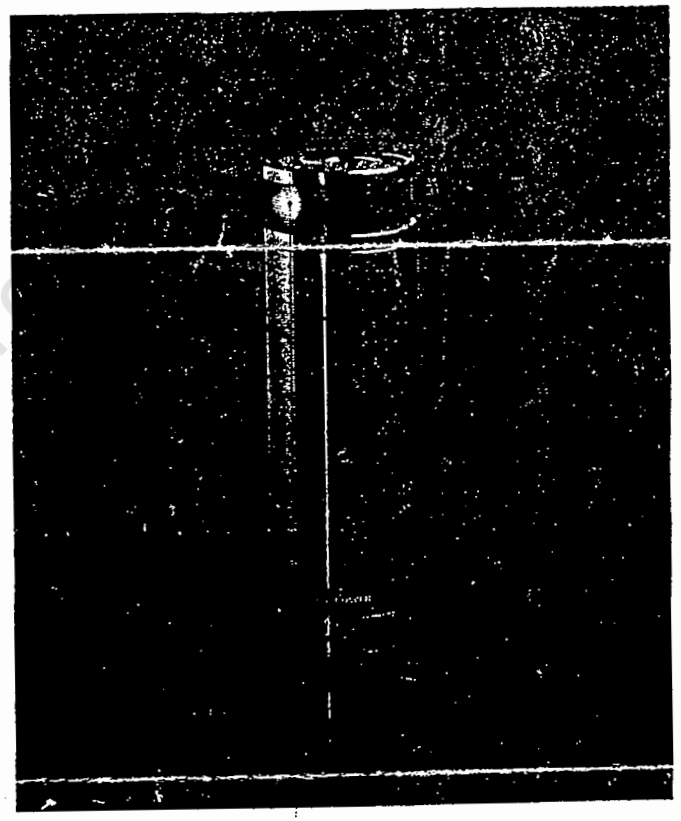

SOLARJACK

THE REVOLUTIONARY NEW D.C. SOLAR SUBMERSIBLE PUMP, A UNIQUE SUBSTITUTE FOR A WINDMILL

SYSTEM PERFORMANCE:

Water capacity in m^3/day as a function of irradiation ($^{kWh}/_{m^2day}$) and head (m).

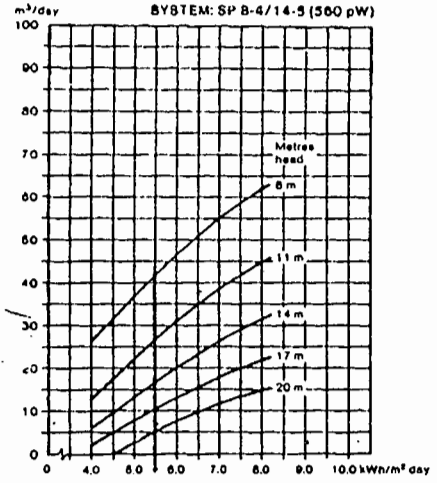

Total number of modules: 14
Modules in series in one row: 7
Number of rows in parallel: 2

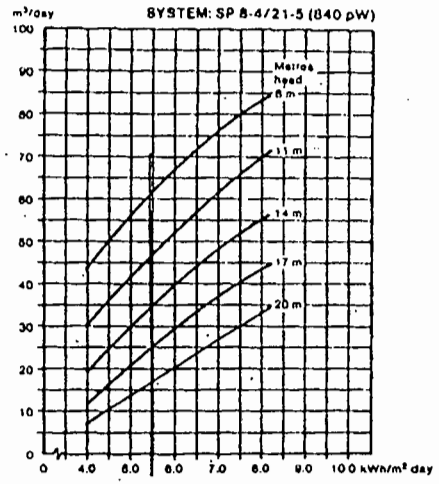

Total number of modules: 21
Modules in series in one row: 7
Number of rows in parallel: 3

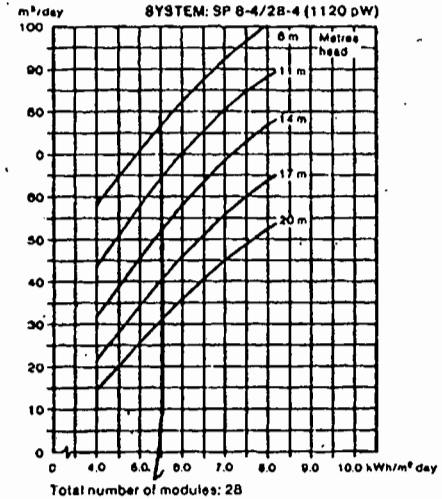

Total number of modules: 28
Modules in series in one row: 7
Number of rows in parallel: 4

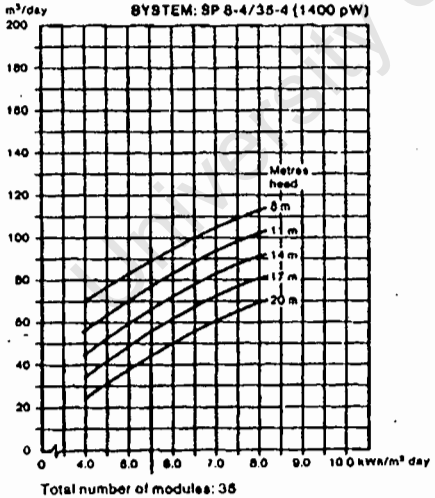

Total number of modules: 35
Modules in series in one row: 7
Number of rows in parallel: 5

The performance curves are based on the conditions:
AMBIENT TEMPERATURE : 30°C average, 35°C max., 20°C min.
OUTPUT VOLTAGE : 101.5 VDC.

SYSTEM PERFORMANCE:

Water capacity in m^3/day as a function of irradiation ($^{kWh}/_{m^2day}$) and head (m).

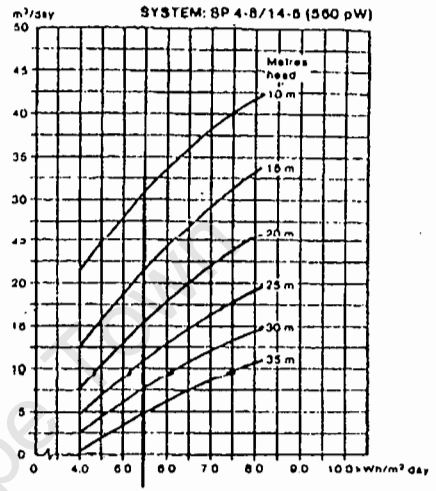

Total number of modules: 14
Modules in series in one row: 7
Number of rows in parallel: 2

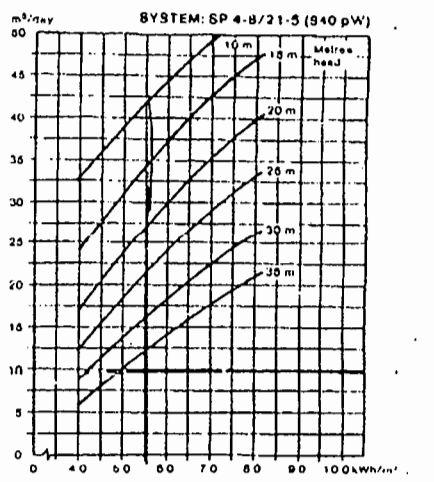

Total number of modules: 21
Modules in series in one row: 7
Number of rows in parallel: 3

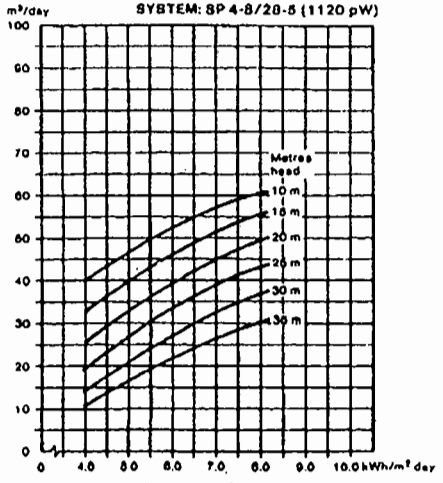

Total number of modules: 28
Modules in series in one row: 7
Number of rows in parallel: 4

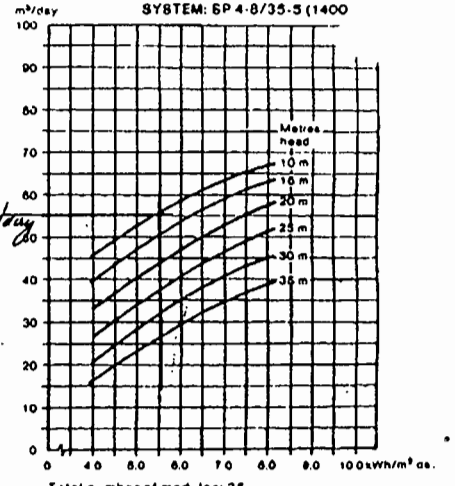

Total number of modules: 35
Modules in series in one row: 7
Number of rows in parallel: 5

The performance curves are based on the conditions:
AMBIENT TEMPERATURE : 30°C average, 35°C max., 20°C min.
OUTPUT VOLTAGE : 101.5 VDC.

SIEMENS

SPECIFICATIONS

ELECTRICAL CHARACTERISTICS:

	MODEL M55	*MODEL M45*	*MODEL M75*	*MODEL M40*	*MODEL M65*	*MODEL M35*	*MODEL M20*
Max. Power, Watts	53 Wp	48 Wp	48 Wp	40 Wp	43 Wp	37 Wp	22 Wp
Open Circuit Voltage (Voc)	21.7	21.6	19.8	19.5	18.0	18.0	18.0
Short Circuit Current (Isc)	3.35	3.2	3.35	3.0	3.32	3.0	1.68
Voltage at Load	17.4	17.3	15.9	15.7	14.6	14.5	14.5
Amperage at Load	3.05	2.78	3.02	2.55	2.95	2.56	1.52

NOTES: 1. Rated electrical characteristics are within 10% of measured values at Standard Test Conditions of: 1000 W/m^2, 25°C cell temperature and solar spectral irradiance per ASTM E 892.

2. Under normal conditions, a photovoltaic module may experience conditions that produce more current and/or voltage than reported at standard test conditions. Accordingly, the values of Isc and Voc marked on UL Listed modules should be multiplied by a factor of 1.25 when determining component voltage ratings, conductor capacities, fuse sizes, and size of controls connected to the module output. Refer to Section 690-8 of the National Electric Code for an additional multiplying factor of 1.25 which may be applicable.

PHYSICAL CHARACTERISTICS:

No. Cells in Series	36	36	33	33	30	30	30
Cell Size	4.05" (102.9 mm) Sq.						1/2 of 4.05" cell
Module - Length:	50.9" (1293 mm)		48" (1219 mm)		42.6" (1083 mm)		22.4" (569 mm)
- Width:	13" (330 mm)						
- Depth:	1.4" (36 mm)						
Weight	12.6 lb (5.7 kg)		11.6 lb (5.2 kg)		10.5 lb (4.8 kg)		5.6 lb (2.5 kg)
Mounting Holes: Across Length of Module	49.8" (1265 mm)		46.9" (1191 mm)		41.5" (1054 mm)		21.3" (541 mm)
Inner Set	25.3" (643 mm)						None
Across the Width of Module	11.3" (287 mm)						
Diameter	0.26" (6.6 mm)						
Wiring Provisions	2 Junction Covers for 8 to 14 AWG wire						18 AWG, 2-conductor cable attached
Maximum System Open Circuit Voltage	600V						20V
Factory Installed Bypass Diodes	Yes	Yes	Yes	Yes	Yes	Yes	No

APPLICATION

M55, M45, M75 and M40

The M55 and M45 have 36 cells in series and are well suited for all solar electric applications, including battery charging in hot climates, direct connection to a DC motor, and operation with a peak power tracking controller.

The M75 and M40, with 33 cells in series, are designed as battery charging solar electric modules for all but the hottest climates where the extra voltage of the M55 or M45 may be needed. The M75 and M40 may also be used for direct connection in selected DC motor applications. A regulator is needed when the M55, M45, M75 or M40 are used to charge a battery.

M20, M65 and M35

These self-regulating modules are designed for direct battery connection. They are intended to meet the needs of those who require electrical power for many applications, particularly lighting, appliances, and other equipment in remote homes, or on recreational vehicles and boats. While the M20 is intended for 12 volt systems only, the M65 and M35 are rated for use in high voltage systems.

Each of these modules has 30 cells in series. They are self-regulating when used to charge batteries of the proper capacity because their electrical characteristics are an excellent match to the charging requirements of a lead acid battery. For more information, see the section titled *'Self Regulation.'*

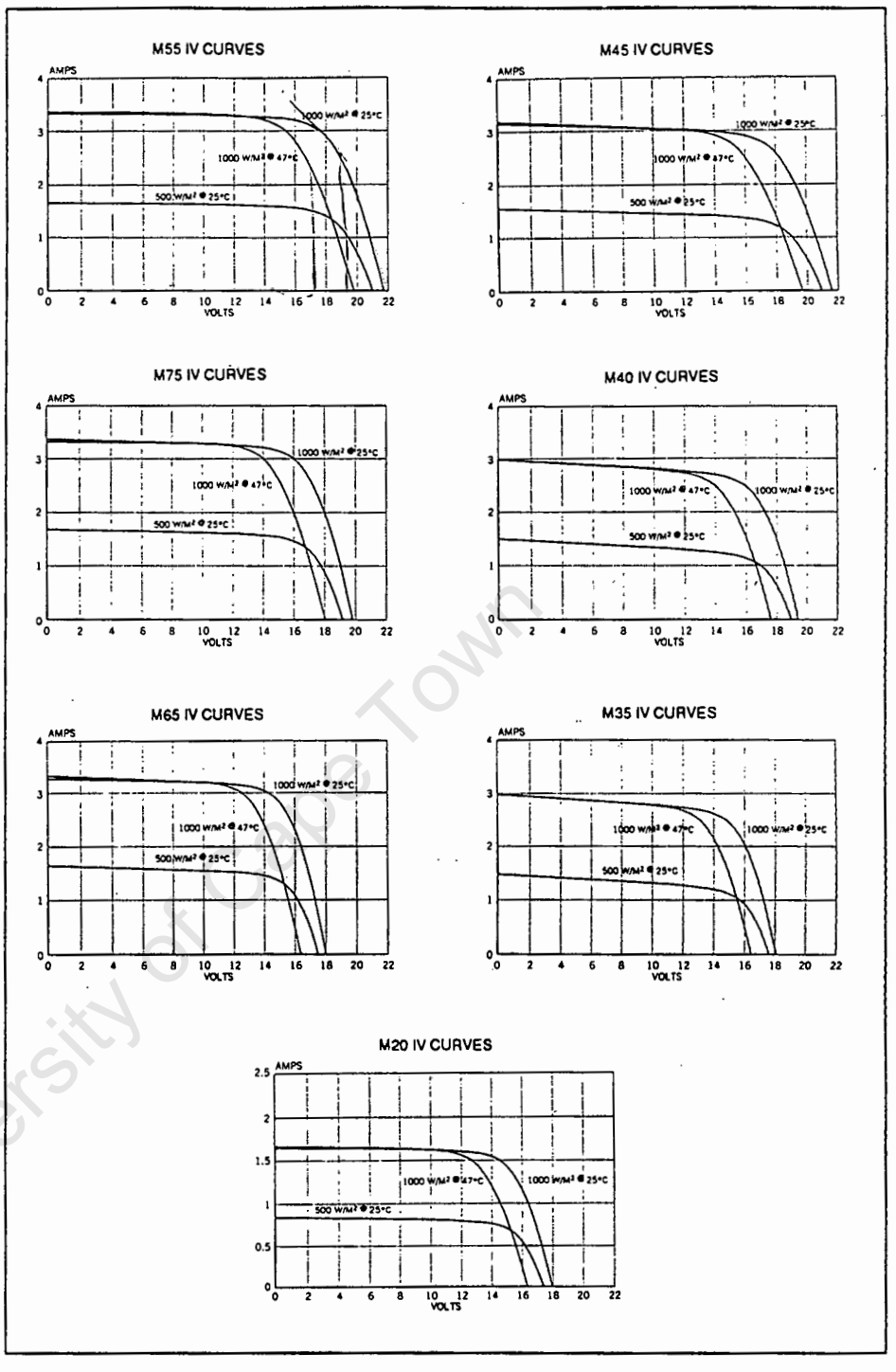

General Information

These Siemens Solar Industries modules utilize high efficiency, single crystal silicon cells which are laminated to tempered glass with EVA. The cells are antireflective coated for improved efficiency. The laminated package is supported by a metal frame. The wiring method provided for each module does not require the use of special cable assemblies. All the modules are equipped with junction covers into which interconnect wiring is installed, except the M20, which is equipped for interconnection with a two-conductor cable.

Using HEXFET III in PWM Inverters for Motor Drives and UPS Systems

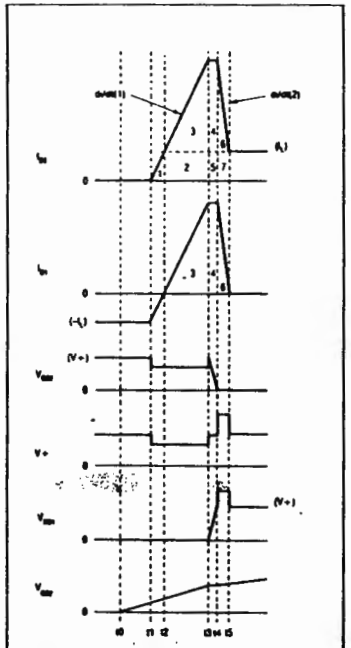

Figure 14. Idealized turn-on waveforms for Fig. 13

Calculation of Switching Losses

The losses incurred during commutation may be predicted from Figure 14.

Conduction losses are ignored and only those losses produced when devices are simultaneously carrying current and blocking voltage are considered.

The losses in HEXFET 2 are as follows:

t1 - t2. The drain current builds up to the value of the load current while supporting the available voltage (dc rail voltage minus the drop in the circuit inductance.)

t2 - t3. Both the load current and the rising diode recovery current are carried while blocking the available voltage.

t3 - t4. Some losses incurred during this period but not a significant amount since the drain voltage is falling rapidly.

As the losses in HEXFET 2 decline the losses in HEXFET 1 increase:

t3 - t4. Some losses incurred as the voltage across the diode increases.

t4 - t5. The final phase of the diode recovery current producing losses, since the diode now blocks the available voltage.

The losses in HEXFET 1 and HEXFET 2 have two basic origins: the conduction of the load current by HEXFET 2 during the period t0 - t3 and the passage of diode recovery current through both devices during the period t1 - t5.

Estimation of the total losses is simplified if it is assumed that the effect of the circuit inductance is neutral, in that while it reduces the available voltage during one part of the switching cycle, it increases it during another. (If the breakdown voltage of the HEXFET is exceeded then this energy will be dissipated in avalanche breakdown, which is permitted with HEXFET III devices, provided the repetitive avalanche ratings are respected). Therefore, if it is assumed that all charge transfer takes place between supply rails whose voltage remains constant at the nominal value, the total losses during commutation of the inverter leg may be calculated approximately by multiplying the dc rail voltage by the various transfers of charge that occur. If a series inductor with its own clamping circuit is located in the dc rail, then energy stored in this inductor is not dissipated in the HEXFET but in the clamp circuit.

Thus the losses in HEXFET 2 are given by the rail voltage times the charge represented by areas 1, 2 and 3 in Figure 14. The losses in HEXFET 1 are given by the rail voltage times the charge represented by area 6. Losses associated with areas 4 and 5 are distributed between the two HEXFETs. The total losses are therefore approximately equal to the rail voltage multiplied by the charge represented by areas 1, 2, 3, 4, 5 and 6. Areas 3, 4 and 6 represent the Q_{RR} of the diode. Areas 1, 2 and 5 are a function of the load current and the rate of rise of diode recovery current, di/dt.

Thus the total commutation energy loss may be expressed as:

$$E = V_{dc}\,[(\text{Area } 3 + \text{Area } 4 + \text{Area } 6) + (\text{Area } 2 + \text{Area } 5) + (\text{Area } 1)]$$

$$= V_{dc}\left[Q_{RR} + I_L\,(t_4 - t_2) + (t_2 - t_1)^2 \cdot \frac{di/dt}{2}\right]$$

$$= V_{dc}\left(Q_{RR} + I_L\sqrt{\frac{2Q_{RR}}{di/dt}} + \frac{I_L^2}{2di/dt}\right) \qquad (1)$$

Where I_L is the load current at the time of the commutation.

This gives the energy loss for the pulse at one value of drain current. From Figure 20 it can be seen that to a first approximation Q_{RR} is linearly related to drain current and therefore, assuming a sinusoidal load current, can be expressed as:

$$Q_{RR}(i) = K \cdot i(t) = K \cdot I_L \sin(\omega t),$$

and:

$$Q_{RR}(\theta) = K \cdot K_L \sin\theta, \text{ where } 0 < \theta < \pi \qquad (2)$$

Substituting into (1) for Q_{RR} gives the energy dissipated when a commutation occurs at a current value of I sin θ.

$$E(\theta) = V_{dc}\left[K \cdot I_L \sin\theta + I_L \sin\theta\sqrt{\frac{2KI_L \sin\theta}{di/dt}} + \frac{I_L^2 \sin^2\theta}{2\,di/dt}\right] \qquad (3)$$

The power loss due to commutation during that switching cycle is given by:

$$P(\theta) = V_{dc} \cdot f_s\left[K \cdot I_L \sin\theta + I_L \sin\theta\sqrt{\frac{2KI_L \sin\theta}{di/dt}} + \frac{I_L^2 \sin^2\theta}{2\,di/dt}\right] \qquad (4)$$

Where f_s is the switching frequency

Since the switching frequency is approximately two orders of magnitude greater than the output frequency, equation (4) can be taken as representing the power loss due to commutation expressed as a continuous function of θ.

The average power loss due to commutation during one half cycle of output current is therefore given by:

$$P_{ave} = \frac{V_{dc} \cdot f_s}{\pi}\left[K \cdot I_L \int_0^\pi \sin\theta\,d\theta + I_L\sqrt{\frac{2KI_L}{di/dt}}\int_0^\pi \sin^{3/2}\theta\,d\theta + \frac{I_L^2}{2di/dt}\int_0^\pi \sin^2\theta\,d\theta\right]$$

$$= \frac{V_{dc} \cdot f_s \cdot I_L}{\pi}\left[2K + 2.47\sqrt{\frac{KI_L}{di/dt}} + 0.785\,\frac{I_L}{di/dt}\right] \qquad (5)$$

This represents the sum of the commutation power loss in both HEXFETs in that inverter "leg" (or "pole").

The process for determining the commutation losses is therefore:

(1) Read the typical value for Q_{RR} from the data sheet.

(2) Adjust Q_{RR} for di/dt and temperature, using the graphs shown in Figure 17 and Figure 19.

(3) Using this value of Q_{RR} obtain K from the equation:

$$K = Q_{RR} / I_F$$

where I_F is the test current specified in the typical Q_{RR} rating in the data sheet.

(4) Substitute K along with di/dt and I_L in equation (5) to obtain the commutation power loss.

Turn-Off Losses

As Figure 21 shows, turn-off losses are small compared with conduction losses and diode recovery losses. Therefore turn-off losses do not significantly affect loss calculations and can be ignored.

The load current is carried either by the channel of one HEXFET or by the body-drain diode of the other. If carried by the channel of a HEXFET the power dissipation in the HEXFET during that period is given by:

$$P_d = i_d \cdot R_{DS(on)}$$

$R_{DS(on)}$ is a function of the die temperature and, to a lesser extent, of the instantaneous value of the drain current. HEXFET data sheets include graphs of $R_{DS(on)}$ versus temperature and $R_{DS(on)}$ versus drain current.

During the period when the load current is being carried by the body-drain diode of one of the HEXFETs the power dissipation is given by:

$$P_d = i_d \cdot V_{SD}$$

V_{SD}, the forward drop of the body-drain diode, is a function of the load current. HEXFET data sheets incorporate a graph showing V_{SD} versus diode current.

Calculation of Conduction Losses

Heat sinking must be sized for worst-case dissipation, which occurs when the load power factor is unity and the longest MOSFET conduction periods coincide with the peaks of the load current. As will be seen, diode conduction losses are much less than MOSFET forward conduction losses, so that although diode losses increase as the load phase angle moves away from 0°, the total losses are reduced. Similarly total losses are greatest when the modulation depth is unity (assuming sinusoidal modulation).

Under these conditions the MOSFET losses may be calculated as follows. Assume a load current waveform or the form $I_L \cdot \sin\theta$. During a switching cycle occuring approximately at a time corresponding to the angle θ, the MOSFET will conduct in the forward direction for a proportion of the cycle given by:

MOSFET pulse width = 1/2 (1 + sin θ)

The proportion of the cycle for which the diode conducts is given by:

Diode pulse = 1/2 (1 − sin θ)

Therefore the MOSFET power loss during a pulse occuring at angle θ is:

$$P(\theta) = I_L^2\,R = I_L^2 \sin\theta \cdot 1/2\,(1 + \sin\theta) \cdot R_{DS(on)} = 1/2\,I_L^2\,R_{DS(on)}\,(\sin^2\theta + \sin^3\theta)$$

The average power loss over one half cycle is given by:

$$P_{ave} = \frac{I_L^2\,R_{DS(on)}}{2\pi}\int_0^\pi (\sin^2\theta + \sin^3\theta)\,d\theta = 0.462\,I_L^2\,R_{DS(on)}$$

Figure 24 shows how losses vary with load power factor.

The diode conduction losses for a switching cycle at angle θ are given by:

$$P(\theta) = I_L \cdot V_{SD} = I_L \sin\theta \cdot 1/2\,(1 - \sin\theta) \cdot V_{SD}$$

Where V_{SD} is the forward diode drop. To simplify calculations this is assumed to be constant for all values of current.

The average power loss due to diode conduction over one half cycle is therefore given:

$$P_{ave} = \frac{I_L \cdot V_{SD}}{2\pi}\int_0^\pi (\sin\theta - \sin^2\theta)\,d\theta = 0.068 \cdot I_L \cdot V_{SD}$$

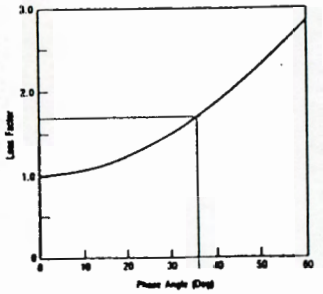

Figure 24. Diode conduction losses versus phase angle

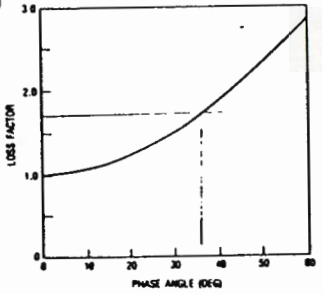

Figure 25. Diode conduction versus phase angle

APPENDIX 1.4: INVERTER LOSS CALCULATION

(Extract from Hexfet Designer's Manual)

APPENDIX 2: PHOTOVOLTAIC TECHNOLOGY WITH IMPURE SILICON

Research Newsletter

Vol 20, No 2 Southern California Edison 3rd Quarter, 1991

Advanced Solar Energy Research May Yield Breakthrough

Southern California Edison has been a major participant in the research and demonstration of solar technology for 15 years. During April, in conjunction with Texas Instruments, Edison announced the development of a new photovoltaic technology which has the potential to revolutionize the market for solar energy. A low-cost manufacturing process utilizing cheap and abundant materials in a sturdy, portable, and flexible design means that "solar spheral" photovoltaics may allow Edison and its customers to finally join in the long-sought benefits of solar energy.

A new, sturdy, low-cost solar cell, developed jointly by Edison Research and Texas Instruments, Inc. (TI), has the potential to make residential rooftop photovoltaics affordable and widely available. This technological breakthrough is in keeping with Edison's corporate strategy, which calls for expanded use of alternate and renewable forms of energy, as well as environmental protection.

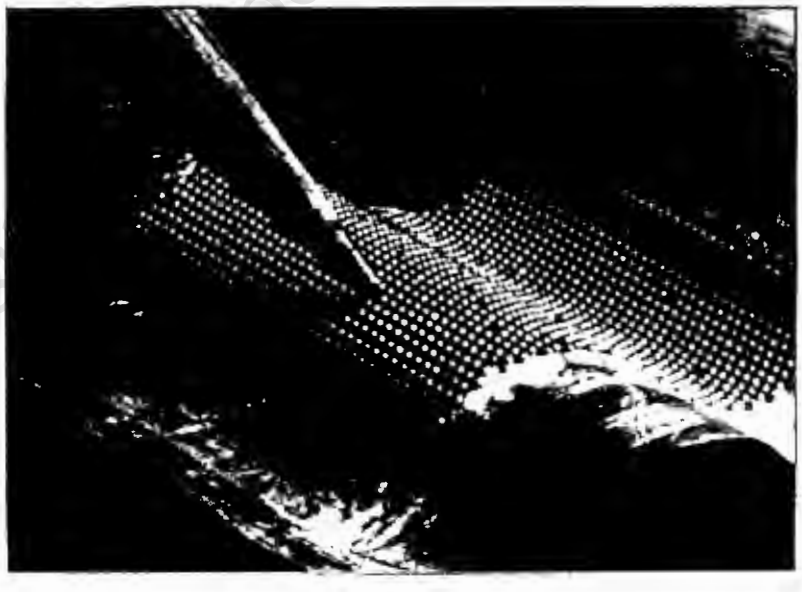

Figure 1: Thousands of BB-sized silicon spheres, embedded into thin, pliable aluminum in a low-cost manufacturing process, are the solar-energy breakthrough known as "solar spheral."

SOLAR SPHERAL IS DIFFERENT

As with all photovoltaic cells the Edison/TI cell turns solar energy into electricity. But the new technology, known as solar spheral, surpasses existing photovoltaic (PV)

IN THIS ISSUE:

• Steam Turbine Performance Evaluation (p.5)

Figure 2: To create a solar spheral cell, about 17,000 silicon spheres are bonded, through heat and pressure, to perforated aluminum foil. Because each sphere turns sunlight into electricity, the cell as a whole can work well even if individual spheres fail.

processes by combining inexpensive materials with low-cost manufacturing equipment to reduce the cost of solar-cell energy by as much as 80 percent.

A conventional solar cell is sliced from ingots made of high-grade silicon which, as a raw material, costs as much as $35 a pound. Thirty to fifty percent of this costly material is lost in the slicing process. In contrast, the solar spheral technology's metallurgical-grade silicon — considered virtually unusable until now — costs about $1 a pound.

MANUFACTURING

In manufacturing solar spheral cells, low-cost production methods convert the low-grade silicon material into solar beads. As the tiny spheres are formed, impurities are pushed to the surface of the spheres where they are etched away. To create a cell, about 17,000 of the spheres are embedded into four-inch squares of thin perforated aluminum foil (Figure 2). Heat and pressure form a bond between the spheres and the aluminum. Insulation is applied, and a second layer of aluminum foil (without holes) is bonded to the bottom of the spheres. Because each of a cell's 17,000 spheres works independently, individual sphere failure has a negligible impact on the overall cell.

Following six years of joint research and a combined investment of $10 million to develop the solar spheral technology, Edison and Texas Instruments have started a pilot line. Small amounts of solar spheres will be made in order to confirm projected manufacturing costs through actual operations on the factory floor. Small-scale production of prototype cells will begin during the second half of 1991, with field-testing the rest of the year. If the cost targets are met, the two companies anticipate commercial availability as early as 1994.

HOW IT WORKS

The conversion of sunlight into electricity in a photovoltaic cell is based on the effect of light entering a solar cell, exciting an electron, and allowing it to move. In Figure 3, a conventional silicon solar cell helps demonstrate this process of conversion.

The cell has two regions: a narrow one on top, rich in electrons (⊕), and a wider one on the bottom, deficient in electrons (⊕). The electrons that move through these regions are the electricity. Very important is the energy barrier between the two regions; without it, the electricity would not flow.

When light enters a solar cell, an electron (⊕) absorbs its energy. This

extra energy allows the electron to leave its home and move freely. If the electron is in the upper region of the photocell, the barrier prevents it from crossing into the lower area and losing its energy. If the electron is in the deficient region, the barrier will attract it over to the electron-rich side. The vacancies left behind as the electrons move about are called holes (⊖).

When an "external load" (such as a light bulb or electric motor) is connected by wires to the rich and deficient PV regions while sunlight is being absorbed, electrons will flow through one wire to the load, then return to the deficient region where they will fill the vacancies, or holes, left by departing electrons. From there they start their journeys again.

The new Edison/TI solar spheral cell differs from a conventional solar cell in that each sphere is an operating cell, having all the features of the conventional cell pictured. The aluminum foils provide the front and back contacts.

PHOTOVOLTAIC HISTORY AT EDISON

Edison's involvement with Texas Instruments is only the most recent in a series of efforts started in 1976 to accelerate the development of cost-effective and environmentally clean PV systems.

Photovoltaics had their first demonstration at Edison in 1978 when a two-kilowatt system, dedicated to operating a patio fountain, was installed at the Edison General Office in Rosemead. At the time, it was the largest system in the nation. From that success evolved Edison's effort to seek out and encourage promising techniques for making low-cost solar cells, and to deploy and compare a variety of solar cell systems within the service territory.

Edison Research has worked with private companies, universities, and other research organizations to examine a wide variety of promising PV technologies. The Company has installed some of them in

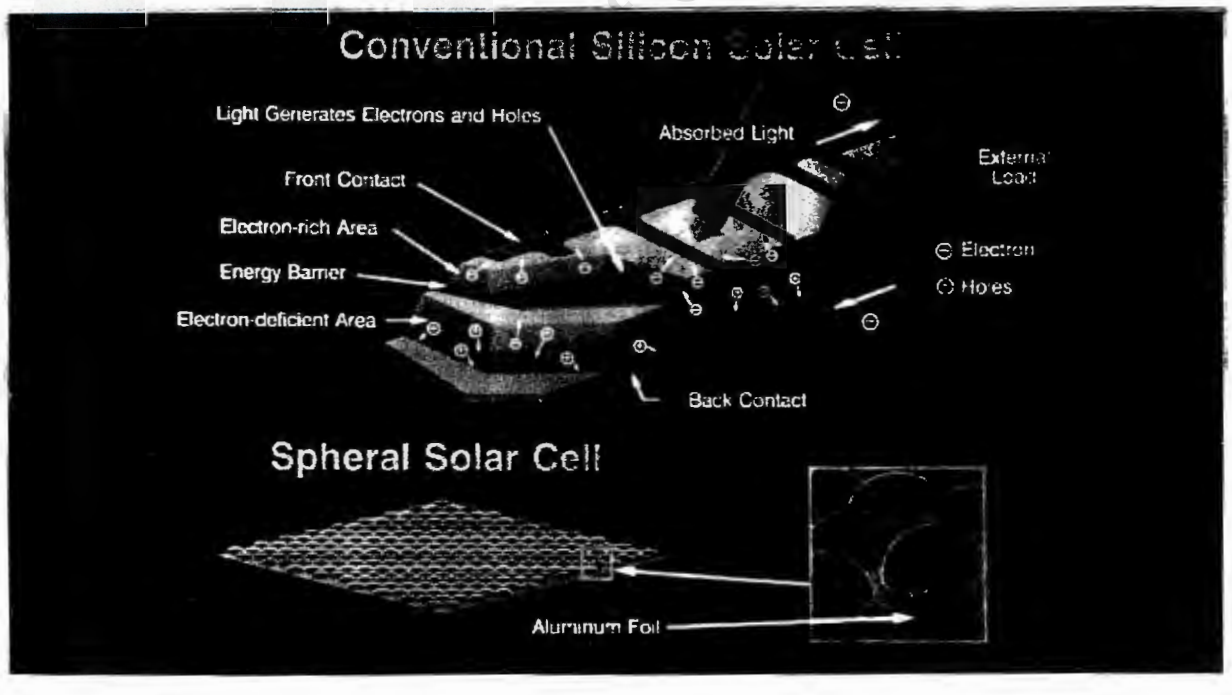

Figure 3: Solar cells are constructed of silicon, a semiconductor. The solar-excited electrons moving across the energy barrier create electricity, which can be conducted out of the cell to do work ("external load"). The solar spheral cell, depicted as a sea of bubbles, reproduces this technology in a sturdier and cheaper form.

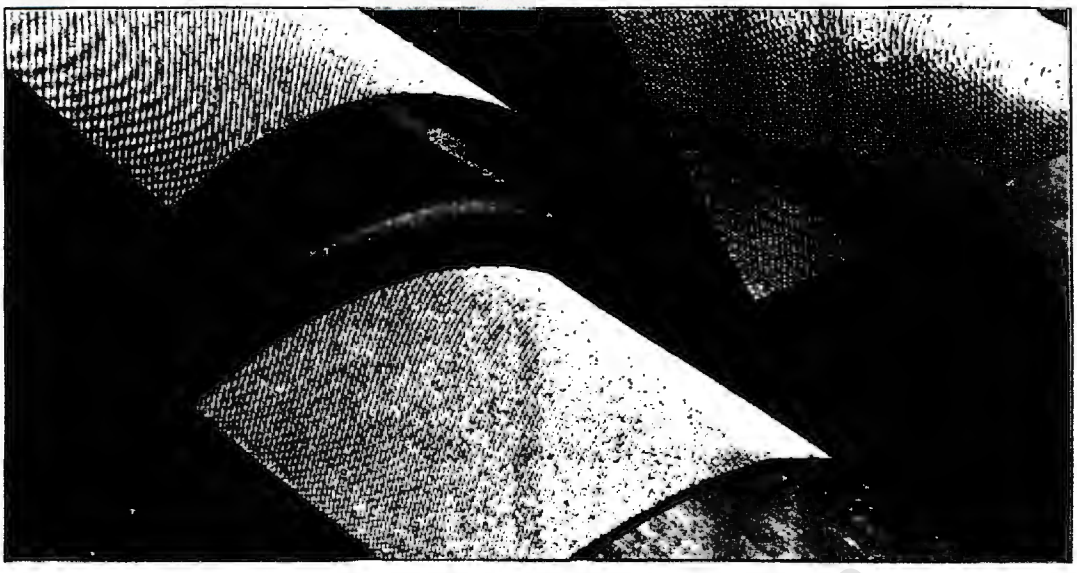

Figure 4: One hundred square feet of solar spheral cells on a south-facing roof can produce approximately one-third the electricity used each year in a typical Southern California residence. Cell configurations for rooftop deployment are currently being defined.

demonstrations to gain operating and maintenance data and to speed the advent of low-cost, mass-produced PVs.

In the 1980s, Edison installed photovoltaic systems that were connected to the electric transmission and distribution grid. The most prominent was a large-scale, central-station power plant built in 1982 near Hesperia, California. The world's largest at the time, the one-megawatt facility built by ARCO Solar confirmed that the barriers to widespread PV deployment were economic, not technical.

Since 1990, Edison has expanded its efforts to off-grid applications usually involving remote customers who are beyond the economic feasibility of distribution-line extensions. Such customers may do without electricity or they may generate their own with a diesel motor. In either case, a stand-alone PV system is likely to be a preferable alternative.

BENEFITS

Implementation of the solar spheral project will have lasting benefits to Edison's customers — atop homes and businesses in metropolitan areas — and to it's operations. A summer daytime-peaking utility like Edison can benefit from both PV uses because, by shaving the demand peak, PVs reduce fossil fuel consumption, reduce high marginal costs associated with running peak-time generation, and may obviate the need for new power plant construction. Also, summer is the worst time of year for air pollution in Southern California. Photovoltaics provide peak-time energy without producing any pollution. During the course of one year, 100 square feet of cells on the south-facing roof of a home can produce about 2,000 kilowatt hours of electricity. That's roughly one-third the annual consumption in an average Southern California residence.

In addition to being an emission-free, in-Basin source of generation,

(Continued on page 8)

ADVANCED SOLAR ENERGY *(Continued from page 4)*

other benefits of widespread PV deployment include:

(1) Reduced need for transmission lines;

(2) Reduced power losses associated with transmission and distribution, yielding greater energy efficiency for utilities and customers;

(3) Increased photovoltaic penetration could mean deferred utility distribution equipment changeouts, and lengthened equipment lifetimes.

The debut of solar spheral PVs creates opportunities for many compatible innovations. For instance, dc/ac converters and batteries with the capacity for deep charge/discharge to accompany this technology are still being perfected. But with its experience, technology base and millions of customers, Edison is well positioned to usher in the era of widespread photovoltaic use.

About the Author:
Nick W. Patapoff, Jr. is a Senior Research Engineer with 20 years of service at Edison. Formerly with the Electric System Planning Division, Mr. Patapoff joined Research in 1976. Since that time, he has concentrated his efforts in the solar field; he is co-developer and project manager of the solar spheral technology. A registered California Electrical Engineer, Mr. Patapoff holds a BSEE and an MBA from the University of Southern California.

Southern California Edison
P. O. Box 800
Rosemead, CA 91770

Editor: B. C. Olsan
Technical Writer: M. K. Fitzpatrick
Coordinator: C. Barrows

Research Newsletter is produced by the Research Division of Southern California Edison Company. Single copies are available upon request. Please address all inquiries to:
Editor, Research Newsletter
Room 449
Southern California Edison
P. O. Box 800
Rosemead, CA 91770

APPENDIX 3: FEASIBILITY OF USING INDUCTION MOTOR FOR SOLAR APPLICATION

(Extract from BSc Project Proposal, J.L.Davies, UCT 1990)

The three main factors that affect the suitability of a motor are its cost, efficiency and maintenance required. Efficiency is of particular importance as the cost of the system is very high.

Before a three phase motor can be recommended, the characteristics of a dc motor need to be known so that the two types of motors can be compared.

1. Direct current motors

These motors are currently being used by Mono Pump to pump water using solar energy. The motors used by Monopump are manufactured by Baldor and range from 0,2 to 0,75 kW depending on the requirements of the customer. The most common motor used is 0.37 kW and costs around R1500. At rated power, the efficiency of this motor is 85%. Mr Peter Burrow with the Technical Research Department at Monopump Head Office said that the motors are run at about 80% efficiency.

The dc motor cannot be run directly off the solar panels as the voltage of the panels must be matched to the required motor voltage. To achieve this, a DC to DC convertor is used. Mr burrow gave the efficiency of the convertor as about 80%. The converter costs around R1200 as quoted by the Monopump branch in Cape Town.

If the efficiency of the motor is taken as 80% and the efficiency of the converter as 80%, the overall efficiency of the motor - converter combination is 64%. This is the efficiency at rated values and is probably similar to the efficiencies achieved under reasonably bright sunlight. The efficiency is unknown when the system operates at lower sunlight intensities and hence lower power.

A major disadvantage of the dc motor is the fact that it has brushes. Brushes do not last indefinetely and thus the system is not maintenance-free. The brushes of the motors used by Monopump last between one and two years. This may seem like a long time, but most of the customers are in remote areas and as each customer has to be serviced individually, maintenance costs are high.

2. Synchronous motors

Synchronous motors fall into two categories, permanent magnet synchronous motors and synchronous motors with separately excited rotors.

2.1. Permanent magnet synchronous motors

This is the type of motor which was originally intended for this project. The rotor of this type of motor consists of permanent magnets which are arranged in a variety of different configurations. There are two possiblities for obtaining a permanent magnet synchronous motor. Such a motor could be bought commercially or the rotor of an induction motor could be removed and replaced by a rotor made up of permanent magnets.

a) Bought permanent magnet motors

Meyer said that Femco quoted a price of R450 for a 0,37 kW permanent magnet motor. It is highly unlikely that Femco ever sold such a motor as they do not supply any permanent magnet motors. Research was done to find the actual prices of these motors.

Permanent magnet motors are new on the market and are sold as servo motors. Bosch and Bircraft are two of the companies that sell this type of motor. The motors offer maintenance-free operation as there are no brushes.

Information on the Bosch motors are given in appendix I. Efficiency figures were not given by Bosch, but Bircrat said that the efficiency of their motors was marginally better than that of induction motors. These motors are not stocked in the country and have to be ordered according to the requirements of the customer. The motor required would cost around R3500.

b) Motor with rotor constructed with discrete permanent magnets

The problem with bought permanent magnet motors is the high cost. To get around this problem, the feasibilty of building a permanent magnet rotor needs to be investigated.

Rare-earth permanent magnets of high energy densities are being produced by Vacodym and Vacomax. Some of the Vacodym magnets have been specifically designed to be used in motors. Kopp electonics are the sole agents for these magnets and are based in Johannesburg. Dirk Venter at the Kopp Electronics Head Office recommended that the Vacodym 370 HR magnets be used for such an application. These are the only ones in stock which show suitable magnetic characteristics. Magnets used in these motors need to have high energy densities, high stability to demagnetizing fields and they must be able to operate at high temperatures. The characteristic curves for the 370HR magnets are shown in Appendix I.

Magnets of different shapes could be ordered or manufactured according to customer specifications, but this would add between 50 and 200% to the original price. The size of the 370 HR magnets are 20mm x 10mm x 5mm with the axis of the magnetic field perpendicular to the 20mm x 10mm face. For a bulk order (greater than ten magnets), the cost of these magnets is R81 each.

In a paper published by G. Souques, a configuration is described which uses rectangular magnets in the rotor of a synchronous motor. The magnetic field of these magnets is perpendicular to the largest face. Such a configuration could thus be constructed using the 370 HR magnets. The magnetic flux lines of this configuration are shown in Appendix II. One such arrangement using the 370 HR is shown in figure 4.

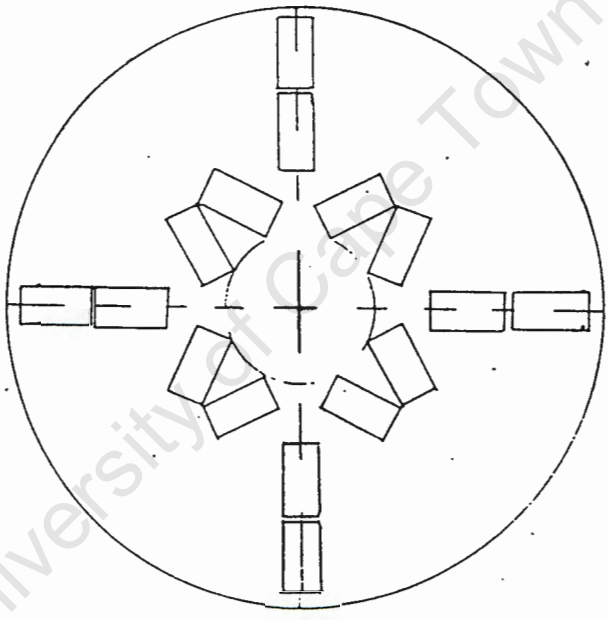

Figure 4 : Magnet configuration of permanent magnet rotor

The above arrangement uses 16 magnets which would cost a total of R1300. To complete the assemby of a synchronous motor, an induction motor would also have to be purchased to provide a stator. This would cost in the vicinity of R500. The overall cost of the entire motor would therefore not be less than R1800, which is still fairly expensive. The torque of such a motor is also uncertain.

2.2 Separately exited synchronous motors

Such a motor is obtained by exciting the rotor field of a three phase alternator. This type of motor has brushes and is therefore not maintenance-free. Inherent losses are incurred as the rotor needs to be excited with direct current.

Enquiries as to the efficiency of alternators from Lucas, Johannesburg, revealed that they were around 50% over the load range. On inspection of one such alternator it could be seen that the slots were not completely filled with windings which corroborated that this was not an efficient design.

Although this is a low cost option, the efficiencies of these motors are too low for them to be used in this project.

3. Induction Motors

Squirrel cage induction motors are both inexpensive and maintenance-free. The only drawback is that for this size of motor they are not as efficient as either DC motors or permanent magnet synchronous motors. The efficiency of these induction motors is between 64 and 68 % at rated load.

Mr John Shultz of GEC Special Machines seemed confident that by oversizing an induction motor an improvement in efficiency could be obtained. He also said that if this was not possible, he was prepared to design an induction motor that would meet the required standard (i.e efficiency of around 85%). The design would be done free of charge, although the production of the motor would cost more than an ordinary induction motor. He was unable to quote the exact price, but the cost would still be less than both a synchronous or a dc motor.

It therefore seems that the best type of motor for the project is an induction motor. An efficient induction motor would not be obtainable within the time limits of this project. However, the induction motor supplied by MLT Drives could therefore be used for the purposes of this project.

APPENDIX 4: MOTOR PERFORMANCE

Experimental Motor Performance
(60 Hz. 45v)

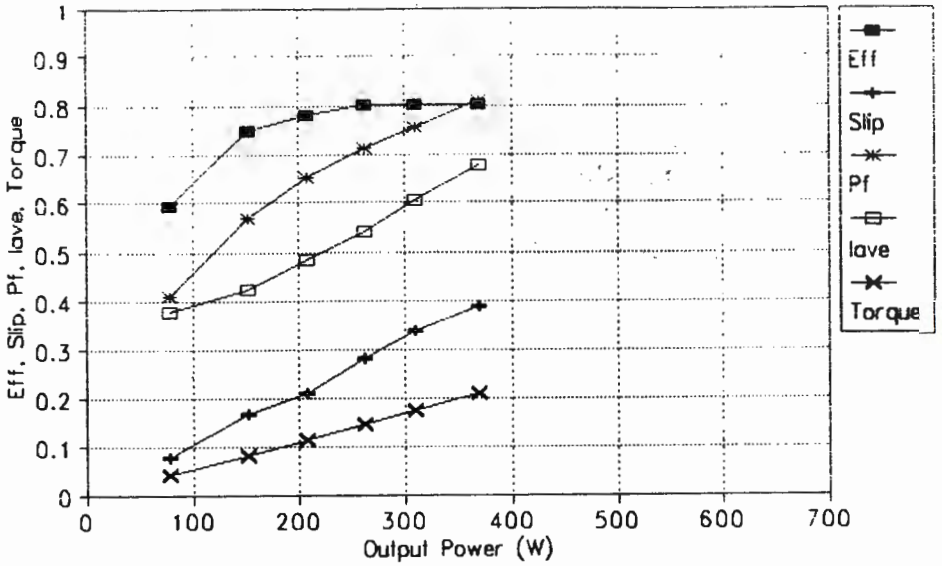

Experimental Motor Performance
(60 Hz. 63.5v)

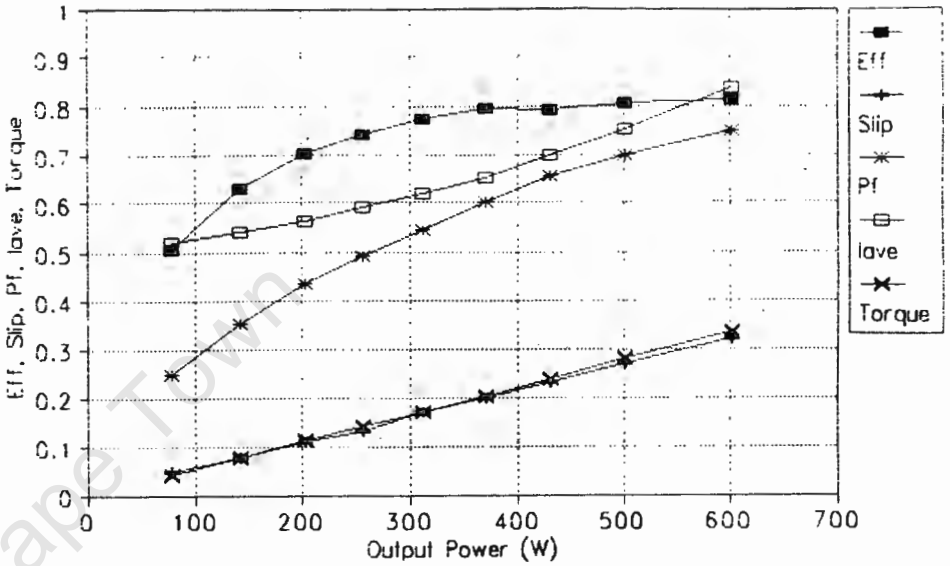

Experimental Motor Performance
(50Hz. 63v)

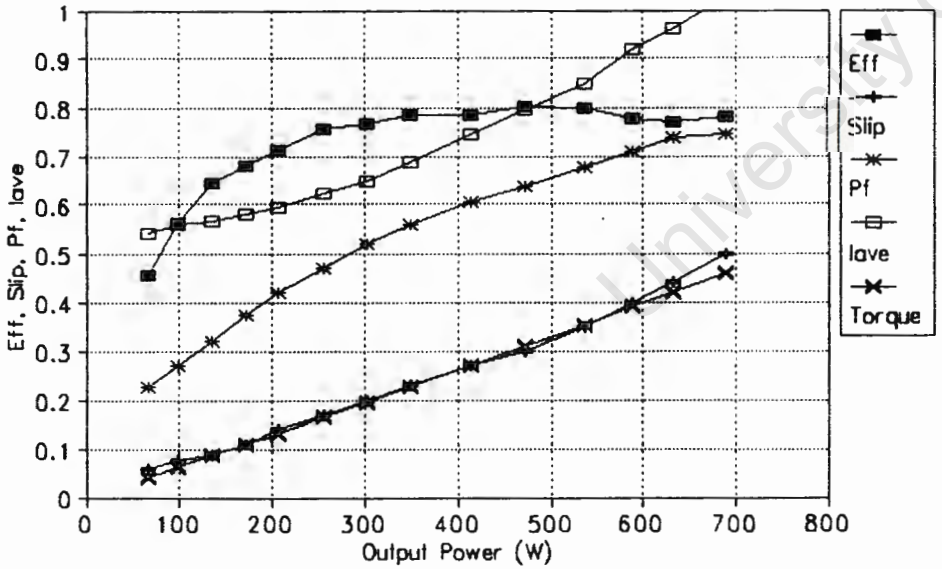

Experimental Motor Performance
(60Hz. 55v)

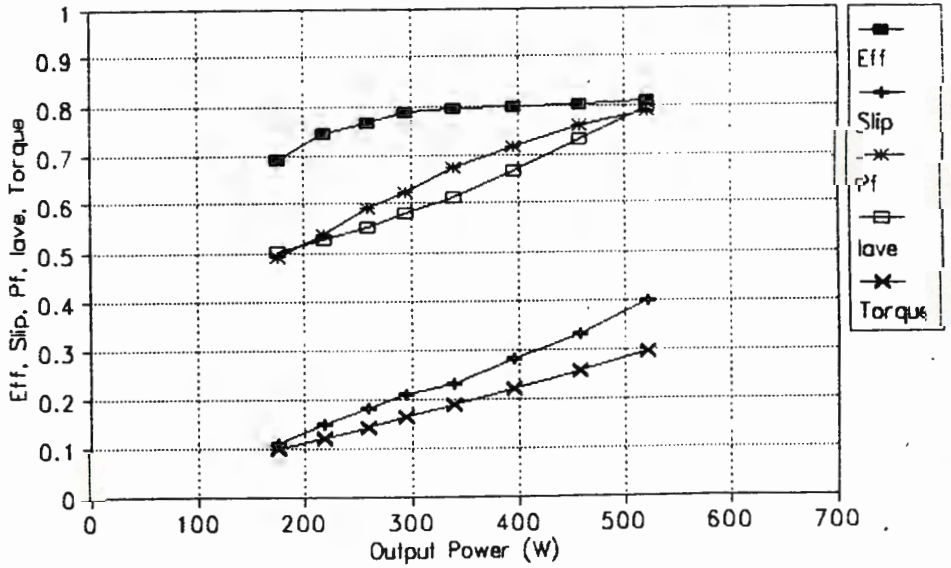

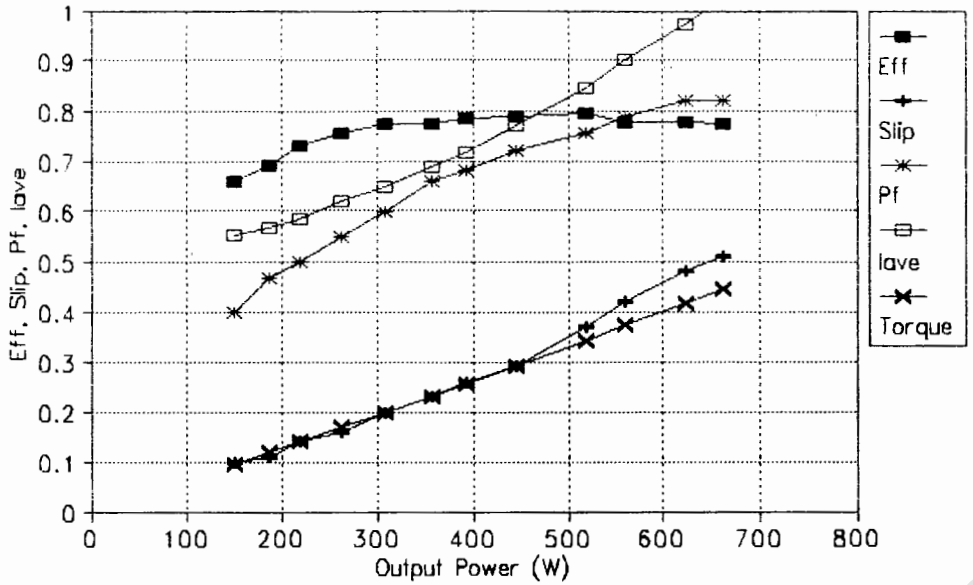

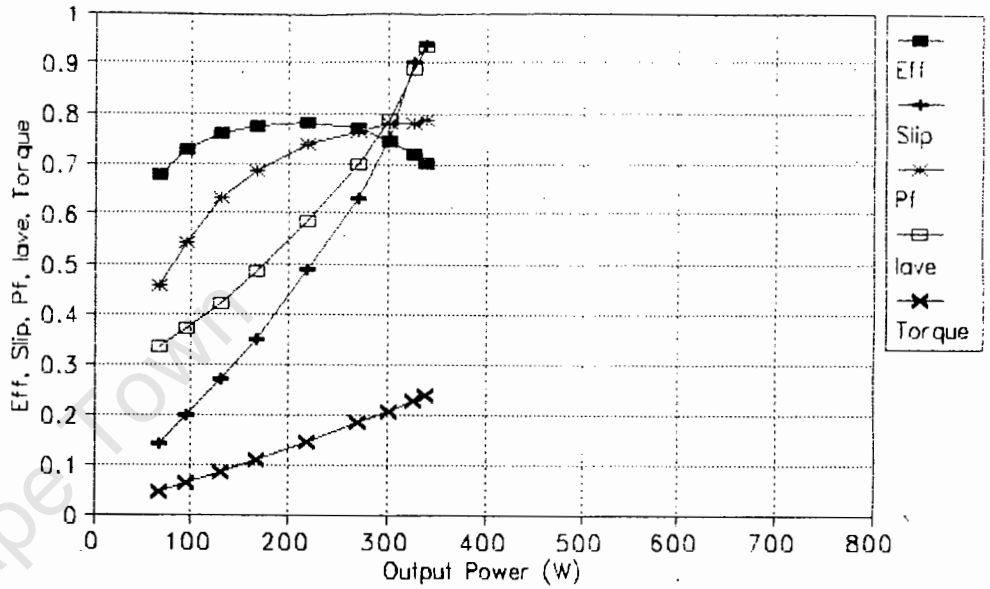

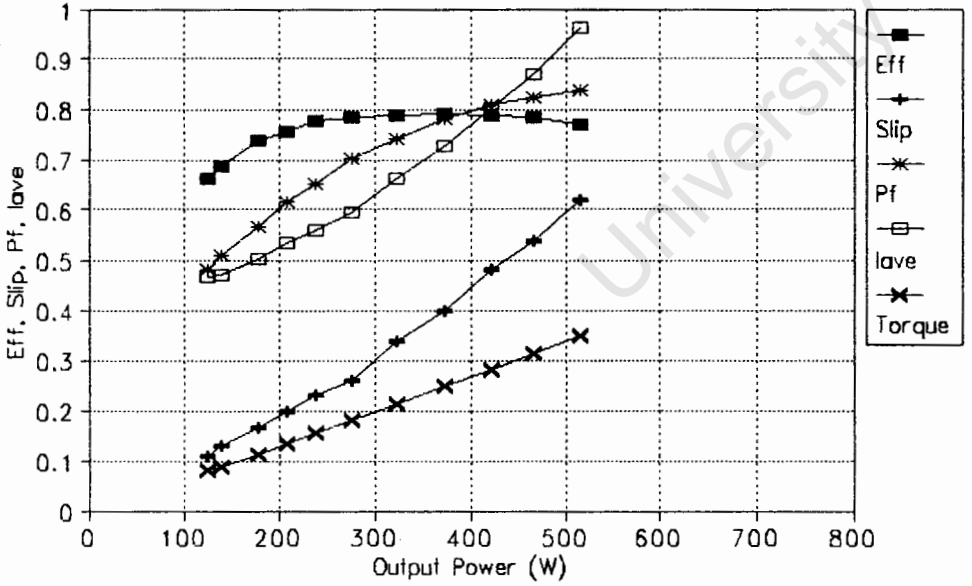

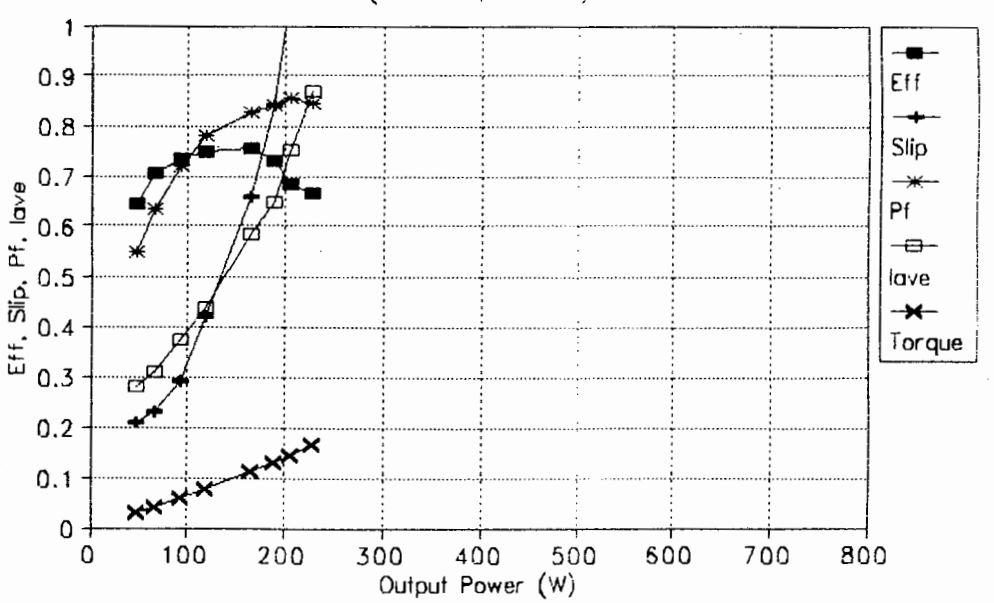

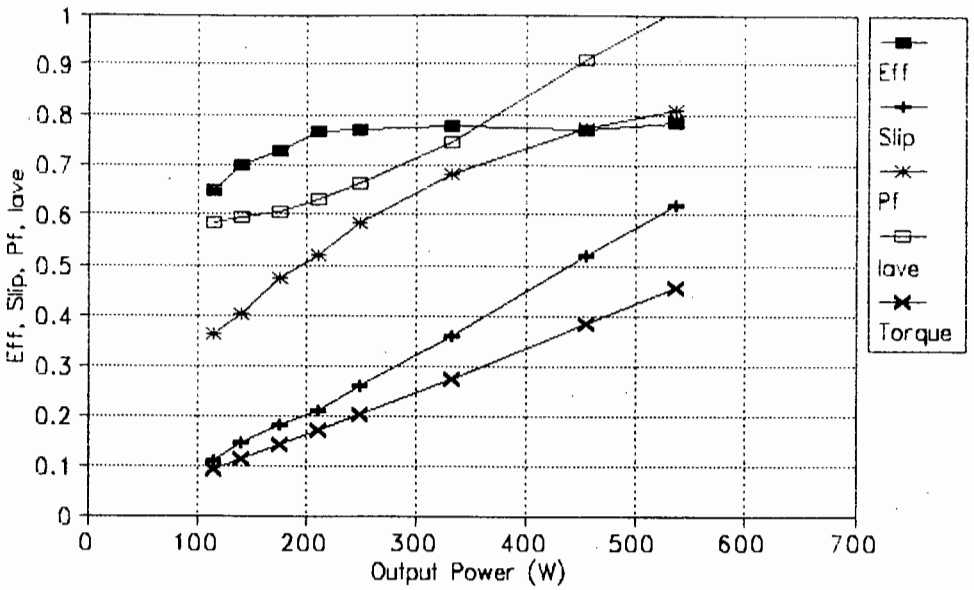

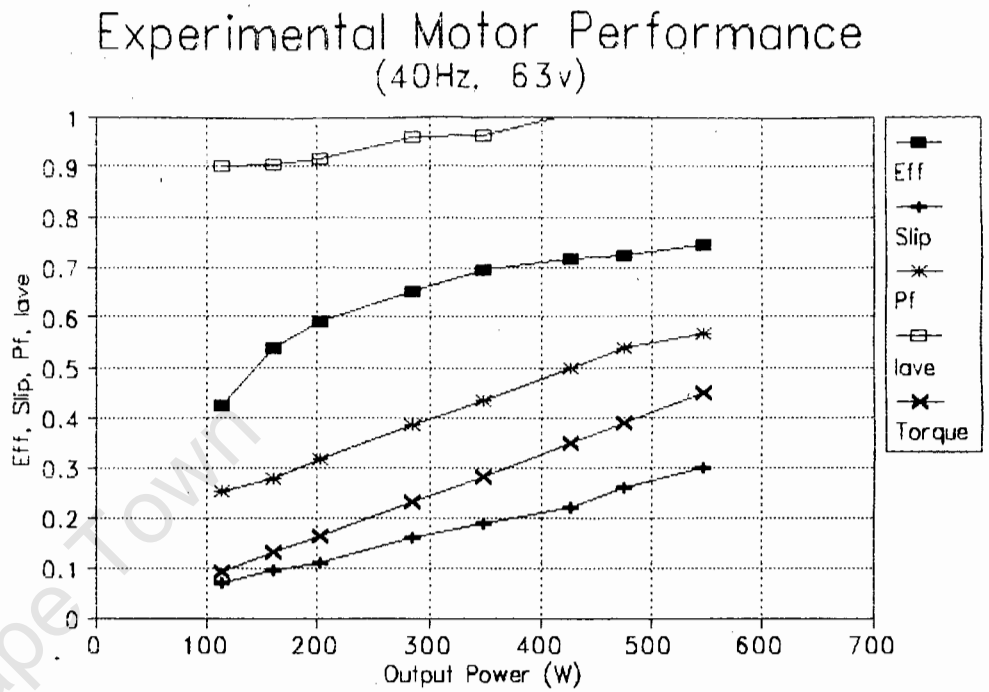

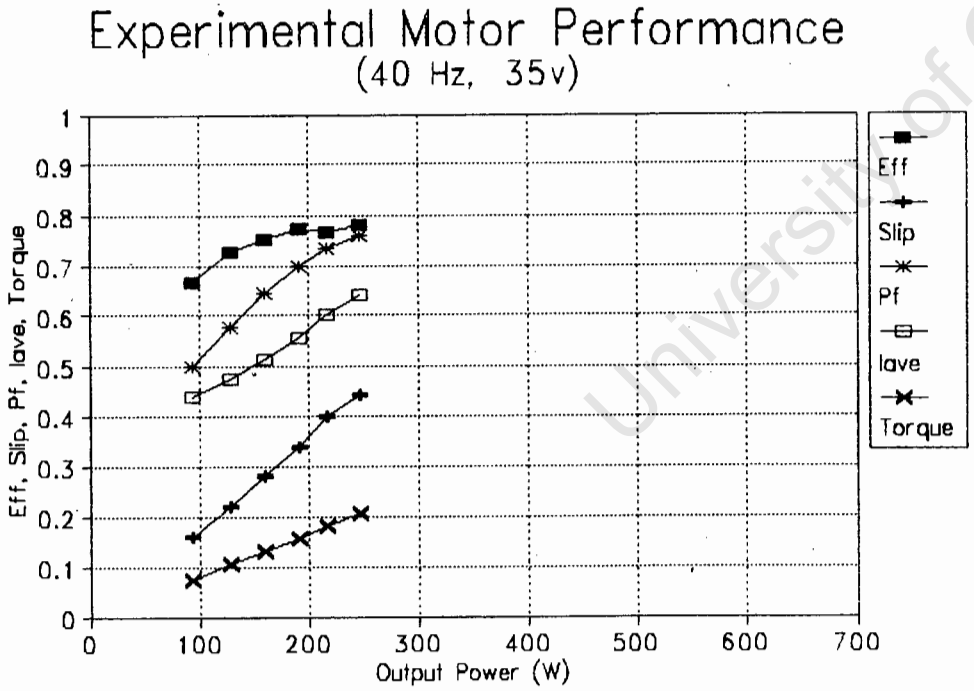

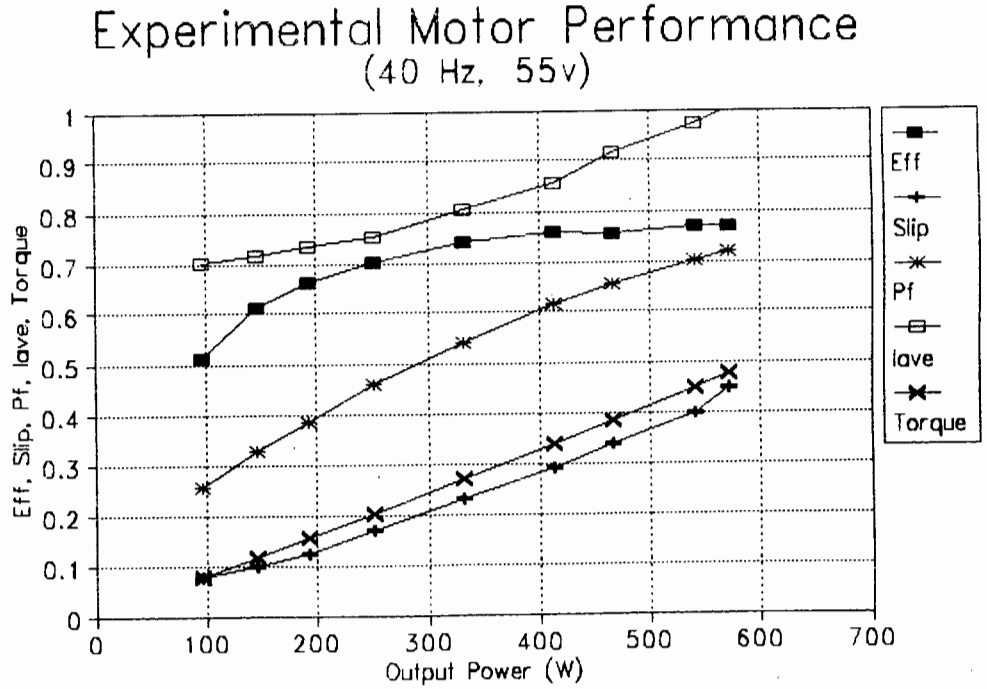

Experimental Motor Performance
(30 Hz, 35v)

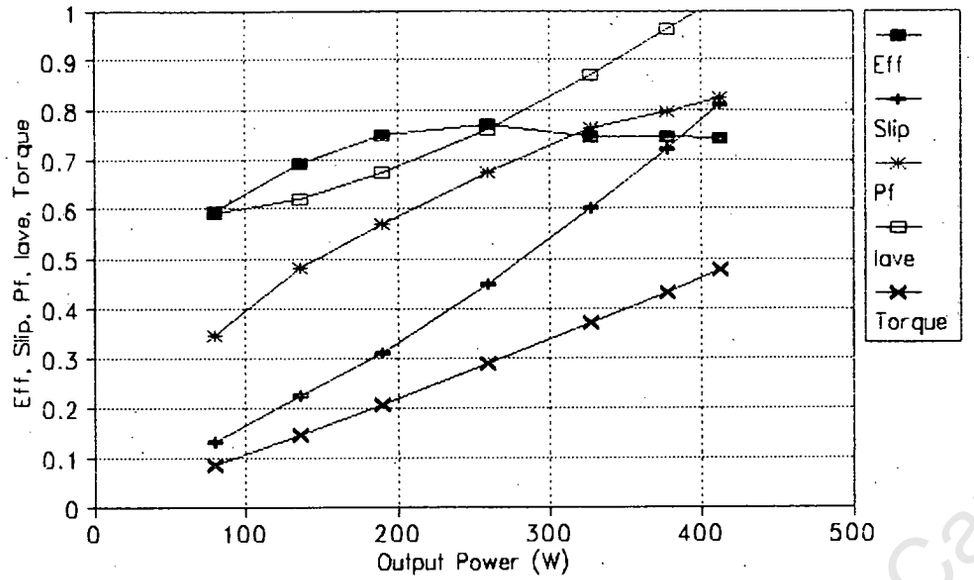

Experimental Motor Performance
(40 Hz, 25v)

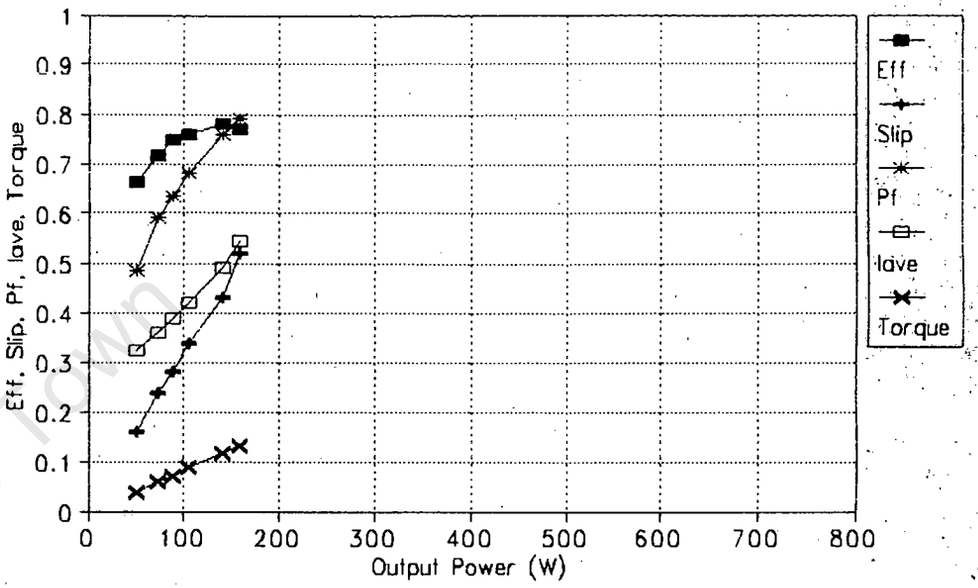

Experimental Motor Performance
(30 Hz, 25v)

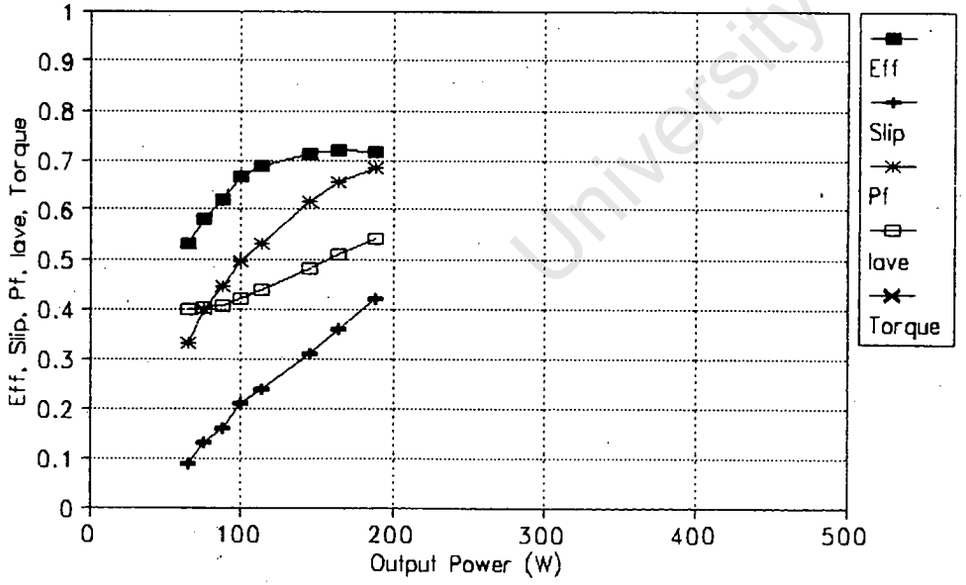

Experimental Motor Performance
(30 Hz, 45v)

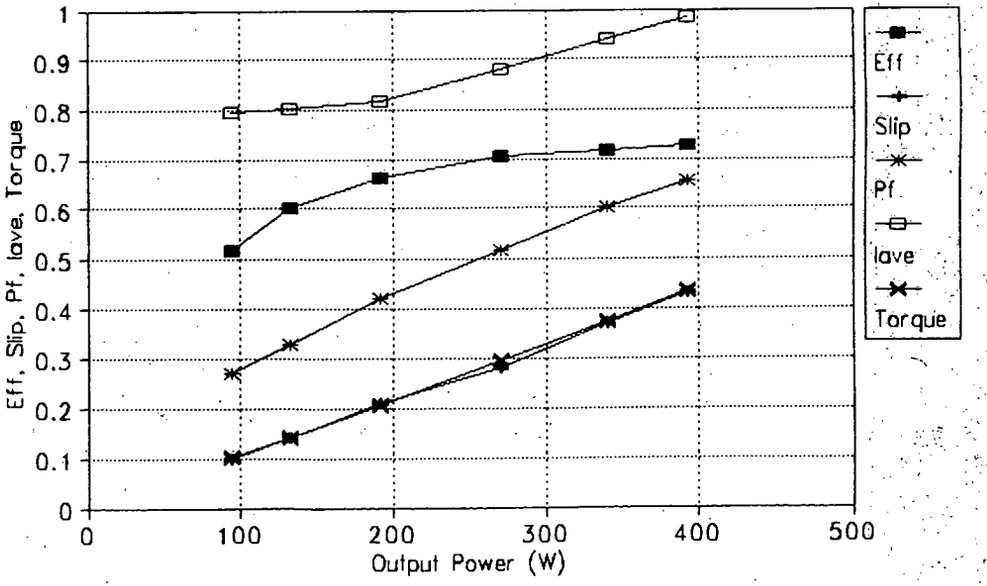

Efficiencies at 40 Hz

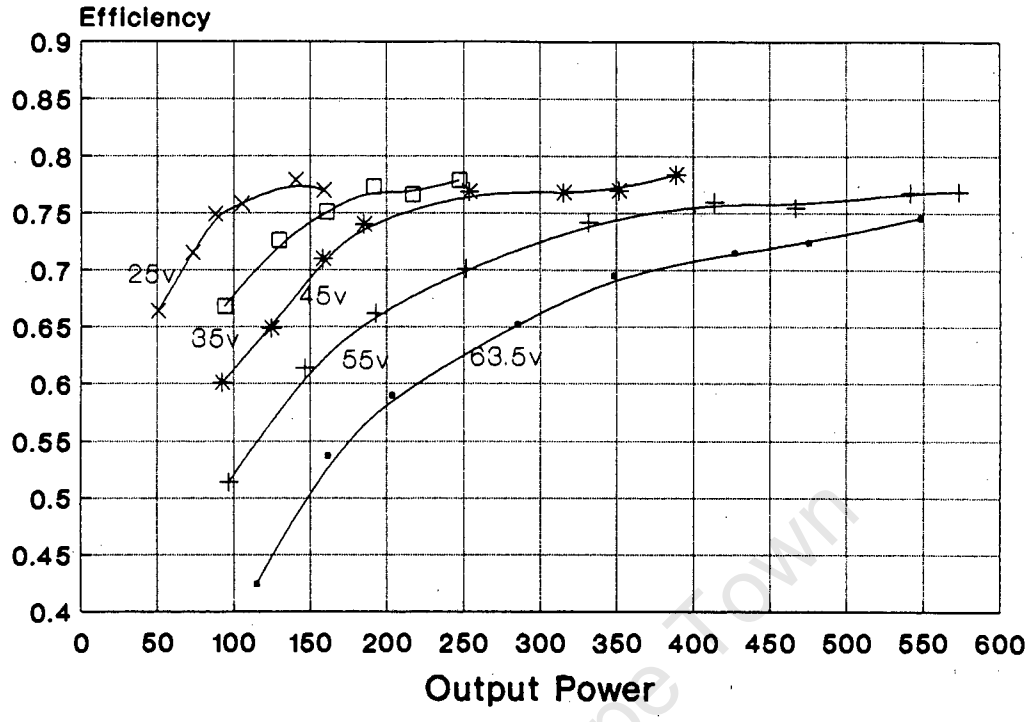

Efficiencies at 50 Hz

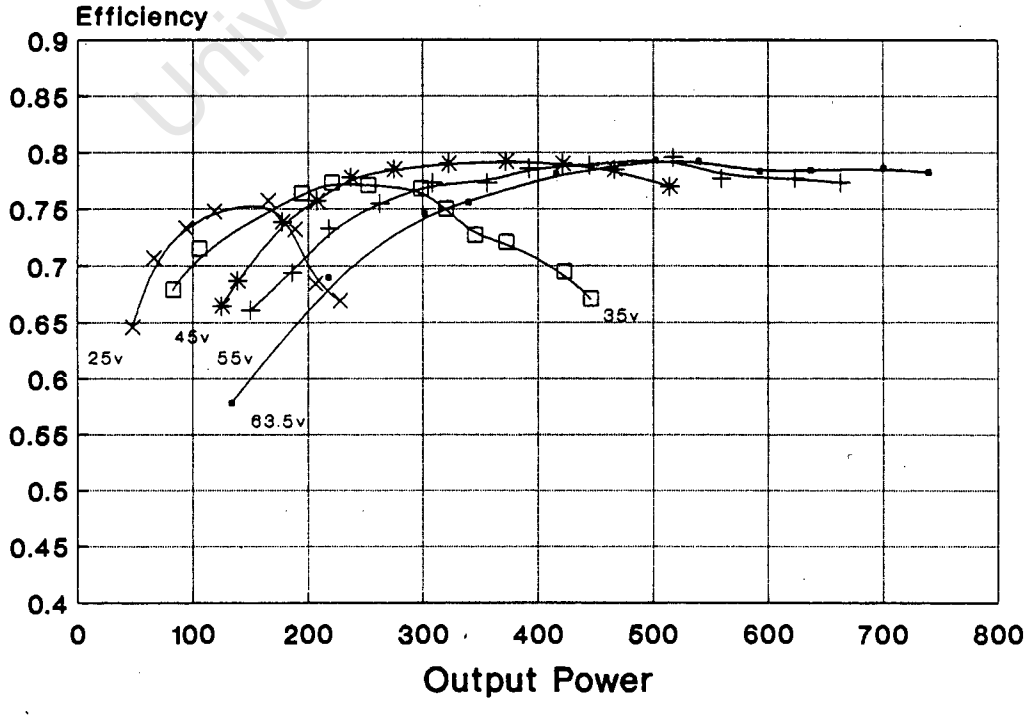

Efficiencies at 30 Hz

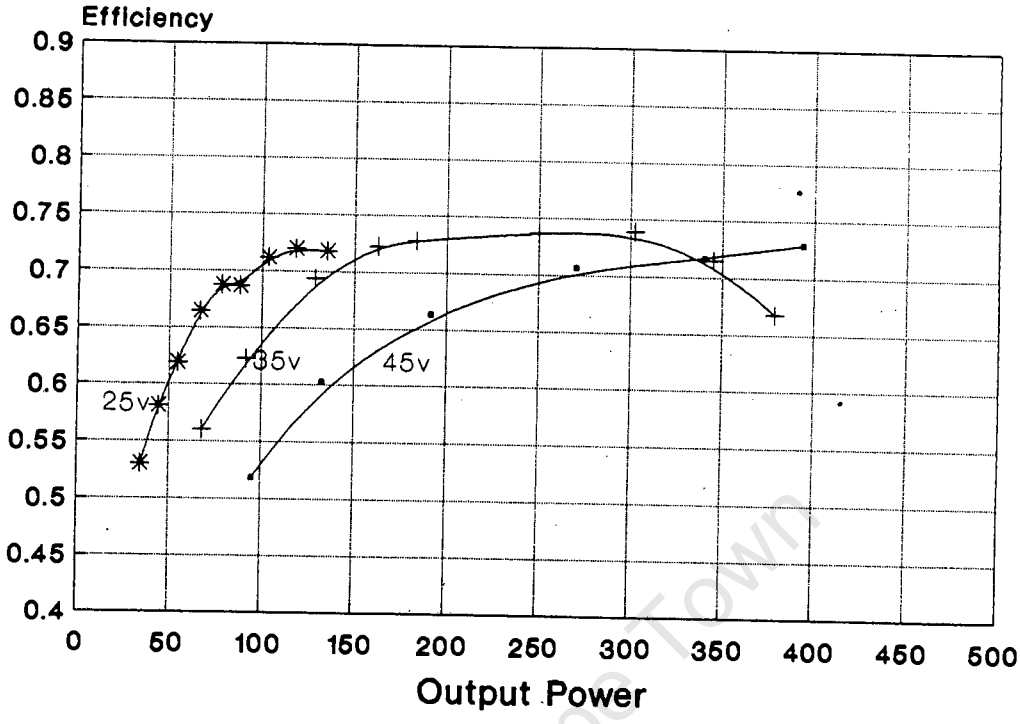

Efficiencies at 20 Hz

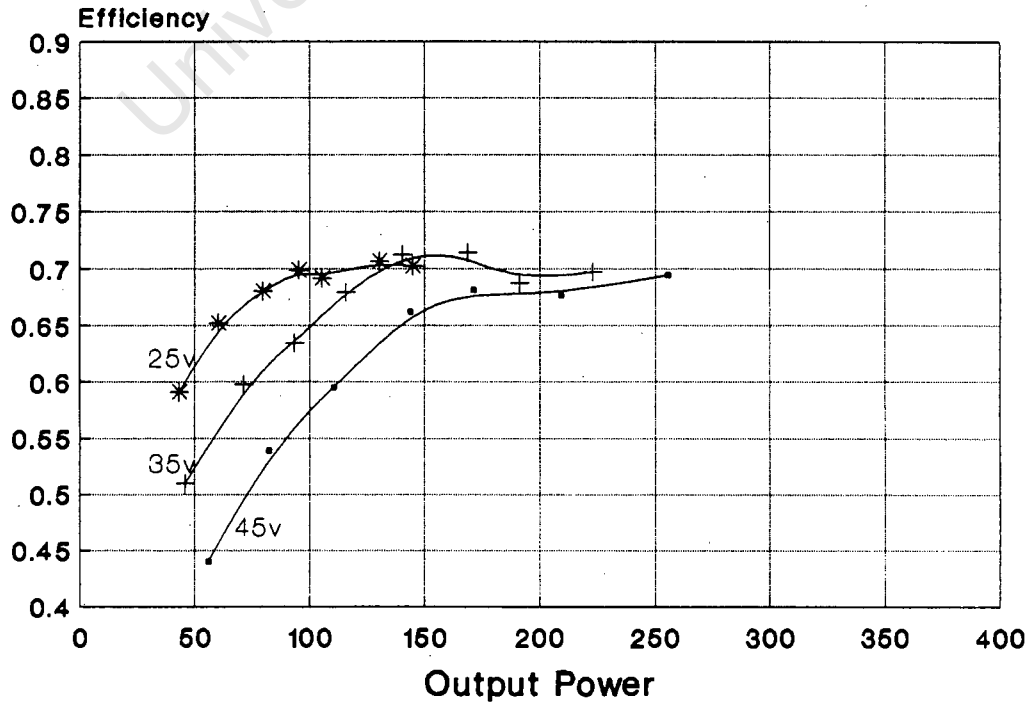

APPENDIX 4.2: THEORETICAL MOTOR PERFORMANCE

THEORETICAL PREDICIONS FOR INDUCTION MOTOR

CIRCUIT PARAMETERS FROM NO-LOAD AND BLOCKED ROTOR TESTS:

$F := 80$

$R1 := .737 \quad ; \quad X1 := 0.003251 \cdot 2 \cdot \pi \cdot F \cdot j$

$R2 := .226 + .0055 \cdot F \quad ; \quad X2 := (4.599 - .02696 \cdot F) \cdot .001 \cdot 2 \cdot \pi \cdot F \cdot j$

$$Rc := \left[5.585 + .131 \cdot F + .106 \cdot F^{1.24}\right] \cdot \frac{F}{3 \cdot 13.44^2}$$

$Xm := .054 \cdot 2 \cdot \pi \cdot F \cdot j$

$$S := \begin{bmatrix} .005 \\ .01 \\ .015 \\ .02 \\ .025 \\ .03 \\ .035 \\ .04 \\ .045 \\ .05 \\ .055 \\ .06 \\ .07 \\ .08 \\ .09 \end{bmatrix} \qquad i := 0,1 \ldots 14$$

$$V1 := \begin{bmatrix} 63.5 \\ 55 \\ 50 \\ 45 \\ 40 \\ 35 \\ 30 \end{bmatrix} \qquad j := 0,1 \ldots 6$$

$$E_{i,j} := V1_j - (R1 + X1) \cdot \frac{V1_j}{R1 + X1 + \left[\frac{1}{Rc + Xm} + \frac{1}{\frac{R2}{S_i} + X2}\right]^{-1}}$$

$$I1_{i,j} := \frac{V1_j - E_{i,j}}{R1 + X1} \qquad I2_{i,j} := \frac{E_{i,j}}{\frac{R2}{S_i} + X2} \qquad I0_{i,j} := \frac{E_{i,j}}{Rc + Xm}$$

$$I1mod_{i,j} := \sqrt{\left[Re\left[I1_{i,j}\right]\right]^2 + \left[Im\left[I1_{i,j}\right]\right]^2}$$

$$I2mod_{i,j} := \sqrt{\left[Re\left[I2_{i,j}\right]\right]^2 + \left[Im\left[I2_{i,j}\right]\right]^2}$$

$$I0_{i,j} := \sqrt{\left[Re\left[I0_{i,j}\right]\right]^2 + \left[Im\left[I0_{i,j}\right]\right]^2}$$

$$Pout_{i,j} := 3\, R2 \left[\frac{1 - S_i}{S_i}\right] \left[I2mod_{i,j}\right]^2$$

$$Ef_{i,j} := \frac{Pout_{i,j}}{Pout_{i,j} + 3\left[R1\left[I1mod_{i,j}\right]^2 + R2\left[I2mod_{i,j}\right]^2 + \left[I0_{i,j}\right]^2 Rc\right]}$$

$$PF_{i,j} := \cos\left[\arg\left[I1_{i,j}\right]\right]$$

$$I_{i,j} := \frac{I1mod_{i,j}}{10}$$

$$T_{i,j} := \frac{Pout_{i,j}}{\left[1 - S_i\right] \cdot \pi \cdot F \cdot 10}$$

$$s_i := S_i \cdot 10$$

WRITEPRN(JEFFIC) := Ef
APPENDPRN(JEFFIC) := Pout
APPENDPRN(JEFFIC) := V1

$V1_0 = 63.5$

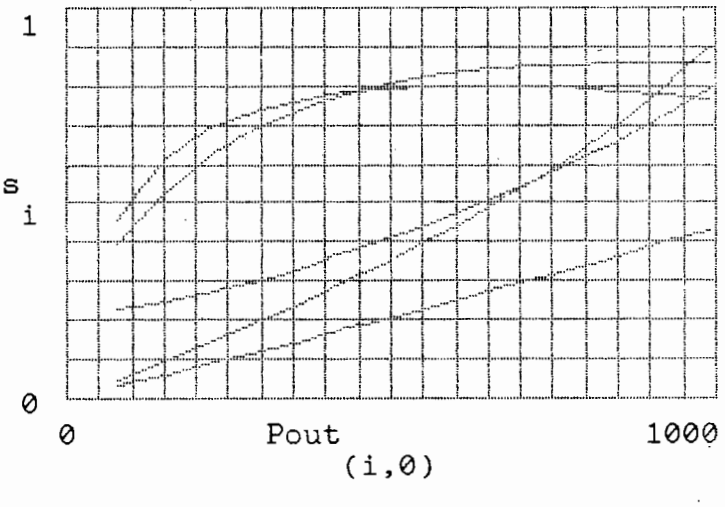

$Ef_{(i,0)}, T_{(i,0)}, PF_{(i,0)}, I_{(i,0)}, s_i$

Ef i,0	I i,0	PF i,0	T i,0	Pout i,0
0.458146	0.227949	0.3976	0.031632	79.101246
0.618463	0.248676	0.531216	0.062552	155.637068
0.696376	0.275073	0.628891	0.092701	229.489222
0.739968	0.305386	0.698187	0.122029	300.558967
0.766044	0.338288	0.746993	0.15049	368.766781

0.782003	0.372832	0.781494	0.178045	434.051851
0.791613	0.408352	0.806054	0.204663	496.371358
0.796994	0.444382	0.823632	0.230319	555.699609
0.79943	0.480589	0.836221	0.254992	612.027022
0.799741	0.516733	0.845172	0.278672	665.359007
0.79848	0.552638	0.851414	0.301348	715.714776
0.796028	0.588171	0.855598	0.323019	763.126097
0.788578	0.657752	0.859524	0.36336	849.297642
0.778837	0.724944	0.859373	0.39976	924.330883
0.767641	0.789446	0.856515	0.432344	988.804326

V1 = 55
  1

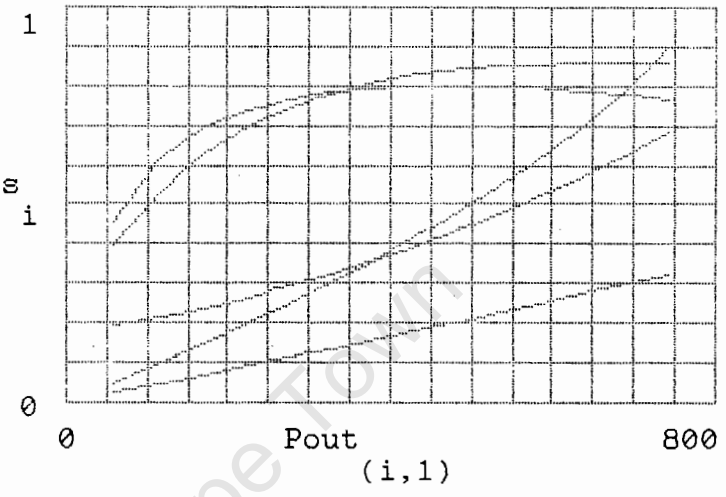

Ef ,T ,PF ,I ,s
(i,1) (i,1) (i,1) (i,1) i

V1 = 50
  2

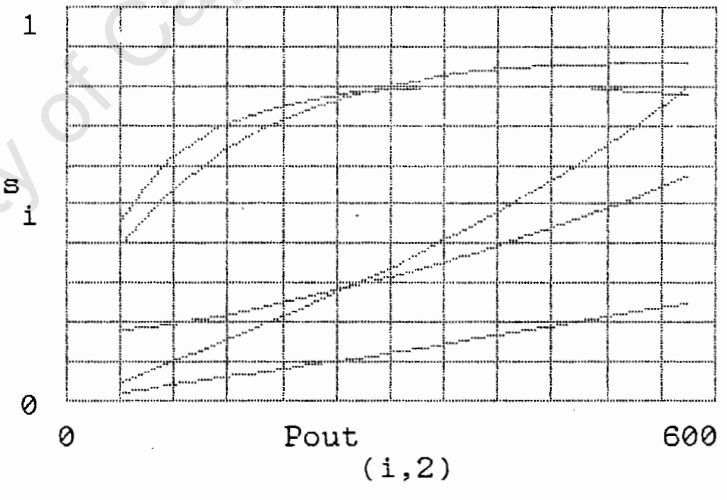

Ef ,T ,PF ,I ,s
(i,2) (i,2) (i,2) (i,2) i

V1 = 45
  3

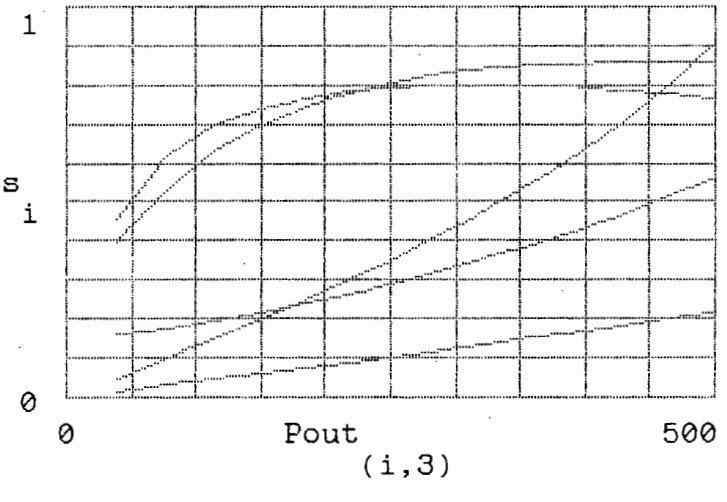

Ef ,T ,PF ,I ,s
(i,3) (i,3) (i,3) (i,3) i

V1 = 40

4

Ef (i,4), T (i,4), PF (i,4), I (i,4), s i

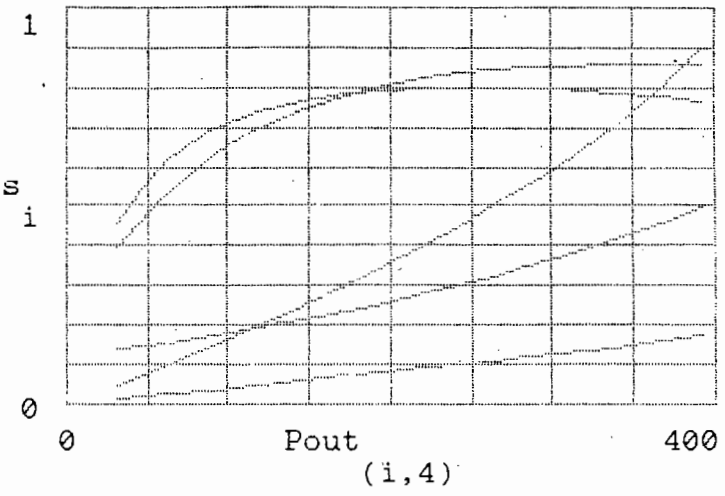

V1 = 35
5

Ef (i,5), T (i,5), PF (i,5), I (i,5), s i

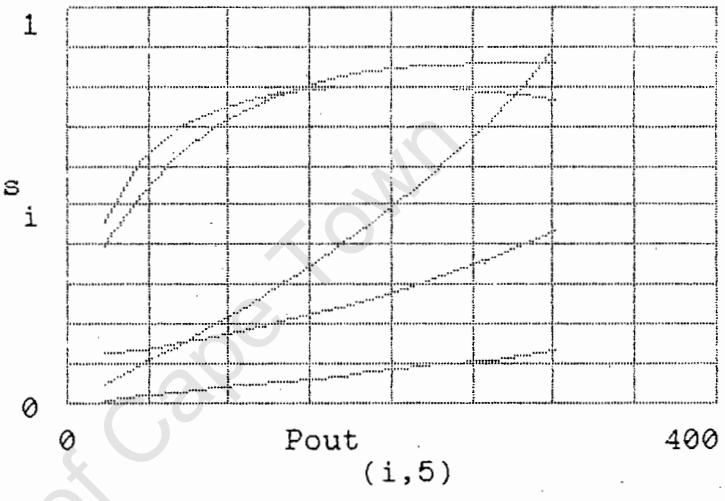

APPENDIX 4.3: CALCULATION OF MOTOR PARAMETERS

The motor parameters were obtained from no-load and blocked rotor tests conducted at frequencies of 25 and 50Hz. The motor is oversized and hence it is necessary to conduct the no-load test at a voltage which is close to the expected operating voltage. For an input power of 350W and assuming a motor/inverter efficiency of 0.67, the output power delivered by the motor is 235W. The output torque capability is limited by the flux, which is proportional to the square of the voltage. In order to obtain an estimate of the voltage at which to conduct the no-load test, the flux is assumed to decrease in proportion to the output power. Hence,

$$V_{nl}^2 = \frac{235}{750} \cdot 63.5^2$$

$$V_{nl} = 35.5 v_{ln}$$

At a frequency of 25Hz a square root voltage frequency curve was followed and thus $V_{nl25} = 25 v_{ln}$

For a torque of 1Nm the current was found to be 2.8A, and this value was used in conducting the blocked rotor test. The following readings were obtained:

Blocked rotor:

Frequency = 50Hz:
V_{llav} = 11.85v
I_{av} = 2.7A RMS
Pin = 27W

Frequency = 25Hz:
V_{llav} = 7.5v
I_{av} = 2.7A RMS
Pin = 24W

No-Load:

Frequency = 50Hz:
V_{llav} = 60.3v
I_{av} = 1.9A RMS
Pin = 33W

Frequency = 25Hz:
V_{llav} = 43.3v
I_{av} = 2.75A RMS
Pin = 31W

Measured DC stator resistance = R_{lav} = 1.27Ω

therefore,

$$r_1 = \frac{(235+65)}{235+25} \cdot R_1/2$$

$$= 0.737$$

From blocked rotor test:

$r_{2(50)} = 0.5$; $r_{2(25)} = 0.363$
$l_{2(50)} = 3.521\text{mH}$; $l_{2(25)} = 3.521\text{mH}$
$l2(50) = 3.521\text{mH}$; $l_{2(25)} = 3.925\text{mH}$

The input power curves for the no-load tests are shown below. The no-load losses consist of friction and windage losses, iron losses and stator resistance losses.

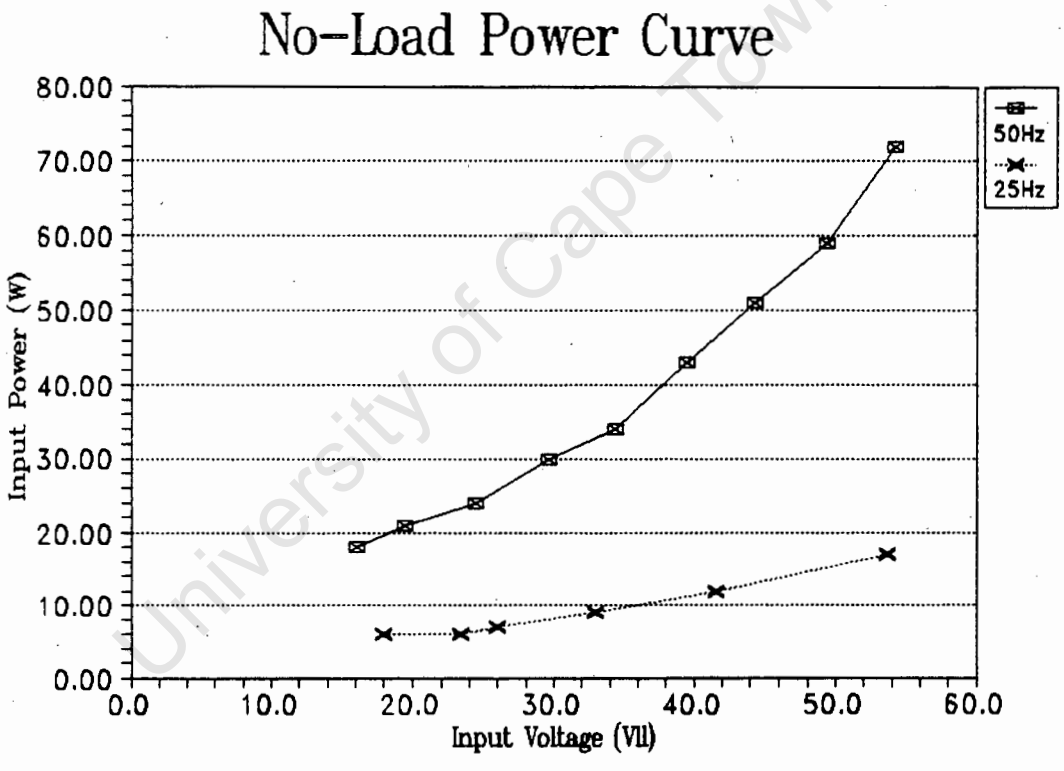

From the above graph, $Pmech_{(50)} = 13$ W
$Pmech_{(25)} = 5.5$ W

$Piron_{(50)} = 12.1$W
$Piron_{(25)} = 8.9$W

APPENDIX 5: DESIGN OF SYSTEM COMPONENTS

APPENDIX 5.1: INVERTER CIRCUIT

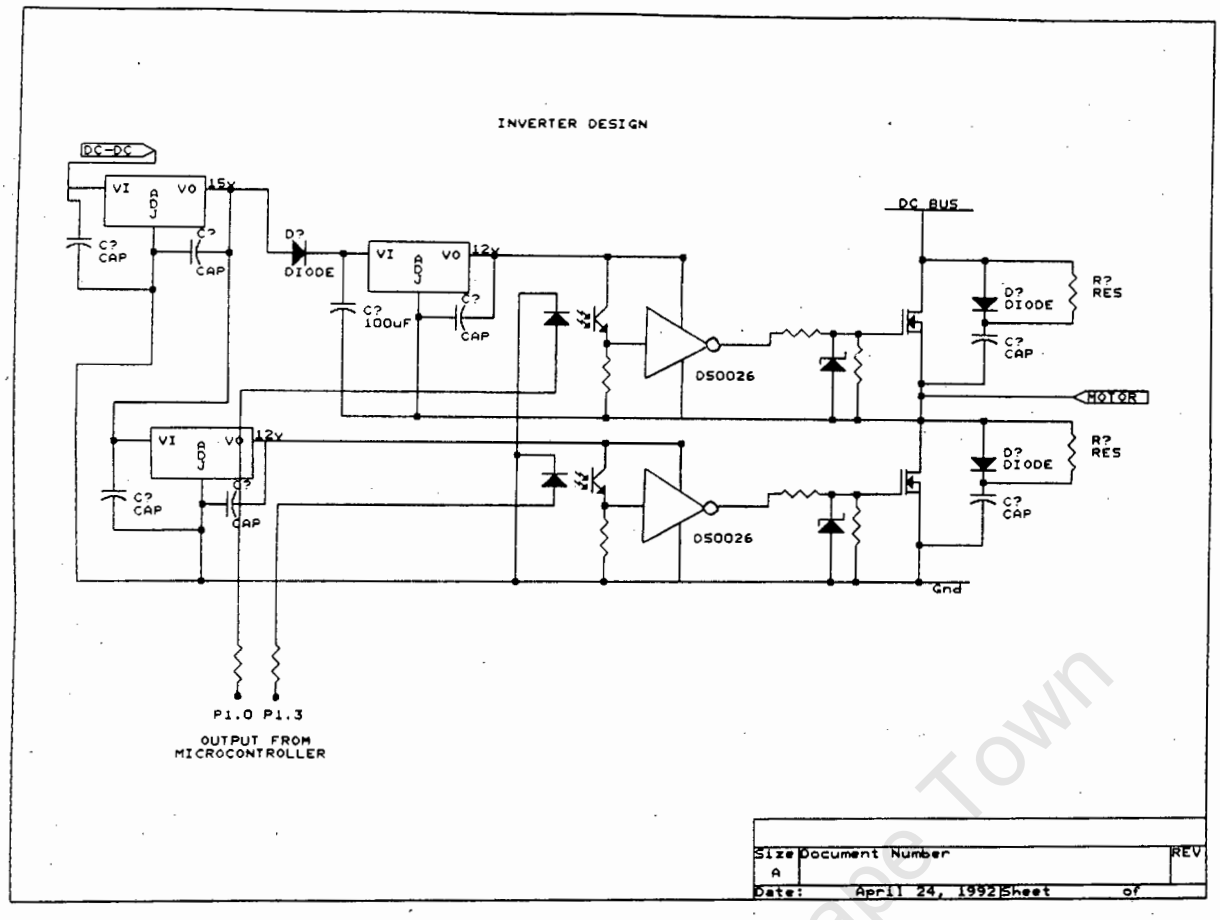

CALCULATION OF SNUBBER COMPONENTS

The turn-off snubber network is shown below and component values for the resistance R_S and capacitance C_S must be determined.

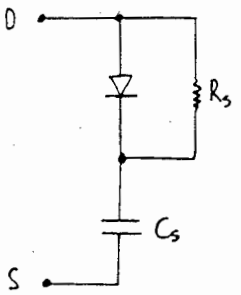

Figure: Turn-off snubber network

At turn-off the principal current flows at first through the diode D_S and then charges the capacitor C_S. Its voltage is nearly identical with the drain-source voltage V_{ds} and increases until the free-wheeling diode begins to conduct. The dissipation of the energy stored in C_S takes place in the suppression resistor R_S at the next turn-on. From an AEG technical information document[30], the snubber components are recommended as follows:

(These components were deisigned for IGBT modules, but the same method can be used for MOSFETs.)

$$C_S \geq \frac{i_{DM}}{dV_{ds}/dt}$$

$$R_{Smin} \geq \frac{V_{ds}}{I_{DRM}}; \qquad R_{Smax} \leq \frac{t_{fg\ min}}{4C_S},$$

where:
- i_{DM} = highest value of drain current to be turned-off
- dV_{ds}/dt = rate of rise of voltage at turn-off
- V_{ds} = drain source voltage immediately prior to turn-on
- I_{DRM} = maximum permissible repetitive peak current
- $t_{fg\ min}$ = minimum duration of forward gate-source voltage

The above parameters were determined at the highest switching frequency and at this frequency the peak current was measured to be 4A. For a DC voltage of 85v and a rise time of 2_us, the capacitor C_S was found to be 0.098_uF. R_{Smax} was found to be 1000 ohms for a gate-source transition time of 400_us.

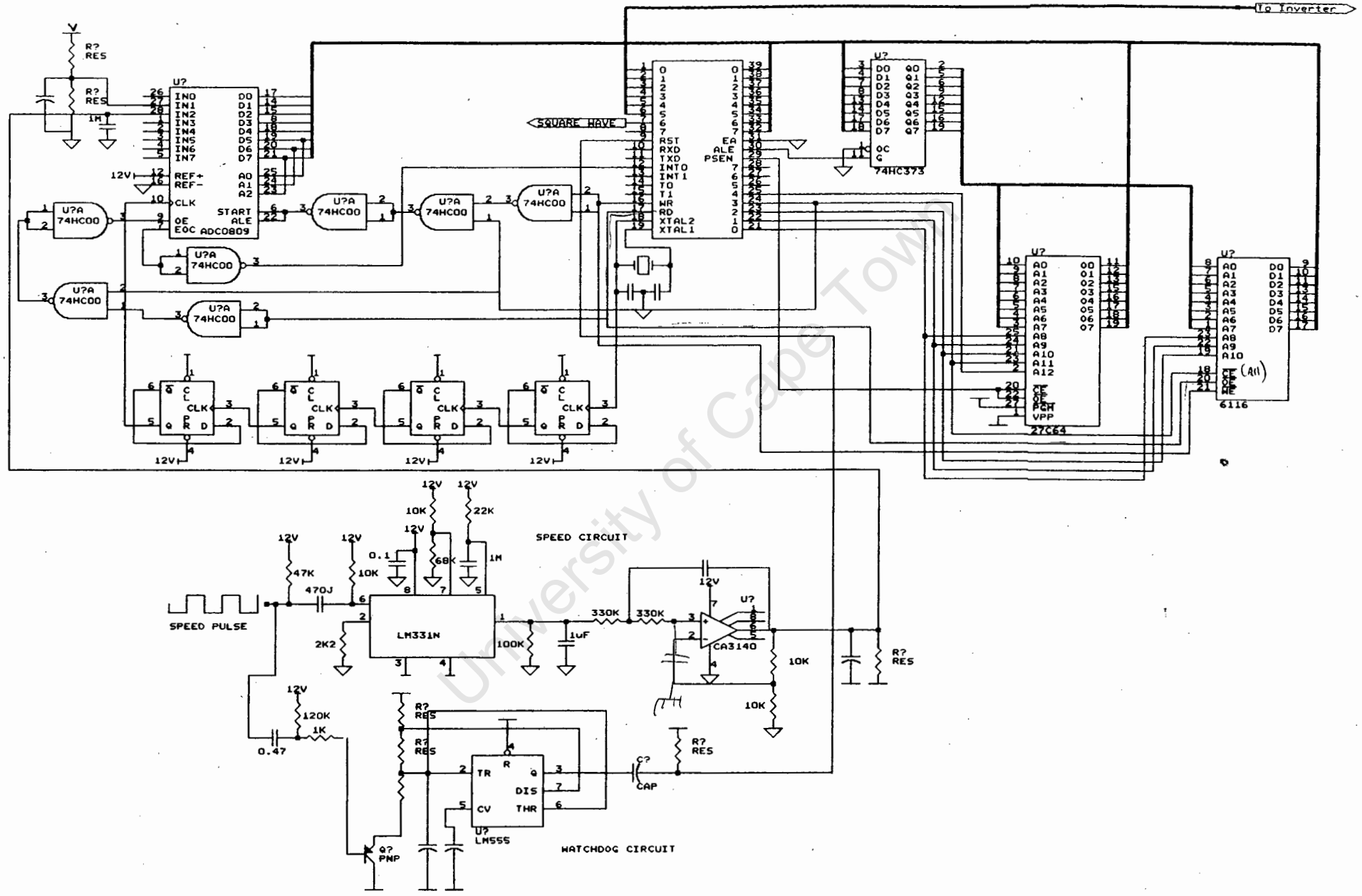

APPENDIX 5.2: MICROCONTROLLER CIRCUIT

APPENDIX 5.3: DC-DC CONVERTER CIRCUIT

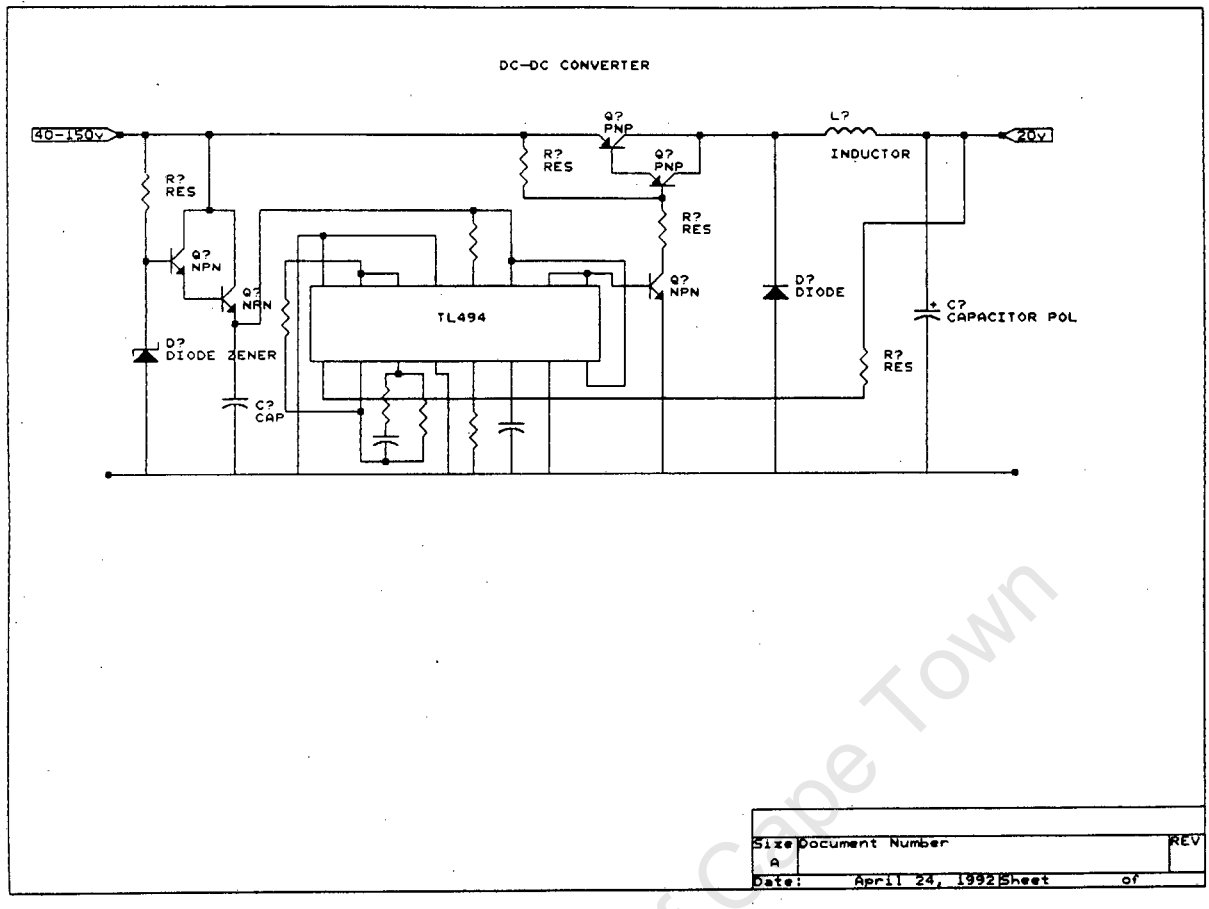

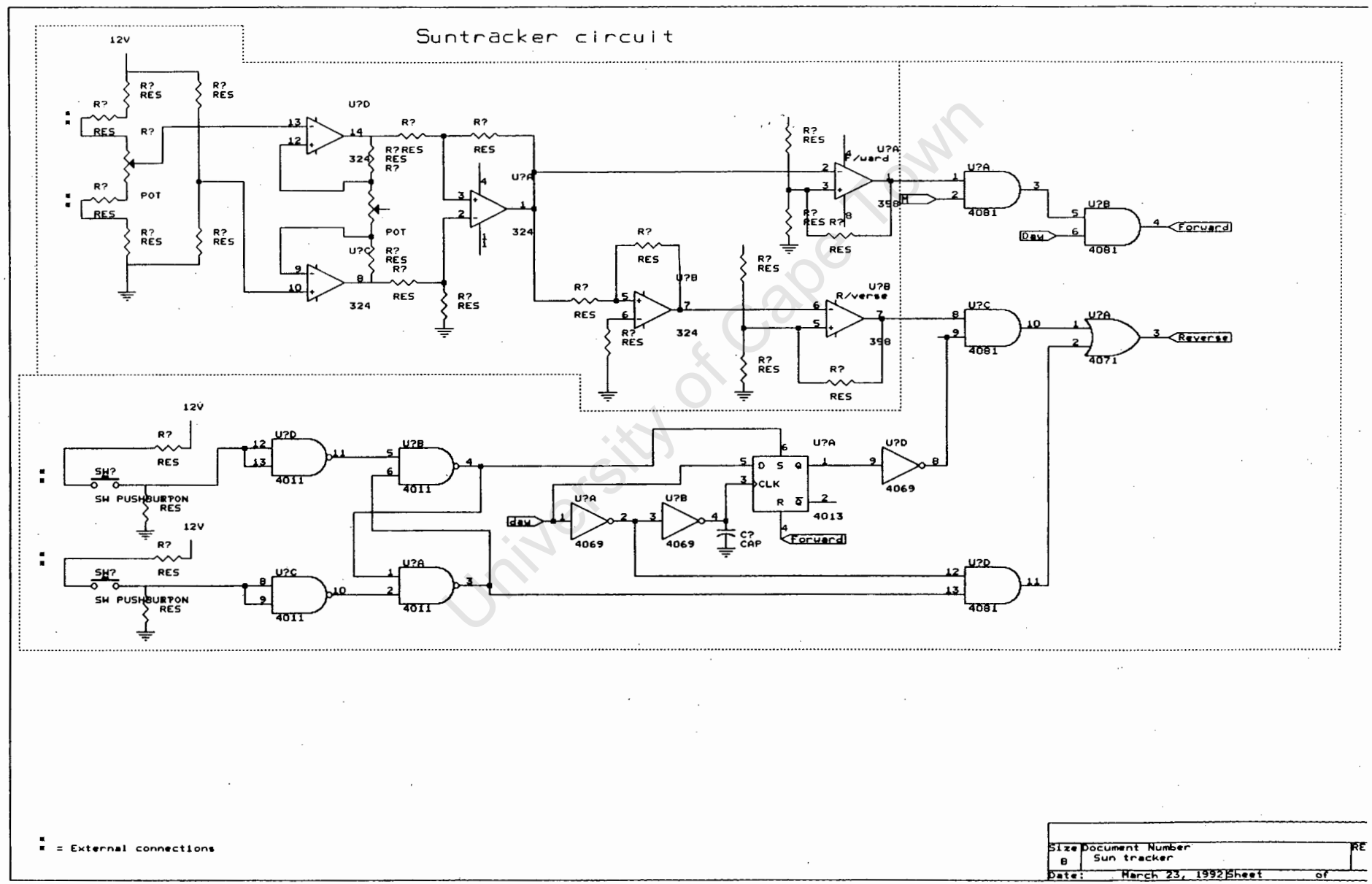

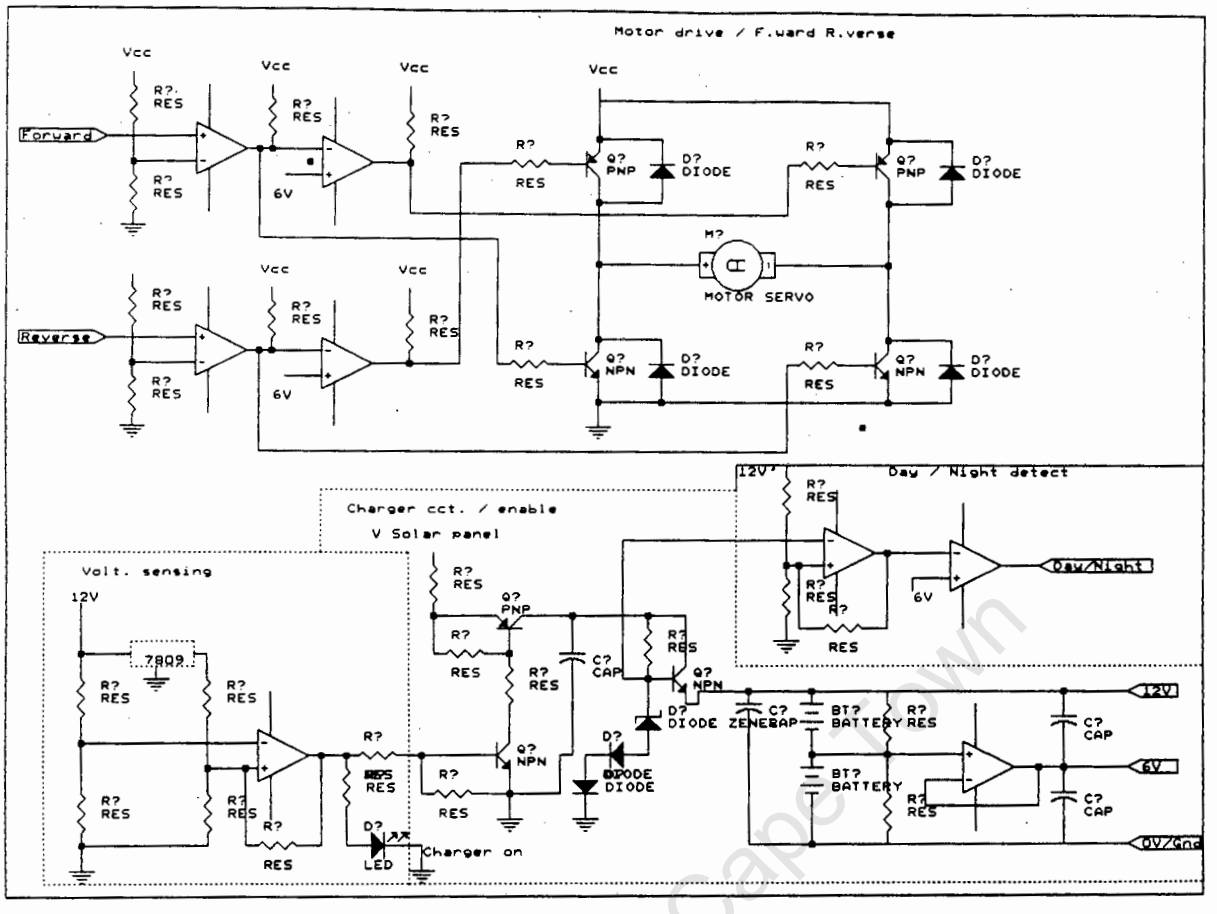

APPENDIX 6: OPERATION OF 8031 MICROCONTROLLER

DESCRIPTION OF 8031 ARCHITECTURE

The 8031 is a member of the Intel MCS-51 family. Some of its features are :

- 8-bit CPU optimized for control purposes
- Extensive Boolean processing
- 64K Program Memory address space
- 64K Data Memory address space
- 128 Bytes of on-chip Data RAM
- 32 bidirectional I/O Lines
- Two 16-bit timers
- Interrupt structure with two priority levels

1. Memory Organization Structure

Separate space is provided for the Data Memory and the Program Memory. 16-bit Data Memory addresses are generated through the DPTR register. Program Memory can only be read, and this is done by the Program Store Enable (/PSEN) signal. To access external Data Memory, the /RD and /WR signals are used. In order to access RAM, the DPTR register is used with the following two instructions :

MOVX A,@DPTR , which moves data from the address supplied from the DPTR to the Accumulator.

MOVX @DPTR,A , which moves data from the Accumulator to the address supplied by the DPTR

To access lookup tables in Program memory, two instructions are available. Since these instructions access only Program Memory, the lookup tables can only be read and not updated. The instructions are shown below :

MOVC A,@A+DPTR , which reads Program Memory at A+DPTR

MOVC @A+DPTR,A , which reads Program Memory at A+DPTR

2. Internal Data Memory

Internal Data Memory addresses are always one byte wide. The lowest 32 bytes are grouped into 4 banks of 8 registers. Program instructions call out these registers as R0 through R7. Two bits in the Program Status Word select which register bank is in use. This allows a more efficient use of code space, as register instructions are shorter than instructions that use direct addressing.

The next 16 bytes above the register banks form a block of bit-addressable memory space. The 128 bits in this area can be manipulated by a wide range of instructions which address the bits directly. The bit addresses in this area are 00H through 7FH.

Special Function Registers include the port latches, timers and peripheral controls. These are only accessed by direct addressing.

3. Interrupt Structure

The 8031 provides 5 interrupt sources, 2 external interrupts, 2 timer interrupts and a serial port interrupt. What follows is an overview of this interrupt structure.

3.1 Interrupt Enables

Each of the interrupt sources can be individually enabled or disabled by setting or clearing a bit in the Interrupt Enable (IE) register. This register also has a global disable bit, which can be cleared to disable all interrupts at once.

3.2 Interrupt Priorities

Each interrupt source can also be individually programmed to one of two priority levels by setting or clearing a bit in the Interrupt Priority (IP) register.

A low-priority interrupt can be interrupted by a high-priority interrupt, but not by another low-priority interrupt. A high priority interrupt cannot be interrupted by another interrupt source.

3.3 Operation of Timers

When these interrupts are configured as 16-bit Timers, they count up with two registers and cause an interrupt when an overflow occurs. After they have caused an interrupt, they continue counting up. When an interrupt is received, it is therefore necessary to reload the registers with the required values.

APPENDIX 7: PROGRAM LISTING

```
$ DATE(26-09-90)
$ PAGEWIDTH(100)
$ TITLE(Power_Track)
;-----------------------------------------
;
;* VARIABLE DEFINITIONS: This section defines
;  variables which are stored in internal RAM and
;  are directly addressable. The variables are
;  either bit or byte addressable.

FLAG1      BIT        7FH
FLAG2      BIT        7EH
FLAG3      BIT        7DH
FLAG4      BIT        7CH
FLAG5      BIT        7BH
FLAG6      BIT        77H
GEAR       BIT        7AH
SWITCH     BIT        79H
READY      BIT        78H
STRTUP     BIT        77H
PSTREF     BIT        76H
REBOOT     BIT        75H
;
NEWVAL     DATA       2CH
MASK       DATA       2BH
TMPCHK     DATA       2AH
STDPL      DATA       29H
TOHSET     DATA       28H
TOLSET     DATA       27H
TMPDPH     DATA       26H
TMPVAL     DATA       25H
STDPH      DATA       24H
VOLTS      DATA       23H
SPEED      DATA       22H
VREF       DATA       21H
NOLD1      DATA       30H
NOLD2      DATA       31H

;
;* RECEIVING INTERRUPTS: This section directs
; the program counter when the controller is
; reset or a service routine is received

ORG 0000H
           JMP START
ORG 0003H
           JMP INTRPT
ORG 000BH
           JMP TIMERO
ORG 001BH
           JMP TIMERI
;
;* MAIN PROGRAM: The main program is purely
responsible for setting up the status of the
interrupts and initializing variables.

ORG 0030H
START:

; Initializing Variables:

           MOV R3,#020D
```

```
          MOV R7,#00H             ;R7 is used as an offset to point to
                                  ; the next voltage and frequency.  There
                                  ; are 108 frequency values over 0 - 80Hz.
          MOV STDPH,#00H
          MOV STDPL,#00H
          MOV TMPCHK,#00H
          MOV TMOD,#00010001B
          MOV VREF,#170D          ;Reference voltage at which
                                  ;panel voltage is initially maintained
          CLR GEAR
          CLR READY
          CLR SWITCH
          CLR REBOOT

; Interrupt status set:

          MOV TH1,#0FFH           ;Timer 1 interrupts first so that a table
          MOV TL1,#00H            ;can be set up before  timer 0
                                  ;comes into operation
          MOV TL0,#01H
          MOV TH0,#00H
          MOV TOLSET,#0D0H
          MOV TOHSET,#0FFH

          ORL TCON,#01010001B     ; Timer Control
          ORL IE,#10001011B       ; Interrupts timer 0, timer 1
                                  ;  and interrupt 0 are enabled
          MOV MASK,#10000010B     ; This is variable is used later to
                                  ;  create a third priority level
          ORL IP,#00000011B       ; Timer 0 and interrupt 0 are
                                  ;  assigned high priority levels

IDLE:     NOP
          JMP IDLE
;
;
;-------------------------------------------------
;         SERVICE ROUTINE TIMERO
;
;This service routine sequentially outputs the
;elements of the three-phase table that has been
;set up by timer 1
;
TIMERO:   MOV TH0,TOHSET          ;Speed of timer 0 is determined
          MOV TL0,TOLSET          ; by variables TOHSET and TOLSET,
                                  ; each of which is set for the required
                                  ; frequency in the timer 1 routine
          PUSH ACC
          PUSH DPL
          PUSH DPH
          MOV A,STDPL
          JNZ NOTRAN              ;If the pointer passes through zero,
                                  ; it is possible that a change in modes
                                  ; (above or below 40Hz) could occur.
          JNB READY,NOTRAN        ;Change in modes if bit READY is set
          CLR READY
          MOV A,STDPH
          CPL ACC.0               ;Toggle bit to address different
                                  ; table if a change in modes occurs
          MOV STDPH,A
NOTRAN:   MOV DPH,STDPH           ;Address of new table element
          MOV DPL,STDPL           ; loaded into DPL and DPH
          MOVX A,@DPTR            ;New element is read in.
          MOV NEWVAL,A
```

```
          MOV P1,A
          NOP                    ; Wait 15uS before writing out the new value
          NOP
          NOP
          NOP
          INC DPL                ; Update pointer for next element
          MOV STDPL,DPL
          POP DPH
          POP DPL
          POP ACC
          MOV P1,NEWVAL
          RETI
;-----------------------------------------
;         SERVICE ROUTINE INTRPT
;This service routine is used to indicate when
;the ADC has completed its latest conversion.
;A third priority level is created because the
;timer 1 routine is still in progress.
;
INTRPT:   PUSH IE
          MOV IE,#MASK
          CALL LABEL
          CLR FLAG2              ;Flag2 is set when the
                                 ; interrupt is receeived
          POP IE
          RET
LABEL:    RETI
;
;-------------------------------------------------
;         SERVICE ROUTINE TIMERI
;This routine forms the core of the controller
;operation. It sets up a three-phase table in
;RAM for timer 0 to access and it determines the
;speed of timer 0.

TIMERI:   DJNZ R6,DELPOW         ;R6 determines the sampling
                                 ; rate of timer 1
          MOV R6,#15D            ;During start up the sampling rate
                                 ; is slower than for normal operation
          JB STRTUP,GETPOW
          MOV R6,#02D

GETPOW:   MOV A,#40H             ;Address of speed signal
          CALL GETVAL
          MOV SPEED,A

          MOV A,#20H             ;Address of voltage signal
          CALL GETVAL
          MOV VOLTS,A

          CALL STRTIN            ;Checks if start up is necessary
          JB STRTUP,BYPASS
          CALL CONTR             ;Controller routine to determine
                                 ; new frequency and voltage
BYPASS:   CALL SETVLT            ;Uses look-up table to get new voltage
          CALL SWOVER            ;Checks if a change in modes is required
          CALL TABLE             ;Creates a table for timer 0 to access
          CALL THRSEQ            ;Generates three-phase table in RAM
          CALL WAITSW            ;Waits for a zero crossing
          CALL RESUME            ;New frequency is updated
DELPOW:   RETI
;-----------------------------------------
;         SUBROUTINE GETVAL
;This subroutine interfaces with the ADC to
```

```
;accumulator before the subroutine is called.
;The value that is read in is placed in the accumulator.

GETVAL:   SETB FLAG2
          MOV DPTR,#0800H        ;ADC selected at this address
          MOVX @DPTR,A
WAIT1:    NOP
          JB FLAG2,WAIT1         ;Waits for interrupt to be received
          MOV DPTR,#0800H
          MOVX A,@DPTR
          RET
;-------------------------------------------------------------
;         SUBROUTINE STRTIN
;Subroutine sets the new frequency during start up

STRTIN:   CLR STRTUP
          CLR C
          MOV A,SPEED
          SUBB A,#40D
          JNC ENDLIM             ;Controller routine if speed
                                 ; is above a certain value
          MOV A,SPEED
          JNZ STLMOV
          CALL RESTRT            ;Subroutine called if motor has stalled
          JMP ENDLIM

STLMOV:   CLR REBOOT
          ADD A,#04H             ;New frequ = Speed + 2 during start up.
          CLR ACC.0
          MOV R7,A
          SETB STRTUP
ENDLIM:   RET
;-------------------------------------------
;         SUBROUTINE RESTRT
;Subroutine used if the motor has stalled
;If the speed was zero, try the lowest
;frequency, if it stays zero then
;disable the MOSFETs and the watchdog will
;reboot after a 3 second delay.

RESTRT:
JNB REBOOT,WASZRO
          MOV P1,#0FFH           ;Switches off the MOSFETs
          CLR IE.1               ;Disables Timer 0
WASZRO:   SETB REBOOT


          MOV R7,#00H
          SETB STRTUP
          RET
;-------------------------------------------
;         SUBROUTINE CONTR
;This subroutine determines the new operating
;frequency. At the end of the routine, a number
;is left in R7 which indicates the new frequency
;and voltage. The controller maintains the
;panels at a fixed voltage, which is slowly
;adjusted to maximize the speed.

CONTR :   MOV A,VOLTS
          CLR C
          SUBB A,VREF
          JC TOFAST
          JZ ENDADJ              ;No adjustment to the frequency is required
```

```
          DEC A
          JZ ENDADJ
          INC R7                ;The voltage is too high so
          INC R7                ; the frequency is increased
          JMP ENDADJ

TOFAST:   DEC R7                ;The voltage is too low and so
          DEC R7                ; the frequency is lowered

          CPL A                 ;If the voltage is significantly less
          CLR C                 ; than Vref then the frequency
          SUBB A,#08D           ; is decreased 4 times
          JC ENDADJ
          MOV A,R7
          SUBB A,#06H
          MOV R7,A

ENDADJ:   DJNZ R5,ENDFRQ
          MOV R5,#25D           ;After every 25th sample Vref is adjusted
          CALL AVESPD

          SUBB A,SPEED
          JC SPDINC
          JMP SPDDEC

SPDINC:   JB PSTREF,INCREF
          JMP DECREF

SPDDEC:   JB PSTREF,DECREF
          JMP INCREF

DECREF:   DEC VREF              ;The reference voltage is decreased
          CLR PSTREF
          JMP UPDATE

INCREF:   INC VREF              ;The reference voltage is increased
          SETB PSTREF
          JMP UPDATE

UPDATE:   MOV NOLD2,NOLD1
          MOV NOLD1,SPEED
ENDFRQ:   RET

;-------------------------------------------------
;         SUBROUTINE AVESPD
;This subroutine determines the average speed of
;the previous two readings, Nold1 and Nold2

AVESPD:   CLR C
          MOV A,NOLD1
          RR A
          CLR ACC.7
          MOV B,A
          MOV A,NOLD2
          RR A
          CLR ACC.7
          ADD A,B           ;A contains the average speed
          RET

;-----------------------------------------
;         SUBROUTINE SETVLT
;Gets the start address of the new voltage
;table to be accessed
```

```
MOVC A,@A+DPTR          ;Use R7 as an offset to the base address
          MOV TMPDPH,A
          MOV A,R7
          INC A
          MOVC A,@A+DPTR
          MOV DPL,A                 ;Data pointer is updated
          MOV DPH,TMPDPH
          RET
;-------------------------------------------------------
;         SUBROUTINE SWOVER
;This routine indicates to timer 0 that a
;change in modes is about to occur

SWOVER:   MOV A,DPH                 ;High frequency mode tables are
                                    ; stored in a different memory
                                    ; section (from 0800H)
          XRL A,TMPCHK
          MOV C,ACC.3
          MOV SWITCH,C              ;Change in modes if switch is set
          MOV A,DPH
          MOV TMPCHK,A
          RET

;-------------------------------------------------------
;         SUBROUTINE TABLE
;This subroutine generates a three-phase table
in RAM by calling in READBL, SNGSEQ and THRSEQ.

TABLE:    CALL READBL
          CALL SNGSEQ
          CALL THRSEQ
          RET

;-------------------------------------------------------
;         SUBROUTINE READBL
;
;This subroutine reads in the PWM voltage block
;sizes and stores them in internal RAM.

READBL:   MOV A,DPH
          MOV C,ACC.3
          MOV GEAR,C                ;High/low frequency mode
          MOV R1,£40H               ;Start address of internal RAM
          MOV R0,£00H
NXTBYT:   MOV A,R0
          MOVC A,@A+DPTR            ;Read in the next element
          MOV @R1,A
          INC R1
          INC R0
          INC A
          JNZ NXTBYT          ;At end of ROM table, last element is OFFH
          DEC R1
          DEC R0
          DEC R0
LIFEAS:   DEC R0
          MOV A,R0
          MOVC A,@A+DPTR            ;ROM table is read backwards
                                    ; to get a half cycle
          MOV @R1,A
```

```
            INC R1
            MOV A,R0
            JNZ LIFEAS
            CPL GEAR
            JNB GEAR,NXTBYT         ;Process is repeated if
                                    ; in high frequency mode
            MOV A,DPH
            MOV C,ACC.3
            MOV GEAR,C
            MOV A,#0FFH             ;The last element in the RAM
                                    ; table is also 0FFH
            MOV @R1,A
            RET
;-------------------------------------------------------------
;           SUBROUTINE SNGSEQ
;
;This subroutine generates a sequence of 1's
;and 0's which simulates the single
;phase PWM voltage. These 1's and 0's are stored
;in external RAM. There are a total of 256 values.
;
SNGSEQ:     MOV DPTR,#0200H         ;Base of single phase table
            CLR FLAG1
            CLR FLAG3
NXTHLF:     MOV R1,#40H
NXTBLK:     MOV A,@R1
            JZ NOCHGE
            MOV R4,A
            INC A
            JNZ CONTIN
            CPL FLAG3
            JB FLAG3,NXTHLF         ;Process is repeated to get
                                    ; the second half of the cycle
            JMP ENDSQ1
CONTIN:     JB FLAG1,OUT1
            MOV A,#00H              ;'00' written to RAM
            JMP EXTMEM
OUT1:       MOV A,#01H              ;'01' written to RAM
EXTMEM:     MOVX @DPTR,A
            INC DPTR
            DJNZ R4,EXTMEM
NOCHGE:     CPL FLAG1
            INC R1
            JMP NXTBLK
ENDSQ1:     RET
;
;-------------------------------------------------------------
;           SUBROUTINE THRSEQ
;
;This subroutine generates a sequence of 1's and
;0's in six bits per byte. These 1's and 0's are
;the controls for a three phase PWM voltage
;waveform. They are stored in external RAM.
;
THRSEQ:     MOV DPTR,#0200H         ;Base address of single phase table
NXTLOC:     MOV B,#00H
            MOV R0,DPL
            MOVX A,@DPTR
            MOV C;ACC.0
            MOV B.0,C               ;Phase A element placed in B.0
```

```
            MOV A,DPL

            JB GEAR,HIFRQA
            ADD A,£85D              ;Offset for low frequency mode
            JMP LOFRQA
HIFRQA:     ADD A,£43D              ;Offset for high frequency mode

LOFRQA:     MOV DPL,A
            MOVX A,@DPTR
            MOV C,ACC.0
            MOV B.1,C               ;Phase B element placed in B.1
            MOV A,DPL

            JB GEAR,HIFRQB
            ADD A,£86D
            JMP LOFRQB
HIFRQB:     ADD A,£43D

LOFRQB:     MOV DPL,A
            MOVX A,@DPTR
            MOV C,ACC.0
            MOV B.2,C               ;Phase C element placed in B.1
            MOV A,B
            RL A
            RL A
            RL A
            CPL A
            ANL A,£00111000B
            ADD A,B                 ;Complements of all phases stored
                                    ; in bits B.3,B.4 and B.5

            MOV B,A
            MOV A,R0
            RLC A
            JC SQUARE
            SETB ACC.7
            JMP LSTWRD
SQUARE:     CLR ACC.7
LSTWRD:     ANL A,£10000000B
            ADD A,B             ;A square wave is created in B.7 so that
                                ; the PWM signals are  synchronized and
                                ; easily viewed on an oscilloscope
            MOV DPL,R0
            DEC DPH
            DEC DPH
            JNB GEAR,LOADDR
            INC DPH
LOADDR:     CPL A
            MOVX @DPTR,A
            MOV DPH,£02H
            INC DPL
            MOV A,DPL
            JNZ NXTLOC
            RET
;-------------------------------------------------------
;           SUBROUTINE WAITSW
;Waits for address of timer 0 to pass through
;zero so that synchronous switching can take
;place if there is a change in modes

WAITSW:     MOV A,STDPL
```

```
            JNZ WAITSW
            MOV C,SWITCH
            MOV READY,C
            RET
;-------------------------------------------------------------
;           SUBROUTINE RESUME
; Sets up new timer 0 speed values

RESUME:     MOV DPTR,£0500H
            MOV A,R7
            MOVC A,@A+DPTR
            MOV TOLSET,A
            MOV A,R7
            INC A
            MOVC A,@A+DPTR
            MOV TOHSET,A
            RET
;-------------------------------------------------------------

ORG 0500H

;Linearized frequency table:

DB 195,251, 244,252, 160,253, 013,254, 013,254
DB 013,254, 013,254, 045,254, 045,254, 045,254
DB 089,254, 145,254, 170,254, 188,254, 222,254
DB 232,254, 249,254, 016,255, 024,255, 035,255
DB 048,255, 059,255, 066,255, 074,255, 083,255
DB 089,255, 094,255, 102,255, 107,255, 114,255
DB 118,255, 121,255, 127,255, 130,255, 135,255
DB 140,255, 143,255, 145,255, 148,255, 152,255
DB 155,255, 157,255, 160,255, 162,255, 165,255
DB 166,255, 169,255, 171,255, 173,255, 175,255
DB 177,255, 178,255, 180,255, 182,255, 183,255
DB 184,255  107,255, 110,255, 113,255, 114,255
DB 118,255, 120,255, 121,255, 124,255, 127,255
DB 129,255, 130,255, 133,255, 135,255, 137,255
DB 139,255, 140,255, 143,255, 144,255, 145,255
DB 147,255, 148,255, 150,255, 152,255, 153,255
DB 155,255, 156,255, 157,255, 158,255, 159,255
DB 160,255, 162,255, 163,255, 165,255, 166,255
DB 167,255, 168,255, 169,255, 170,255, 171,255
DB 172,255, 173,255, 174,255, 175,255, 175,255
DB 176,255, 176,255, 177,255, 177,255, 177,255
DB 178,255, 178,255, 179,255, 179,255, 179,255
DB 179,255, 179,255, 179,255, 179,255, 179,255
DB 179,255, 179,255, 179,255, 179,255, 179,255
DB 179,255, 179,255, 179,255, 179,255, 179,255
DB 179,255, 179,255, 179,255,

ORG 0600H
;Voltage table:
DB 03H,000H, 03H,000H, 03H,000H, 03H,000H, 03H,000H
DB 03H,000H, 03H,000H, 03H,000H, 03H,000H, 03H,000H
DB 03H,060H, 03H,060H, 03H,060H, 03H,080H, 03H,080H
DB 03H,080H, 03H,080H, 03H,0A0H, 03H,0A0H, 03H,0A0H
DB 03H,0A0H, 03H,0A0H, 03H,0C0H, 03H,0C0H, 03H,0C0H
DB 03H,0C0H, 03H,0E0H, 03H,0E0H, 03H,0E0H, 04H,000H
DB 04H,000H, 04H,000H, 04H,020H, 04H,020H, 04H,020H
DB 04H,020H, 04H,020H, 04H,040H, 04H,040H, 04H,040H
```

```
DB 04H,040H, 04H,040H, 04H,040H, 04H,060H, 04H,060H
DB 04H,060H, 04H,080H, 04H,080H, 04H,080H, 04H,0A0H
DB 04H,0A0H, 04H,0A0H, 04H,0A0H, 04H,0A0H, 04H,0C0H
DB 04H,0C0H, 08H,000H, 08H,000H, 08H,000H, 08H,000H
DB 08H,000H, 08H,000H, 08H,000H, 08H,000H, 08H,000H
DB 08H,000H, 08H,000H, 08H,000H, 08H,000H, 08H,000H
DB 08H,000H, 08h,000h, 08H,000H, 08H,000H, 08H,000H
DB 08H,020H, 08H,020H, 08H,020H, 08H,020H, 08H,020H
DB 08H,020H, 08H,020H, 08H,020H, 08H,020H, 08H,020H
DB 08H,020H, 08H,020H, 08H,020H, 08H,020H, 08H,020H
DB 08H,020H, 08H,020H, 08H,040H, 08H,040H, 08H,040H
DB 08H,040H, 08H,040H, 08H,040H, 08H,040H, 08H,040H
DB 08H,040H, 08H,040H, 08H,040H, 08H,040H, 08H,040H
DB 08H,040H, 08H,040H, 08H.040H, 08H,040H, 08H,040H
DB 08H,040H, 08H,040H, 08H,040H, 08H,040H, 08H,040H
DB 08H,040H, 08H,040H, 08H,040H, 08H,040H, 08H,040H
DB 08H,040H, 08H,040H, 08H,040H, 08H,040H, 08H,040H
DB 08H,040H, 08H,040H, 08H,040H
```

(29)

```
;PWM Ratios: (Low frequency mode)
ORG 0300H
DB 2,2,2,2,2,2,2,2,2,3,2,2,2,3,2,2,2,3,2,2,2,3,2,2,2,3,3,1,2,1,4,0FFH
ORG 0320H
DB 2,2,2,2,2,2,2,2,3,2,2,2,2,3,1,2,2,3,1,2,2,3,1,2,2,3,1,2,2,3,3,6,0FFH
ORG 0340H
DB 2,2,2,2,1,2,2,2,3,1,2,2,3,1,2,2,3,1,2,2,3,1,2,2,3,1,2,2,4,1,2,2,4,3,6,0FFH
ORG 0360H
DB 2,2,2,2,1,2,2,2,3,1,2,2,3,1,2,2,3,1,2,2,3,1,2,2,4,1,2,2,4,1,2,2,4,2,6,0FFH
ORG 0380H
DB 2,2,2,2,2,2,2,2,3,1,2,2,3,1,2,2,3,1,2,2,4,1,2,2,4,2,6,2,6,0FFH
ORG 03A0H
DB 2,2,2,2,2,2,2,2,3,1,2,2,3,1,2,2,4,2,6,2,6,2,6,2,8,0FFH
ORG 03C0H
DB 2,2,2,3,1,2,2,2,3,1,2,2,3,1,2,2,3,2,6,2,6,2,7,2,8,0FFH
ORG 03E0H
DB 2,2,2,2,2,5,3,6,2,6,2,6,2,7,2,7,2,8,0FFH
ORG 0400H
DB 4,4,3,5,3,6,2,6,2,6,2,7,2,7,1,8,0FFH
ORG 0420H
DB 4,5,3,5,3,6,2,6,2,6,2,7,1,7,1,8,0FFH → 80%, 15 SW
ORG 0440H
DB 4,5,3,5,3,6,2,6,2,7,1,7,1,7,1,8,0FFH → 80%
ORG 0460H
DB 4,4,3,5,3,6,2,6,2,7,1,7,1,8,1,8,0FFH
ORG 0480H
DB 4,4,3,5,3,6,2,7,1,7,1,7,1,8,1,8,0FFH
ORG 04A0H
DB 4,4,3,5,3,6,2,7,1,7,1,8,1,24,0FFH
ORG 04C0H
DB 4,5,3,5,2,6,2,7,1,8,1,40,0FFH → 90%
ORG 04E0H
DB 4,5,3,6,2,6,2,7,1,56,0FFH → 100%, n=15

;PWM Ratios: (High frequency mode)
ORG 0800H
DB 2,2,1,3,1,3,1,38,0ffH
ORG 0820H
DB 2,4,1,50,0ffH
ORG 0840H
DB 2,4,1,50,0FFH
```

APPENDIX 7.2: PWM RATIOS FOR INVERTER CONTROL

TABLE III

ELIMINATION OF 5TH, 7TH, AND 11TH HARMONICS OF THREE-PHASE INVERTER, SWITCHING ANGLES AND FUNDAMENTAL-WAVE AMPLITUDES

V_{max} 1	α_1	α_2	α_3	α_4	V_{max} 1	α_1	α_2	α_3	α_4
0.01	23.13	39.96	60.11	73.93	0.60	23.37	32.21	56.25	77.93
0.03	23.23	39.77	60.22	77.86	0.61	23.33	31.73	66.42	77.97
0.04	23.29	37.59	60.33	79.79	0.62	23.37	31.73	66.59	77.83
0.05	23.32	36.45	63.45	72.72	0.64	23.35	31.41	66.77	77.93
0.06	20.49	37.31	60.56	73.66	0.65	23.33	31.22	66.95	77.99
0.08	20.58	37.17	60.67	73.59	0.66	23.33	33.95	67.14	77.91
0.10	20.65	37.03	60.73	73.52	0.67	23.25	33.67	67.32	77.92
0.10	23.77	35.89	60.30	73.46	0.69	23.19	30.39	67.51	77.93
0.11	23.87	38.75	61.32	73.43	0.70	23.12	30.09	67.73	77.95
0.13	23.96	38.63	61.14	73.33	0.71	23.03	22.73	67.93	77.94
0.14	21.35	38.46	61.25	73.27	0.73	22.93	29.46	68.10	77.98
0.15	21.14	38.32	61.37	73.21	0.74	22.81	29.13	63.30	78.02
0.17	21.23	38.17	61.49	73.15	0.75	22.67	28.79	68.51	73.02
0.18	21.32	33.03	61.61	73.09	0.76	22.52	28.43	68.71	78.03
0.19	21.41	37.89	61.73	73.03	0.71	22.34	28.06	68.97	73.05
0.20	21.53	37.73	51.85	70.27	0.79	22.14	27.61	69.14	73.06
0.22	21.53	37.57	61.97	78.91	0.80	21.92	27.29	69.35	73.09
0.23	21.67	37.44	62.10	73.86	0.81	21.69	26.93	57.57	78.39
0.24	21.76	37.22	62.22	78.80	0.83	21.42	26.43	69.79	73.33
0.25	21.84	37.13	62.35	73.75	0.84	21.14	26.37	70.01	73.13
0.27	21.93	36.98	62.47	73.73	0.85	20.83	23.65	70.24	73.13
0.28	22.01	36.83	62.60	78.65	0.87	20.53	25.23	70.47	78.13
0.29	22.09	36.67	62.72	73.63	0.88	20.20	24.80	70.69	73.39
0.31	22.17	35.51	62.86	78.55	0.89	19.85	24.38	70.73	73.08
0.32	22.25	34.36	62.99	73.50	0.90	19.51	23.95	71.16	78.37
0.33	22.33	34.19	63.12	73.45	0.92	19.14	23.53	71.43	79.06
0.34	22.40	34.03	53.25	73.41	0.93	18.77	23.11	71.64	73.05
0.36	22.48	33.87	63.39	73.37	0.94	18.39	22.73	71.32	73.34
0.37	22.55	35.73	63.52	78.32	0.95	18.31	22.22	72.14	78.03
0.31	22.62	35.58	63.66	73.28	0.97	17.62	21.83	72.40	73.01
0.39	22.69	35.37	63.09	78.24	0.98	17.22	21.48	72.67	73.33
0.41	22.75	33.19	63.93	73.21	0.99	16.83	21.08	72.95	73.04
0.42	22.82	35.02	64.39	73.17	1.01	16.43	20.67	73.23	73.06
0.43	22.88	34.84	64.22	73.14	1.02	16.32	20.32	73.33	73.22
0.45	22.94	34.66	64.36	73.11	1.03	15.61	19.92	73.13	73.14
0.46	23.00	34.43	64.51	73.08	1.04	15.22	19.54	74.23	73.21
0.47	23.05	34.29	64.46	73.05	1.06	14.79	19.15	74.02	73.31
0.49	23.13	34.11	64.81	73.03	1.07	14.36	18.73	75.34	73.43
0.50	23.15	33.91	64.96	70.00	1.08	13.92	18.42	75.21	70.64
0.51	23.19	33.72	65.11	77.28	1.09	13.47	13.32	76.35	73.99
0.52	23.24	33.52	65.27	77.96	1.11	13.01	17.62	76.49	77.23
0.53	23.27	33.31	65.42	77.94	1.12	12.51	17.28	77.45	77.74
0.54	23.30	33.13	65.59	77.93	1.13	11.97	16.76	78.46	33.45
0.56	23.32	32.97	65.75	77.92	1.13	11.39	16.25	79.11	31.53
0.57	23.35	32.47	65.91	77.91	1.16	10.91	13.68	81.12	33.33
0.59	23.37	32.43	46.33	77.30	1.17	9.43	14.32	86.41	37.53

TABLE IV

ELIMINATION OF 5TH, 7TH, 11TH, AND 13TH HARMONICS OF THREE-PHASE INVERTER, SWITCHING ANGLES AND FUNDAMENTAL-WAVE AMPLITUDES

V_{max} 1	α_1	α_2	α_3	α_4	α_5	V_{max} 1	α_1	α_2	α_3	α_4	α_5
0.01	19.99	23.25	37.99	40.07	59.99	0.59	14.64	22.53	34.33	44.19	54.71
0.03	19.73	20.12	29.77	43.18	59.73	0.60	14.54	22.53	34.22	44.28	54.59
0.04	19.67	20.17	39.65	43.28	59.67	0.61	14.43	22.62	34.09	44.37	54.47
0.05	19.53	20.21	39.54	40.37	59.56	0.62	14.23	22.67	33.74	44.46	54.34
0.06	19.44	20.29	39.42	43.46	59.45	0.64	14.17	22.71	33.91	44.54	54.22
0.03	19.33	20.33	39.30	43.55	59.34	0.65	14.34	22.76	33.67	44.63	54.39
0.09	19.22	20.43	39.13	43.64	59.22	0.66	13.92	22.83	33.53	44.72	53.97
0.10	19.11	20.46	39.07	43.74	59.11	0.67	13.80	22.04	33.39	44.30	53.84
0.11	19.99	20.52	38.95	40.83	57.30	0.69	13.67	22.83	33.25	44.89	53.71
0.13	13.88	20.53	38.84	43.93	58.83	0.73	13.34	23.92	33.10	44.97	53.58
0.14	13.77	20.63	38.72	41.01	58.73	0.71	13.42	22.96	32.96	45.05	53.45
0.15	18.65	20.69	38.60	41.10	58.67	0.73	13.27	22.99	32.81	45.14	53.32
0.17	18.54	20.73	38.48	41.20	58.55	0.74	13.16	23.03	32.66	45.22	51.17
0.18	18.43	20.81	38.36	41.29	58.44	0.75	13.03	23.05	32.51	45.30	53.06
0.19	18.31	20.85	38.24	41.39	58.33	0.76	12.91	23.13	32.35	45.38	52.92
0.21	18.23	20.92	38.13	41.47	58.22	0.78	12.73	23.13	32.21	45.46	52.79
0.22	18.33	20.97	38.01	41.56	58.10	0.79	12.65	23.16	32.06	45.53	52.65
0.23	17.97	21.04	37.89	41.65	57.99	0.80	12.52	23.13	31.90	45.61	52.51
0.24	17.85	21.07	37.77	41.73	57.88	0.81	12.33	23.21	31.74	45.69	52.37
0.25	17.74	21.15	37.65	41.82	57.77	0.83	12.25	23.23	31.53	45.76	52.27
0.27	17.62	21.21	37.53	41.93	57.65	0.84	12.12	23.25	31.42	45.93	52.09
0.28	17.51	21.26	37.40	42.02	57.54	0.85	11.92	23.27	31.25	45.93	51.94
0.29	17.73	21.32	37.28	42.12	57.42	0.87	11.85	23.28	31.09	45.97	51.79
0.31	17.23	21.33	37.16	42.21	57.31	0.88	11.72	23.33	33.92	46.03	51.64
0.32	17.14	21.43	37.04	42.30	57.13	0.89	11.58	23.33	32.74	46.10	51.48
0.33	17.05	21.49	36.91	42.39	57.03	0.90	11.44	23.31	30.55	46.15	51.33
0.34	16.97	21.58	36.79	42.48	56.96	0.92	11.29	23.31	30.29	46.21	51.16
0.36	16.11	21.63	36.67	42.57	56.85	0.93	11.15	23.31	30.02	46.26	51.03
0.37	16.70	21.65	36.54	42.66	56.73	0.94	11.02	23.33	29.91	46.31	50.82
0.33	16.53	21.71	36.42	42.78	56.62	0.95	10.38	23.29	29.01	46.35	50.54
0.39	16.46	21.75	36.29	42.85	56.53	0.97	10.74	23.27	29.61	46.38	50.46
0.41	16.34	21.82	36.17	42.94	56.39	0.98	10.59	23.24	29.41	46.41	50.27
0.42	16.22	21.87	36.04	43.03	56.27	0.99	10.45	23.21	29.19	46.43	50.06
0.43	16.11	21.93	35.92	43.12	56.15	1.01	10.33	23.17	28.97	46.43	49.85
0.45	15.93	22.03	35.73	43.21	56.01	1.02	10.15	23.12	28.75	46.41	49.62
0.46	15.87	22.03	35.66	43.39	55.92	1.03	9.99	23.07	28.51	46.40	49.27
0.47	15.75	22.03	35.53	43.39	55.83	1.04	9.84	23.02	28.26	46.35	49.11
0.49	15.63	22.13	35.41	43.48	55.53	1.06	9.68	22.91	28.00	46.28	48.81
0.50	15.51	22.13	35.28	43.57	55.56	1.07	9.52	22.81	27.72	46.17	49.48
0.51	15.39	22.24	35.15	41.66	55.44	1.03	9.35	22.69	27.43	46.03	48.09
0.52	15.27	22.32	35.02	41.75	55.32	1.09	9.17	22.34	27.10	45.76	47.64
0.53	15.15	22.34	34.37	43.84	55.20	1.11	8.99	22.36	26.79	45.42	47.37
0.55	15.03	22.33	34.72	43.93	55.03	1.12	8.72	22.13	26.35	44.99	45.33
0.56	14.91	22.43	34.62	44.02	54.96	1.13	8.57	21.91	25.37	44.34	45.10
0.57	14.73	22.43	34.49	44.11	54.84	1.15	8.30	21.31	25.21	43.53	43.65
						1.13	7.88	22.19	22.92	23.47	43.47

```
;TRUE BASIC PROGRAM TO GENERATE PWM RATIOS

CLEAR
LET D = 2000          ;Sets resolution of superimposed sine wave
LET P = 128           ;Sets the number of divisions per cycle
LET OFB = 15          ;Sets the number of switches per cycle
let w = 80            ;Sets the modulation factor

PRINT W;"%";
LET Z = 100/W
LET Itmp = 0
LET TOTAL = 0
LET M = 0
LET J = 0
LET C = OFB + 0.5
LET B = 2 * (2*OFB + 1)
FOR I = 0 TO D
    LET Y = SIN ((I/D)*PI)        ;Generates sine wave
    IF I < M*(D/C) + D/B THEN
        LET F = (Z/(D/B))*(I-(M*D/C))
    ELSE
        LET F = Z - (Z/(D/B)) * (I-(M*D/C + D/B))
    END IF                                    ;Generates triangular wave

    IF I - (M*D/C + D/C) > 0.5 THEN LET M = M + 1
    LET Jtmp = J
    IF (F - Y) < 0.05 AND (Y-F) < 0.05 THEN
        LET J = 0
    ELSE
        LET J = 1         ;'1' or '0' created
    END IF
    IF Jtmp = 1 AND J = 0 THEN
         PRINT INT(0.5+((I-Itmp)*P/D));
         LET TOTAL = INT(0.5 + ((I-Itmp)*P/D)) + TOTAL
         LET Itmp = I
    END IF
NEXT I
PRINT TOTAL
LET W = W + 2
GET KEY ZZ
END
```

APPENDIX 8: HARMONIC CONTENT OF PWM WAVEFORMS

Voltage Waveforms

1) Frequency = 50 Hz

Sinusoidal Modulation

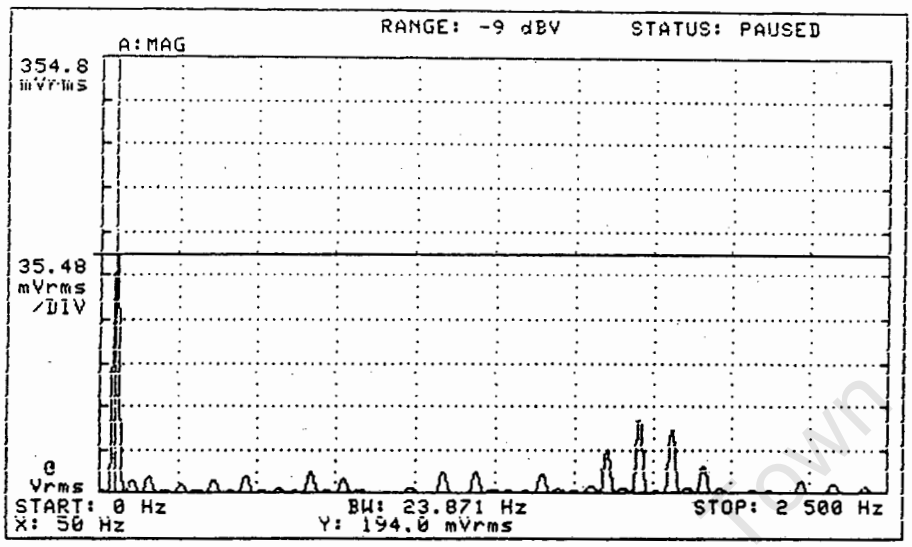

Harmonic Elimination

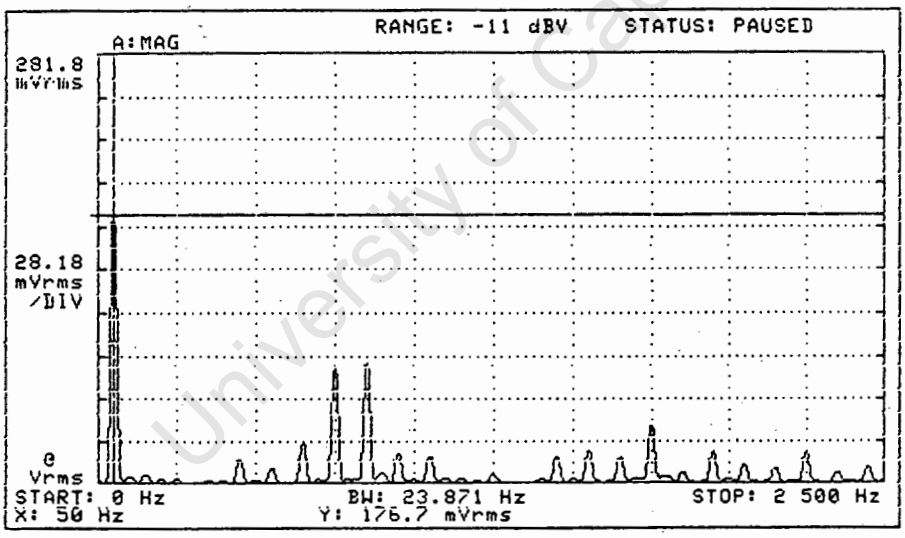

2) Frequency = 35 Hz

Sinusoidal Modulation

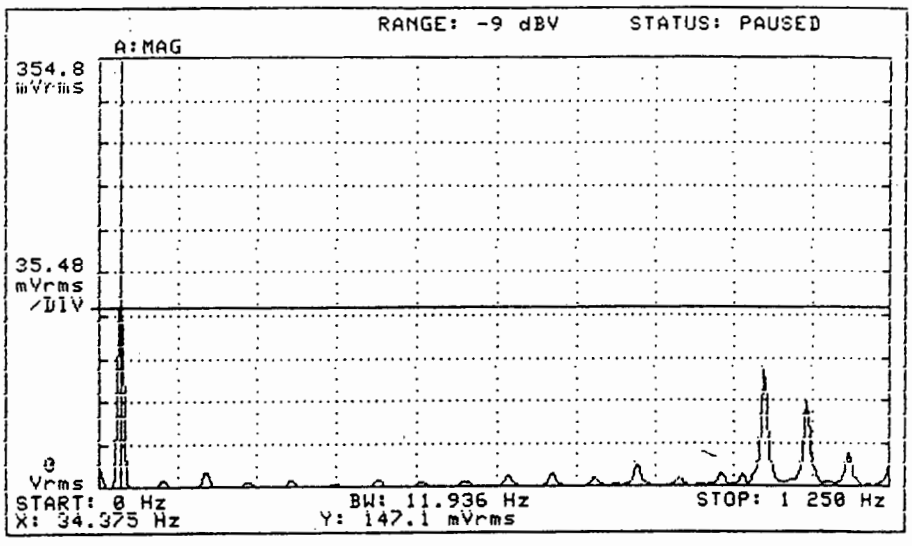

Harmonic Elimination

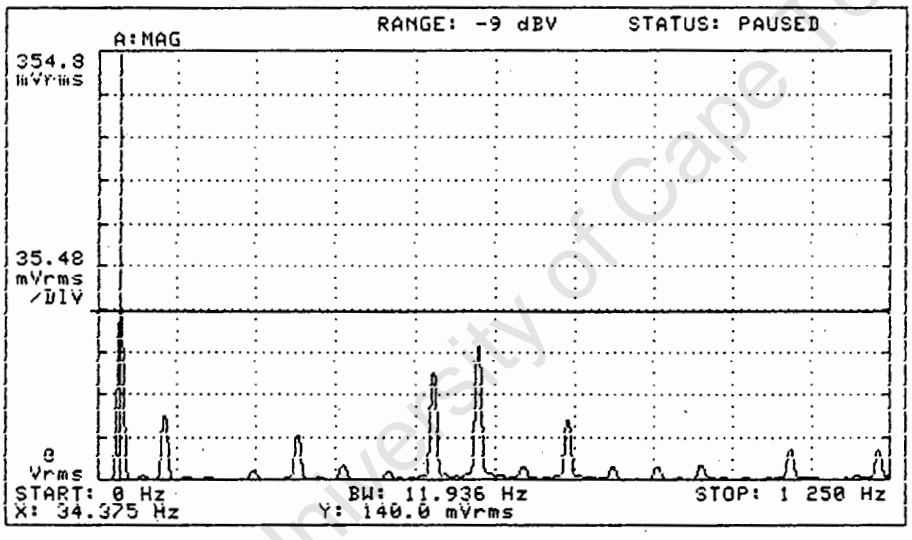

3) Frequency = 20 Hz

Sinusoidal Modulation

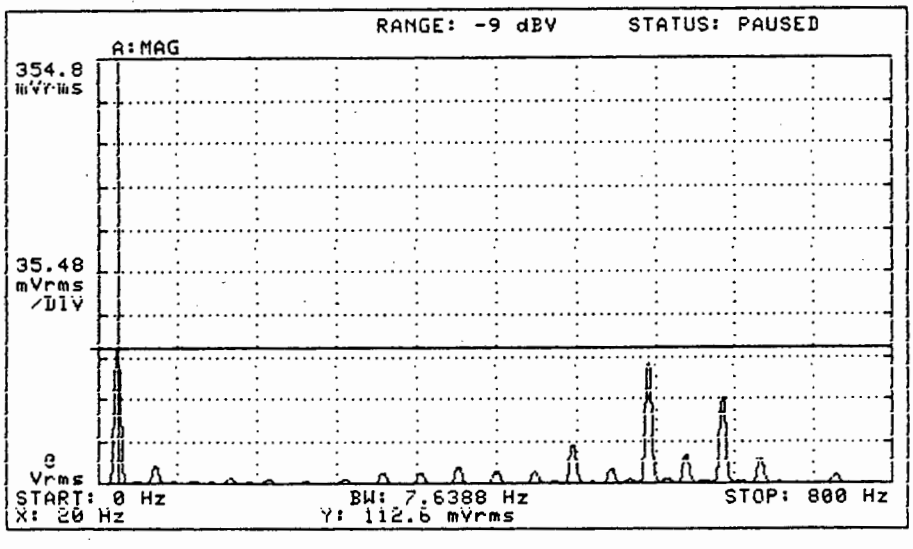

Harmonic Elimination

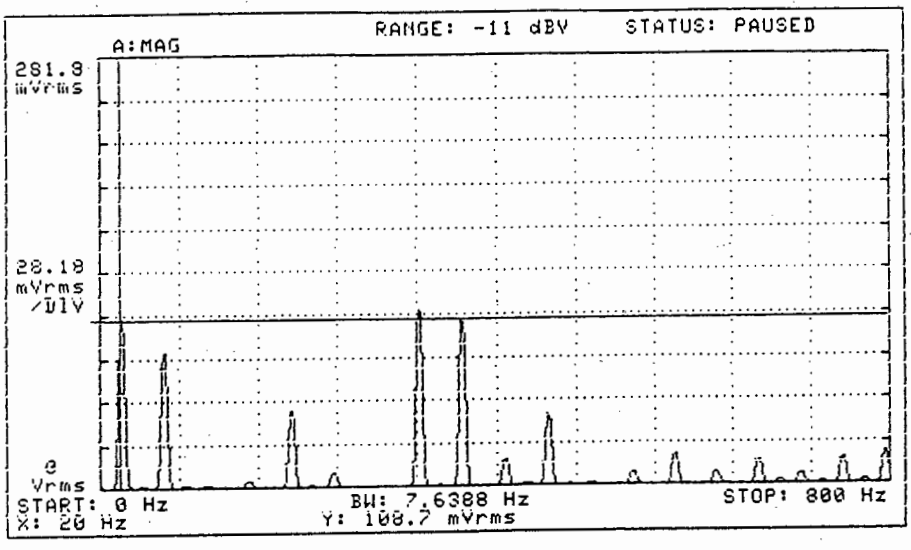

Current Waveforms

1) Frequency = 50 Hz

Sinusoidal Modulation

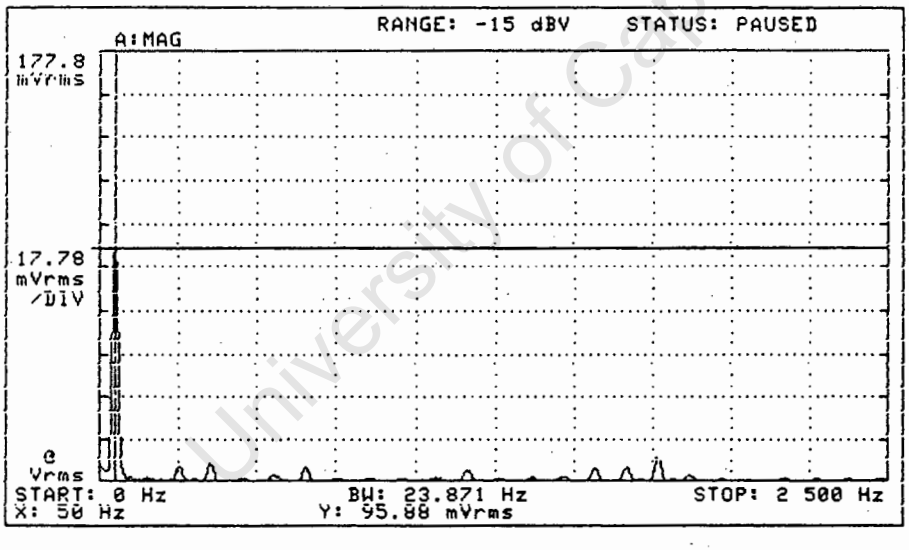

Harmonic Elimination

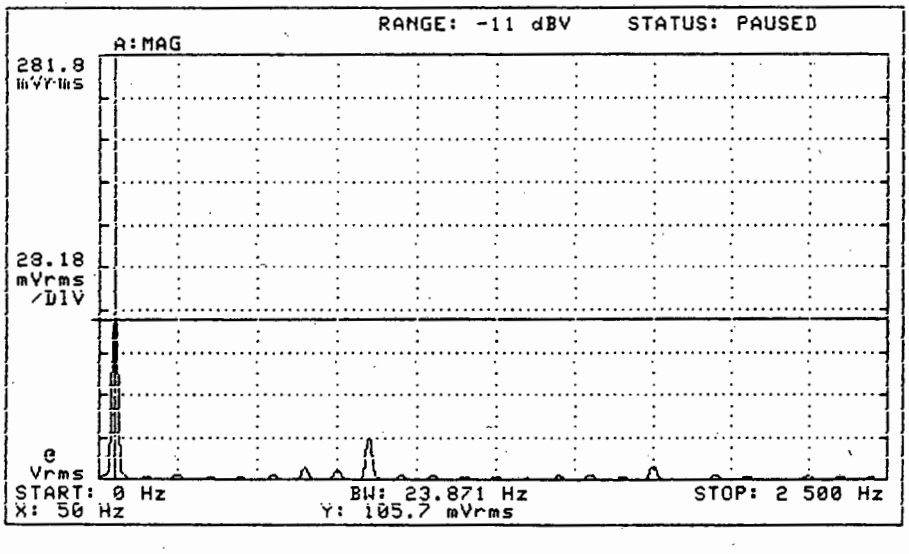

2) Frequency = 35 Hz

Sinusoidal Modulation

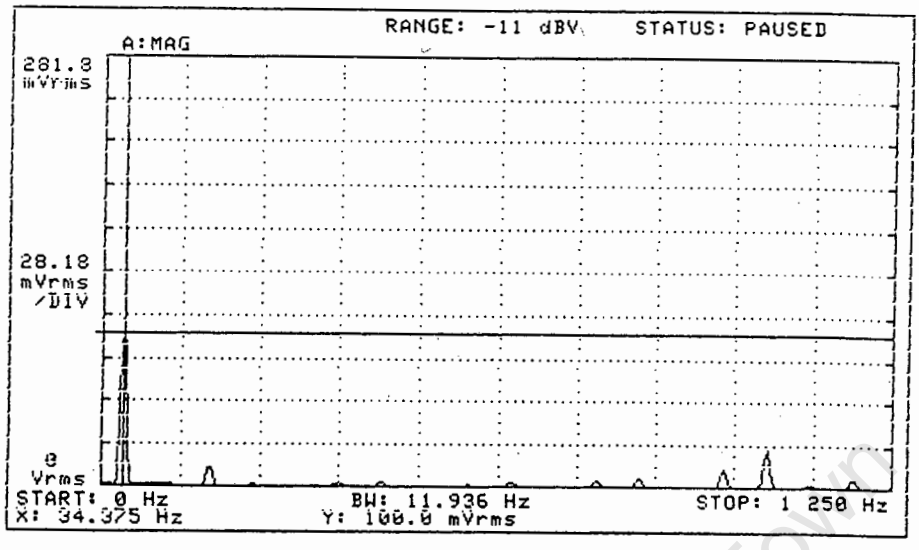

Harmonic Elimination

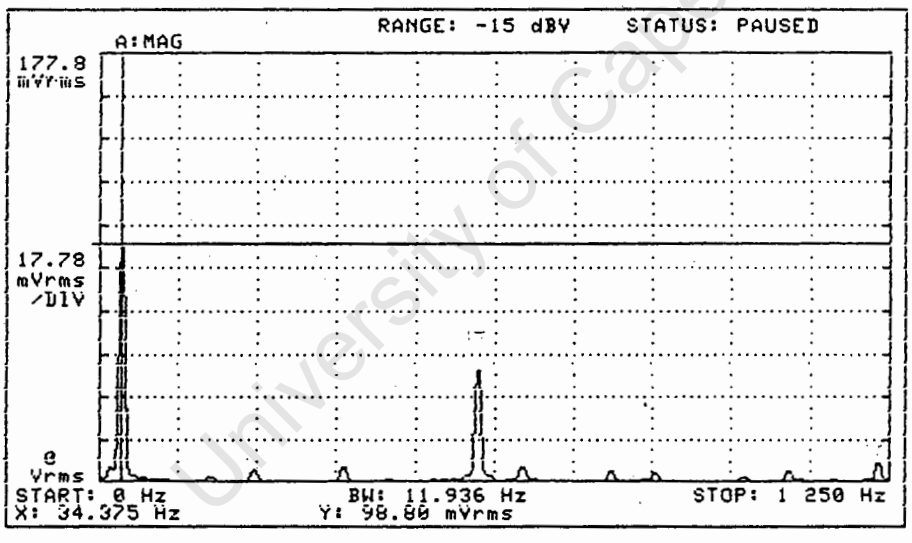

3) Frequency = 20 Hz

Sinusoidal Modulation

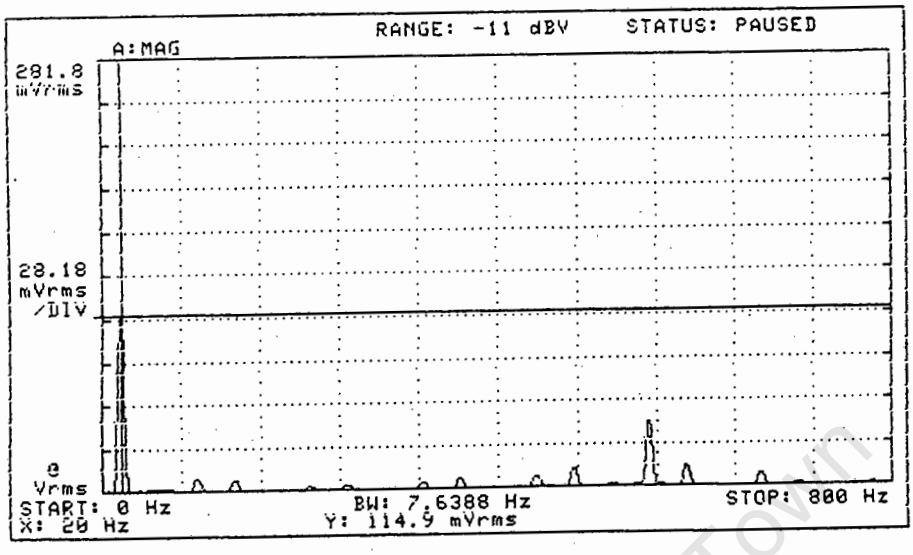

Harmonic Elimination